COMPUTATIONAL MODELS IN WAVE ANALYSES

W. ROLAND B. BAKER, B.Eng., P.Eng.

COMPUTATIONAL MODELS

IN

WAVE ANALYSES

by

© W. Roland B. Baker, B.Eng, P.Eng.

A thesis submitted to the School of Graduate
Studies in partial fulfilment of the
requirements for the degree of
Master of Engineering

Faculty of Engineering and Applied Science
Memorial University of Newfoundland
January 1992

St. John's Newfoundland Canada

ISBN 0-315-73755-1

To Lorne and Beryl
Without whom this work would not be possible.

ABSTRACT

The use of microcomputer technology to solve many of the iterative and tedious computations encountered in the engineering field is becoming prominent. Coastal Engineering is one of the many fields in engineering where the presence of the microcomputer is being felt. The need to compete efficiently and economically in the engineering market requires the accessibility to and use of computer software to speed up some of the menial tasks. This thesis presents the development and demonstrated use of three (3) such software packages. The data encryption software, CADGRID, water wave refraction and diffraction software, MUNWAVE, and the water basin response software, LONGWAVE, were developed using the Microsoft, QuickBasic program development software on a 80386 CPU based microcomputer sytem with 80387 coprocessor. The plotting routines were written using the Hewlett Packard Graphics Language (HPGL). The programs CADGRID and LONGWAVE will work in either EGA, VGA, CGA or Hercules monochrome graphics mode with VGA recommended. The program MUNWAVE will only operate in EGA graphics mode.

ACKNOWLEDGEMENTS

I would like to take this opportunity to thank Dr. T.R. Chari, Associate Dean of Graduate Studies, who was instrumental in my admission to the Master of Engineering Program; my supervisor, Dr. J.H. Allen, for his guidance as well as moral and financial support; the Offshore Awards Liaison Commitee, Ocean Studies Task Force for the Career Development Fellowship recommendation and the Provincial Government of Newfoundland and Labrador, Department of Career Development, for the award; and finally my many fellow graduate students who supported me in my studies.

TABLE OF CONTENTS

Chapter 3
COMPUTERIZED HYDROGRAPHIC DATA MANIPULATION

Chapter 4

COMPUTATIONAL MODEL FOR HARBOUR RESPONSE TO LONG PERIOD WATER WAVES

Chapter 5
COMPUTATIONAL MODEL FOR ON-SHORE WATER WAVE PROPAGATION

Chapter 6
ANALYSES USING THE COMPUTER PROGRAMS

Chapter 7
Discussion and Conclusions

LIST OF FIGURES

LIST OF FIGURES

LIST OF FIGURES

LIST OF FIGURES

LIST OF FIGURES

LIST OF FIGURES

LIST OF TABLES

NOMENCLATURE

The nomenclature adopted for the work presented in this thesis is, for the most part, as published by the International Association for Hydraulic Research (IAHR), 1989. The symbols used by various authors referenced in this thesis were reproduced with definitions as required. Symbols used are as follows,

$(1/\beta)^{1/2}$	: refraction coefficient.
α	: angle wave makes with shoreline.
α_0	: angle deep water wave makes with shoreline.
θ	: angle ray makes with a shore normal.
θ_0	: angle deep water ray makes with a shore normal.
ϕ	: velocity potential.
ϕ_{Lat}	: latitude (+/-) northern/southern hemispheres.
ω_e	: earth's angular rotation (7.27×10^{-5} rad/sec).
C	: wave celerity.
C_0	: deep water wave celerity.
C_g	: wave group celerity, typically $C_0/2$.
F_C	: Coriolis parameter.
g	: gravitational acceleration.
h	: water depth.
H_0	: deep water wave height.
L	: wave length.
s	: distance along a ray path.
t	: elapsed time.
T	: wave period.

Chapter 1
INTRODUCTION

1.0 Introduction

The province of Newfoundland and Labrador is located on the east coast of Canada (see Fig. 1.1). The province has an extensive shoreline with many well protected harbours. The most notable of the harbours is St. John's Harbour which is located on the east coast of the island portion of the province. The harbour has been a safe haven for sea vessels travelling the treacherous North Atlantic Ocean for approximately 500 years. The harbour is unique in its geometry with a narrow entrance channel and its north-south orientation of the major water basin (see insert, Fig. 1.1).

The activity in oil exploration over the past two decades on the Grand Banks, located southeast of the province, has led to exploitable oil field finds, one of which is the Hibernia oil field. A production agreement has been signed between the two levels of government and the oil industry to develop this field.

The increase in off-shore petroleum exploration and subsequent production will in turn increase the need for safe harbours

with few inconveniences. Many harbours have been proposed as construction and supply sites for the off-shore petroleum industry. One proposal is the development of Freshwater Bay (see insert Fig. 1.1), located southeast of St. John's Harbour, as an off-shore petroleum supply base (see Fig. 1.2). The tidal range in the St. John's Bay area is semi diurnal and of the order of approximately one (1) metre.

The development of Freshwater Bay as a service port for the off-shore would provide the opportunity for proper radial growth of City of St. John's as well as provide much needed services required by the petroleum industry.

The project in summary entails the construction of access roads, tunnel, breakwater, wharves and dredging of the existing pond at the southern end of the bay to the depth required by deep sea vessels (see Fig. 1.2). The harbour basin created by this development and the effect of the breakwater need to be examined for response to wave activity entering from the Atlantic Ocean through St. John's Bay.

In the majority of cases, the effect of encroaching waves on harbour basins has been restricted to the analysis of short period wave phenomenon with localized disturbance effects inside the harbour basin. However, the response of the entire harbour basin to long period water waves can be significant if

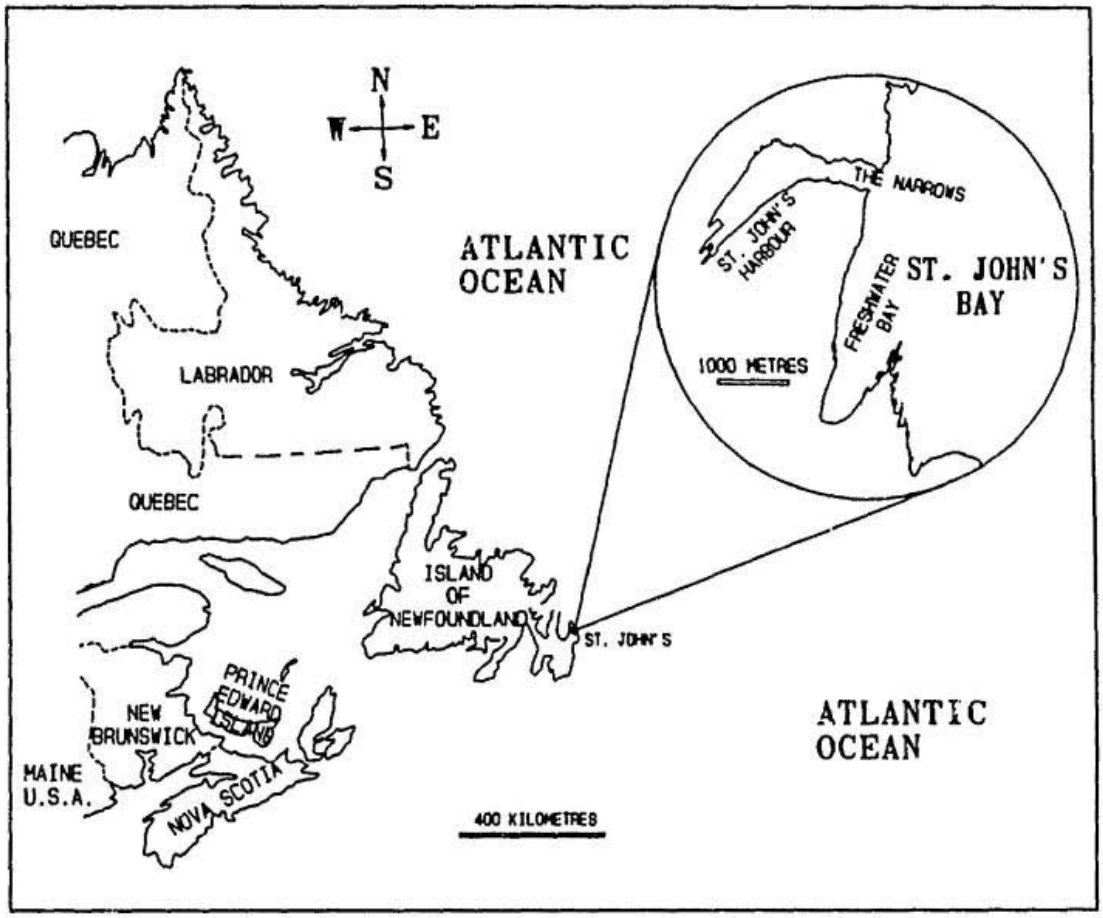

Fig. 1.1 - St. John's Harbour, The Narrows and Freshwater Bay Location Map.

the wave period coincides with the natural response period of the harbour basin. A literature review is presented to familiarize the reader with the various aspects and phenomena which are encountered during water wave propagation.

The natural response period of a harbour basin of simple geometry can be determined analytically using various relationships previously developed.

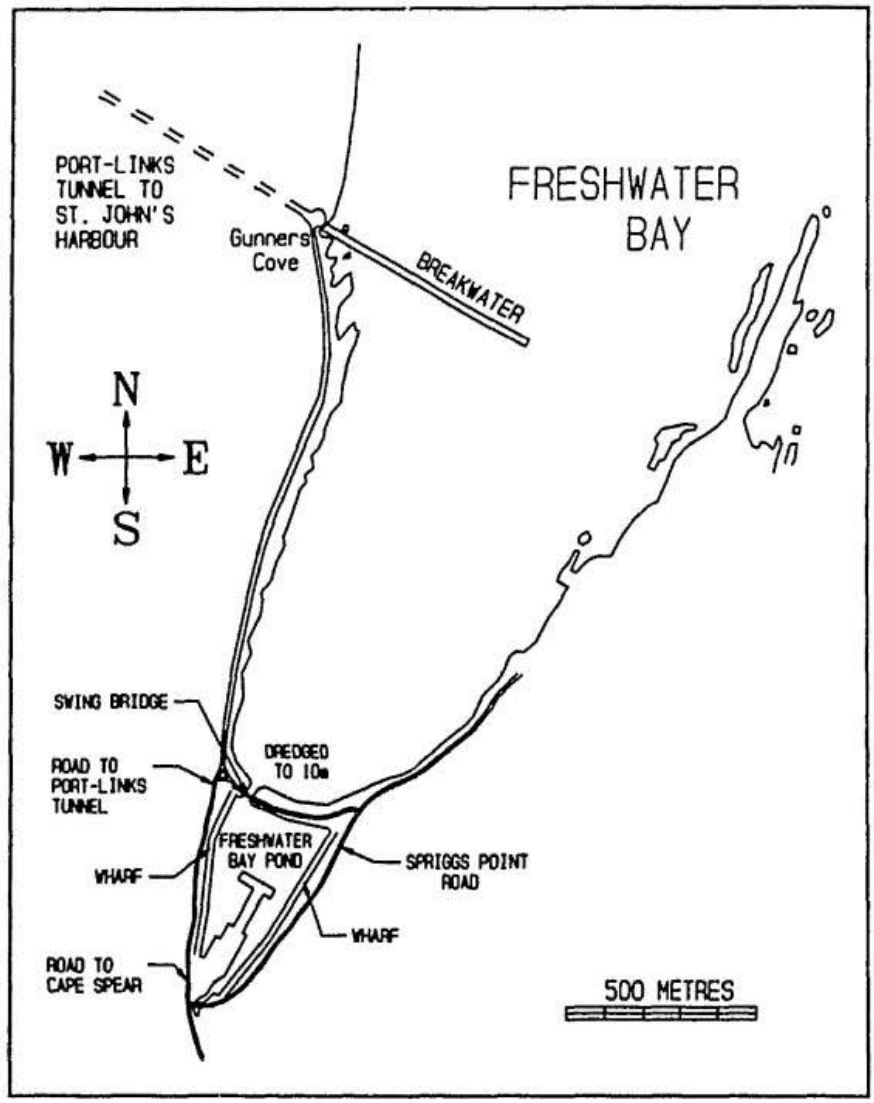

Fig. 1.2 - Freshwater Bay proposed development plan.

However, the response period of an arbitrarily shaped water basin with varying depth is difficult, if not impossible, to determine analytically. Therefore, researchers have devised various methods to determine the response period.

The methods typically used vary with physical models and/or numerical models being used with actual field data as input or used for calibration. Both methods have their merits and pitfalls and usually complement each other as verification tools. The majority of existing numerical models typically require access to large expensive mainframe computer systems which might not be readily available to the practising Coastal Engineer.

The development of personal computer based models to study the response characteristics of a proposed coastal development to encroaching long period water waves is presented in this thesis. The primary attention is focused on the numerical modelling methods of analysis with three (3) software packages developed. One (1) package will serve to input the large amount of hydrographic data typically required for any such analysis and the remaining two (2) are the actual analysis packages. These software packages provide the Coastal Engineer with a series of personal computer based tools to determine quick solutions to coastal wave problems and analyses.

The Freshwater Bay (SOHILCO) Development is selected for analysis to demonstrate a typical analysis procedure using the software packages.

Chapter 2
LITERATURE REVIEW

2.0 Introduction

The work presented in this thesis concerns the response of a harbour basin to long period waves entering the harbour from the ocean. Ocean waves undergo a transformation as they propagate towards the shore and upon reaching the shore. These waves upon entering a harbour can cause oscillations of the harbour basins while undergoing transformation inside. The work undertaken by various researchers in this area is extensive and analysis methods used are typically physical and/or mathematical modelling techniques. Therefore, a literature review concerning the theory with respect to the process of wave transformation, water basin oscillations, and modelling techniques used by various researchers to investigate the phenomenon was undertaken to identify sources of information and possible recommendations as to procedures to use for the work presented in this thesis.

2.1 Wave Theory

The solutions to many wave propagation problems are typically developed using Laplace's wave equation (Dean and Dalrymple,

1984, p.43),

$$\nabla^2\phi = \frac{\partial^2\phi}{\partial x^2} + \frac{\partial^2\phi}{\partial y^2} + \frac{\partial^2\phi}{\partial z^2} = 0 \qquad (2.1)$$

where: ϕ = velocity potential; x,y,z are spacial dimensions.

The equation has many solutions. Therefore, it is necessary to select only those that are applicable to the particular wave motion of interest.

2.1.1 Wave Shoaling, Refraction & Diffraction

Ocean waves undergo a transformation as they propagate from deep water, over varying bathymetry, into shallow water. Wave shoaling, refraction, diffraction and reflection constitute this transformation. Shoaling refers to the change in wave height to maintain the conservation of energy less the energy loss due to bottom friction, refraction to change in direction due to the bathymetry, diffraction to the dispersion of wave energy such as behind breakwaters and reflection to the creation of a waves travelling in the opposite direction as a result of the shoreline or some structure such as a breakwater.

The method used to understand the refraction of water waves typically involves the construction of directional wave rays

at right angles to the wave front or crest. In the past this has been accomplished by hand using a graphical method. The Shore Protection Manual (SPM) gives a good summary and references to the underlying academics of the practical studies from which the graphical method is derived (see SPM, 1984, pp.2-62 to 2-74). The method involves the use of Snell's law directly,

$$\frac{\sin\alpha}{C} = \frac{\sin\alpha_0}{C_0} \qquad (2.2)$$

in conjunction with a graphical template (SPM, 1984, p.2-65). The restriction in this method is the angle between a ray and a tangent to a bathymetric contour which cannot be greater than eighty degrees (80°). A further technique is required whereby smaller spacial increments are used if this situation is encountered (SPM, 1984, p.2-70).

Dean and Dalrymple (1984), pp.100-112 presents the development of a mathematical approach using Snell's law to determine a spatially dependant refraction coefficient which is a measure of the distance between wave rays. The derivation is not presented here. However, the final equations required to determine the refraction coefficient are,

$$\frac{d^2\beta}{ds^2} + p(s)\frac{d\beta}{ds} + q(s)\beta = 0 \qquad (2.3)$$

where:

$$p(s) = -\frac{\cos\theta}{C}\frac{\partial C}{\partial x} - \frac{\sin\theta}{C}\frac{\partial C}{\partial y}$$

$$q(s) = \frac{\sin^2\theta}{C}\frac{\partial^2 C}{\partial x^2} - 2\frac{\sin\theta\cos\theta}{C}\frac{\partial^2 C}{\partial x\partial y} + \frac{\cos^2\theta}{C}\frac{\partial^2 C}{\partial y^2}$$

These equations and the equations following are solved simultaneously for β,

$$\frac{ds}{dt} = C \quad , \quad \frac{dx}{dt} = C\cos\theta \quad , \quad \frac{dy}{dt} = C\sin\theta \tag{2.4}$$

This refraction coefficient is typically used in combination with a shoaling coefficient which determines the wave height along a ray path. It is found using the conservation of energy, $(EnC)_1 b_1 = (EnC)_2 b_2$ assuming minimal energy losses due to bottom friction, where E = wave energy, $n=1/2[1+\{2kh/\sinh(2kh)\}]$, b = distance between wave rays, subscript 1,2 signify positions along the ray path. Substituting the energy equation gives,

$$E = \frac{1}{8}\rho g H^2 \quad , \quad \frac{H_2}{H_1} = \sqrt{\frac{C_{g1}}{C_{g2}}}\sqrt{\frac{b_1}{b_2}} \tag{2.5}$$

Substituting C_0 for position '1' and realizing that the second term on the right is equal to $1/\beta$ we get the equation for wave height transformation during propagation,

$$\frac{H_2}{H_0} = \sqrt{\frac{C_0}{2C_g}}\sqrt{\frac{1}{\beta}} \tag{2.6}$$

The first term on the right is the shoaling coefficient and the second is termed the refraction coefficient.

The increase in accessibility of affordable and relatively

powerful computers has seen a rise in the computational methods developed to study the refraction of water waves. Computational methods in the form of computer programs have been developed to carry out the tedious process of developing these wave rays such as those by Baker and Allen (1990) and Crookshank (1975).

Problems with focusing and crossing of rays, refraction over long distances and the restriction to linear wave theory have been examined by many researchers some of which are presented here.

Peregrine (1986) presented one description of the focusing of water waves. He derived two expressions for the maximum amplitude of a water wave at a focal point,

$$|a_0| = A_1\left\{1 + 2\alpha\sqrt{\frac{kR}{\pi}}\right\}$$
$$|a_0| = A_1\left\{1 + \frac{\alpha}{kA_1\sqrt{2K}}\right\} \qquad (2.7)$$

where:

$$p = \tanh kh \quad ; \quad \frac{C}{C_g} = \left\{\frac{2p}{1 + kh(1-p^2)}\right\}$$
$$K = \frac{C}{C_g}\left\{\frac{9 - 12P^2 + 13p^4 - 2p^6}{p - kh(1-p^2)}\right\}$$

and: A_1= initial amplitude at radius R from the focus; k= wave number; a_0= maximum amplitude; 2α= angle of circular arc containing focusing wave rays; h= water depth.

The second equation incorporates non-linear effects while the first does not. Both equations give increasing maximum amplitude with increasing wave steepness until they are equal then the first equation remains constant. This was observed with kR and α held constant and A_1 permitted to vary. These equations were derived for constant water depth of initially uniform amplitude.

Southgate (1984) presented a ray averaging method for smoothing out the ray crossing and focusing associated with the ray methods. The method consists of determining each rays particular influence in a square area and finding the average amplitude associated with this average. The final equation is,

$$A_{av}e^{iS_{av}} = \frac{1}{d}\sum_{All\ rays}\left\{\frac{e^{iS}}{\sin\zeta}\sqrt{\frac{\overline{bE}}{C_g}}\right\} \qquad (2.8)$$

where:

$$E = A^2 C_g b \quad ; \quad S = \int_{ray} k\,ds + S_0$$

and: A = average amplitude of a ray in the square; A_{av} = average of all rays in square; S = average phase of a ray in the square; S_{av} = average phase of all rays in the square; k = wave number; C_g = group celerity; b = separation of rays; s = path length along a ray from the rays starting point; ζ = angle between the ray and the averaging line; d = length of the averaging line.

This is one example which was summarized from Southgate (1984). The author presents similar methods for various

averaging areas other than a square. One of the side benefits to this method is the smoothing effect of ray crossings and focuses as indicated by the right hand side of the first equation where the ray separation factor, 'b', is now in the numerator.

Liu and Tsay (1985) presented still another method where the bathymetric data is modified using an algorithm developed by the authors. The area to be modified is divided into a series of cross-sections in the y direction. Along each cross section, $x = x_i$ ($i = 1, 2, 3, \ldots, M$), the water depth at each node is denoted as h_j^i ($j = 1, 2, 3, \ldots, M$). An averaged water depth along the cross-section is then calculated,

$$\bar{h}(x_i) = \frac{1}{2}\sum_{j=1}^{N-1}\left\{\frac{(y_{j+1}-y_j)\,(h_{j+1}^i - h_j^i)}{(y_N - y_1)}\right\} \quad i=1,2,\ldots M \tag{2.9}$$

The modified h(x) is then calculated,

$$\bar{h}(x) = \sum_{j=1}^{4} C_{j,i}(x-x_i)^{j-1} \quad , \quad i=1,2,3,\ldots,M-1 \tag{2.10}$$

in, which $C_{j,i}$ is determined by matching water depth $h(x_i)$ at each x_i and by requiring the first and second derivatives of the equation be continuous at each node.

Headland and Chu (1984) suggested governing equations for the refraction of long, finite amplitude (cnoidal) waves in shallow water where cnoidal refers to the theory which best

describes the wave profile and is given by the Jacobian elliptical cosine function. They proposed linear theory be used for waves in deep and transitional water and cnoidal theory in shallow water. The governing equations were developed in the same manner as that presented by Dean and Dalrymple, (1984) for linear theory. The equations are lengthy and are not reproduced here. The authors compared the two theories and noted that the cnoidal rays travel faster, propagate further, refract less and shoal higher than linear rays.

The term diffraction is used to describe the process of lateral spreading of energy perpendicular to a water wave's dominant propagation direction. The usual method of analysis was initially separate from the refraction analysis and typically associated with wave structure interaction. The analysis was carried out using wave diffraction diagrams which provide isolines of relative wave height for various incident wave angles on a semi-infinite breakwater or a given breakwater gap (SPM, 1984, pp.2-75 to 2-108). Dean and Dalrymple (1984), pp.116-124, presents the governing equation and a solution developed by Sommerfeld,

$$F(x,y) = \frac{1+i}{2}\left[e^{-iky}\int_{-\infty}^{\beta} e^{-i\frac{\pi}{2}u^2}du + e^{iky}\int_{-\infty}^{\beta'} e^{-i\frac{\pi}{2}u^2}du\right] \qquad (2.11)$$

where:

$$\beta^2 \equiv \frac{4}{L}(r-y) \quad , \quad \beta'^2 \equiv \frac{4}{L}(r+y)$$

$$r=\sqrt{x^2+y^2} \quad , \quad u=2\pi\left[\sqrt{\frac{2r}{L}}\sin\left(\frac{\theta \pm \theta_0}{2}\right)\right]^2$$

and: x= distance along breakwater positive from tip to butt; y= distance 90° to breakwater in leeward direction; F(x,y)= complex amplitude (Ae^{-iky}); A= amplitude; L= wavelength; θ= $\tan^{-1}(y/x)$; θ_0= incident angle.

The solution for F(x,y) may be found using fresnel integrals,

$$\int_0^u \cos\left(\frac{\pi u^2}{2}\right)du \quad , \quad \int_0^u \sin\left(\frac{\pi u^2}{2}\right)du$$

This method was used by Baker and Allen (1990) and Crookshank (1975) in their ray tracking programs.

Efforts to investigate the combined refraction-diffraction problem using the mild slope equation developed by Berkoff,

$$\frac{\partial}{\partial x}\left(CC_g\frac{\partial \phi}{\partial x}\right)+\frac{\partial}{\partial y}\left(CC_g\frac{\partial \phi}{\partial y}\right)+\sigma^2\frac{C_g}{C}\phi = 0 \qquad (2.12)$$

where: ϕ(x,y)= complex velocity potential, x and y are horizontal dimensions; σ= angular frequency ($2\pi/T$); T= wave period; C(x,y)= wave celerity (σ/k); k(x,y)= wave number given by $\sigma^2 = gk\tanh(kh)$; $n=1/2\{1+2kh/\sinh(2kh)\}$; h(x,y)= still water depth; C_g(x,y)= group celerity (nC); g= acceleration due to gravity.

have been made by various researchers such as Liu and Tsay (1983), Ebersole (1985) and Panchang et al. (1988, 1990). The mild slope equation has the effect of smoothing over areas where ray crossings and focal points occur by introducing the

diffraction of wave energy which opposes the concentration of energy which occurs at the ray focuses.

2.1.2 Wave Reflection

The reflection of water waves is a phenomenon that occurs as a wave propagates on shore. The ability of a shoreline or structure to reflect a wave is typically denoted by a reflection coefficient. Dean and Dalrymple (1984), p.339, present Miche's theory for the approximate reflection coefficient of beach slopes,

$$k_r = \frac{\left(\frac{2\beta}{\pi}\right)^{\frac{1}{2}} \frac{\sin^2\beta}{\pi}}{\frac{H_0}{L_0}} \qquad (2.13)$$

where: β= beach slope; H_0, L_0 = deep water wave height and length respectively.

The SPM (1984), pp.2-112 to 2-129, presents a more detailed explanation for reflections from vertical walls, plane slopes, revetments, beaches, breakwaters and bathymetric variations. Vertical walls typically have a reflection coefficient of one (1). In comparison to Miche's theory, the SPM presents a theory developed by Battjes based on a surf similarity parameter,

$$\xi = \frac{1.0}{\cot\theta\sqrt{\frac{H_i}{L_0}}} \qquad (2.14)$$

where: ξ = surf similarity parameter; θ = beach angle; H_i = incident wave height; L_0= deep water wave length.

and further expanded upon by others to incorporate the slope surface roughness effects (see Fig.2-65, SPM, 1984, p. 2-118).

More modifications are then required for structures with armour stone. These structures dissipate more wave energy and typically have a lower reflection coefficient. The SPM, pp.2-120 to 2-121, provides a figure relating the ratio of incident height over breaking height at the toe of the structure (H_i/H_b) to size of armour stone, breaking wave length and beach slope $\{(d_b/L_b)\cot\theta\}$ and a table for number of layers of armour stone, to determine the two extra factors required (α_1, α_2). These factors are then used to correct the reflection coefficient derived previously.

Seelig (1983) reported similar findings during his study and proposed various empirical equations to determine the reflection coefficient for smooth slopes and breakwaters and jetties,

$$k_r = \tanh(a\xi^b) \quad ; \quad a=0.1,\ b=2.0 \qquad (2.15)$$

$$k_r = \frac{\alpha\xi^2}{\xi^2+\beta} \quad ; \quad \alpha=1.0,\ \beta=5.5 \qquad (2.16)$$

where: $\xi = m/(H_i/L_0)^{1/2}$ and m = beach slope.

The coefficients α and β are taken to be 0.6 and 6.6 respectively for breakwaters and jetties.

The SPM, pp.2-122 to 2-125, also presents a method to determine the reflection coefficient of bathymetric variations such as smooth steps and sinusoidal shaped bed forms. The reflection coefficient for smooth steps is related to the ratio of the (deepest depth) divided by (shallower depth), $(=d_1/d_2)$ and the (step length) divided by (sum of the depths), $\{=l/(d_1+d_2)\}$ and figures constructed from experimental data. The coefficient for sinusoidal bars is handled in much the same way. The ratios of bar amplitude to length and bar amplitude to the depth from still water level to mean bed level and two figures are used to determine the maximum reflection coefficient.

The SPM, pp.2-124 to 2-129, also discusses trapped waves at structures that have no beaches fronting them. The SPM provides formulae to determine the seaward distance that a slope must extend to trap waves and long shore distance the reflected wave will travel before returning to the shoreline,

$$\frac{X_m}{d_s} = \frac{1}{\sin^2\alpha} - 1$$

$$\frac{Y_m}{d_s} = \frac{1}{\sin^2\alpha}[\pi - 2\alpha + \sin(2\alpha)] \qquad (2.17)$$

where: X_m = max slope distance; d_s = water depth at toe of structure; α = angle between a wave ray and the shore normal; Y_m = long shore distance for reflected wave return.

Wiegel (1964), pp. 72-74, discusses the Mach stem effect which usually occurs with solitary waves. The typical reflection patterns are depicted in Fig. 2.1. Wiegel (1964) also presents figures which give the coefficients to determine the height of the reflected wave and Mach stem, using the incident wave height, for typical incident wave angles as reported by Perroud.

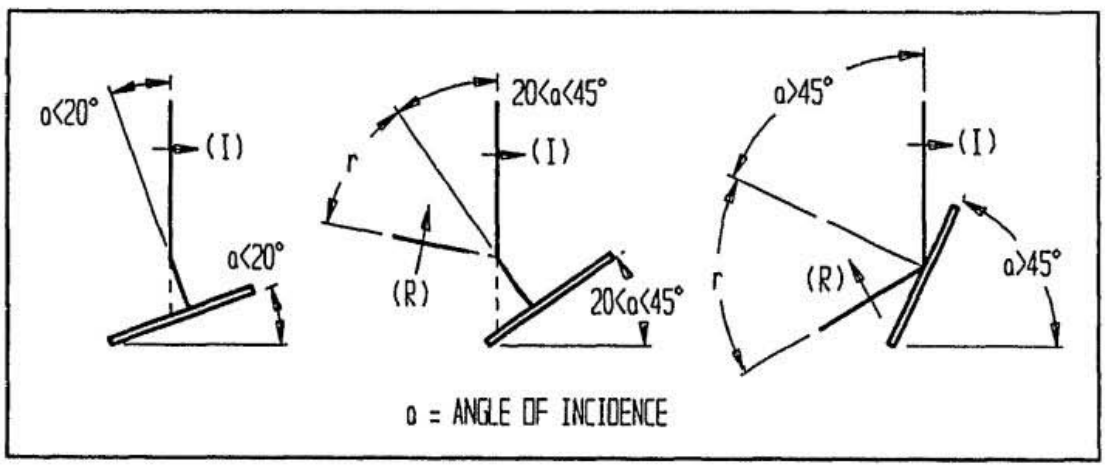

Fig. 2.1 - Reflection patterns of solitary wave (Wiegel, 1964, p.72).

2.1.3 Wave Energy Dissipation

The development of friction terms to describe the effect of bottom or sea bed friction on long waves is presented in Dean and Dalrymple (1984), pp.146-154 and pp.261-282. Charts providing friction factors over land and constant depth bottom are presented in SPM, pp.3-68 to 3-69. The methods used to incorporate the effects of bottom friction on wave propagation for long and short period waves are numerous.

Hsaio and Shemdin (1978) investigated the bottom friction mechanism in detail using the relationship,

$$\frac{1}{E}\frac{dE}{dt} = -\frac{4}{3}\frac{C_f \omega^3 H}{g \sinh^3 kh} \qquad (2.18)$$

where: E= wave energy; t= time; ω= wave frequency; H= wave height; k= wave number; h= water depth.

and proposed a method for calculating the friction coefficient from field measurements. The method uses a friction coefficient diagram first proposed by Jonsson and later expanded upon by Kamphuis through a series of laboratory tests. The diagram is similar to the standard Stanton diagram whereby the friction factor, C_f, and relative roughness, a/k, are plotted versus the Reynolds number, Re. A comparable diagram was presented in Dean and Dalrymple (1984), p.266, which was excerpted from the work of Kamphuis. The Reynolds number was determined using,

$$Re = \frac{aU_m}{\upsilon} \tag{2.19}$$

where: U_m= maximum wave orbital velocity; a= orbital amplitude; υ= kinematic viscosity.

The relative roughness, a/k_s, was determined using an equation for sand motion,

$$\frac{\gamma_s T^2}{\rho D_s} = 240\left(\frac{2a}{D_s}\right)^{\frac{4}{3}}\left(\frac{\rho\gamma_s D_s^3}{\mu^2}\right)^{-\frac{1}{9}} \quad , \quad \gamma_s = (\rho_s - \rho)g \tag{2.20}$$

where: ρ= water density; ρ_s= sand density; T= wave period; D_s= mean sand diameter; μ= dynamic viscosity.

to determine if bottom ripples are present which can be expected if this equation is satisfied. The authors found that the ripple slope, ζ/λ_s (height to length), had a functional dependence on a dimensionless stress parameter θ_s defined as,

$$\theta_s = \frac{\rho U_m^2}{\gamma_s D_s} \tag{2.21}$$

and the ripples vanished at $\theta_s \geq 2.5\text{x}10^2$. The ripple heights, if present, were then determined using a diagram which depicts the functional dependence of λ_s/a on U_m/w, where w is the fall velocity of sand. The relative roughness k_s was then taken as the ripple height and where no ripples were present as D_s. They also compared percolation dissipation,

$$\frac{1}{E}\frac{dE}{dt} = -k\sqrt{\alpha\beta}\,\frac{\tanh\sqrt{\frac{\alpha}{\beta}}kd}{\cosh^2 kh} \tag{2.22}$$

where: α,β = horizontal and vertical coefficients of permeability respectively; d= thickness of sand layer.

bottom motion dissipation, assuming a viscoelastic bottom obtaining the dispersion equation,

$$k = \frac{\omega^2}{g}\frac{1+\tanh kh\Omega}{\tanh kh+\Omega} \qquad (2.23)$$

where: Ω= function of wave bottom properties; k= complex wave number in which the imaginary part is a measure of energy dissipation.

mechanisms to the bottom friction mechanism. They concluded that all three mechanism are dominant in dissipating wave energy in shallow water. They also showed that the overall friction coefficient varies considerably above and below the widely used value of 10^{-2} and knowledge of the bottom sediment is essential in determining the appropriate value.

Wang and Christensen (1986) suggested friction factor formulae, developed for the investigation of storm surges resulting from hurricanes, dependant on the type of coastal topography,

smooth ocean bottom : $$f' = \frac{0.32}{[\ln(365d+1)]^2} \qquad (2.24)$$

rough ocean bottom : $$f' = \frac{0.32}{[\ln(20d+1)]^2} \qquad (2.25)$$

mangrove areas : $$f_e' = \frac{0.32}{[\ln(21d+1)]^2} + 0.07d \qquad (2.26)$$

forested areas : $$f_e' = \frac{0.31}{[\ln(22d+1)]^2} + 0.048d \qquad (2.27)$$

grassy areas : $$f' = \frac{0.32}{[\ln(2.7d+1)]^2} \qquad (2.28)$$

urban developed areas :

$$f_e' = \frac{0.32}{[\ln(122d+1)]^2}(1-\varepsilon) + MC_D dD \qquad (2.29)$$

where: C_D in equation (2.29) is determined from,

$C_D = 0.355\, e^{29000M}$:one row high-rise building areas.

$C_D = 1.05 + 5200M$: staggered medium-rise building areas.

$C_D = 1.04 + 1800M$:staggered residential areas.

and: M= number of buildings per square meter; d= water depth; D= average dimension of building in meters; ε= empirical coefficient developed by the authors.

The bed shear stress to be used in wave dissipation analysis is then found by substituting the appropriate f′ or f_e' value in the following,

$$\tau_b = \frac{f'\rho u_m^2}{2} \qquad (2.30)$$

where: ρ= density of water, u_m= spatial mean velocity in the local vertical.

The first two formulae are applicable to the work presented in this paper. The remaining formulae were included for information purposes.

The previous discussions concerned studying friction dissipation using bed shear stresses, etc. However, Leendertse (1968), Raney (1977), Dronkers (1972) and Falconer et al. (1986) used a form of the Chezy friction coefficient, discussed later, in their studies while Wang and Christensen used the Mannings coefficient. The relationship between the Manning and Chezy number is commonly known and can be found in any hydraulics text.

2.1.4 Wave and Current Interaction

The study to be carried out for this thesis does not deal with wave and current interaction. However, provisions are made in the models to include this phenomenon. Therefore, some references to pertinent literature were obtained.

Yoo et al. (1988) presented, via their comparison of mathematical models, several governing equations for studying wave-current interaction in small, bigger and large areas,

(A) waves in a small area:

$$\frac{D^2\varphi}{Dt^2} + \frac{\partial U_i}{\partial x_i}\frac{D\varphi}{Dt} - \frac{\partial}{\partial x_i} nC^2 \frac{\partial \varphi}{\partial x_i} + (1-n)\sigma_0^2\varphi = 0 \qquad (2.31)$$

where:

$$\frac{D}{Dt} = \frac{\partial}{\partial t} + U_i \frac{\partial}{\partial x_i} \quad ; \quad \sigma_0^2 = gk\tanh(kd)$$

$$\sigma = \sigma_0 + K_i U_i \quad ; \quad C = \frac{\sigma_0}{k} \quad ; \quad n = \frac{1}{2}\left(1 + \frac{2kd}{\sinh(2kd)}\right)$$

and: φ= velocity potential at mean water depth; U= current velocity; i= 1,2 as in conventional tensor notation; d= water depth; σ_0= angular frequency relative to water mass; k= separation factor; σ= angular frequency relative to sea bed; K= wave number vector.

such as wave current interaction at a port entrance. This governing equation is of the elliptic type. However, with a few manipulations hyperbolic equations were developed,

$$\frac{\partial \zeta}{\partial t} + \left(1 + \frac{K_i U_i}{\sigma_0}\right) \frac{1}{n} \frac{\partial}{\delta_{x_i}} (nR_i) = 0$$

$$\frac{\partial R_i}{\partial t} + \left(1 + \frac{K_i U_i}{\sigma_0}\right) C^2 \frac{\partial \zeta}{\partial x_i} = 0 \qquad (2.32)$$

where:

$$\zeta = \frac{\eta}{\sigma_0} \quad ; \quad R_i = \frac{K_i}{K} \frac{\eta}{K} \quad ; \quad K = \sqrt{K_1^2 + K_2^2}$$

and: η= water surface elevation.

Unlike the elliptic governing equations these hyperbolic equations had the capability to handle external as well as internal diffraction.

(B) waves in a bigger area: harmonic forms were introduced for various variables,

$$\varphi = -igAe^{i\theta} \quad ; \quad \zeta = Ae^{i\theta} \quad ; \quad R_i = P_i e^{i\theta}$$

$$A = \frac{a}{\sigma_0} \quad ; \quad P = \frac{a}{K}$$

where: i= $(-1)^{1/2}$; θ= wave phase; a= complex wave amplitude.

and a parabolic type governing equation developed,

$$i\left\{2\sigma_0\left[\frac{\partial A}{\partial t}+U_i\frac{\partial A}{\partial x_i}+nC\frac{\partial A}{\partial x}\right]+\frac{\partial u_i a}{\partial x_i}+A\frac{\partial(\sigma_0 nC)}{\partial x}\right\} - \frac{D^2A}{Dt^2}-\frac{\partial U_i}{\partial x_i}\frac{DA}{Dt}+\frac{\partial}{\partial x_i}\left(nC^2\frac{\partial A}{\partial x_i}\right)=0 \tag{2.33}$$

where: x= principal direction of propagation.

Likewise modifications were made and hyperbolic governing equations developed,

$$\frac{\partial A}{\partial t}+i\sigma_0 A+\left(1+\frac{K_i U_i}{\sigma_0}\right)\frac{1}{n}\frac{\partial(nP_i)}{\partial x_i}=0 \tag{2.34}$$

$$\frac{\partial P_i}{\partial t}+i\sigma_0 P_i+\left(1+\frac{K_i U_i}{\sigma_0}\right)C^2\frac{\partial A}{\partial x_i}=0 \tag{2.35}$$

for the description of wave climate on slowly varying current.

(C) waves in large areas: existing kinematic conservation equation used for ray tracking was modified to include diffraction effects,

$$\frac{\partial\omega}{\partial t}+\frac{1}{2a}\frac{\partial}{\partial x_i}(U_i+nC_i)a^2+\frac{S_{ij}}{\rho g a}\frac{\partial U_j}{\partial x_i}=0 \tag{2.36}$$

$$\frac{\partial K_i}{\partial t}+(U_j+nC_j)\frac{\partial K_i}{\partial x_j}+K_j\frac{\partial U_j}{\partial x_i}+\frac{\sigma_0(2n-1)}{2d}\frac{\partial d}{\partial x_i} + \frac{nC}{2ka}\left(\frac{1}{a}\frac{\partial a}{\partial x_i}\frac{\partial^2 a}{\partial x_j^2}-\frac{\partial^3 a}{\partial x_i\partial x_j^2}\right)=0 \tag{2.37}$$

$$S_{ij}=\left\{n\frac{K_i}{k}\frac{K_j}{k}+\left(n-\frac{1}{2}\right)\delta_{ij}\right\}\frac{1}{2}\rho g a^2 \tag{2.38}$$

where: j=1,2; δ_{ij}=1 at i=j ; δ_{ij}=0 at i≠j;
S_{ij}= radiation stress tensor.

The authors' finite difference grid model was used to solve these various governing equations and in most instances the results were acceptable. All the equations presented here also incorporate the refraction and diffraction of the wave as well as the current effect.

Yamaguchi (1986) developed a numerical method to simulate near shore current based on finite amplitude wave theory. The total method consisted of wave transformation and near shore current method in combination with cnoidal wave theory. The governing equations of wave number components for the wave transformation model were derived from the irrotational condition of wave number components giving the following wave number component conservation equations and nonlinear dispersion relation,

$$\frac{\partial k_x}{\partial t}+\frac{\partial}{\partial x}\left\{k_x\left(\frac{\partial \sigma_m}{\partial k}\cos\theta+U\right)\right\}+\frac{\partial}{\partial y}\left\{k_x\left(\frac{\partial \sigma_m}{\partial k}\sin\theta+V\right)\right\}$$
$$=k_x\left[\frac{\partial\left\{\frac{\partial \sigma_m}{\partial k}\cos\theta\right\}}{\partial x}+\frac{\partial\left\{\frac{\partial \sigma_m}{\partial k}\sin\theta\right\}}{\partial y}\right] \qquad (2.39)$$
$$+k_x\frac{\partial V}{\partial y}-k_y\frac{\partial V}{\partial x}-\frac{\partial \sigma_m}{\partial D}\frac{\partial D}{\partial x}-\frac{\partial \sigma_m}{\partial H}\frac{\partial H}{\partial x}$$

$$\frac{\partial k_y}{\partial t}+\frac{\partial}{\partial x}\left\{k_y\left(\frac{\partial \sigma_m}{\partial k}\cos\theta+U\right)\right\}+\frac{\partial}{\partial y}\left\{k_y\left(\frac{\partial \sigma_m}{\partial k}\sin\theta+V\right)\right\}$$
$$=k_y\left[\frac{\partial\left\{\frac{\partial \sigma_m}{\partial k}\cos\theta\right\}}{\partial x}+\frac{\partial\left\{\frac{\partial \sigma_m}{\partial k}\sin\theta\right\}}{\partial y}\right] \qquad (2.40)$$
$$+k_y\frac{\partial U}{\partial x}-k_x\frac{\partial U}{\partial y}-\frac{\partial \sigma_m}{\partial D}\frac{\partial D}{\partial y}-\frac{\partial \sigma_m}{\partial H}\frac{\partial H}{\partial y}$$

where: k_x, k_y = wave number components; U,V = two dimensional current components; k= wave number, θ= wave direction; $\partial\sigma_m/\partial k$ = propagation velocity corresponding to the group velocity; σ_m= relative angular frequency; D=(h+η)= water depth, h, plus the mean water level variation, η; H= wave height.

The energy balance equation used was,

$$\frac{\partial}{\partial t}\left(E_n - \frac{M_x^2+M_y^2}{2\rho D}\right) + \frac{\partial}{\partial x}\left(UE_n + F_x - \frac{M_x^2+M_y^2}{2\rho D}\tilde{U}\right) + \frac{\partial}{\partial y}\left(VE_n + F_y - \frac{M_x^2+M_y^2}{2\rho D}\tilde{V}\right) + S_{xx}\frac{\partial U}{\partial x} + S_{xy}\frac{\partial V}{\partial x} + S_{yx}\frac{\partial U}{\partial y} + S_{yy}\frac{\partial V}{\partial y} - \frac{M_x}{\rho D}\frac{\partial S_{xx}}{\partial x} - \frac{M_y}{\rho D}\frac{\partial S_{xy}}{\partial x} - \frac{M_x}{\rho D}\frac{\partial S_{yx}}{\partial y} - \frac{M_y}{\rho D}\frac{\partial S_{yy}}{\partial y} = -E_{bw} \qquad (2.41)$$

where:

$$\tilde{U} = U + \frac{M_x}{\rho D} \quad ; \quad \tilde{V} = V + \frac{M_y}{\rho D} \quad ; \quad M = \overline{\int_{-D}^{\xi} \rho u\, dz}$$

$$M_x = M\cos\theta \quad ; \quad M_y = M\sin\theta$$

$$E_n = E_p + E_k \quad ; \quad E_p = \frac{\rho g\overline{\xi^2}}{2} \quad ; \quad E_k = \frac{1}{2}\left\{\overline{\int_{-D}^{\xi} \rho\,(u^2+w^2)\, dz}\right\}$$

$$F = \overline{\int_{-D}^{\xi} (\rho u^2 + p)\, dz} - \frac{\rho g D^2}{2} \quad ; \quad F_x = F\cos\theta \quad ; \quad F_y = F\sin\theta$$

$$S_{11} = \overline{\int_{-D}^{\xi} (\rho u^2 + p)\, dz} - \frac{\rho g D^2}{2} \quad ; \quad S_{22} = \overline{\int_{-D}^{\xi} p\, dz} - \frac{\rho g D^2}{2}$$

$$S_{xx} = S_{11}\cos^2\theta + S_{22}\sin^2\theta - \frac{M_x^2}{\rho D}$$

$$S_{xy} = S_{yx} = (S_{11} - S_{22})\cos\theta - \frac{M_x M_y}{\rho D}$$

$$S_{yy} = S_{11}\sin^2\theta + S_{22}\cos^2\theta - \frac{M_y^2}{\rho D}$$

and: ξ= surface displacement; u,w = horizontal wave induced vertical particle velocity components, p= wave pressure; g= gravitational acceleration; E_p= potential energy; E_k= kinetic energy and the overline means time average over one wave period.

The near shore current model was developed using the vertically integrated continuity and momentum equations,

$$\frac{\partial \rho D}{\partial t} + \frac{\partial \tilde{M}_x}{\partial x} + \frac{\partial \tilde{M}_y}{\partial y} = 0 \tag{2.42}$$

$$\begin{aligned} &\frac{\partial \tilde{M}_x}{\partial t} + \frac{\partial (\tilde{U}\tilde{M}_x)}{\partial x} + \frac{\partial (\tilde{U}\tilde{M}_y)}{\partial y} \\ &= -\rho g D \frac{\partial \eta}{\partial x} + \frac{\partial}{\partial x}\left(\overline{\varepsilon} D \frac{\partial \tilde{U}}{\partial x}\right) + \frac{\partial}{\partial y}\left(\overline{\varepsilon} D \frac{\partial \tilde{U}}{\partial y}\right) \\ &\quad - \left(\frac{\partial S_{xx}}{\partial x} + \frac{\partial S_{xy}}{\partial y} + \tau_{bx}\right) \end{aligned} \tag{2.43}$$

$$\begin{aligned} &\frac{\partial \tilde{M}_y}{\partial t} + \frac{\partial (\tilde{V}\tilde{M}_x)}{\partial x} + \frac{\partial (\tilde{V}\tilde{M}_y)}{\partial y} \\ &= -\rho g D \frac{\partial \eta}{\partial y} + \frac{\partial}{\partial x}\left(\overline{\varepsilon} D \frac{\partial \tilde{V}}{\partial x}\right) + \frac{\partial}{\partial y}\left(\overline{\varepsilon} D \frac{\partial \tilde{V}}{\partial y}\right) \\ &\quad - \left(\frac{\partial S_{yx}}{\partial x} + \frac{\partial S_{yy}}{\partial y} + \tau_{by}\right) \end{aligned} \tag{2.44}$$

where:

$$\tilde{M}_x = \rho D\tilde{U} \quad ; \quad \tilde{M}_y = \rho D\tilde{V} \quad ; \quad \overline{L} = N_c \rho l_x \sqrt{gD}$$

$$\tau_{bx} = \rho C_f (u_b \cos\theta + U)\sqrt{(u_b \cos\theta + U)^2 + (u_b \sin\theta + V)^2}$$

$$\tau_{by} = \rho C_f (u_b \sin\theta + V)\sqrt{(u_b \cos\theta + U)^2 + (u_b \sin\theta + V)^2}$$

and: l_x= distance measured from shore; N_c= lateral mixing coefficient; C_f= bottom friction coefficient in the wave-current system.

Although the model developed using these equations is primarily interested in the area of the surf zone, some of the method used are applicable to long wave current interaction such as the near shore current model.

Raichlen and Lee (1984) conducted experiments to examine the interaction of long period waves and current. They concluded that a linear superposition of the water particle velocities of a wave and those of a current alone can adequately describe the total velocity of current and wave combined.

Ismail (1984) conducted experiments to examine the interaction of surface waves and non-uniform current (jet). As regards to wave motion, the results of the experiment indicated an increase in wave amplitude as the waves propagated into the jet and a set-up was formed at the jet source. With respect to current behaviour, the results indicated that the depth averaged mean current velocity at the jet longitudinal axis decreased in the presence of a wave which was accompanied by

an increase in the spreading of the jet. Also, the vertical velocity profile of the current was modified in that the mean velocity decreased near the bottom and increased near the surface.

Jonsson and Christoffersen (1984) presented a method to examine the effect of current on water wave refraction. They developed a series of coefficients for determining the wave height incorporating current, refraction, shoaling and energy dissipation,

$$\frac{H}{H_{st}} = \sqrt{\frac{\omega_r}{\omega_{r,st}}}\sqrt{\frac{C_{ga,st}}{C_{ga}}}\sqrt{\frac{De_{st}}{De}}\sqrt{\frac{AJ}{A_{st}J_{st}}} \qquad (2.45)$$

where: ω_r= relative angular frequency; C_{ga}= absolute group celerity; De = distance between rays; A= wave dissipative action; J= Jacobian; subscript 'st' means start.

These coefficients were developed for linear waves. However, the authors present a method to determine the coefficients for non-linear conditions by substitution of the non-linear wave energy density in the equations used to develop the above coefficients.

2.1.5 Long Period Waves

Seiche or ***seiching*** is the term used to describe the oscillation or resonance of a water basin as the result of some causative force (Dean & Dalrymple, 1984, p.144; U.S. Army Corps of Engineers (SPM), 1984, p. 3-96). Wiegel, 1964, p.115, disagrees with this and states that *seiching* refers to the 'free' oscillation of a water basin. The definition provided by Dean & Dalrymple and the SPM is adopted for the description of a harbour *seiching* phenomenon. The terms *seiching*, oscillation and resonance have the same definition throughout this work and are sometimes interchanged with those of the original authors.

A *seiche* is considered as a long period wave due to the typical period range of 20 seconds to several minutes even hours (Wiegel, 1964; Easton, 1984) and the large wavelength associated with this range of periods. In fact, the tidal motion of a harbour can be considered as a seiche with a period of approximately twelve (12) hours.

Long period waves can be generated by atmospheric disturbances, sea bottom movement or incorporated as bound long waves in wave groups. These waves are very durable and are purely reflected from beaches with a slope greater than 0.83% as well as vertical walls (see Baker, 1989). Upon

entering a harbour, this reflective property of long period waves between harbour boundaries can result in harbour resonance (see Bowers, 1982) or *seiching* which, depending on basin geometry, can be very complex.

The term bound long wave refers to long waves which are bound or travel with wave groups. These types of long period waves occur more frequently than the free long period waves generated by atmospheric disturbances. To date, there is no agreement as to if the bound long wave really travels with a wave group or is in fact a result of the wave group. Methods to estimate the bound long wave using random wave measurements have been developed and verified (see Vis et al, 1985; List, 1986; Barthel and Funke, 1984; Ottesen Hansen, 1980). The method involves spectral manipulation of the recorded wave data giving rise to the long wave climate.

Mansard and Barthel (1984) conducted experiments on the shoaling properties of bound long waves. Their investigation indicated a distinct trend in the increase of the bound long wave during shoaling and document the relationship between the bound long waves and the 'groupiness' factor of the incident wave group. They also document an increase in magnitude of low frequency oscillations in the shallow region of the experimental set up. The information available concerning bound long waves is minimal. However, research is continuing,

as this is an important phenomenon which is usually overlooked in long period wave studies.

The water motion associated with a *seiche* is typically very large in the horizontal direction with minimal vertical movement. Wiegel (1964), p.115, presents a typical motion where moored vessels were surging or swaying up to five (5) feet during a three (3) minute period oscillation with vertical water motions in the order of 0.1 to 0.2 feet (30 to 60 millimetres).

2.1.6 Water Basin Oscillations

Analytical expressions have been developed to determine the free oscillation period of water basins with simple geometry based on the Merian equation,

$$T_n = \frac{2 L_b}{n\sqrt{gh}} \qquad (2.46)$$

where: T_n= oscillation period corresponding to mode n; n= number of nodes in the basin; L_b= length of basin in longest direction; h= water depth; g= gravitational acceleration

(see Dean and Dalrymple, 1984, pp.148-149 for modified versions of (2.46)). The first two oscillation modes of a simple rectangular harbour are depicted in Fig. 2.2.

All the equations developed from the Merian equation are

unidirectional with the harbour geometry being described as simple mathematical functions. Wiegel (1964), pp.116, presents a form of the Merian equation for the coupled oscillations of a rectangular, constant depth water basin,

$$T_{mn} = \frac{2\lambda}{\sqrt{gh\left[m^2 + \left(\frac{\lambda n}{B}\right)^2\right]}} \qquad (2.47)$$

where: T_{mn}= oscillation period; λ= length of basin in longest direction; B= width of basin; m & n are integers describing the nodality of the basin oscillation.

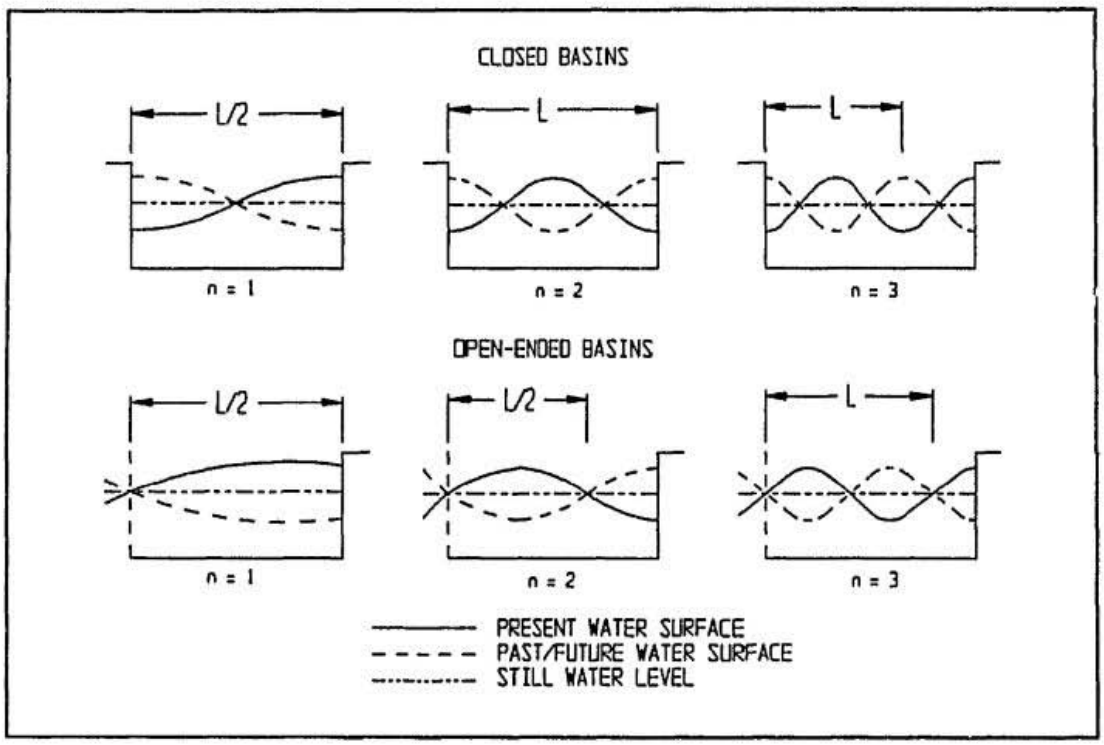

Fig. 2.2 - Surface profiles for oscillating waves in closed and open-ended basin.

Wiegel also presents the equations for the free surface of rectangular and circular basins of constant depth,

$$y_s = a_0 \sin\frac{2\pi t}{T}\cos\frac{m\pi x}{\lambda}\cos\frac{n\pi z}{B} \qquad \text{: rectangular} \quad (2.48)$$

where: x,z = horizontal coordinates with the origin at one corner and z the direction of incident wave advance; a_0= oscillation amplitude coefficient.

$$y_s = a\frac{kT}{2\pi}\sin\frac{2\pi t}{T}\cos n\theta \cdot J_n(kr) \qquad \text{: circular} \quad (2.49)$$

where: the origin is at the centre of the basin; r= radius; a= amplitude; θ= angle, n= any integer; J_n= Bessel function of order n.

Easton (1984) presented the derivation of a formula for the free oscillation periods of an idealized rectangular basin of constant depth,

$$T = \frac{2\pi}{C} = \frac{2L_b}{\sqrt{gh}}\sqrt{m^2 + \left(\frac{L_b n}{B}\right)^2} \qquad (2.50)$$

which agrees with Wiegel (1964).

These equations cannot be used to study arbitrarily shaped water basins, such as those found in nature. However, they can provide a 'rough' estimate of *seiche* periods for various modes if the basin geometries are idealized as simple geometric shapes. A mathematical model developed from the governing equations of motion and mass conservation of a fluid (Dean and Dalrymple , 1984, pp.16-19,133-137),

Equations of motion:

$$\frac{\partial U}{\partial t} + U\frac{\partial U}{\partial x} + V\frac{\partial U}{\partial y} + g\frac{\partial \eta}{\partial x} - \frac{1}{\rho}\left(\frac{\partial \tau_{xx}}{\partial x} + \frac{\partial \tau_{yx}}{\partial y}\right) - \frac{[\tau_{zx}(\eta) - \tau_{zx}(-h)]}{\rho(h+\eta)} = 0 \qquad (2.51)$$

$$\frac{\partial V}{\partial t} + U\frac{\partial V}{\partial x} + V\frac{\partial V}{\partial y} + g\frac{\partial \eta}{\partial y} - \frac{1}{\rho}\left(\frac{\partial \tau_{xy}}{\partial x} + \frac{\partial \tau_{yy}}{\partial y}\right) - \frac{[\tau_{zy}(\eta) - \tau_{zy}(-h)]}{\rho(h+\eta)} = 0 \qquad (2.52)$$

Continuity equation:

$$\frac{\partial \eta}{\partial t} + \frac{\partial [U(h+\eta)]}{\partial x} + \frac{\partial [V(h+\eta)]}{\partial y} = 0 \qquad (2.53)$$

where: U & V = depth averaged horizontal velocities in the x & y directions; ρ= fluid density; τ= shear stress; η= fluid surface above mean level; h= fluid depth; t= time.

or physical model is typically used to study the response of an arbitrarily shaped water basin, such as a harbour, to long period waves entering the basin.

2.1.7 Coriolis Effect

The Coriolis effect, also referred to as the Coriolis Force, is a result of the earth's eastward rotation. The effect occurs whereby an object in motion, not fixed to the earth, shows an apparent deflection clockwise (to the right) in the northern hemisphere and counterclockwise (to the left) in the southern hemisphere (Pipkin et al., 1987, p.97).

The Coriolis effect can play a significant role in long period wave propagation when the wave frequency is of the same order

as the earth's angular rotation frequency. Researchers typically include the coriolis parameter,

$$F_c = 2\omega_E \sin\phi_{Lat} \qquad (2.54)$$

(see Dean and Dalrymple, 1984, p.154) in the governing equations when developing mathematical models to study long period wave phenomena such as *seiching* or waves of tidal origin.

2.2 Modelling

The modelling of wave phenomena in harbours reduces the risk of unsatisfactory behaviour resulting from expansions or major renovations. Certain studies are best modelled mathematically while others must be physically modelled. Invariably, there arise situations where studies are within the capability of both types of models. In these instances, the cost advantage of the mathematical model must be balanced against the risk that some hydraulic feature might be overlooked whereas the physical model will typically show all features. (Olliver, 1982)

Researchers have developed various mathematical models to study long period wave phenomena of various forms such as Leendertse (1968), Shemdin et al. (1970), Dronkers (1972), Wilson et al.(1972), Houston (1977), Raney (1977), Chen

(1981), Gaillard (1982), Botes et al. (1984), Easton (1984), Falconer et al. (1986), Skovgaard et al. (1984) and Coeffe et al. (1984). These researchers typically verified their models with either a physical model or field measurements.

Some researchers have presented discussion papers giving the advantages and disadvantages of both modelling techniques such as Bowers (1982), Berenguer et al.(1986). Berenguer et al. (1986) describe both modelling techniques as complimentary tools that require validation via field measurements where possible. Bowers (1982) describes the types of mathematical models in use and comments on ability of the models to represent various wave effects. He concluded that time dependant long wave mathematical models can be used to study resonance for preliminary harbour design with the best layouts resulting from the mathematical model study examined in greater detail via a physical model.

Sunderman et al. (1972) conducted a comparison study of a mathematical model for tidal waves and a physical model. They showed that the mathematical model predicted the response of the physical model very well. The results from both models were not verified against actual field data. However, their study indicated the effectiveness of a mathematical model in reproducing the results of a physical model.

2.2.1 Physical Models

Physical models are, as the name suggests, scaled representations of the actual size or prototype phenomenon being studied. The model to prototype scale relationships required to investigate water wave phenomena are typically developed using Froudian similitude; $(F_r)_m = (F_r)_p$, where F_r is the Froude number and the subscripts m and p refer to model and prototype respectively (see Sharp, 1981, pp.35 and 57 to 64).

The work presented in this thesis is related to long period wave phenomena. The wave celerity is typically found using the relationship; $C = (gh)^{1/2}$. This relationship can be rearranged in the form of a Froude number; $C/(gh)^{1/2}$. Substituting into the Froudian similitude relationship presented above, a celerity scale relationship is developed;

$$\left(\frac{C_m}{C_p}\right)^2 = \frac{h_m}{h_p} \tag{2.55}$$

and substituting $C = L/T$, a time scale relationship is developed,

$$\frac{T_m}{T_p} = \frac{\frac{L_m}{L_p}}{\sqrt{\frac{h_m}{h_p}}} \tag{2.56}$$

These relationships are valid for shallow water waves with a depth to wavelength ratio less than 1/20. However, where the waves travel over varying bathymetry, it is possible to have transitional water waves. In this instance the above relationships are not valid and another relationship has to be developed using the transitional water wave celerity equation,

$$C^2 = \left(\frac{gL}{2\pi}\right)\tanh\left(\frac{2\pi h}{L}\right) \tag{2.57}$$

and substituting into the Froudian relationship using C = L/T gives the time scale relationship for the general case,

$$\frac{T_m}{T_p} = \sqrt{\left[\frac{L_m}{L_p}\right]\left[\frac{\tanh\left(\frac{2\pi h_p}{L_p}\right)}{\tanh\left(\frac{2\pi h_m}{L_m}\right)}\right]} \tag{2.58}$$

The horizontal scale of a long period wave model is typically governed by the actual physical area to hold the model. The typical horizontal scale used for the study of water basin response to long period waves or *seiching* is on the order of 1:1000 to 1:2000 (see Biesel, 1954). This horizontal scale if used for the vertical could result in a very small water depth in the model making it difficult to model the waves. Therefore, a distorted model is typically used giving rise to a larger vertical scale and subsequent water depth in the model. Given the prototype wave period and water depth the maximum distortion permitted to model the waves can be

determined from (see Biesel, 1954),

$$\frac{\left(\frac{h_m}{h_p}\right)}{\left(\frac{L_m}{L_p}\right)} < \sqrt{\frac{6T_p^2}{h_p}} \qquad (2.59)$$

The long period waves are highly reflective. Therefore, the model and prototype reflection coefficients should be the same for proper simulation. The wave height scale can be determined from a relationship for the reflection coefficient of smooth impermeable slopes as proposed by Miche (see Whalin and Chatham, 1974),

$$R = \frac{H_r}{H_i} = \frac{\tau'}{\pi}(2\alpha\sin^2\alpha)\left(\frac{L_0}{H_0}\right) \qquad (2.60)$$

where: R= reflection coefficient; H_r & H_i = reflected & incident wave heights respectively; $\tau' = 0.8$, an empirical coefficient; α= average slope in radians; L_0 & H_0 = equivalent deep water wave length & height respectively.

Assuming the empirical slope coefficient can be made equal in model and prototype and that α is proportional to h/L a wave height relationship can be developed (see Baker, 1989),

$$\frac{H_{0m}}{H_{0p}} = \left(\frac{L_{0m}}{L_{0p}}\right)\left[\frac{\phi\alpha_p\sin^2\phi\alpha_p}{\alpha_p\sin^2\alpha_p}\right] \quad , \quad \phi = \left(\frac{h_m}{h_p}\right)\left(\frac{L_p}{L_m}\right) \qquad (2.61)$$

This relationship indicates that the effect of scale distortion can be reduced by modifying the model wave heights.

The distorted model scale also presents problems with fluid viscosity and surface tension when the same fluid is used in both. Viscous and surface tension scale relationships can be developed using dimensionless parameters relating the fluid viscosity, υ, and surface tension ,σ, to water depth (see Baker, 1989),

$$\frac{\nu_m}{\nu_p} = \left(\frac{h_m}{h_p}\right)^{\frac{3}{2}} \quad , \quad \frac{\sigma_m}{\sigma_p} = \left(\frac{h_m}{h_p}\right)^2 \tag{2.62}$$

Assuming the same fluid in model and prototype, these relationships indicate the necessity to reduce the effects introduced by the surface tension and viscosity of the fluid. Le Mehaute recommends a minimum water depth of two (2) centimetres for viscous effects to be negligible and Kirschmer recommends a minimum value for water depth and wave height of five (5) and two (2) centimetres respectively to minimize the surface tension scale effects (see Kohlhase and Dette, 1980).

The boundaries for physical models are of primary concern as well. Waves reflected from necessary boundaries in the model which are not in the prototype, such as the walls of a wave tank can affect the results of a model study. This effect is minimized by the installation of filters at all boundaries not included in the study. These filters can be very large when compared with the actual model size. Biesel (1954) recommends a minimum filter width proportional to the model wave length and of the order of size equivalent to one wave length. The

offshore distance to be modelled is also directly proportional to the wave length. This distance and resulting area can be very large, such as that required to study water basin response to tidal fluctuations where the prototype ocean boundary is located at the amphidromic point. Depending on geographic location, the amphidromic point can be located outside the continental shelf if it is not located on land.

The costs of undertaking a physical model study can be high depending on the complexity of the study and the number of models required. A typical harbour resonance study might require the construction of more than one model at different scales if the wave period range to be studied is very large. The effects due to scale reduction also requires supplemental modifications to the model or resulting data. The relative cost of a physical model can be reduced by conducting mathematical simulations prior to model design and construction. This effort can provide a better understanding of the phenomenon being investigated and eliminate the trial and error method of constructing models to determine the conditions for maximum response.

2.2.2 Mathematical Models

The mathematical models are typically based on formulations

of the water motion and continuity, equations provided earlier, using finite difference, finite element or variational calculus techniques. The mathematical models are invariably verified/calibrated using actual recorded data and/or a physical model.

Yoo et al. (1989), present a lengthy discussion on the various mathematical models in use for wave current interaction as previously mentioned. They categorize the models inter-period, evolution and period averaging where each group contains various models which may be named after the type of governing equation such as hyperbolic, elliptic, parabolic and Boussinesq. The authors recommend a, hyperbolic evolution, inter-period model when investigating the response of water basins.

The mathematical models developed to study harbour response to long period waves were typically developed using the transitional equations of motion, (2.51) and (2.52), and the conservation of mass 'continuity' equation (2.53), for a fluid. The equations are easily modelled using either finite element or difference techniques with suitable boundary conditions.

Thacker (1978) presented a paper comparing the two techniques. He found the finite element technique to be computationally

more expensive for two reasons. The first is that the equations are coupled and computation time must be devoted to inverting the equations at each time step which is not required in the finite difference technique. The second is the smaller time step required than that for the finite difference technique. The finite element technique was found to more accurate than the finite difference technique when the same computational grid was used. However, Thacker states that the level of performance provided by the finite-element technique can be obtained more economically by using a finer computational grid with the finite difference technique.

Other successful attempts involved variational calculus (Lee and Raichlen, 1970) and mirroring techniques (Kohlhase et al., 1978). Lee and Raichlen developed their model based on a harbour of arbitrary shape with constant depth. The use of these models to investigate harbours with varying bathymetry such as presented in this thesis is questionable.

2.2.2.1 Finite Difference Models

The most prominent contribution was made by Leendertse (1968). The governing equations used were the equations of motion and continuity with minor modifications (ref. (2.51), (2.52) & (2.53)). He included the effects of bed friction by including

terms based on the Chezy coefficient rather than retain the shear stress terms,

$$\frac{gU\sqrt{U^2+V^2}}{C^2(h+\xi)} \quad , \quad \frac{gV\sqrt{U^2+V^2}}{C^2(h+\xi)} \qquad (2.63)$$

where: C= chezy coefficient; ξ= water surface elevation.

The coriolis parameter was also included in the governing equations.

Leendertse developed a time marching central difference method using a space staggered grid coordinate scheme to study tidal flow. A space staggered scheme was used where velocities, water levels and depths were described at different grid points (see Fig. 2.3). The solution to the governing equations, using finite difference approximations, was a multistep operation in time in such a way that the terms containing space derivatives and the Coriolis parameter are taken alternating forward and backward. The individual

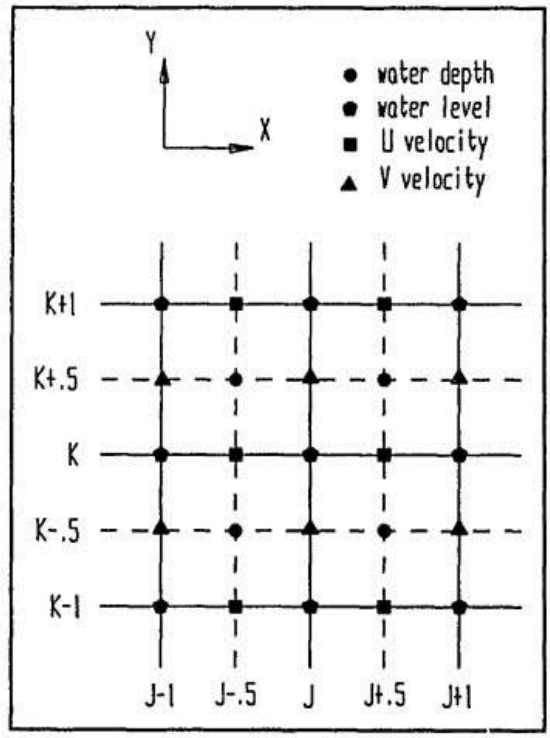

Fig. 2.3 - Space staggered finite difference scheme.

operations each have two time intervals. The first operation was taken from time 'n' to 'n+½' and the second from 'n+½' to 'n+1'. Values of the fields of ξ, U, and V at time 'n+½' were obtained from the same fields at time 'n' by an operation which was implicit in ξ and U and explicit in V. Then the same fields at time 'n+1' were computed from the fields at time 'n+½' using an operation which was implicit in ξ and V and explicit in U. Leendertse investigated the stability of the finite difference scheme and found the model to be unconditionally stable.

The model is well suited for arbitrarily shaped harbours with varying bathymetry. Research has been undertaken by other researchers using the techniques described in Leendertse's work (Dronkers, 1972; Raney, 1977; Botes et al., 1984; Hou, 1985).

Dronkers (1972) improved on Leendertse's model and presented a lengthy discussion of implicit versus explicit finite difference techniques along with the problems encountered with space staggered grid arrangements. He describes an

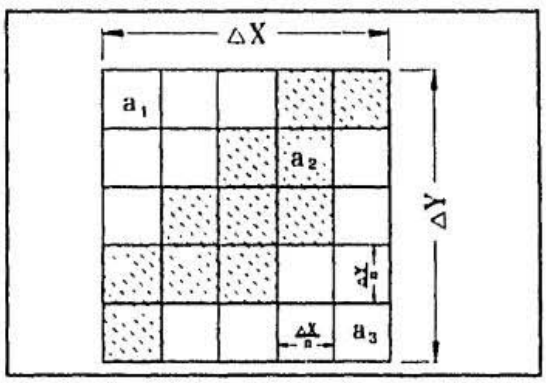

Fig. 2.4 - Schematization of a grid space.

explicit method as one where the water levels and velocities at a future time step are immediately computed from those of the previous time step and an implicit method where the water levels and velocities are obtained after the simultaneous solution of a set of linear equations.

Dronkers (1972) developed a method to modify the Chezy friction coefficient over a grid space area to represent local bathymetric features, such as shoals and gullies, that might not be represented with the grid resolution used. This was accomplished by developing a sub-grid of ($\Delta x/n$) by ($\Delta y/n$) grid spaces as depicted if Fig. 2.4.

The basic formulation of the method to determine the modified Chezy coefficients was,

$$\overline{Ca^{3/2}} = \frac{1}{\Delta x \Delta y}\left\{\int_0^x \int_0^y C(x,y)\, a^{\frac{3}{2}}(x,y)\, dx dy\right\} \qquad (2.64)$$

where: C(x,y)= Chezy coefficient of a sub-grid at location x,y inside the grid space being examined;
a(x,y)= water depth at the sub grid location.

and the modified value C_m was obtained from,

$$C_m a_m^{\frac{3}{2}} = \overline{Ca^{\frac{3}{2}}} \qquad (2.65)$$

where: a_m=the mean depth of the grid space.

Raney (1977) used a model similar to Leendertse's and included the effect of wind stress at the water surface,

$$L_x = \frac{T_x}{(h+\eta)} \quad ; \quad L_y = \frac{T_y}{(h+\eta)} \tag{2.66}$$

where: T_x & T_y = wind stress components acting on the surface.

to study tidal circulation in Los Angeles and Long Beach Harbours. The modified Chezy coefficient of Dronkers was not used. However, the bottom friction and Coriolis parameters of Leendertse were used in the model. Raney obtained satisfactory results when compared to historical tide records.

Botes et al. (1984) modified Leendertse's model to investigate the response of the cooling water intake basin of the Koeberg Nuclear Power Station, South Africa, to long period waves. The authors obtained satisfactory results and provide excellent reporting on the calibration of their model using a physical model and field data along with the selection of model time step versus model grid size via the Courant number. The Courant number relates the prototype wave celerity to that in the numerical model,

$$C_r = \frac{C_p}{C_m} = \sqrt{gh}\frac{\Delta t}{\Delta l} \quad or \quad \Delta t = \frac{(\Delta l)\, C_r}{\sqrt{gh}} \tag{2.67}$$

where: C_r= Courant number; Δt= model time increment; Δs= model grid space used; $(gh)^{1/2}$= long wave celerity; p & m = prototype & model respectively.

Botes et al. (1984), also give the approximate lower limit for wave description (number of points per wave length), from Leendertse's work, as $T/\Delta t$ = 9.6 and $L/\Delta l$ = 10.6. They

obtained reasonable results for Courant numbers of 1, 1.7 and 2.2. However, a Courant number of 3.0 resulted in poor results. Subsequent trials using a finer grid would give reasonable results as this would allow larger time steps. However, computational time would also increase due to the larger grid area.

Hou (1985) used Leendertse's method with no modifications to develop a model to study the oscillations in Taichung Harbour, Taiwan. This decision was made after carrying out an evaluation of existing numerical models in the public domain. The results were compared well with the results from a physical model.

Falconer et al. (1986) developed a nested model based on an implicit finite difference, space staggered grid system which resembles Leendertse's model. The model was comprised of a fine resolution finite difference grid system representing an idealized rectangular harbour surrounded by a coarser resolution grid representing the offshore.

The computational strategy was similar to Leendertse. However the governing equations were modified to include Reynolds stress components and an advective-diffusion equation was attached to permit the evaluation of a conservative tracer,

Motion equations:

$$\frac{\partial UH}{\partial t}+\beta\left[\frac{\partial U^2H}{\partial x}+\frac{\partial UVH}{\partial y}\right]-fVH+gH\frac{\partial \eta}{\partial x}+\frac{\tau_{bx}}{\rho}-\frac{1}{\rho}\left[\frac{\partial H\sigma_{xx}}{\partial x}+\frac{\partial H\tau_{xy}}{\partial y}\right]=0 \qquad (2.68)$$

$$\frac{\partial VH}{\partial t}+\beta\left[\frac{\partial UVH}{\partial x}+\frac{\partial V^2H}{\partial y}\right]-fUH+gH\frac{\partial \eta}{\partial y}+\frac{\tau_{by}}{\rho}-\frac{1}{\rho}\left[\frac{\partial H\tau_{yx}}{\partial x}+\frac{\partial H\sigma_{yy}}{\partial y}\right]=0 \qquad (2.69)$$

Continuity equation:

$$\frac{\partial \eta}{\partial t}+\frac{\partial UH}{\partial x}+\frac{\partial VH}{\partial y}=0 \qquad (2.70)$$

Advective-diffusion equation:

$$\frac{\partial HS}{\partial t}+\left[\frac{\partial SUH}{\partial x}+\frac{\partial SVH}{\partial y}\right]= \frac{\partial}{\partial x}\left[HD_{xx}\frac{\partial s}{\partial x}+HD_{xy}\frac{\partial s}{\partial y}\right]+\frac{\partial}{\partial y}\left[HD_{yx}\frac{\partial s}{\partial x}+HD_{yy}\frac{\partial s}{\partial y}\right] \qquad (2.71)$$

where: η= water surface elevation above mean water level; t= time; U & V = depth mean velocity in x & y directions; H= total depth of flow; β= momentum correction factor for non-uniform vertical velocity profile; f= Coriolis parameter, g= gravitational acceleration; τ_{bx}, τ_{by}= bed shear stress components in x & y directions; ρ= fluid density; $\sigma_{xx}, \tau_{xy}, \tau_{yx}, \sigma_{yy}$ = Reynolds stress components in x & y directions; s = conservative tracer; $D_{xx}, D_{xy}, D_{yx}, D_{yy}$ = depth mean longitudinal dispersion and turbulent diffusion tensor coefficients in x,y directions.

The Chezy coefficient was determined using the Colebrook-White equation,

$$C=\sqrt{\frac{8g}{f}}=-2\sqrt{8g}\log_{10}\left[\frac{k_s}{12R}+\frac{2.5}{Re\sqrt{f}}\right] \qquad (2.72)$$

where: f= Darcy friction factor; k_s= Length parameter characteristic of bed roughness; R= hydraulic radius; Re = Reynolds number.

and used in the standard quadratic friction law for bed shear stress.

Calculations performed using the coarse grid system outside the nested grid supplied the boundary conditions for the nested model. The data obtained from their work was encouraging with a close correlation achieved in the nested numerical model with a physical model. However, they observed a deterioration in accuracy for Courant numbers greater than eight (8). The Courant number is high when compared to that of Botes, et al. The reasons for this are numerous and depend on the difference in grid sizes and time steps. The Falconer et al. (1986) model used two (2) sizes of grids and were investigating tidal flushing which has relative long time period allowing larger time steps. Botes et al. (1984) used a fixed grid size and were investigating the basin response to waves with periods much less than the tidal periods. These are obvious differences in the two models that account for the range in Courant number as noted.

Wilson et al. (1972) developed a model by combining the equations of motion and continuity into one second order partial differential equation and eliminated the time constraint by assuming a solution which depended on the angular frequency of the mode of oscillation,

$$h\left[\frac{\partial^2 \xi}{\partial x^2}+\frac{\partial^2 \xi}{\partial y^2}\right]+\frac{\partial h}{\partial x}\frac{\partial \xi}{\partial x}+\frac{\partial h}{\partial y}\frac{\partial \xi}{\partial y}+\left(\frac{\omega^2}{g}\right)\xi = 0 \qquad (2.73)$$

where: h= water depth at position x,y; ξ= water surface elevation above datum at position x,y; ω= angular eigen frequency of a mode of free motion.

Development of the same equation is presented in Dean & Dalrymple (1984), p.168 as an exercise. The Wilson (1972) model involves taking central differences on an unequally spaced grid, forming an eigenvalue array incorporating appropriate boundary conditions. The 'free undamped' oscillations periods of the harbour are then determined from this array and the eigenvectors produced during this operation give the water surface elevations corresponding to the eigenvalues. This model has some disadvantages in that determination of eigenvalues using a very large number of nodes requires a fair amount of computer memory and time. Also, analysis beyond the point of determining the free oscillations is not possible. It is interesting to note that Wilson, et al, used Leendertse's time marching technique as one of the verification models for their model.

Easton (1984) presented a model similar to Wilson's. However he used the linearized frictionless long wave equations and continuity equation (Dean and Dalrymple, 1984, pp.136-137) and an idealized harbour of constant depth. His presentation was made to show the general derivation of a model similar to Wilson's. He also presents similar derivations for an analytical and finite element solution using the same equations. The models are not useful other than to educate the reader.

Chapter 3
COMPUTERIZED HYDROGRAPHIC DATA MANIPULATION

3.0 Introduction

The numerical analysis of wave phenomenon using a computer requires the relevant data to be in a form that can be readily recognized by the computer software. The analyses undertaken in this thesis require the input of hydrographic information in the form of water depths, shoreline, latitudes and longitudes for a grid area to be examined. This information is readily available in the form of hydrographic charts published by the Canadian Hydrographic Service, Department of the Environment, Ottawa, Canada. The data transfer is accomplished using the CADKEY ®, computer aided drafting software package and a compatible digitizing board to digitize the hydrographic charts. The CADKEY software is capable of producing a sequential data file in ASCII format which can then be used by other software. The sequential file contains information for the CADKEY software to display the digitized chart using this file. The term 'graphical database' is used throughout this thesis to describe the resulting sequential file. A full description of the CADKEY software is beyond the scope of this thesis and the reader is referred to the CADKEY manuals provided in the references (see Cadkey, 1989).

The graphical database contains more information than is required and typically is on the order of 300,000 bytes in length. Therefore, routines were developed to extract the required information and create a 'modified database' typically on the order of 50,000 bytes. The modified database in conjunction with a 'sort database' was used to generate the required 'grid database' containing the interpolated water depths and latitudes in an equally spaced grid for a particular area represented in the modified database.

The routines for creation of the modified and grid databases from the graphical database were combined into one software package. The package was given the name CADGRID and the logic flow is presented in Fig. 3.1.

The specific methods and routines that make up the CADGRID software package were original with the exception of a contouring routine. This routine, contained in the data file output section, is as presented by Crookshank (1975). The routine was translated to the QuickBasic language using the original fortran version with commands added to give the screen output required.

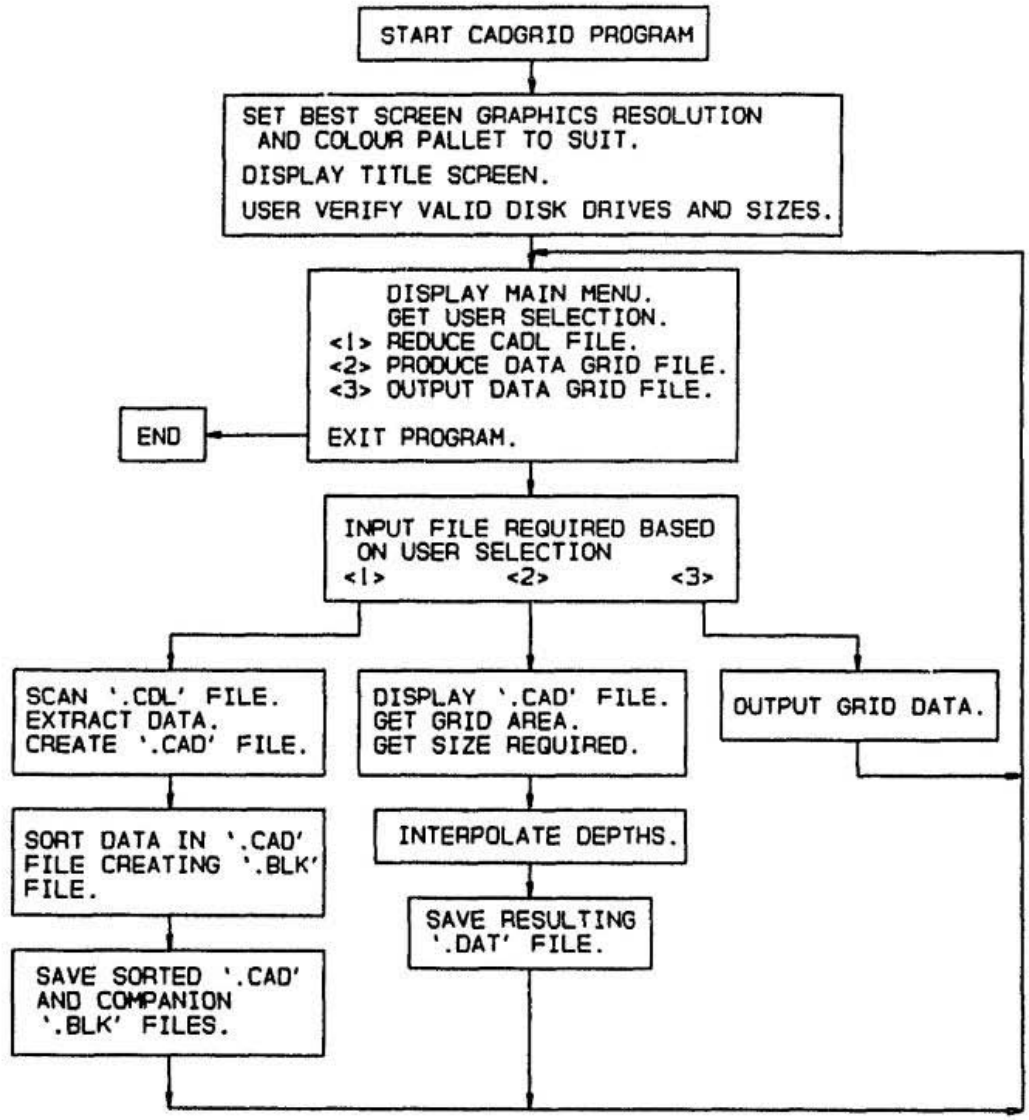

Fig. 3.1 - CADGRID software package logic flow chart.

3.1 Computer Hardware/Software

The computer system used was a 80386 based microcomputer with 80387 maths coprocessor, one (1) megabyte memory, forty (40) megabyte hard drive, 5.25 inch high density floppy and MS-DOS ©, Version 3.30. The CADGRID program was written to execute using Hercules ® Monochrome, EGA or VGA resolution graphics. However, EGA or VGA resolution is recommended for proper colour displays.

The digitizing process and graphical database creation was accomplished using CADKEY as previously mentioned and a GTCO ® Digipad 5 Series, digitizing board in high resolution mode. The modified and grid database creation routines were written and compiled using the Microsoft ® QuickBASIC ©, Version 4.5, program development software package. This language was used for the generous graphics options and its compatibility with other languages such as Fortran and C. QuickBASIC is also menu driven with built in compiler to create an executable file which can be executed on any compatible microcomputer. The plotter output routines were written for a HP 7475A Graphics Plotter using the Hewlett Packard Graphics Language, (HP-7475A, 1983), and encoded using the QuickBASIC program development language.

3.2 Digitizing Process

The digitizing of hydrographic chart data is accomplished using the digitizing option of the CADKEY software package and a digitizing board. The CADKEY software has the ability to create graphical database files using entries in the form of 'data primitives' or 'entities' which can be assigned to a maximum of 255 different levels or layers. This ability provides the necessary versatility for manipulation of the final graphical database. The digitized drawing is output as an ASCII text file consisting of the information required plus extraneous data required by the CADKEY package which forms the graphical database.

3.2.1 Graphical Database Production

The setup and initialization of the CADKEY software and digitizing board are not presented here. The reader is referred to the CADKEY and digitizing board manuals for these procedures. The procedure, presented in this thesis, starts from the point where CADKEY is in the digitizing mode.

The first step is to designate a digitizing origin, scale and x-axis. The designated origin and x-axis should be accessible from any part of the drawing and within the range of the

digitizing board. This is to ensure that a chart larger than the range of the board can be digitized by moving the chart and redesignating the same origin and x-axis for the next area to be digitized. The range of a digitizing board varies with size and type used. The scales provided on the chart can be used to assign the digitizing scale.

The remaining step is to digitize the required water depth, shoreline, high tide level and latitude/longitude coordinate information contained on the chart. The longitude information is not required for the investigation presented in this thesis. However, the inclusion of the longitude information provides a complete graphical database and will then be present for other work if required.

It is not essential to follow a particular sequence. However, the entity to level relationships presented in Table 3.1 should be used in conjunction with this software.

The water depths provided on a chart can be in feet, meters and fathoms depending on the chart used. Therefore, provisions are made in the software to convert the digitized depths to the units required during creation of the modified database.

The z coordinate, used for digitizing the entities, is set using the CADKEY, ALT-D instruction which alters the

Table 3.1 - CADKEY entity to level relationships.

LEVEL	CONTENTS
1	Shoreline and land elevations.
2	Depth data points and contours.
3	Latitude and longitude values and locations.
4	Note containing digitizing units for water depths, land elevations and distances.
5	Latitude and longitude grid lines, miscellaneous notes such as place names, instructions, etc.

construction depth, z coordinate, of the drawing. Any point digitized is automatically set at the specified depth. The depth is set to zero (0) and all shoreline digitized by creating line entities. This depth then becomes the datum for the entire chart and is typically the lowest normal tide depth. The high tide level is usually indicated adjacent to the shoreline as a denser black line and the value can be determined from a tide table typically found on the chart.

The construction depth is set to the negative of this value to permit proper location of the shoreline when the water depth datum is changed to another value, such as mid tide simulations. The land contours, if present, can be digitized as well. However, these values should be digitized using a negative construction depth as with the high tide line. These points are not essential in the final calculations presented in this thesis. However, for proper location of the shoreline

and display purposes a negative land value is required. Therefore, a small negative increment on the order of one half (½) the digitizing unit used should be added to the high tide mark, if the land contours are not included. The water depths are digitized by altering the construction depth as previously mentioned for each depth value provided on the chart. However, these values are entered in the positive z direction to separate them from land.

The latitude and longitude angles are input as label entities which have a leader and arrow for designators. The label for each entry consists of two lines and has the following format,

Latitude on first line => ###:##:##

Longitude on second line => ###:##:##

where each numerical position is degrees:minutes:seconds, and the arrow tip location digitized as the intersection of the latitude and longitude grid line entities. The longitude angles are not required for the investigations presented in this thesis. However, they should be included to provide a full and complete database.

The complete digitized chart is visually inspected for digitizing errors by switching the CADKEY view to one which gives a profile view. Severe errors are easily detectable using this method. Another method used to check for errors, is to utilize the colour options provided by the CADKEY software.

A specific colour can be used to represent alternate depths or ranges of depths which would make visual inspection easier.

The graphical database is created by using the CADKEY FILES/CADL/OUTPUT/ALL_DSP/ALL instruction sequence after ensuring the required levels, one through four, are turned on and all entities are displayed. This instruction sequence creates an ASCII text file in the location specified, typically on hard disk and contains the following information in the form of CADKEY entities,

LINE $x_1, y_1, z_1, x_2, y_2, z_2$, colour, level, line type, group number, subgroup number, pen number.

where superscripts 1 & 2 indicate start and end coordinates in world coordinates.

POINT x, y, z, colour, level, group number, subgroup number, pen number.

where x, y & z are in world coordinates.

LABEL x_1, y_1, x_2, y_2, x_3, y_3, arrow type, x, y, **(lines of text including carriage returns)**, rotation angle, character height, character aspect ratio, mirror text flag, VIEW primitive reference number, colour, level, font number, group number, subgroup number, pen number.

where all x & y are in view coordinates and x_3, y_3 are the coordinates of the arrow tip.

TEXT x, y, **(lines of text including carriage returns)**, rotation angle, character height, character aspect ratio, mirror text flag, VIEW primitive reference number, colour, level, font number, group number, subgroup number, pen number

The "**underlined bold**" text above indicates the information extracted during the creation of the modified database.

3.2.2 Digitizing Accuracy

The accuracy attained when digitizing information from a hydrographic chart is related to the point digitized, the point's relation to the identifying symbol used on the chart and the care taken in using the digitizing puck.

The Arabic symbols on the charts providing the water depths typically cover a chart area of approximately two (2) by three (3) millimetres. This small area can represent a large area depending on the scale of the chart. This area would represent an equivalent area of 15,000 square meters on a 1:50,000 scale hydrographic chart. The data is used, assuming the value provided is representative of the area covered by the symbol, and errors minimized by using the approximate centre of the numeric symbol for digitizing purposes (see Fig. 3.2).

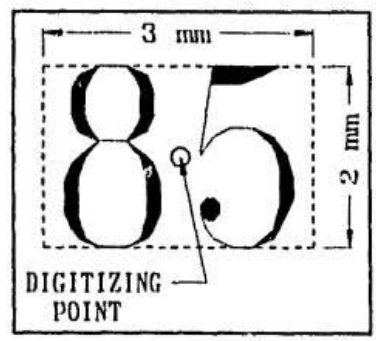

Fig. 3.2 - Depth data point digitized.

The lines depicting the shoreline, high tide level and land

contours range in thickness from approximately one tenth (1/10) to three tenths (3/10) of a millimetre. Again, using a typical scale of 1:50,000, the width represented by the lines are five (5) and fifteen (15) meters respectively. Also, inaccuracies occur if an insufficient number of entities are used to represent any curvature or severe changes in direction of the line on the chart. To overcome these inaccuracies, the centre of the lines were used in digitizing and a sufficient number of line segments were digitized to represent the major features represented by the line. The number and extent of line segments digitized is left to the educated judgement of the person doing the digitizing.

A parallax error is also introduced by the digitizing puck and its relation to the board and the point being digitized (see Fig. 3.3). The viewing angle should be 90° to minimize the errors. This further emphasizes the care which must be exercised when digitizing the chart information.

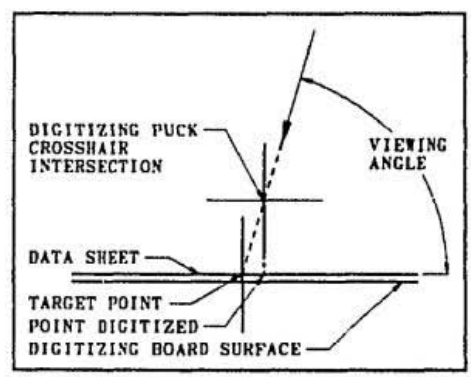

Fig. 3.3 - Parallax digitizing errors.

3.3 Modified Database Production

The graphical database output from the CADKEY digitizing process is on the order of 300,000 bytes. This is a result of the extraneous data produced by the CADKEY program which is not required for the work presented in this thesis. Computer routines were developed to extract the necessary data from the graphical database using the QuickBASIC program development language and output the modified database.

The routine developed uses the string manipulation routines contained in the QuickBASIC software package. The routine initially scans through the graphical database to determine the most negative z coordinate and the maximum and minimum values for both the horizontal coordinates and line length. These parameters are used as control parameters for the extraction procedure and display purposes. Provisions are included for the user to have control over certain aspects of the extraction process. These provisions are the maximum length of a line entity and the high tide increment as discussed on p. 61 which is indicated by the most negative z coordinate. These parameters are input and verified by the user.

The extraction routine assumes a single point at each end of a line entity in the graphical database. This causes prob'.ems

during the interpolation of grid database depths. Therefore, the maximum line length, as input by the user, is used to segment relatively long line entities by creating points along the line entities which exceed the maximum length. The depth conversion factor is included to permit digitizing of the water depth points by eliminating the need to manually convert the depth values to the units required.

The modified database output from this process is in the form of a random access file on disk containing a record whose contents are the x coordinate, y coordinate and water depth as the z coordinate for each point. The physical size reduction of the database is typically 60%.

The graphical and modified databases contain the required information in random order. This creates problems with search routines and speed of computation when trying to interpolate an orderly grid database. Therefore, a sorting routine was developed to minimize these problems and speed up the process.

3.3.1 Sort Database Production

The modified database is contained in a data file in random order. Various techniques of sorting were tried, such as sorting on x coordinate and sub-sorting on y coordinate, and

a block sorting routine was found to the most effective for the searching process required during grid database production.

The block sort routine divides the modified database into blocks which have dimensions of one tenth (1/10) the maximum x dimension by one tenth (1/10) the maximum y dimension for a final total block array of 100. The modified database points are then sorted into these blocks using a combination march and swapping sequence on the random access file records altering the database itself. The process starts with the first block (1,1) and the first database record. If this record does not belong in the block it is flagged as the swap location and a search is made through the database file until a valid record is found and swapped with the flagged record. The next record after the swapped record is then checked for its suitability and either flagged as the swap location, if not suitable, or left as it is. This process is continued throughout the database for each block until the last record has been flagged or left. The process is progressive, in that, once a record has been swapped or left, it is not checked again. This method reduces the amount of time required to sort the modified database file.

The final output of this routine is a companion 'sort database' containing the start record of each block and the

number of modified database records in each block as well as the physical block dimensions. Both files are then given a permanent file name by the user and stored for future use in developing grid databases.

3.4 Grid Database Production

The development of the grid database is written independent of the modified database production. This permits the creation of the modified database to be performed on various graphical databases prior to grid database production. Also, the requirement to create a modified database for every grid database required is eliminated. The routines developed for grid database production rely heavily on the graphics capability of the QuickBASIC software package.

The routine displays the full modified database on the computer screen overlain with the block areas generated during the sort database production and stored in a companion file for the particular modified database being used. The user is then requested to designate the area required using cursor movement and various key presses indicated on screen by the software. The user has the option to redo the grid area designation if required.

The routine requests the grid spacing required and provides the user with the minimum size which the available computer memory will permit. The available memory constraint is not considered a problem as the typical minimum size indicated for grid sizes is for grid arrays on the order of 300 by 300 grid points. This size of grid is felt to be more than sufficient to represent the designated area for the analyses undertaken in this thesis.

3.4.1 Grid Point Interpolation

The grid database is to be of equal spaces in the horizontal coordinate system. However, the modified database, even with the blocksort database, is still randomly spaced. Therefore, search and interpolation routines were developed to estimate the water depths required for the grid database.

The development of the interpolation routines was based on linear interpolation techniques using formulae developed assuming the existence of four or three interpolation points as presented in Fig. 3.5 to Fig. 3.9, inclusive. These figures show the point to be interpolated lying in the plane of the interpolation points. The point required can be located outside the plane as depicted in Fig. 3.10. Conditions were included whereby the interpolated value is forced to be within

the range of the interpolation points. If the interpolated value is higher than the point values, the highest value is used and the lowest value if the interpolated value is lower. This form of conditioning was felt to be adequate with the accuracy provided by the digitizing process.

The search routine developed to locate the nearest interpolation points involves a search of four blocks of points using the information contained in the companion sort database. The four blocks selected depend on the location of the target point within the source block. The interpolation point search using the block configuration supplied by the companion blocksort file is depicted in Fig. 3.6.

The particular blocks to be searched for the nearest interpolation points depend on the location quadrant of the target point within the source block, (i, j) (see Fig. 3.6). The arrangement depicted here is for a central location within the grid area specified previously. The search pattern is still valid for source blocks located at the ends of the area. However, the blocks searched are only those available. The particular blocks searched with respect to the quadrant location of the target point is presented in Table 3.2. This method reduces the time required for the location of the nearest interpolation points by eliminating the need to search the entire modified database. The actual selection of points

within the search routine is based on a comparison of the radial distance between a database point and target point. Constraints were added to ensure the arrangement of selected points is as depicted in Fig. 3.5 to Fig. 3.9, wherever possible.

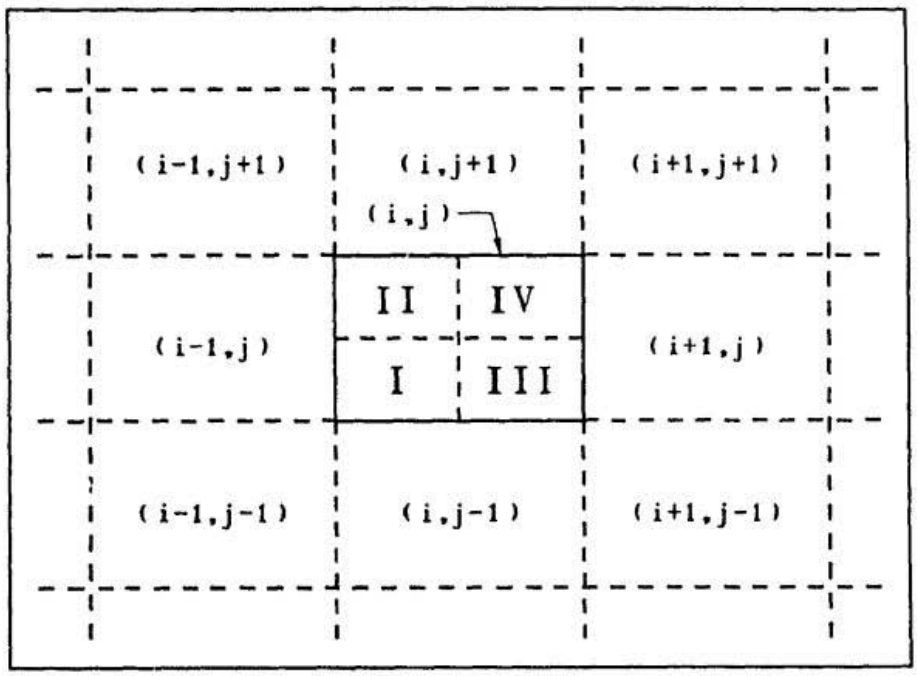

Fig. 3.4 - Interpolation point search. Block configuration and usage.

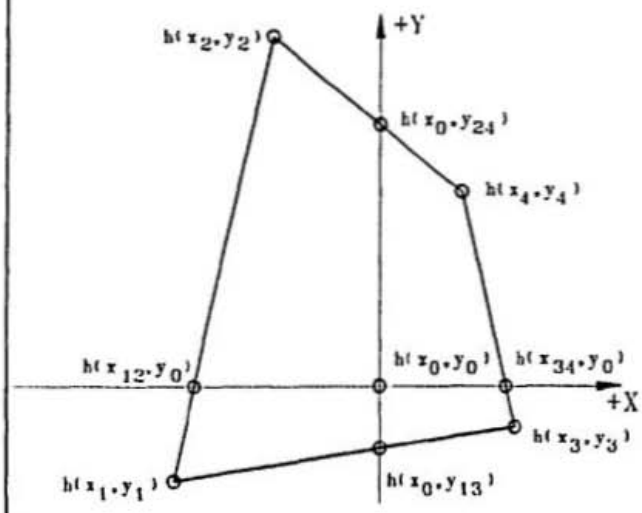

$$x_{12} = \left[\frac{y_0 - y_1}{y_2 - y_1}\right](x_2 - x_1) + x_1$$

$$x_{34} = \left[\frac{y_0 - y_3}{y_4 - y_3}\right](x_4 - x_3) + x_3$$

$$y_{13} = \left[\frac{x_0 - x_1}{x_3 - x_1}\right](y_3 - y_1) + y_1$$

$$y_{24} = \left[\frac{x_0 - x_2}{x_4 - x_2}\right](y_4 - y_2) + y_2$$

$$h(x_{34}, y_0) = [h(x_4, y_4) - h(x_3, y_3)]\sqrt{\frac{(x_{34} - x_3)^2 + (y_0 - y_3)^2}{(x_4 - x_3)^2 + (y_4 - y_3)^2}} + h(x_3, y_3)$$

$$h(x_{12}, y_0) = [h(x_2, y_2) - h(x_1, y_1)]\sqrt{\frac{(x_{12} - x_1)^2 + (y_0 - y_1)^2}{(x_2 - x_1)^2 + (y_2 - y_1)^2}} + h(x_1, y_1)$$

$$h(x_0, y_{13}) = [h(x_3, y_3) - h(x_1, y_1)]\sqrt{\frac{(x_0 - x_1)^2 + (y_{13} - y_1)^2}{(x_3 - x_1)^2 + (y_3 - y_1)^2}} + h(x_1, y_1)$$

$$h(x_0, y_{24}) = [h(x_4, y_4) - h(x_2, y_2)]\sqrt{\frac{(x_0 - x_2)^2 + (y_{24} - y_2)^2}{(x_4 - x_2)^2 + (y_4 - y_2)^2}} + h(x_2, y_2)$$

$$\frac{\partial h}{\partial x} = \frac{h(x_{34}, y_0) - h(x_{12}, y_0)}{x_{34} - x_{12}} \quad ; \quad \frac{\partial h}{\partial y} = \frac{h(x_0, y_{24}) - h(x_0, y_{13})}{y_{24} - y_{13}}$$

$$h(x_0, y_0) = h(x_1, y_1) - \frac{\partial h}{\partial x}(x_1 - x_0) - \frac{\partial h}{\partial y}(y_1 - y_0)$$

Fig. 3.5 - Four point interpolation.

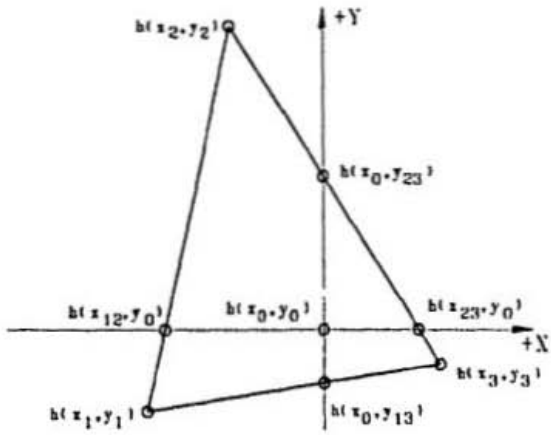

$$y_{23} = \left[\frac{x_0 - x_3}{x_2 - x_3}\right](y_2 - y_3) + y_3$$

$$x_{23} = \left[\frac{y_0 - y_3}{y_2 - y_3}\right](x_2 - x_3) + x_3$$

x_{12} , y_{13} : *see four point interpolation.*

$$h(x_0, y_{23}) = [h(x_2, y_2) - h(x_3, y_3)]\sqrt{\frac{(x_0 - x_3)^2 + (y_{23} - y_3)^2}{(x_2 - x_3)^2 + (y_2 - y_3)^2}} + h(x_3, y_3)$$

$$h(x_{23}, y_0) = [h(x_2, y_2) - h(x_3, y_3)]\sqrt{\frac{(x_{23} - x_3)^2 + (y_0 - y_3)^2}{(x_2 - x_3)^2 + (y_2 - y_3)^2}} + h(x_3, y_3)$$

$h(x_0, y_{13})$, $h(x_{12}, y_0)$: *see four point interpolation.*

$$\frac{\partial h}{\partial x} = \frac{h(x_{23}, y_0) - h(x_{12}, y_0)}{x_{23} - x_{12}} \quad ; \quad \frac{\partial h}{\partial y} = \frac{h(x_0, y_{23}) - h(x_0, y_{13})}{y_{23} - y_{13}}$$

$$h(x_0, y_0) = h(x_1, y_1) - \frac{\partial h}{\partial x}(x_1 - x_0) - \frac{\partial h}{\partial y}(y_1 - y_0)$$

Fig. 3.6 - Three point interpolation - condition (a).

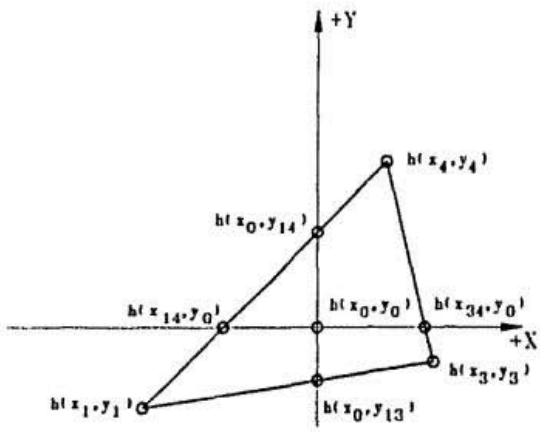

$$x_{14} = \left[\frac{y_0-y_1}{y_4-y_1}\right](x_4-x_1) + x_1$$

$$y_{14} = \left[\frac{x_0-x_1}{x_4-x_1}\right](y_4-y_1) + y_1$$

x_{34} , y_{13} : *see four point interpolation.*

$$h(x_{14},y_0) = [h(x_4,y_4)-h(x_1,y_1)]\sqrt{\frac{(x_{14}-x_1)^2+(y_0-y_1)^2}{(x_4-x_1)^2+(y_4-y_1)^2}} + h(x_1,y_1)$$

$$h(x_0,y_{14}) = [h(x_4,y_4)-h(x_1,y_1)]\sqrt{\frac{(x_0-x_1)^2+(y_{14}-y_1)^2}{(x_4-x_1)^2+(y_4-y_1)^2}} + h(x_1,y_1)$$

$h(x_{34},y_0)$, $h(x_0,y_{13})$: *see four point interpolation.*

$$\frac{\partial h}{\partial x} = \frac{h(x_{34},y_0)-h(x_{14},y_0)}{x_{34}-x_{14}} \quad ; \quad \frac{\partial h}{\partial y} = \frac{h(x_0,y_{14})-h(x_0,y_{13})}{y_{14}-y_{13}}$$

$$h(x_0,y_0) = h(x_1,y_1) - \frac{\partial h}{\partial x}(x_1-x_0) - \frac{\partial h}{\partial y}(y_1-y_0)$$

Fig. 3.7 - Three point interpolation - condition (b).

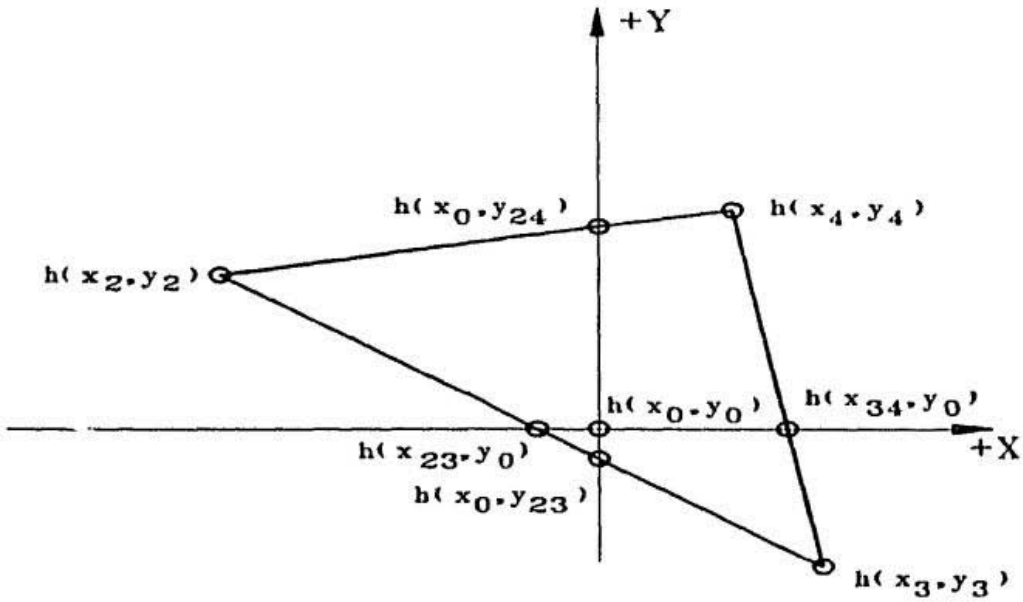

$x_{34}, y_{24}, h(x_0, y_{24}), h(x_{34}, y_0)$: *see four point interpolation.*

$x_{23}, y_{23}, h(x_{23}, y_0), h(x_0, y_{23})$: *see condition (a).*

$$\frac{\partial h}{\partial x} = \frac{h(x_{34}, y_0) - h(x_{23}, y_0)}{x_{34} - x_{23}} \quad ; \quad \frac{\partial h}{\partial y} = \frac{h(x_0, y_{24}) - h(x_0, y_{23})}{y_{24} - y_{23}}$$

$$h(x_0, y_0) = h(x_2, y_2) - \frac{\partial h}{\partial x}(x_2 - x_0) - \frac{\partial h}{\partial y}(y_2 - y_0)$$

Fig. 3.8 - Three point interpolation - condition (c).

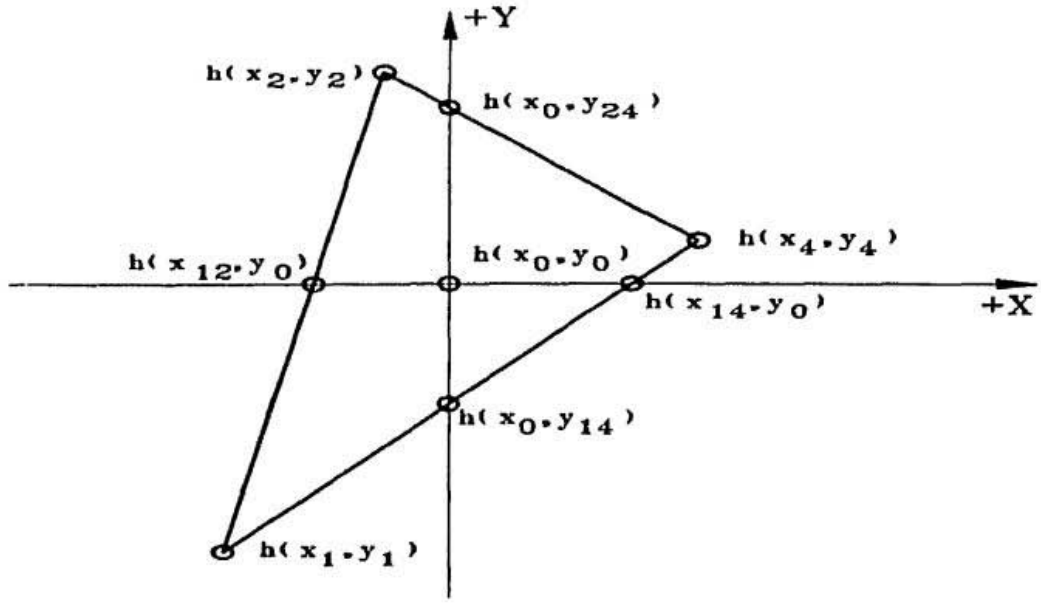

x_{12} , y_{24} , $h(x_{12}, y_0)$, $h(x_0, y_{24})$: *see four point interpolation.*

x_{14} , y_{14} , $h(x_{14}, y_0)$, $h(x_0, y_{14})$: *see condition (b).*

$$\frac{\partial h}{\partial x} = \frac{h(x_{14}, y_0) - h(x_{12}, y_0)}{x_{14} - x_{12}} \quad ; \quad \frac{\partial h}{\partial y} = \frac{h(x_0, y_{24}) - h(x_0, y_{14})}{y_{24} - y_{14}}$$

$$h(x_0, y_0) = h(x_1, y_1) - \frac{\partial h}{\partial x}(x_1 - x_0) - \frac{\partial h}{\partial y}(y_1 - y_0)$$

Fig. 3.9 - Three point interpolation - condition (d).

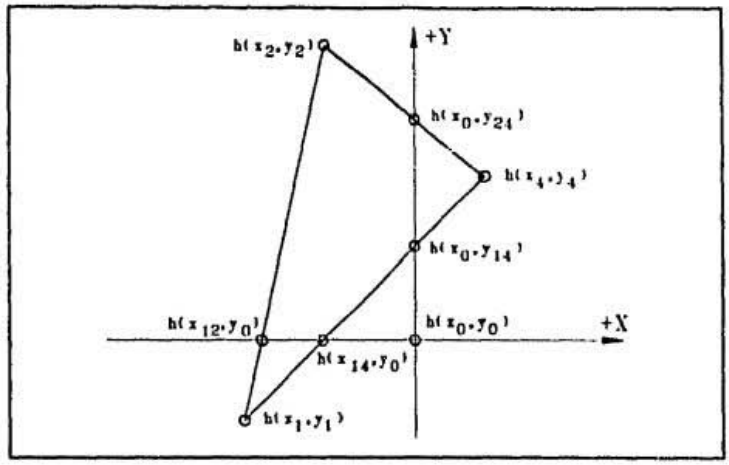

Fig. 3.10 - Three point interpolation - condition (e).

Table 3.2 - Search block by target point quadrant location.

Source Block Quadrant	Data Blocks Searched
I	(i,j), (i-1,j), (i-1,j-1), (i,j-1)
II	(i,j), (i-1,j), (i-1,j+1), (i,j+1)
III	(i,j), (i+1,j), (i+1,j-1), (i,j-1)
IV	(i,j), (i+1,j), (i+1,j+1), (i,j+1)

The final output from this routine is an equally spaced depth grid database located on hard or floppy disk in ASCII format. This file contains the grid spacing, number of grid points in the two directions as well as the interpolated water depths. The ASCII format was used to permit the visual verification of the interpolated values using text editing software.

3.4.2 Grid Point Latitude Interpolation

The hydrographic charts used to create the graphical database are typically produced using some form of projection method such as mercator, transverse mercator, polyconic, etc. The coordinate data digitized and carried through to the modified database have not been adjusted to remove the distortion effects of the projection method used to create the hydrographic chart. The errors introduced are felt to be at a minimum due to the relatively small chart areas required to undertake the tasks presented in this thesis.

The latitude angle required for the investigations presented in this thesis is determined for the grid location (1,1). The angle required at other grid locations is determined using the average change in latitude in both the vertical and horizontal directions in the following formula,

$$\frac{d\phi_{Lat}}{ds} = \left(\frac{\partial \phi_{Lat}}{\partial x}\right)\left(\frac{\partial x}{\partial s}\right) + \left(\frac{\partial \phi_{Lat}}{\partial y}\right)\left(\frac{\partial y}{\partial s}\right) \qquad (3.25)$$

where:

$$\frac{\partial x}{\partial s} = \frac{\partial x}{\sqrt{(\partial x)^2 + (\partial y)^2}} \quad , \quad \frac{\partial y}{\partial s} = \frac{\partial y}{\sqrt{(\partial x)^2 + (\partial y)^2}} \quad , \quad ds = \partial s$$

The change in latitude for both the x and y directions is determined by finding all the rates of change in latitude for all points having the same longitude as previously digitized and contained in the modified database. These rates of change

are then summed and averaged using the total number of occurrences. The subsequent rate of change is then used to determine the latitude of grid location (1,1) as selected by the user. the subsequent latitude and rates of change are then added to the end of the grid database generated. The longitude angle is not required for the investigations presented in this thesis. However, a similar method is provided to determine the longitude angle at each location if required with the necessary information placed at the end of the depth database.

3.4.3 Grid Database Hardcopy Output

The hardcopy outputs provided by the CADGRID program are in the form of a text output of the grid parameters including interpolated water depths and a contour map of the grid area using the interpolated depths. The text copy requires a printer and the contour plot requires a HP-7475A or equivalent plotter compatible with HPGL. Both outputs can also be diverted to the screen or disk file by the user. The plotter graphics image can be output to a graphics printer using a conversion utility, such as JetPlotter ®, which prints a HPGL plot file to a graphics printer.

Chapter 4

Computational Model for Harbour Response to Long Period Water Waves

4.0 Introduction

The computational model and subsequent computer software program developed to analyze the response of a water basin to long period water waves was based on the model and program, presented by Leendertse (1967), developed to study long period wave motion. The numerical method uses finite difference techniques to solve the general equations of motion and continuity in four dimensions. The input data are specified on a space staggered grid system in the horizontal (x,y) plane with the z axis being vertical, positive upwards. The computational method is executed using alternating implicit and explicit methods in time as well as direction over the computational grid system.

4.1 Governing Equations

The development of the governing equations for the computational model is discussed in detail by Leendertse (1967) and again in Leendertse (1970). Dean and Dalrymple (1984) also present a similar derivation. A brief description

of the derivation process is presented.

Water wave propagation can be described using the two dimensional, partial-differential, equations for long period water wave motion,

$$\frac{\partial u}{\partial t} + u\frac{\partial u}{\partial x} + v\frac{\partial u}{\partial y} + w\frac{\partial u}{\partial z} + \frac{1}{\rho}\frac{\partial p}{\partial x} = X \qquad (4.1)$$

$$\frac{\partial v}{\partial t} + u\frac{\partial v}{\partial x} + v\frac{\partial v}{\partial y} + w\frac{\partial v}{\partial z} + \frac{1}{\rho}\frac{\partial p}{\partial y} = Y \qquad (4.2)$$

$$\frac{\partial w}{\partial t} + u\frac{\partial w}{\partial x} + v\frac{\partial w}{\partial y} + w\frac{\partial w}{\partial z} + \frac{1}{\rho}\frac{\partial p}{\partial z} = Z \qquad (4.3)$$

and mass conservation,

$$\frac{\partial u}{\partial x} + \frac{\partial v}{\partial y} + \frac{\partial w}{\partial z} = 0 \qquad (4.4)$$

where (x,y,z) are the spacial coordinates with (x,y) being the horizontal coordinates and z the vertical conforming to the cartesian coordinate system (see Fig.4.1), (u,v,w) are velocity components in the corresponding (x,y,z) coordinate system, P is pressure, ρ is density and (X,Y,Z) are the extraneous forces due to earths rotation, tide generating force caused by celestial

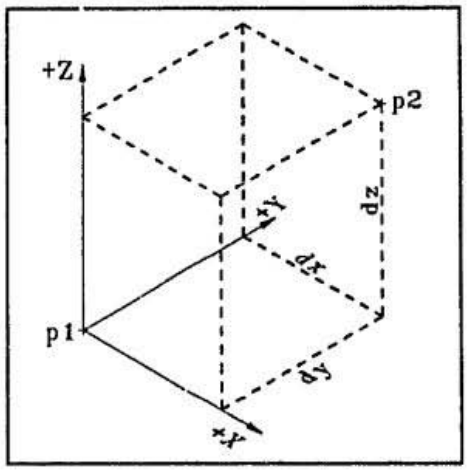

Fig.4.1 - Cartesian coordinate system.

bodies and the gravity forces in the z direction.

The vertical acceleration was neglected as it is very small when compared with the acceleration of the gravity field. Equations (4.1), (4.2) and (4.4), were vertically integrated introducing the vertically averaged velocity components;

$$U=\frac{1}{h+\zeta}\int_{-h}^{\zeta} u\,dz \quad ; \quad V=\frac{1}{h+\zeta}\int_{-h}^{\zeta} v\,dz$$

the surface and bottom boundary conditions;

$$w(\zeta)=\frac{\partial\zeta}{\partial t}+u\frac{\partial\zeta}{\partial x}+v\frac{\partial\zeta}{\partial y} \quad ; \quad w(-h)+u\frac{\partial h}{\partial x}+v\frac{\partial h}{\partial y}=0$$

assuming hydrostatic pressure distribution, the pressure in terms of water surface elevation, water depth and atmospheric pressure;

$$\frac{\partial p}{\partial x}=\rho g\frac{\partial\zeta}{\partial x}+\frac{\partial p_0}{\partial x} \quad ; \quad \frac{\partial p}{\partial y}=\rho g\frac{\partial\zeta}{\partial y}+\frac{\partial p_0}{\partial x}$$

the Coriolis parameter, f_c, as part of the extraneous force;

$$X=f_c v+K_x \quad ; \quad Y=-f_c u+K_y$$

and the bottom friction terms using the Chezy coefficient, C_h, and neglecting internal frictional losses,

$$K_x=F_x-\frac{\rho g U\sqrt{U^2+V^2}}{C_h^2} \quad ; \quad K_y=F_y-\frac{\rho g V\sqrt{U^2+V^2}}{C_h^2}$$

The resulting governing equations for the numerical model,

neglecting the remaining extraneous forces components (i.e. $F_x=0$ and $F_y=0$), are

$$\frac{\partial U}{\partial t}+U\frac{\partial U}{\partial x}+V\frac{\partial U}{\partial y}-f_c V+g\frac{\partial \zeta}{\partial x}+\frac{gU\sqrt{U^2+V^2}}{C_h^2(h+\zeta)}=0 \qquad (4.5)$$

$$\frac{\partial V}{\partial t}+U\frac{\partial V}{\partial x}+V\frac{\partial V}{\partial y}+f_c U+g\frac{\partial \zeta}{\partial y}+\frac{gV\sqrt{U^2+V^2}}{C_h^2(h+\zeta)}=0 \qquad (4.6)$$

$$\frac{\partial \zeta}{\partial t}+\frac{\partial[(h+\zeta)U]}{\partial x}+\frac{\partial[(h+\zeta)V]}{\partial y}=0 \qquad (4.7)$$

4.2 Computational Model

The computational model was based on a space staggered grid system where the velocity components, water surface elevation and water depth are specified at differing grid point locations. The space staggered grid structure as previously described has the X-velocity, 'U', described at 'j+½, k', Y-velocity, 'V', at 'j, k+½', water surface elevation, 'ζ', at 'j, k', and the water depth to datum, 'h', and Chezy coefficient, 'C_h', at 'j+½, k+½'. A computer model cannot recognize variables using non-integer identifiers. Therefore, the system used to identify grid positions was modified to permit the identification of various grid point positions and parameters as required by a computer. The staggered grid system was further divided into rows and columns as depicted

in Fig.4.2. The modified grid point locations are identified by 'n' rows and 'm' columns with each 'n,m' position identifying the location of $h_{j+\frac{1}{2},k+\frac{1}{2}}$, $C_{h\,j+\frac{1}{2},k+\frac{1}{2}}$, $U_{j+\frac{1}{2},k}$, $V_{j,k+\frac{1}{2}}$, and $\zeta_{j,k}$.

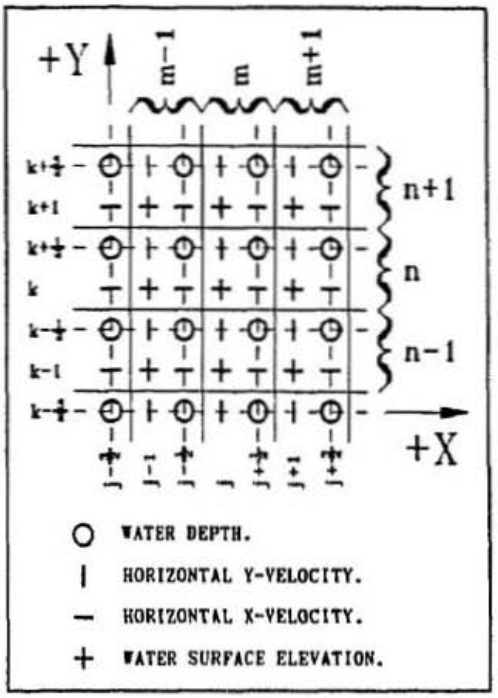

Fig.4.2 - Computational grid for long period wave propagation.

A multi-step operation in time was used such that the terms containing space derivatives and the Coriolis force, 'f_c', are generally taken alternating forward and backward. Two time steps are used and indicated as in the original work by Leendertse (1967) as superscripts in the form of 't', 't+½' and 't+1' for the initial, first and second 'half time steps' respectively.

The first step in the multi-step operation is to determine 'U', 'V' and 'ζ' at time 't+½' from the values at time 't' using an operation which is implicit in 'ζ' & 'U' using equations (4.5) & (4.7) and explicit in 'V' using equation (4.6). The next step in the operation is to determine 'U', 'V' and 'ζ' at time 't+1' from the values at time 't+½' using an operation which is implicit in 'ζ' & 'V' using equations

(4.6) & (4.7) and explicit in 'U' using equation (4.5).

The following notation was used in the approximation of the finite difference equations,

$$\left\{\begin{array}{c}\Delta x=\Delta y=\Delta s\\ j,k=0,\pm\frac{1}{2},\pm 1,\pm\frac{3}{2}\\ t=0,\frac{1}{2},1,\frac{3}{2},2\end{array}\right\} \quad ; \quad \left\{\begin{array}{c}U\\V\\\zeta\\h\\C_h\\f_c\end{array}\right\}_{n,m}^{t} = \left\{\begin{array}{l}U_{j+\frac{1}{2},k}\\V_{j,k+\frac{1}{2}}\\\zeta_{j,k}\\h_{j+\frac{1}{2},k+\frac{1}{2}}\\C_{h\ j+\frac{1}{2},k+\frac{1}{2}}\\f_{c\ j+\frac{1}{2},k+\frac{1}{2}}\end{array}\right\}^{t}$$

4.2.1 Implicit Computation for Horizontal Velocity 'U' and Water Surface Elevation 'ζ'

The velocity component in the x-direction, 'U', is approximated by solving equation (4.5) in the finite difference format,

at j+½,k (n,m):

$$\frac{\partial U}{\partial t} = \overline{\overline{V}}^{t}\left[f - \left\langle\frac{\partial U}{\partial y}\right\rangle^{t}\right] - U^{t+\frac{1}{2}}\left\langle\frac{\partial U}{\partial x}\right\rangle^{t} - g\left\langle\frac{\partial \zeta}{\partial x}\right\rangle^{t+\frac{1}{2}} - gU^{t}R_x^{t} \qquad (4.8)$$

where:

$$\left\langle \frac{\partial U}{\partial t} \right\rangle_{j+\frac{1}{2},k} = \frac{U_{n,m}^{t+\frac{1}{2}} - U_{n,m}^{t}}{\tau} \quad ; \quad \tau = \frac{\Delta t}{2}$$

$$\bar{\bar{V}}_{j+\frac{1}{2},k}^{t} = \frac{V_{n,m+1}^{t} + V_{n,m}^{t} + V_{n-1,m}^{t} + V_{n-1,m+1}^{t}}{4}$$

$$\left\langle \frac{\partial U}{\partial y} \right\rangle_{j+\frac{1}{2},k}^{t} = \frac{U_{n+1,m}^{t} - U_{n-1,m}^{t}}{2\Delta s} \quad ; \quad \left\langle \frac{\partial U}{\partial x} \right\rangle_{j+\frac{1}{2},k}^{t} = \frac{U_{n,m+1}^{t} - U_{n,m-1}^{t}}{2\Delta s}$$

$$\left\langle \frac{\partial \zeta}{\partial x} \right\rangle_{j+\frac{1}{2},k}^{t+\frac{1}{2}} = \frac{\zeta_{n,m+1}^{t+\frac{1}{2}} - \zeta_{n,m}^{t+\frac{1}{2}}}{\Delta s} \quad ; \quad R_{x\,j+\frac{1}{2},k}^{t} = \frac{\sqrt{(U_{n,m}^{t})^2 + (\bar{\bar{V}}_{n,m}^{t})^2}}{(\bar{h}^{y} + \zeta^{xt})\,(\bar{C}_{h}^{y})^2}$$

$$\bar{h}_{j+\frac{1}{2},k}^{y} = \frac{h_{n,m} + h_{n-1,m}}{2} \quad ; \quad \bar{C}_{hj+\frac{1}{2},k}^{y} = \frac{C_{hn,m} + C_{hn-1,m}}{2} \quad ; \quad \zeta_{j+\frac{1}{2},k}^{xt} = \frac{\zeta_{n,m+1}^{t} + \zeta_{n,m}^{t}}{2}$$

Expanding the terms containing parameters at the time level $t+\frac{1}{2}$ and re-writing the equation, an expression for the velocity, U, and water surface elevation, ζ, at time level $t+\frac{1}{2}$ in terms of the previous time level, t, is obtained,

$$\begin{aligned} &-\frac{g\tau}{\Delta s}\zeta_{n,m}^{t+\frac{1}{2}} + \left[1 + \tau\left\langle \frac{\partial U}{\partial x} \right\rangle_{n,m}^{t}\right] U_{n,m}^{t+\frac{1}{2}} + \frac{g\tau}{\Delta s}\zeta_{n,m+1}^{t+\frac{1}{2}} \\ &= U_{n,m}^{t}\left[1 - g\tau R_{x\,n,m}^{t}\right] + \tau\bar{\bar{V}}_{n,m}^{t}\left[f_{c\,n,m} - \left\langle \frac{\partial U}{\partial y} \right\rangle_{n,m}^{t}\right] \end{aligned} \qquad (4.19)$$

The water surface elevation at time $t+\frac{1}{2}$ is determined by solving equation (4.7) in the finite difference form,

at j,k (n,m):

$$\frac{\partial \zeta}{\partial t} = -\left\langle \frac{\partial [(h+\zeta)\,U]}{\partial x} \right\rangle^{t+\frac{1}{2}} - \left\langle \frac{\partial [(h+\zeta)\,V]}{\partial y} \right\rangle^{t} \qquad (4.20)$$

where:

$$\left\langle \frac{\partial \zeta}{\partial t} \right\rangle_{j,k} = \frac{\zeta_{n,m}^{t+\frac{1}{2}} - \zeta_{n,m}^{t}}{\tau} \quad ; \quad \tau = \frac{\Delta t}{2}$$

$$\left\langle \frac{\partial [(h+\zeta)\, U]}{\partial x} \right\rangle_{j,k}^{t+\frac{1}{2}} = \frac{\left(\bar{h}^{y}_{j+\frac{1}{2},k} + \zeta^{x\ t+\frac{1}{2}}_{j+\frac{1}{2},k}\right) U^{t+\frac{1}{2}}_{j+\frac{1}{2},k} - \left(\bar{h}^{y}_{j-\frac{1}{2},k} + \zeta^{x\ t+\frac{1}{2}}_{j-\frac{1}{2},k}\right) U^{t+\frac{1}{2}}_{j-\frac{1}{2},k}}{\Delta S}$$

$$\left\langle \frac{\partial [(h+\zeta)\, V]}{\partial y} \right\rangle_{j,k}^{t} = \frac{\left(\bar{h}^{x}_{j,k+\frac{1}{2}} + \zeta^{y\ t}_{j,k+\frac{1}{2}}\right) V^{t}_{j,k+\frac{1}{2}} - \left(\bar{h}^{x}_{j,k-\frac{1}{2}} + \zeta^{y\ t}_{j,k-\frac{1}{2}}\right) V^{t}_{j,k-\frac{1}{2}}}{\Delta S}$$

$$\bar{h}^{y}_{j+\frac{1}{2},k} = \frac{h_{n,m} + h_{n-1,m}}{2} \quad ; \quad \bar{h}^{x}_{j,k+\frac{1}{2}} = \frac{h_{n,m} + h_{n,m-1}}{2}$$

$$\zeta^{x}_{j+\frac{1}{2},k} = \frac{\zeta_{n,m} + \zeta_{n,m+1}}{2} \quad ; \quad \zeta^{y}_{j,k+\frac{1}{2}} = \frac{\zeta_{n+1,m} + \zeta_{n,m}}{2}$$

$$U_{j+\frac{1}{2},k} = U_{n,m} \quad ; \quad U_{j-\frac{1}{2},k} = U_{n,m-1} \quad ; \quad V_{j,k+\frac{1}{2}} = V_{n,m} \quad ; \quad V_{j,k-\frac{1}{2}} = V_{n-1,m}$$

Expanding the terms containing parameters at time level t+½ and re-writing the equation, a relationship is developed from the conservation of mass equation for the water surface elevation at time level t+½,

$$\zeta_{n,m}^{t+\frac{1}{2}} + \frac{\tau}{2\Delta S}\left\{\begin{array}{c} U_{n,m}^{t+\frac{1}{2}}\left[h_{n,m} + h_{n-1,m} + \zeta_{n,m}^{t+\frac{1}{2}} + \zeta_{n,m+1}^{t+\frac{1}{2}}\right] \\ - U_{n,m-1}^{t+\frac{1}{2}}\left[h_{n,m-1} + h_{n-1,m-1} + \zeta_{n,m-1}^{t+\frac{1}{2}} + \zeta_{n,m}^{t+\frac{1}{2}}\right] \end{array}\right\} \qquad (4.21)$$

$$=$$

$$\zeta_{n,m}^{t} - \frac{\tau}{2\Delta S}\left\{\begin{array}{c} V_{n,m}^{t}\left[h_{n,m} + h_{n,m-1} + \zeta_{n+1,m}^{t} + \zeta_{n,m}^{t}\right] \\ - V_{n-1,m}^{t}\left[h_{n-1,m} + h_{n-1,m-1} + \zeta_{n,m}^{t} + \zeta_{n-1,m}^{t}\right] \end{array}\right\}$$

Introducing the following into equation (4.19)

$$r = \frac{g\tau}{\Delta s} \quad ; \quad a_{n,m} = 1 + \tau \left\langle \frac{\partial U}{\partial x} \right\rangle^{t}_{n,m}$$

$$B_{n,m} = U^{t}_{n,m}\left[1 - g\tau R^{t}_{x\,n,m}\right] + \tau \overline{V}^{t}_{n,m}\left[f_{c\,n,m} - \left\langle \frac{\partial U}{\partial x} \right\rangle^{t}_{n,m}\right]$$

provides a more workable form of the equation,

$$-r\zeta^{t+\frac{1}{2}}_{n,m} + a_{n,m}U^{t+\frac{1}{2}}_{n,m} + r\zeta^{t+\frac{1}{2}}_{n,m+1} = B_{n,m} \tag{4.22}$$

Similarly, introducing the following into equation (4.21);

$$\chi^{t}_{x\,n,m} = \frac{\tau}{2\Delta s}\left[h_{n,m} + h_{n-1,m} + \zeta^{t}_{n,m} + \zeta^{t}_{n,m+1}\right]$$

$$\chi^{t}_{y\,n,m} = \frac{\tau}{2\Delta s}\left[h_{n,m} + h_{n,m-1} + \zeta^{t}_{n+1,m} + \zeta^{t}_{n,m}\right]$$

$$A_{n,m} = \zeta^{t}_{n,m} - \chi^{t}_{y\,n,m}V^{t}_{n,m} + \chi^{t}_{y\,n-1,m}V^{t}_{n-1,m}$$

provides a more workable form of this equation,

$$\zeta^{t+\frac{1}{2}}_{n,m} + \chi^{t+\frac{1}{2}}_{x\,n,m}U^{t+\frac{1}{2}}_{n,m} - \chi^{t+\frac{1}{2}}_{x\,n,m-1}U^{t+\frac{1}{2}}_{n,m-1} = A_{n,m} \tag{4.23}$$

A system of linear equations can be constructed relating the water surface elevations and horizontal, 'U', velocity along a row of computational points in the grid system. In matrix form, using the notation presented in equations (4.22) and (4.23), for a single row, 'n', of computational points, the simultaneous system is,

$$\begin{bmatrix} 1 & \chi_{x\,m}^{t+\frac{1}{2}} & 0 & 0 & 0 & 0 & 0 & 0 \\ -r & a_m & r & 0 & 0 & 0 & 0 & 0 \\ 0 & -\chi_{x\,m}^{t+\frac{1}{2}} & 1 & \chi_{x\,m+1}^{t+\frac{1}{2}} & 0 & 0 & 0 & 0 \\ 0 & 0 & -r & a_{m+1} & r & 0 & 0 & 0 \\ \cdot & \cdot & \cdot & \cdot & \cdot & \cdot & \cdot & \cdot \\ \cdot & \cdot & \cdot & \cdot & \cdot & \cdot & \cdot & \cdot \\ \cdot & \cdot & \cdot & \cdot & \cdot & \cdot & \cdot & \cdot \\ 0 & 0 & 0 & 0 & 0 & 0 & -\chi_{x\,I-1}^{t+\frac{1}{2}} & 1 \end{bmatrix} \begin{bmatrix} \zeta_m^{t+\frac{1}{2}} \\ U_m^{t+\frac{1}{2}} \\ \zeta_{m+1}^{t+\frac{1}{2}} \\ U_{m+1}^{t+\frac{1}{2}} \\ \zeta_{m+2}^{t+\frac{1}{2}} \\ \cdot \\ \cdot \\ \zeta_I^{t+\frac{1}{2}} \end{bmatrix} = \begin{bmatrix} A_m \\ B_m \\ A_{m+1} \\ B_{m+1} \\ A_{m+2} \\ \cdot \\ \cdot \\ A_I \end{bmatrix} + \begin{bmatrix} \chi_{x\,m-1}^{t+\frac{1}{2}} U_{m-1}^{t+\frac{1}{2}} \\ 0 \\ 0 \\ 0 \\ 0 \\ 0 \\ 0 \\ \chi_{x\,I}^{t+\frac{1}{2}} U_I^{t+\frac{1}{2}} \end{bmatrix} \qquad (4.24)$$

The values of the vector ($\zeta_{n,m}$, $U_{n,m}$, $\zeta_{n,m+1}$, $U_{n,m+1}$, ..., ζ_I) is determined using a process of elimination of unknowns. Starting with the first equation of (4.24) the water surface elevation ζ_m is expressed as a function of the unknown velocity U_m,

$$\zeta_{n,m}^{t+\frac{1}{2}} = -P_{n,m} U_{n,m}^{t+\frac{1}{2}} + Q_{n,m} \qquad (4.25)$$

where:
$$P_{n,m} = \chi_{x\,n,m}^{t+\frac{1}{2}} \quad ; \quad Q_{n,m} = A_{n,m} + \chi_{x\,n,m-1}^{t+\frac{1}{2}} U_{n,m-1}^{t+\frac{1}{2}}$$

Substituting (4.25) into the second equation of (4.24) and expressing $U_{n,m}$ as a function of $\zeta_{n,m+1}$ gives,

$$U_{n,m}^{t+\frac{1}{2}} = -R_{n,m} \zeta_{n,m+1}^{t+\frac{1}{2}} + S_{n,m} \qquad (4.26)$$

where:

$$R_{n,m} = \frac{r}{rP_{n,m} + a_{n,m}} \quad ; \quad S_{n,m} = \frac{B_{n,m} + rQ_{n,m}}{rP_{n,m} + a_{n,m}}$$

Substituting (4.26) into the third equation of (4.24) and expressing $\zeta_{n,m+1}$ in terms of the velocity $U_{n,m+1}$, the following relationship is developed,

$$\zeta_{n,m+1}^{t+\frac{1}{2}} = -P_{n,m+1} U_{n,m+1}^{t+\frac{1}{2}} + Q_{n,m+1} \qquad (4.28)$$

where:

$$P_{n,m+1} = \frac{\chi_{x\,n,m+1}^{t+\frac{1}{2}}}{1 + \chi_{x\,n,m}^{t+\frac{1}{2}} R_{n,m}} \quad ; \quad Q_{n,m+1} = \frac{A_{n,m+1} + \chi_{n,m}^{t+\frac{1}{2}} S_{n,m}}{1 + \chi_{x\,n,m}^{t+\frac{1}{2}} R_{n,m}}$$

Generally the following recursive formulae can be written,

$$\zeta_{n,m}^{t+\frac{1}{2}} = -P_{n,m} U_{n,m}^{t+\frac{1}{2}} + Q_{n,m} \qquad (4.30)$$

$$U_{n,m-1}^{t+\frac{1}{2}} = -R_{n,m-1} \zeta_{n,m}^{t+\frac{1}{2}} + S_{n,m-1} \qquad (4.31)$$

where:

$$P_{n,m} = \frac{\chi_{x\,n,m}^{t+\frac{1}{2}}}{1 + \chi_{x\,n,m-1}^{t+\frac{1}{2}} R_{n,m-1}} \quad ; \quad Q_{n,m} = \frac{A_{n,m} + \chi_{x\,n,m-1}^{t+\frac{1}{2}} S_{n,m-1}}{1 + \chi_{x\,n,m-1}^{t+\frac{1}{2}} R_{n,m-1}}$$

$$R_{n,m-1} = \frac{r}{a_{n,m-1} + r P_{n,m-1}} \quad ; \quad S_{n,m-1} = \frac{B_{n,m-1} + r Q_{n,m-1}}{a_{n,m-1} + r P_{n,m-1}}$$

The recursion coefficients, P, Q, R and S are determined starting at the lower bound, given the water surface elevation at this bound, and proceeding to the upper bound. If the velocity at the upper bound is known, the water surface elevations and velocities are then determined in descending order starting at the upper bound.

This sequence is executed for every row of computational points in the grid system to determine the first estimate for the water surface elevation and horizontal, 'U', velocities for the first half time step.

The water surface required in the solution for the non-linear expression presented in equation (4.21) is determined by an iterative process. The first estimate for the water surface elevation at time level 't+½' is made by the implicit procedure of taking the nonlinear term at time level 't'. Next, the value thus computed is used in (4.21) for the actual computation. This iteration can be repeated several times.

4.2.2 Explicit Computation for Horizontal Velocity 'V'

The velocity, 'V', in the other direction can now be estimated explicitly using equation (4.6) in the following finite difference form since the velocity 'U' in the Coriolis term is already known,

at j,k+½ (n,m);

$$\frac{\partial V}{\partial t} = -\overline{\overline{U}}^{t+\frac{1}{2}}\left[f_c + \left\langle \frac{\partial V}{\partial x} \right\rangle^t\right] - V^{t+\frac{1}{2}}\left\langle \frac{\partial V}{\partial y} \right\rangle^t - g\left\langle \frac{\partial \zeta}{\partial y} \right\rangle^t - gV^{t+\frac{1}{2}} R_y^{t+\frac{1}{2}} \qquad (4.33)$$

where:

$$\frac{\partial V}{\partial t} = \frac{V_{n,m}^{t+\frac{1}{2}} - V_{n,m}^{t}}{\tau} \quad ; \quad \tau = \frac{\Delta t}{2}$$

$$\overline{\overline{U}}_{j,k+\frac{1}{2}}^{t+\frac{1}{2}} = \frac{U_{n,m}^{t+\frac{1}{2}} + U_{n+1,m}^{t+\frac{1}{2}} + U_{n+1,m-1}^{t+\frac{1}{2}} + U_{n,m-1}^{t+\frac{1}{2}}}{4}$$

$$\left\langle \frac{\partial V}{\partial x} \right\rangle_{j,k+\frac{1}{2}}^{t} = \frac{V_{n,m+1}^{t} - V_{n,m-1}^{t}}{2\Delta s} \quad ; \quad \left\langle \frac{\partial V}{\partial y} \right\rangle_{j,k+\frac{1}{2}}^{t} = \frac{V_{n+1,m}^{t} - V_{n-1,m}^{t}}{2\Delta s}$$

$$\left\langle \frac{\partial \zeta}{\partial y} \right\rangle_{j,k+\frac{1}{2}}^{t} = \frac{\zeta_{n+1,m}^{t} - \zeta_{n,m}^{t}}{\Delta s} \quad ; \quad R_{y\,j,k+\frac{1}{2}}^{t+\frac{1}{2}} = \frac{\sqrt{(\overline{\overline{U}}_{n,m}^{t+\frac{1}{2}})^2 + (V_{n,m}^{t})^2}}{(\overline{h}^{x} + \zeta^{y\,t+\frac{1}{2}})\ (\overline{C_h}^{x})^2}$$

$$\overline{h}_{j,k+\frac{1}{2}} = \frac{h_{n,m} + h_{n,m-1}}{2} \quad ; \quad \overline{C_h}^{x}_{j,k+\frac{1}{2}} = \frac{C_{h\,n,m} + C_{h\,n,m-1}}{2} \quad ; \quad \zeta_{j,k+\frac{1}{2}}^{t+\frac{1}{2}} = \frac{\zeta_{n+1,m}^{t+\frac{1}{2}} + \zeta_{n,m}^{t+\frac{1}{2}}}{2}$$

Substituting the finite difference approximations containing those parameters at time level '$t+\frac{1}{2}$' and solving for the velocity '$V^{t+\frac{1}{2}}$', the following relationship is developed,

$$V_{n,m}^{t+\frac{1}{2}} = \frac{V_{n,m}^{t} - \tau\left\{\overline{\overline{U}}_{n,m}^{t+\frac{1}{2}}\left[f_{c\,n,m} + \left\langle \frac{\partial V}{\partial x} \right\rangle_{n,m}^{t}\right] + g\left\langle \frac{\partial \zeta}{\partial y} \right\rangle_{n,m}^{t}\right\}}{1 + \tau\left[gR_{y\,n,m}^{t+\frac{1}{2}} + \left\langle \frac{\partial V}{\partial y} \right\rangle_{n,m}^{t}\right]} \qquad (4.34)$$

4.2.3 Implicit Computation for Horizontal Velocity 'V' and Water Surface Elevation 'ζ'

The velocity 'V' and water surface elevation, ζ, for the second half time step, '$t+\frac{1}{2}$' to 't+1', is an implicit

operation using equations (4.6) and (4.7) in the following finite difference forms,

using (4.6) at j,k+½ (n,m):

$$\frac{\partial V}{\partial t} = -\bar{\bar{U}}^{t+\frac{1}{2}}\left[f_c + \left\langle\frac{\partial V}{\partial x}\right\rangle^{t+\frac{1}{2}}\right] - V^{t+1}\left\langle\frac{\partial V}{\partial y}\right\rangle^{t+\frac{1}{2}} - g\left\langle\frac{\partial \zeta}{\partial y}\right\rangle^{t+1} - gV^{t+\frac{1}{2}}R_y^{t+1} \qquad (4.35)$$

where:

$$\left\langle\frac{\partial V}{\partial t}\right\rangle_{j,k+\frac{1}{2}} = \frac{V_{n,m}^{t+1} - V_{n,m}^{t+\frac{1}{2}}}{\tau} \quad ; \quad \tau = \frac{\Delta t}{2}$$

$$\left\langle\frac{\partial V}{\partial x}\right\rangle_{j,k+\frac{1}{2}}^{t+\frac{1}{2}} = \frac{V_{n,m+1}^{t+\frac{1}{2}} - V_{n,m-1}^{t+\frac{1}{2}}}{2\Delta s} \quad ; \quad \left\langle\frac{\partial V}{\partial y}\right\rangle_{j,k+\frac{1}{2}}^{t+\frac{1}{2}} = \frac{V_{n+1,m}^{t+\frac{1}{2}} - V_{n-1,m}^{t+\frac{1}{2}}}{2\Delta s}$$

$$\left\langle\frac{\partial \zeta}{\partial y}\right\rangle_{j,k+\frac{1}{2}}^{t+1} = \frac{\zeta_{n+1,m}^{t+1} - \zeta_{n,m}^{t+1}}{\Delta s} \quad ; \quad R_{y\,j,k+\frac{1}{2}}^{t+1} = \frac{\sqrt{(\bar{\bar{U}}_{n,m}^{t+\frac{1}{2}})^2 + (V_{n,m}^{t+\frac{1}{2}})^2}}{(\bar{h}^y + \zeta^{y\,t+\frac{1}{2}})\ (\overline{C_h}^x)^2}$$

$$\bar{h}_{j,k+\frac{1}{2}}^x = \frac{h_{n,m} + h_{n,m-1}}{2} \quad ; \quad \overline{C_h}_{j,k+\frac{1}{2}}^x = \frac{C_{h\,n,m} + C_{h\,n-1,m}}{2} \quad ; \quad \zeta_{j,k+\frac{1}{2}}^{y\,t+\frac{1}{2}} = \frac{\zeta_{n+1,m}^{t+\frac{1}{2}} + \zeta_{n,m}^{t+\frac{1}{2}}}{2}$$

using (4.7) at j,k (n,m):

$$\frac{\partial \zeta}{\partial t} = -\left\langle\frac{\partial [(h+\zeta)\,U]}{\partial x}\right\rangle^{t+\frac{1}{2}} - \left\langle\frac{\partial [(h+\zeta)\,V]}{\partial y}\right\rangle^{t+1} \qquad (4.36)$$

where:

$$\left\langle\frac{\partial \zeta}{\partial t}\right\rangle_{j,k} = \frac{\zeta_{n,m}^{n+1} - \zeta_{n,m}^{t+\frac{1}{2}}}{\tau} \quad ; \quad \tau = \frac{\Delta t}{2}$$

$$\left\langle\frac{\partial [(h+\zeta)\,U]}{\partial x}\right\rangle_{j,k}^{t+\frac{1}{2}} = \frac{\left(\bar{h}_{j+\frac{1}{2},k}^y + \zeta_{j+\frac{1}{2},k}^{x\,t+\frac{1}{2}}\right)U_{j+\frac{1}{2},k}^{t+\frac{1}{2}} - \left(\bar{h}_{j-\frac{1}{2},k}^y + \zeta_{j-\frac{1}{2},k}^{x\,t+\frac{1}{2}}\right)U_{j-\frac{1}{2},k}^{t+\frac{1}{2}}}{\Delta s}$$

$$\left\langle\frac{\partial [(h+\zeta)\,V]}{\partial y}\right\rangle_{j,k}^{t+1} = \frac{\left(\bar{h}_{j,k+\frac{1}{2}}^x + \zeta_{j,k+\frac{1}{2}}^{y\,t+1}\right)V_{j,k+\frac{1}{2}}^{t+1} - \left(\bar{h}_{j,k-\frac{1}{2}}^x + \zeta_{j,k-\frac{1}{2}}^{y\,t+1}\right)V_{j,k-\frac{1}{2}}^{t+1}}{\Delta s}$$

$$\bar{h}^{y}_{j+\frac{1}{2},k}=\frac{h_{n,m}+h_{n-1,m}}{2}\quad;\quad \bar{h}^{x}_{j,k+\frac{1}{2}}=\frac{h_{n,m}+h_{n,m-1}}{2}$$

$$\zeta^{x}_{j+\frac{1}{2},k}=\frac{\zeta_{n,m}+\zeta_{n,m+1}}{2}\quad;\quad \zeta^{y}_{j,k+\frac{1}{2}}=\frac{\zeta_{n,m}+\zeta_{n+1,m}}{2}$$

$$U_{j+\frac{1}{2},k}=U_{n,m}\quad;\quad U_{j-\frac{1}{2},k}=U_{n,m-1}\quad;\quad V_{j,k+\frac{1}{2}}=V_{n,m}\quad;\quad V_{j,k-\frac{1}{2}}=V_{n-1,m}$$

Expanding the terms containing parameters at the time level 't+1' in equation (4.35) and collecting like terms with respect to time level gives,

$$\begin{aligned}&-\frac{g\tau}{\Delta s}\zeta^{t+1}_{n,m}+\left[1+\tau\left\langle\frac{\partial V}{\partial y}\right\rangle^{t+1}_{n,m}\right]V^{t+1}_{n,m}+\frac{g\tau}{\Delta s}\zeta^{t+1}_{n+1,m}\\&=V^{t+\frac{1}{2}}_{n,m}\left[1-g\tau R^{t+1}_{yn,m}\right]-\tau\bar{\bar{U}}^{t+\frac{1}{2}}_{n,m}\left[f_{cn,m}+\left\langle\frac{\partial V}{\partial x}\right\rangle^{t+\frac{1}{2}}_{n,m}\right]\end{aligned}\qquad(4.37)$$

and introducing the following,

$$r=\frac{g\tau}{\Delta s}\quad;\quad a'_{n,m}=1+\tau\left\langle\frac{\partial V}{\partial y}\right\rangle^{t+\frac{1}{2}}_{n,m}$$

$$B'_{n,m}=V^{t+\frac{1}{2}}_{n,m}\left[1-g\tau R^{t+1}_{yn,m}\right]-\tau\bar{\bar{U}}^{t+\frac{1}{2}}_{n,m}\left[f_{c\,n,m}+\left\langle\frac{\partial V}{\partial x}\right\rangle^{t+\frac{1}{2}}_{n,m}\right]$$

gives the following more workable form of the equation,

$$-r\zeta^{t+1}_{n,m}+a'_{n,m}V^{t+1}_{n,m}+r\zeta^{t+1}_{n+1,m}=B'_{n,m}\qquad(4.38)$$

Similarly, expanding (4.36), the following relationship is developed for the water level elevation at time level 't+1' in terms of the parameter values at time level 't+½',

$$\zeta_{n,m}^{t+1}+\frac{\tau}{2\Delta s}\left\{\begin{array}{c} V_{n,m}^{t+1}\left[h_{n,m}+h_{n,m-1}+\zeta_{n,m}^{t+1}+\zeta_{n+1,m}^{t+1}\right] \\ -V_{n-1,m}^{t+1}\left[h_{n-1,m}+h_{n-1,m-1}+\zeta_{n-1,m}^{t+1}+\zeta_{n,m}^{t+1}\right]\end{array}\right\}$$

$$=\qquad (4.39)$$

$$\zeta_{n,m}^{t+\frac{1}{2}}-\frac{\tau}{2\Delta s}\left\{\begin{array}{c} U_{n,m}^{t+\frac{1}{2}}\left[h_{n,m}+h_{n-1,m}+\zeta_{n,m}^{t+\frac{1}{2}}+\zeta_{n,m+1}^{t+\frac{1}{2}}\right] \\ -U_{n,m-1}^{t+\frac{1}{2}}\left[h_{n,m-1}+h_{n-1,m-1}+\zeta_{n,m-1}^{t+\frac{1}{2}}+\zeta_{n,m}^{t+\frac{1}{2}}\right]\end{array}\right\}$$

and introducing the following,

$$\chi_{x\,n,m}^{t} \quad ; \quad \chi_{y\,n,m}^{t} \qquad \text{:see page 88}$$

$$A'_{n,m}=\zeta_{n,m}^{t+\frac{1}{2}}-\chi_{x\,n,m}^{t+\frac{1}{2}}U_{n,m}^{t+\frac{1}{2}}+\chi_{x\,n,m-1}^{t+\frac{1}{2}}U_{n,m-1}^{t+\frac{1}{2}}$$

gives the following relationship,

$$\zeta_{n,m}^{t+1}+\chi_{y\,n,m}^{t+1}V_{n,m}^{t+1}-\chi_{y\,n-1,m}^{t+1}V_{n-1,m}^{t+1}=A'_{n,m} \qquad (4.40)$$

Using the matrix formulation and solution technique, as previously described, and equations (4.38) and (4.40), the following recursion formulae are developed for the, 'V', velocities in the opposite direction at time level 't+1';

$$\zeta_{n,m}^{t+1}=-P'_{n,m}V_{n,m}^{t+1}+Q'_{n,m} \qquad (4.41)$$

$$V_{n-1,m}^{t+1}=-R'_{n-1,m}\zeta_{n,m}^{t+1}+S'_{n-1,m} \qquad (4.42)$$

where:

$$P'_{n,m}=\frac{\chi_{y\,n,m}^{t+1}}{1+\chi_{y\,n-1,m}^{t+1}R'_{n-1,m}} \quad ; \quad Q'_{n,m}=\frac{A'_{n,m}+\chi_{y\,n-1,m}^{t+1}S'_{n-1,m}}{1+\chi_{y\,n-1,m}^{t+1}R'_{n-1,m}}$$

$$R'_{n-1,m}=\frac{r}{a'_{n-1,m}+rP'_{n-1,m}} \quad ; \quad S'_{n-1,m}=\frac{B'_{n-1,m}+rQ'_{n-1,m}}{a'_{n-1,m}+rP'_{n-1,m}}$$

The recursion coefficients, P′, Q′, R′ and S′ are determined starting at the lower bound, given the water surface elevation at this bound, and proceeding to the upper bound. If the velocity at the upper bound is known, the water surface elevations and velocities are then determined in descending order starting at the upper bound.

This sequence is executed for every column of computational points in the grid system to determine the first estimate for the water surface elevation and horizontal, 'V', velocities for the second half time step.

The water surface required in the solution for the non-linear expression presented in equation (4.39) is determined by an iterative process. The first estimate for the water surface elevation at time level 't+1' is made by the implicit procedure of taking the nonlinear term at time level 't+½'. Next, the value thus computed is used in (4.39) for the actual computation. This iteration can be repeated several times.

4.2.4 Explicit Computation for Horizontal Velocity 'U'

The velocity, 'U', in the other direction is determined explicitly using (4.5) in the following finite difference form,

at j+½,k (n,m):

$$\frac{\partial U}{\partial t} = \overline{\overline{V}}^{t+1}\left[f_c - \left\langle\frac{\partial U}{\partial y}\right\rangle^{t+\frac{1}{2}}\right] - U^{t+1}\left\langle\frac{\partial U}{\partial x}\right\rangle^{t+\frac{1}{2}} - g\left\langle\frac{\partial \zeta}{\partial x}\right\rangle^{t+\frac{1}{2}} - gU^{t+1}R_x^{t+1} \qquad (4.43)$$

where:

$$\left\langle\frac{\partial U}{\partial t}\right\rangle_{j+\frac{1}{2},k} = \frac{U_{n,m}^{t+1} - U_{n,m}^{t+\frac{1}{2}}}{\tau} \quad ; \quad \tau = \frac{\Delta t}{2}$$

$$\overline{\overline{V}}^{t+1}_{j+\frac{1}{2},k} = \frac{V_{n,m}^{t+1} + V_{n-1,m}^{t+1} + V_{n,m+1}^{t+1} + V_{n-1,m+1}^{t+1}}{4}$$

$$\left\langle\frac{\partial U}{\partial x}\right\rangle^{t+\frac{1}{2}}_{j+\frac{1}{2},k} = \frac{U_{n,m+1}^{t+\frac{1}{2}} - U_{n,m-1}^{t+\frac{1}{2}}}{2\Delta s} \quad ; \quad \left\langle\frac{\partial U}{\partial y}\right\rangle^{t+\frac{1}{2}}_{j+\frac{1}{2},k} = \frac{U_{n+1,m}^{t+\frac{1}{2}} - U_{n-1,m}^{t+\frac{1}{2}}}{2\Delta s}$$

$$\left\langle\frac{\partial \zeta}{\partial x}\right\rangle^{t+\frac{1}{2}}_{j+\frac{1}{2},k} = \frac{\zeta_{n,m}^{t+\frac{1}{2}} - \zeta_{n,m-1}^{t+\frac{1}{2}}}{\Delta s} \quad ; \quad R_{x\,j+\frac{1}{2},k}^{t+1} = \frac{\sqrt{(U_{n,m}^{t+\frac{1}{2}})^2 + (\overline{\overline{V}}_{n,m}^{t+1})^2}}{(\overline{h}^y + \zeta^{x\,t+\frac{1}{2}})\,(\overline{C_h}^y)^2}$$

$$\overline{h}^y_{j+\frac{1}{2},k} = \frac{h_{n,m} + h_{n-1,m}}{2} \quad ; \quad \overline{C_h}^y_{j+\frac{1}{2},k} = \frac{C_{h\,n,m} + C_{h\,n-1,m}}{2} \quad ; \quad \zeta^{x\,t+\frac{1}{2}}_{j+\frac{1}{2},k} = \frac{\zeta_{n,m}^{t+\frac{1}{2}} + \zeta_{n,m+1}^{t+\frac{1}{2}}}{2}$$

Solving for 'U' velocity at time level 't+1' gives the following relationship;

$$U_{n,m}^{t+1} = \frac{U_{n,m}^{t+\frac{1}{2}} + \tau\left\{\overline{\overline{V}}_{n,m}^{t+1}\left[f_{c\,n,m} - \left\langle\frac{\partial U}{\partial y}\right\rangle^{t+\frac{1}{2}}_{n,m}\right] - g\left\langle\frac{\partial \zeta}{\partial x}\right\rangle^{t+\frac{1}{2}}_{n,m}\right\}}{1 + \tau\left[gR_{x\,n,m}^{t+1} + \left\langle\frac{\partial U}{\partial x}\right\rangle^{t+\frac{1}{2}}_{n,m}\right]} \qquad (4.44)$$

4.2.5 Boundary Conditions

The computational model boundary conditions for examining the response of a harbour basin to long period water waves are the shore and open boundary conditions.

The shore boundary can vary from fully reflective, such as concrete sea walls, to situations where run-up can occur, such as gradual beaches. The slope at which a long period waves will have a reflection coefficient greater than 0.9 is presented in Table 4.1 for various wave periods.

Table 4.1 - Wave period/slope relationship for reflection coefficient greater than 0.9 on plane slopes.

WAVE PERIOD (seconds)	SLOPE
10	1 on 2.68
50	1 on 13.44
100	1 on 26.88
150	1 on 40.32
200	1 on 53.76
250	1 on 67.20

Incident wave height = 1 m ; Reflection coefficient greater then 0.9 when surf similarity parameter greater than 4.65 (see SPM (1984), Fig. 2-65, p.2-118, for plane slopes).

The shore boundary is assumed to be fully reflective with respect to long period waves for the work presented in this thesis.

The open boundary condition is assumed to be the entrance to the harbour basin where the water surface elevation, velocities and direction are known.

4.2.5.1 Shore Boundary Condition

The shore boundary is assumed to be described at the locations where the depth data is provided and less than or equal to zero. The assumption that the boundary is fully reflective leads to the no flow condition normal to the boundary. Evaluation of the velocity at these boundaries using the previously developed formulae is not possible. Therefore, a weighting factor and linear approximation for each of the differential operations is introduced,

$$\left\langle \frac{\partial U}{\partial x} \right\rangle_{n,m} = (1-\gamma)\left[\frac{U_{n,m+1} - U_{n,m}}{\Delta S}\right] + \gamma\left[\frac{U_{n,m} - U_{n,m-1}}{\Delta S}\right] \qquad (4.45)$$

$$\left\langle \frac{\partial U}{\partial y} \right\rangle_{n,m} = (1-\gamma)\left[\frac{U_{n+1,m} - U_{n,m}}{\Delta S}\right] + \gamma\left[\frac{U_{n,m} - U_{n-1,m}}{\Delta S}\right] \qquad (4.46)$$

$$\left\langle \frac{\partial V}{\partial x} \right\rangle_{n,m} = (1-\gamma)\left[\frac{V_{n,m+1} - V_{n,m}}{\Delta S}\right] + \gamma\left[\frac{V_{n,m} - V_{n,m-1}}{\Delta S}\right] \qquad (4.47)$$

$$\left\langle \frac{\partial V}{\partial y} \right\rangle_{n,m} = (1-\gamma)\left[\frac{V_{n+1,m} - V_{n,m}}{\Delta S}\right] + \gamma\left[\frac{V_{n,m} - V_{n-1,m}}{\Delta S}\right] \qquad (4.48)$$

The weighting factor, γ, is either 0, 0.5 or 1.0, depending on the location of the shore boundary encountered as presented in Table 4.2.

Table 4.2 - Shoreline boundary, off-centre derivative weighting factor, γ.

Boundary Location	$\frac{\partial U}{\partial x}$	$\frac{\partial U}{\partial y}$	$\frac{\partial V}{\partial x}$	$\frac{\partial V}{\partial y}$
X-Direction:				
lower bound	0.0	0.5	0.0	0.5
upper bound	1.0	0.5	1.0	0.5
Y-Direction:				
lower bound	0.5	0.0	0.5	0.0
upper bound	0.5	1.0	0.5	1.0

4.2.5.2 Open Boundary Condition

The water surface elevations are required at the open boundary and are the driving force of the computational model to simulate long period wave propagation in a water basin. The open boundary water surface elevation is assumed to be of a sinusoidal waveform with a constant deep water height and a user specified period. The initial surface elevation is taken to be zero with subsequent time dependant elevations obtained by addition of a surface increment obtained as follows;

$$d\zeta_{x_i} = \zeta_m\{\cos[kx_i - \sigma(t_i + dt)] - \cos[kx_i - \sigma t_i]\}$$

$$\sigma = \frac{2\pi}{T} \quad ; \quad k = \frac{2\pi}{L} \quad ; \quad L = T\sqrt{gd_{x_i}} \tag{4.49}$$

$$\therefore \; d\zeta_{x_i} = \zeta_m\left\{\cos\left[\sigma\left(\frac{x_i}{\sqrt{gd_{x_i}}} - t_i - dt\right)\right] - \cos\left[\sigma\left(\frac{x_i}{\sqrt{gd_{x_i}}} - t_i\right)\right]\right\}$$

where: $d\zeta$= change in water surface elevation; ζ_m= maximum water surface elevation; T= wave period; dt= $\tau/2$ = half time step; t_i, x_i = time, distance from start.

The wave length is chosen to ensure shallow water conditions are met over the entire basin by using the shallow water criterion (Dean & Dalrymple, 1984, p.132) with the maximum water depth, d_{max}, as follows,

$$L_{min} = 20.0 d_{max} \tag{4.50}$$

An estimate of the corresponding wave period is found using equation (4.50) and the linear equation for shallow water wave length,

$$T_{est} = \frac{L_{min}}{\sqrt{gd_{max}}} = 20.0\sqrt{\frac{d_{max}}{g}} \tag{4.51}$$

where: T_{est} = estimated wave period.

Leendertse (1967) recommends a computational resolution of thirty (30) points per wave length, i.e. $L_{min} = 30\Delta s$. An estimate of the wave period to meet this requirement is,

$$T_{est} = \frac{L_{min}}{\sqrt{g d_{max}}} = 30.0 \frac{\Delta s}{\sqrt{g d_{max}}} \qquad (4.52)$$

where: Δs = grid spacing.

The two (2) wave period estimates resulting from equations (4.51) and (4.52) are compared and the largest of the two is taken to be the minimum recommended value to be used for any analysis.

The maximum water surface elevation at the boundary is chosen based on the need to eliminate any possible occurrences of breaking waves by ensuring that the following relationships are not satisfied (Dean & Dalrymple, 1984, p.335);

$$\frac{H_b}{d_{min}} = 0.78 \ , \ \therefore H_b = 0.78 d_{min} \quad \text{:Shallow water.} \qquad (4.53)$$

$$\frac{H_b}{L_0} = \frac{1}{7} \ ; \ L_0 = \frac{g T_{est}^2}{2\pi} \ , \ \therefore H_b = \frac{g T_{est}^2}{14\pi} \quad \text{:Deep water.} \qquad (4.54)$$

$$H_b = 0.218 L_0 \ ; \ L_0 = \frac{g T_{est}^2}{2\pi} \quad \text{:Deep water standing wave.} \qquad (4.55)$$

$$\eta_c = 0.647 H_b \ ; \ \eta_t = 0.353 H_b$$

$$H_b = 1.37 d_{min} \quad \text{:Shallow water standing wave.} \qquad (4.56)$$

where: H_b= breaking wave height corresponding to the estimated period, T_{est}; L_0= deep water wave length; d_{min}= minimum water depth; η_c, η_t = maximum, minimum water surface displacement at breaking; g= acceleration due to gravity.

Taking the minimum of the values determined from the above equations to be the maximum water wave height permitted at the open boundary, H_i, and multiplying by an arbitrary factor of one-half (½) will ensure that wave breaking will not occur.

The water depth varies along the length of the open boundary which results in variable wave height along the boundary. The equivalent deep water wave height, H_0, is determined using the shoaling coefficient,

$$K_{sh} = \frac{H_i}{H_0} = \sqrt{\frac{C_0}{C_i}} \; ; \; C_0 = \frac{gT_{est}}{2\pi} \; ; \; C_i = \sqrt{gd_{x_i}}$$
$$\therefore H_o = H_i \sqrt{\frac{2\pi}{T_{est}} \sqrt{\frac{d_{x_i}}{g}}} \qquad (4.57)$$

The deep water wave height is then used in conjunction with the shoaling coefficient to determine the wave height and subsequent water surface elevations at the boundary resulting in the following relationship,

$$\zeta_0 = \frac{H_o}{2} \; ; \; \zeta_m = \frac{H_i}{2}$$
$$\zeta_m = \zeta_0 \sqrt{\frac{T_{est}}{2\pi} \sqrt{\frac{g}{d_{x_i}}}} \qquad (4.58)$$

Substituting (4.58) into (4.49) gives rise to the final estimate of the change in surface elevation for a particular

location along the open boundary as follows,

$$d\zeta_{x_i} = \zeta_0 \sqrt{\frac{T_{est}}{2\pi}\sqrt{\frac{g}{d_{x_i}}}} \left\{ \begin{array}{l} \cos\left[\frac{2\pi}{T_{est}}\left(\frac{x_i}{\sqrt{gd_{x_i}}} - t_i - dt\right)\right] \\ -\cos\left[\frac{2\pi}{T_{est}}\left(\frac{x_i}{\sqrt{gd_{x_i}}} - t_i\right)\right] \end{array} \right\} \qquad (4.59)$$

where: d = water depth at location x_i along the open boundary; remaining variables as previously described.

The recommended time step, τ, is determined using a Courant number of one (1) at the average depth of the basin, d_{avc}, as follows,

$$C_m = KC_p$$

$$C_m = \frac{\Delta S}{\tau} \; ; \; C_p = \sqrt{gd_{ave}} \; ; \; K = 1 \qquad (4.60)$$

$$\therefore \tau = \frac{\Delta S}{\sqrt{gd_{ave}}}$$

where: C = wave celerity; m,p = model, prototype; K = Courant number; τ = time step; Δs = grid spacing.

The resulting time step introduces local instabilities in the numerical model where the local water depth is very much lower or higher than the average water depth resulting in a non representative Courant number. The elimination of these local instabilities would require the implementation of a variable time step throughout the basin which in turn would increase the computational time and complexity of the computational

model. The selection of the time step using the average depth is felt to be sufficient for the analysis of a water basin on the hole. Analysis of specific areas or locations inside the basin using this software should be undertaken with due consideration of the local instabilities introduced.

4.2.5.3 Chezy Coefficient Determination

The bottom boundary condition assumes a rigid non-porous bottom. The effect of bottom friction on wave motion is described using the Chezy Coefficient for flow in open channels as presented in the previous discussions.

The actual Chezy Coefficient ,C_h, value to be used can be determined using one of the following expressions ;

1. Ganguillet and Kutter, 1869, in Douglas, et al. (1979), p.436:

$$C_h = \frac{23 + \frac{0.0015}{s} + \frac{1}{n}}{1 + \left(23 + \frac{0.0015}{s}\right)\frac{n}{\sqrt{m}}} \qquad (4.61)$$

where: n= Manning's No. (0.025 to 0.035); s= bottom slope; m= hydraulic radius = water depth.

2. Bazin, 1897, in Douglas et al. (1979), p.437:

$$C_h = \frac{86.9}{1 + \frac{k}{\sqrt{m}}} \tag{4.62}$$

where: k= 0.850, 1.303 and 1.750 for very regular surface channels, ordinary and exceptionally rough channels respectively; m= hydraulic radius = water depth.

3. Wang and Christensen (1986):

$$C_h = \sqrt{\frac{2}{f'}} = \sqrt{\frac{[\ln(ad+1)]^2}{.64}} \tag{4.63}$$

where: a= 365 or 20 for smooth and rough seabed respectively; d= water depth; f'= effective friction factor.

4. Leendertse (1967):

$$C_h = 19.4 \ln(.9d) \tag{4.64}$$

where: d= water depth.

Equations (4.61) and (4.62) are used extensively in the examination of water flow in open channels. Equation (4.61) provides a method to incorporate the change in bottom elevation in the direction of flow as well as the effect of bottom friction. Equation (4.62) incorporates the frictional effects only. Equation (4.63) was developed from experimental work examining the propagation of hurricane induced waves on various coastal morphologies. Equation (4.64) was developed using historical tidal information for the Haringvliet, the

Netherlands.

Due to the wide variations in bottom topography typically found in harbour basins, equation (4.61) was selected to be used for the analyses presented in this thesis with a Manning's No. of 0.030. The other equations are available for use in the computer program.

4.3 Computer Model

A solution of the numerical model presented in the previous sections would be a laborious process if attempted manually. A computer program was developed to solve the numerical model for any combination of water basin geometry and wave period selected. The software package was given the name LONGWAVE with the logic flow as presented in Fig. 4.3.

The computational routines were translated from the work presented by Leendertse (1967) in Fortran to the QuickBasic software language. Various routines were developed and added to provide visual and hard copy outputs of the component and/or resultant velocities, water surface elevation, water depth, Chezy coefficient and basin response factor (S_i/S_0).

The program can be run in VGA, EGA, CGA or Hercules monochrome

graphics mode. However, the colour screen displays are only provided while in the EGA or VGA environments. The CGA and Hercules monochrome modes are in black and white. The colours and or line types used for each type of output is provided in Table 4.3.

Table 4.3 - Colour/line type representations for LONGWAVE program output types.

ITEM OUTPUT	OUTPUT TYPE		
	EGA/VGA DISPLAY	CGA/MONO DISPLAY	CONTOUR PLOTS
Shoreline	brown	white	black
Contour: <0 =0 >0	 green red blue	(white) -·-· ···· ——	(black) -··- --·- ——
Vector	red	white	black
Section to save	yellow	white	Not Plotted
Text	red green yellow	white	black

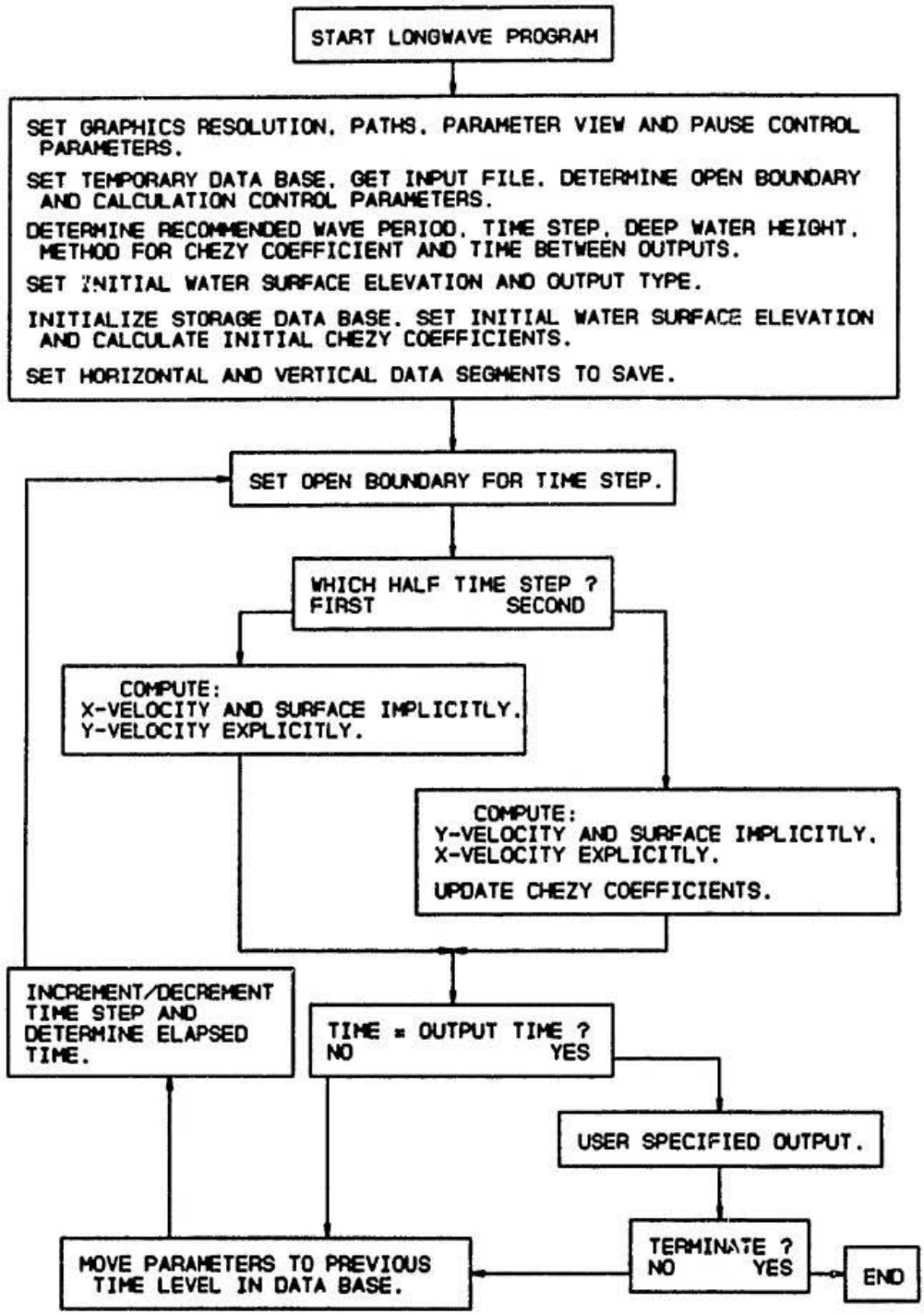

Fig. 4.3 - LONGWAVE software package logic flow chart.

The primary screen contains information for grid database retrieval and type of graphics adapter installed,

```
VIDEO TYPE AND SYSTEM PATHS --
<RIGHT ARROW> to EDIT & <F>inish.

Graphics resolution  [V,E,C,M]      *>V
Path for input FILE  [dr:\dir(s)\]   C:\HARBDATA\
File to be used      [filename]      SJBY100
Path for {.DB} files [dr:\dir(s)\]   E:\
View open boundary values [Y,N]      N
View control parameters   [Y,N]      N
Suppress pauses           [Y,N]      N
```

These parameters are maintained in a program default file titled PARAMS.LGW and are read in automatically at each program run. After the user has completed the above screen a second parameter screen is presented to input and verify the analysis parameters to be used,

```
ANALYSIS PARAMETERS --
<RIGHT ARROW> to EDIT & <F>inish.

Initial water surface elevation      0
Chezy formula to use [L,B,W,G#,N]    G.03
Wave period to use in seconds {>=}   120
Time step to use in seconds   {<=}   4.08
Total time for analysis in seconds   1200
Iterations for non-linear terms     *>1
Output type                [C,T]     C
Time between outputs in seconds      15
Wave angle at boundary in degrees    0
```

These parameters are also maintained in the default file. However, at each running of the program the recommended wave period, time increment and time between outputs are calculated for the grid database input and write over the previously stored parameters.

The time between outputs determines the point at which computations are interrupted and the user can specify the parameter to be contoured and output he/she requires. The contouring routine uses companion rows of data points as specified by the calculation control parameters generated in the early stages of the program. The contour line coordinates are determined using four point linear interpolation and the parameter values obtained from the temporary database generated by the program.

Termination of the program is determined by the total time for analysis or as selected by the user at the end of each output.

Chapter 5
COMPUTATIONAL MODEL FOR ON-SHORE WATER WAVE PROPAGATION

5.0 Introduction

The program LONGWAVE was developed assuming an open boundary condition based on the water depth at the boundary as it compares to the deep water depth for the wave period being examined. The shoaling coefficient was applied to the deep water wave height to obtain a wave height at the boundary. This method omits the effect of wave direction and the change in wave direction due to wave refraction. The prediction and analysis of the refraction pattern of the waves will provide the better open boundary values applied to the LONGWAVE program.

The refraction and resulting concentration/dispersion of wave energy is directly influenced by the geometry of the ocean floor and shoreline. In the past, analysis of this phenomenon was undertaken using a tedious and lengthy process whereby the engineer developed charts of the waveform as it travels over the ocean floor. The analysis was undertaken by constructing wave crest orthogonals or 'rays' starting in deep water regions and propagating these in the shoreward direction. Calculations were carried out in conjunction with the ray

construction at strategic locations to determine the required parameters. This was a time consuming process as lengthy calculations were also required prior to the drawing of the charts. This analysis has become less tedious with the increased use of computer technology in the engineering field and several programs are in daily use. These programs are usually relatively expensive and require the user to have access to large computer systems. The program MUNWAVE is a relatively inexpensive program which can be run on a modest personal computer based system.

5.1 Program Outline

The program outline and sequence for MUNWAVE stemmed from Crookshank (1975) which was written in Fortran and developed for use on a personal computer 'PC' based system. The logic flow and sequence of operation for the program MUNWAVE is presented in Fig. 5.1.

The most visible difference between MUNWAVE and the Crookshank (1975) program HYDRSDC is the sequence in which construction of orthogonals or 'rays' is conducted. MUNWAVE performs the necessary calculations at each time step for all rays instead of one at a time. This permitted better visualization of the wave front on the screen and more efficient detection of

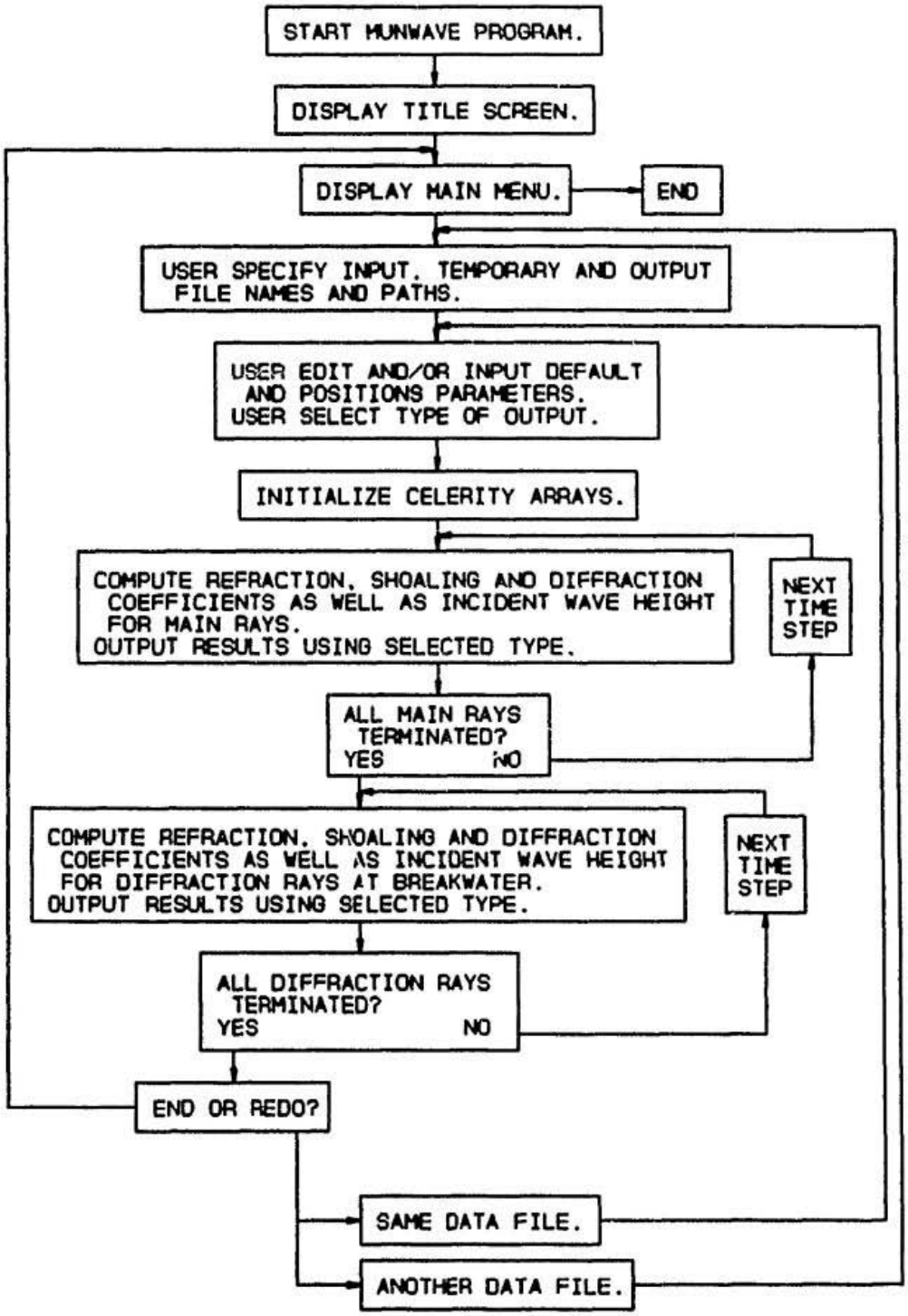

Fig. 5.1 - Logic flowchart for MUNWAVE software package.

caustics or 'ray crossings', a feature which was incorporated. The detection of a caustic situation causes the program to identify these locations and terminates the rays involved. The form of test conducted by the program is such that rays which are not in phase can still cross, situations which emulate similar occurrences in nature. The program develops a linear equation for each iteration on a pair of rays and checks to see if the point of intersection is within the bounds of each iteration on each ray.

Termination of breaking waves is accomplished by performing checks on the wave steepness and water depth. The breaking wave limit for wave steepness is determined by assuming that the ratio of wave height 'H' to wavelength 'L' (H/L) must be less than 0.142. The limit for water depth is provided by the ratio of wave height to water depth 'd' (H/D) being assumed to be 0.78 at breaking. The rays are terminated when these breaking limits are encountered during the iteration calculations.

The ability to plot and examine user defined wave height contours has been incorporated. A simple algorithm was developed utilizing the principle that a plane, identified by three points in space, has a line on its surface where each point along it is at the same vertical height or elevation. The assumption made for this algorithm was that the wave

height distribution is linear. The program uses a simple linear interpolation technique on two lines of a plane to determine the coordinates of the line of equal height.

The method to determine the refraction coefficient used by Crookshank (1975) was modified by developing a numerical technique using a backward difference technique to solve the differential equation for the ray separation factor 'ß' (see p.8, Eq. 2.3).

The method used by Crookshank (1975), specifying a reflection coefficient for the determination of diffraction coefficients, was found to be lacking in that the coefficient was in reality a transmission coefficient. This was discarded and the procedure modified to bring it in line with that used in the Shore Protection Manual (see SPM, 1984, pp.2-77 to 2-92). This procedure assumes a totally energy absorptive breakwater. The program MUNWAVE does not perform reflection calculations and only determines diffraction coefficients on those primary orthogonals which pass the breakwater line and all secondary orthogonals behind the breakwater.

The calculation performed by Crookshank (1975) to determine the shoaling coefficient, applied to the wave height, was for group wave celerity. This was replaced with a similar calculation for the celerity of a single wave as this is the

type of analysis undertaken by the program MUNWAVE.

5.2 Program Description

The program MUNWAVE was developed using the Microsoft, QuickBASIC, software development language. This language provided versatile file manipulation as well as enhanced visual graphics output in an immediate mode.

The overall program is segmented with the first being the initializing process whereby a storage device for temporary files is assigned as well as the location and retrieval of the data file to be used. The necessary data file consists of a grid with horizontal dimension equidistant in the horizontal and vertical directions. The water depth values at the specified grid points are to be positive with those on land negative in sign. The first line in the data file must contain the five control parameters in the order provided in Table 5.1 and separated by commas.

The data file can be constructed using a text editor or by using the program CADGRID. If a text editor is used the grid should be constructed with the bottom left grid point as the origin and proceeding upward. The data input routine requires that each row of data be continuous with no word wrap, line

feed or carriage return values between column entries. The MUNWAVE program requires that the depth data be in metres. Therefore it is important to enter the correct conversion factor as presented in Table 5.2.

Table 5.1 - First line in grid database file required by MUNWAVE.

PARAMETER POSITION	DESCRIPTION
1	Number of columns of data.
2	Number of rows of data.
3	Grid spacing in metres.
4	Current data indicator: 0 - No Current Data. 1 - X and Y Current Data. 2 - Magnitude and Direction.
5	Depth conversion factor to metres.

Table 5.2 - Depth conversion factors for various units to metres.

From	Factor
feet	0.3048
fathoms	1.8288
metres	1.0000

The CADGRID program produces a grid depth database which can be input to the MUNWAVE program with no or little

manipulation. However, the CADGRID program requires access to the CADKEY computer aided drafting package to previously digitize the necessary information.

The next step in operation is for the user to input the wave parameters required for further calculations and includes the following:

1. **Water Depth Increment/Decrement Factor:** this is required to simulate the change in water level due to such phenomenon as tides, storm surges, etc.

2. **Deep Water Wave Period:** the time it takes for a wave crest to travel past a specific point.

3. **Point Time Increment:** this parameter is used for the iteration process. The program calculates a recommended default value which is dependant on the wave period, wavelength and grid spacing.

4. **Number of Point Time Increments between Crest Marks:** the program provides a default value which permits the plotting at one minute intervals and is dependant on the Point Time Increment.

5. **Orthogonal 'Ray' Spacing:** distance between rays in grid space units, eg. 0.5 would be one half the grid space apart.

These parameters can be altered by the user at the start of each analysis run with recommended defaults displayed.

A position edit screen is provided to position the deep water wave crest, breakwater and specific points of interest. The wave crest must be provided for proper program execution. The X and Y cooordinates and water depth are displayed and updated with every move of the cursor. During location of the wave

crest the wave angle is also displayed during selection of the wave crest end position. The significance of the wave angle is presented in Fig. 5.2. However, the breakwater butt and tip positions need not be selected by placing them in the red zone of the edit screen. The program does not recognize the existence of points in this zone during calculations. Also provided are depth contours indicating the deep/transitional and transitional/shallow water limit depth contours related to the particular wave parameters input by the user for proper placement of the wave crest. Specific keyboard operations to accomplish this are displayed at times required.

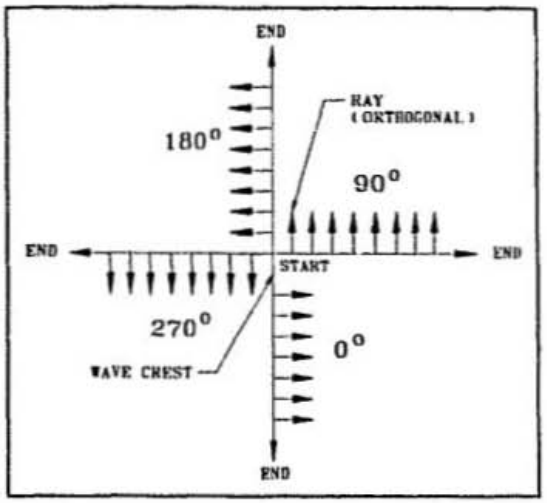

Fig. 5.2 - MUNWAVE wave angle, crest and ray relationship.

The final sequence in this segment is the user designation of type of output required. There are six combinations provided for screen, tabular and plotter output with the user specifying the relevant computer output ports when requested.

The next segment of the program is the number crunching and output portion using the information provided by the user

during execution of the initial segment and contained in the previously digitized water depth data file.

The first operation in this segment is construction of primary rays from the wave crest deep water location to the shoreline and breakwater. The construction of secondary radial orthogonals at the breakwater tip is undertaken after the primary orthogonals have terminated at the shore or edge of grid. The specific locations of interest can now be examined at the bottom of the output screen, if the user has specified screen graphic output mode. Each point is identified on the graphics display as the variables are selected for user examination. The final sequence or operation is the construction of wave height contours. The user inputs the value required using a range generated by the computer during calculations.

The user is prompted at the end of this segment to return to the beginning of the program and input another data file or re-use the same. The user can terminate the program at this point if he/she so wishes.

5.3 Output Types

The type of final output is variable and selected by the user

in the first segment of the program as mentioned previously. Output can be via certain combinations of computer screen, line printer and graphics plotter.

The graphical outputs show the shoreline; ocean floor contours (user selectable); wave ray paths; location of breakers; location of caustics; wave crests; wave height contours(user selectable). The colours vary depending on output device selected (see Table 5.3).

Table 5.3 - MUNWAVE output colour designations.

DISPLAY ITEM	COMPUTER SCREEN	PLOTTER OUTPUT
Background	white	n.a.
Shoreline	black	black
Water depth contours	green and light green	green
Wave ray paths	light blue	blue
Wave crest marks	high white	blue
Breaking wave locations	yellow	green
Ray caustics (crossings)	red	red
Wave heights	brown, light magenta and magenta	magenta
Grid point locations	blue dots	black border tics

The text output can be selected to be displayed on the screen

or printed on a line printer. The text output is in tabular format and gives the data for each time interval and all orthogonals (see Table 5.4).

Table 5.4 - MUNWAVE text output format.

COLUMN	DESCRIPTION
1	Time interval in seconds.
2	Ray (orthogonal) number.
3 & 4	X & Y grid coordinates in grid space units.
5	Interpolated water depth in feet.
6	Refraction coefficient.
7	Shoaling Coefficient.
8	Diffraction coefficient.
9	Incident wave height in feet.
10	wave angle in degrees.

Ray terminations due to shore, breaking and caustics are identified throughout the listing. The same output is provided for both the primary rays and secondary rays resulting from diffraction behind a breakwater. The specific location data is output at the end of the orthogonal listing. The hardcopy printout of the tabular data contains brief descriptions at the start of each of the tables. The grid size and initial wave parameters are output at the start of the primary output. Diffraction information such as initial wave height selected and orthogonal closest to the breakwater tip is output at the start of the secondary output.

5.4 System Requirements

The program was developed on a Hewlett Packard, Vectra (R), Personal Computer, with 40 megabyte hard drive, one megabyte extended memory, VGA graphics board and HP-IB plotter interface. The hardcopy graphics routines were developed using the Hewlett Packard Graphics Language (HP-GL) for an HP7475A eight pen plotter. The program should operate correctly on lesser systems. However, VGA graphics capability and HP-GL compatibility are necessary requirements.

Chapter 6
ANALYSES USING THE COMPUTER PROGRAMS

6.0 Introduction

The application of the computer programs CADGRID, LONGWAVE and MUNWAVE to the real world is a relatively easy process. The program CADGRID using a previously digitized database provides a means to develop grid databases of varying sizes from the same database. These grid databases can then be used as input for the LONGWAVE and MUNWAVE programs developed to study the response of a particular water basin to long period waves as well as the propagation of regular water waves.

The creation of graphical, modified, sort and subsequent grid databases using the CADGRID program for St. John's Bay and the SOHILCO harbour development is presented in this thesis.

The analysis of water wave propagation and basin response using the MUNWAVE and LONGWAVE computer software packages useing the grid databases is presented and discussed.

6.1 Digitized Database

The graphical databases required for the analyses were prepared using CADKEY and a GTCO digitizing pad to digitize the hydrographic chart for The Approaches to St. John's as published by the Canadian Hydrographic Service, Department of The Environment, Ottawa, Canada (see Fig. 6.1). This database file, titled STAPPRCH.PRT, was the main graphical database used to supply the subsequent graphical databases required. The St. John's Bay database file, titled SJBAYROT.PRT, was created using an exerpt from the main database and changing the orientation to provide a vertical boundary at the mouth of the bay (see Fig. 6.2). The Freshwater Bay, SOHILCO harbour development graphical database file, titled SOHILROT.PRT, (see Fig. 6.3) was created using an exerpt from the main graphical database and modified to reflect the proposed harbour improvements. This database was then oriented to provide a vertical boundary at the entrance to the harbour (see Fig. 6.4).

The approximate disk storage required for the graphical databases created is presented in Table 6.1.

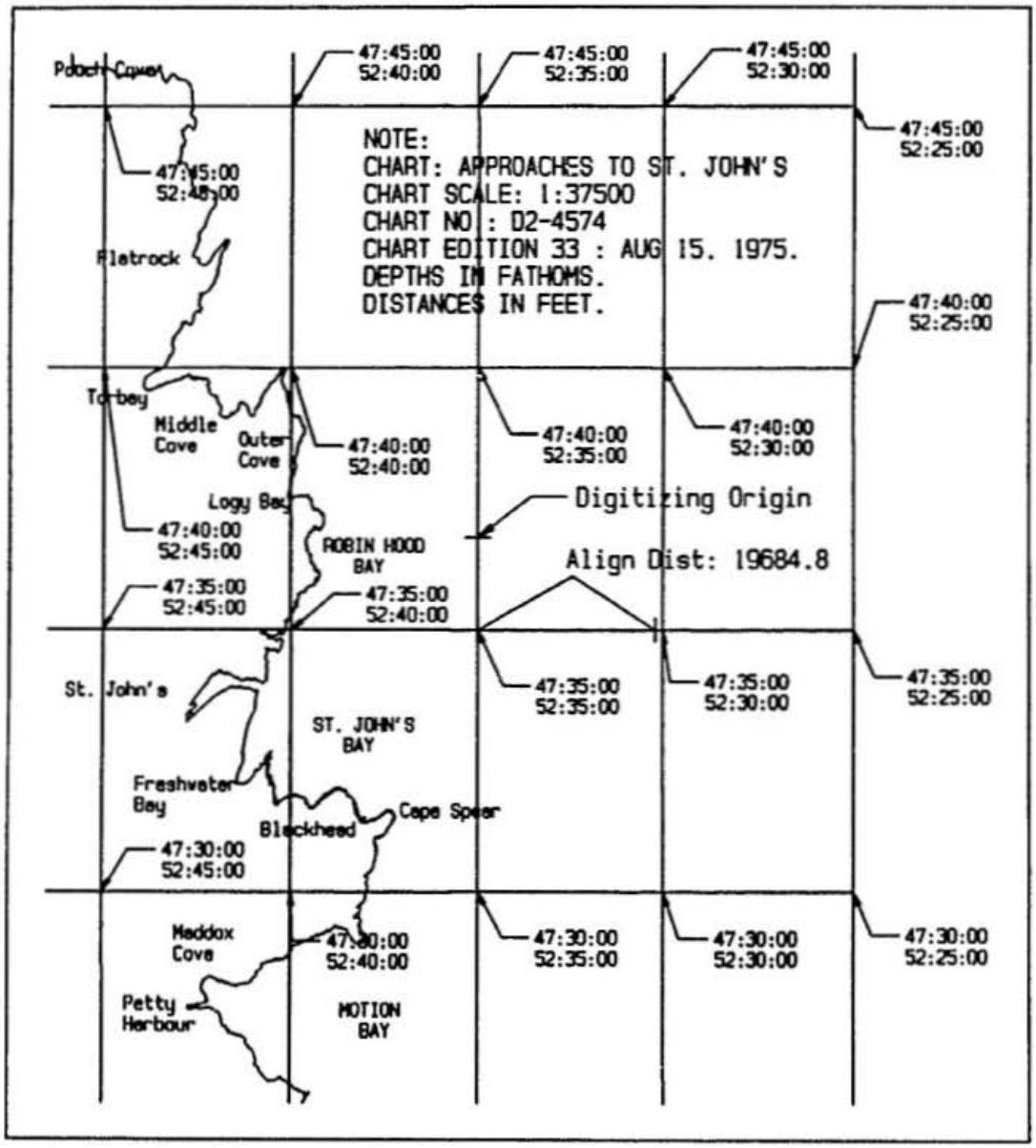

Fig. 6.1 - Graphical database for the Approaches to St. John's.

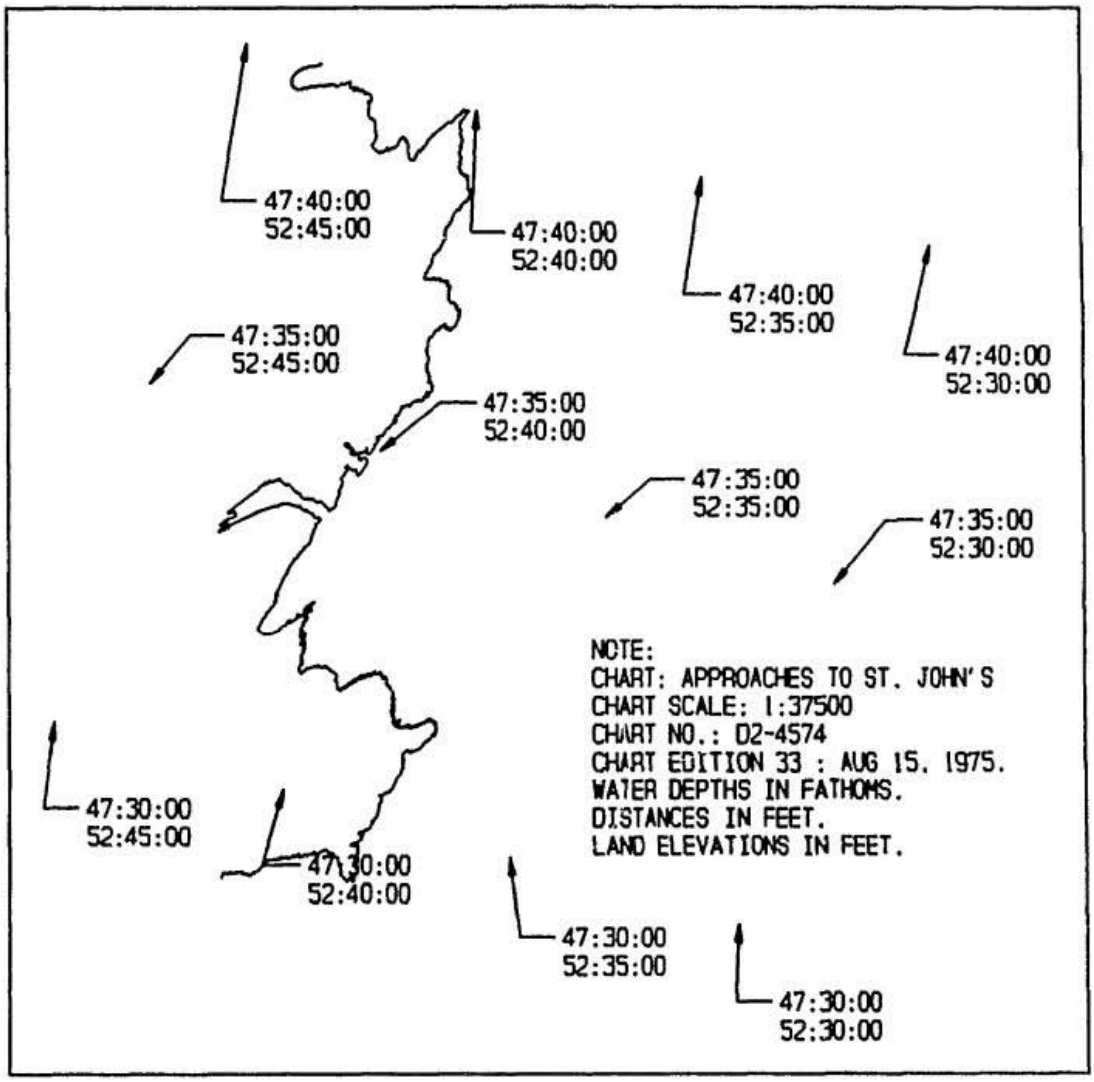

Fig. 6.2 - Graphical database for St. John's Bay extracted from Approaches to St. John's database.

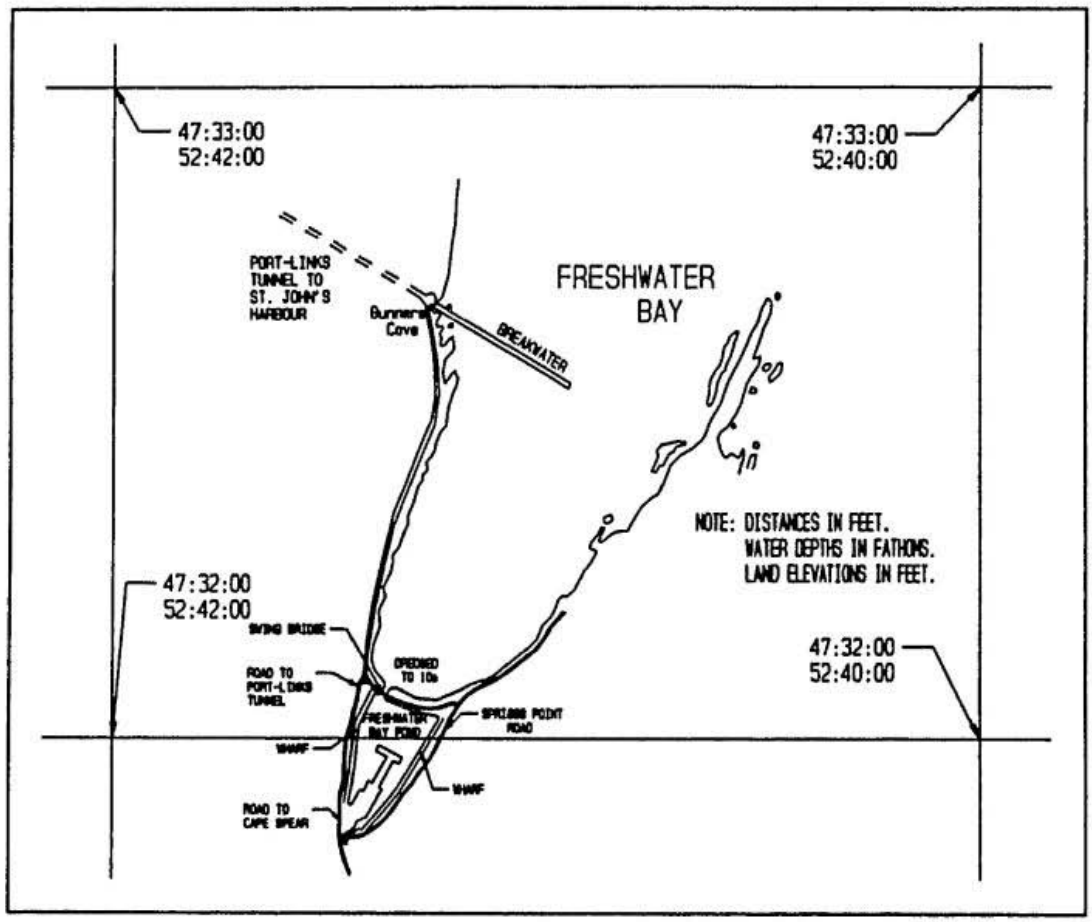

Fig. 6.3 - Database for Freshwater Bay, SOHILCO Harbour Development extracted form St. John's Bay database and modified to show harbour improvements.

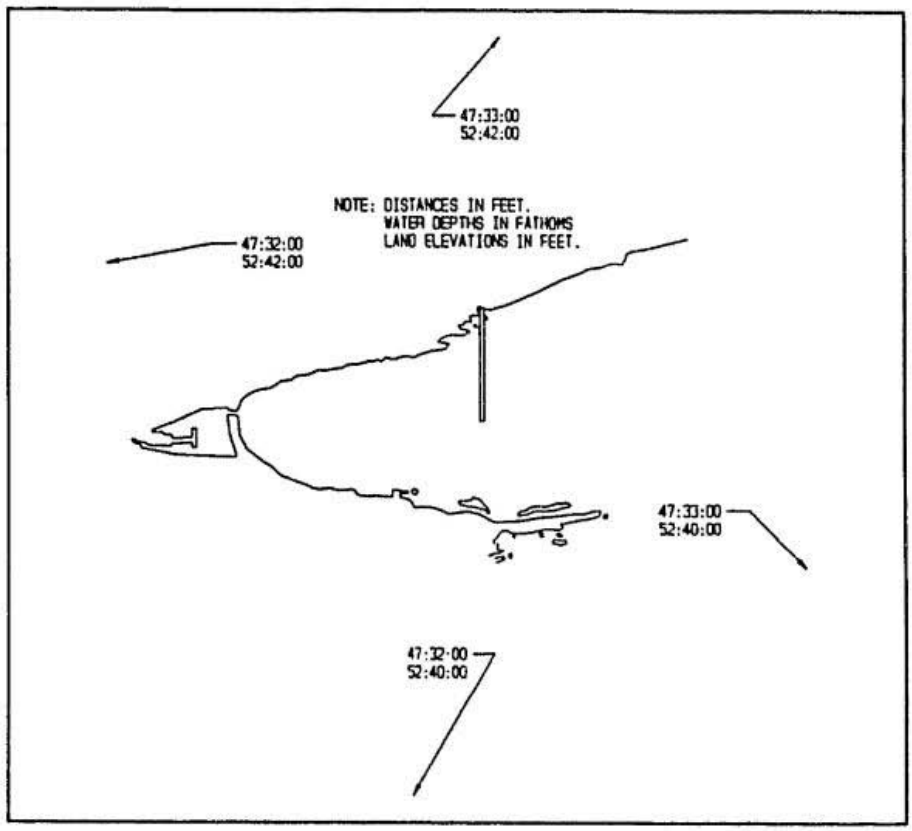

Fig. 6.4 - Final graphical database for Freshwater Bay, SOHILCO Harbour Development.

Table 6.1 - Digitized database file sizes.

FILENAME	SIZE KBYTES
STAPPRCH.PRT	297
SJBAYROT.PRT	297
SOHILROT.PRT	139

6.2 Modified and Sort Database Development

The output files in the form of ASCII text files were then obtained using the CADL output option of the CADKEY software package. These output files were then used as input for the CADGRID program and reduced sorted versions of the databases produced and stored for future use.

Table 6.2 - CADKEY output (.CDL), reduced (.CAD) and sort (.BLK) file sizes in bytes.

BASE FILENAME	'.CDL'	'.CAD'	'.BLK'
SJBAYROT	331464	256944	1267
SOHILROT	128801	87024	1226

6.3 Grid Database Development

The grid database created to study the propagation of water waves into St. John's Bay was developed using the SJBAYROT.CAD and companion SJBAYROT.BLK sort databases as input for the CADGRID program. Two databases were created for the analysis of St. John's Bay, titled SJBY200A.DAT and SJBY100.DAT, having grid space dimensions of 200 and 100 metres respectively. The database SJBY200A.DAT was used with the MUNWAVE program and the SJBY100.DAT database was used with the LONGWAVE program.

The grid databases for the study of the SOHILCO development were developed using the SOHILROT.CAD and companion SOHILROT.BLK sort databases. These databases were used to examine the response behaviour of the proposed harbour to long period waves. Preliminary estimations were made to determine the fundamental response period of an idealized harbour with geometry similar to that encountered in the SOHILCO development. The overall dimensions of the water basins created by the proposed development were obtained from the SOHILROT.PRT graphical database (see Fig. 6.5).

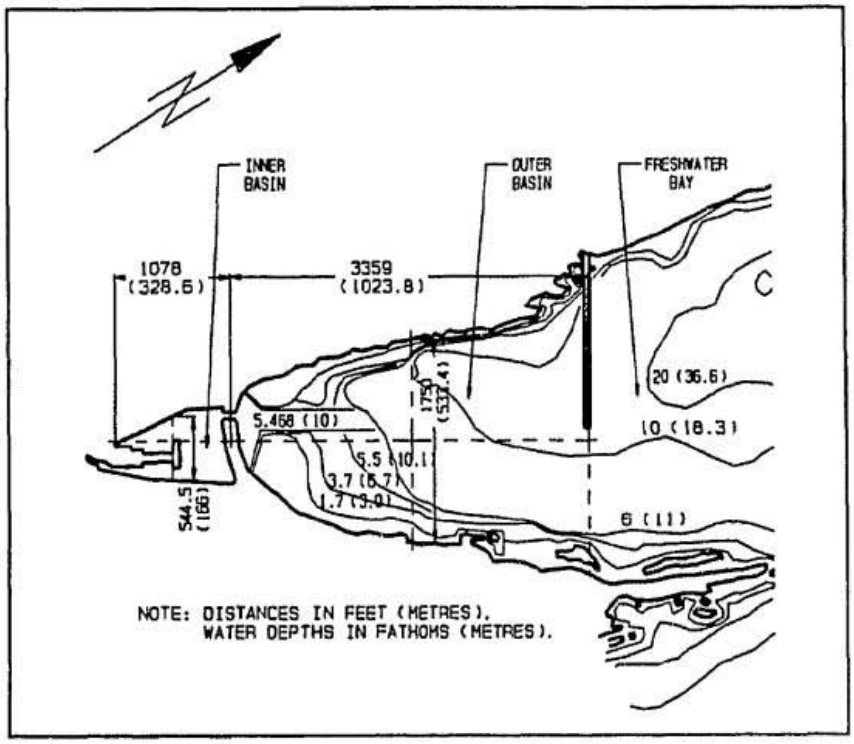

Fig. 6.5 - SOHILCO Harbour Development, depth contours and dimensions.

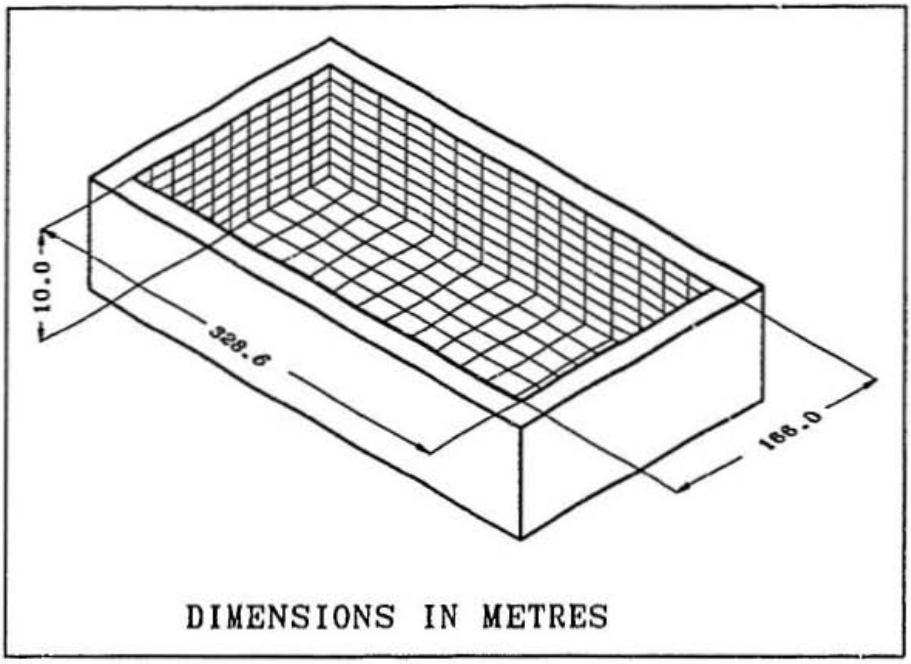

Fig. 6.6 - Idealized inner basin of SOHILCO Harbour development (metres).

The inner water basin created by the development was idealized as presented in Fig. 6.6. The fundamental response period was determined using (Dean and Dalrymple, 1984, p.149),

$$T_F = \frac{2L}{\sqrt{gh}} = \frac{2L}{\sqrt{(9.81)(10)}}$$

$$\approx \underline{0.20L}$$

where L is the length of the water basin in the direction of interest. Therefore, the periods for the inner basin are T_{FEW}=33.2 and T_{FNS}=65.7 seconds for the east-west and north-south directions respectively.

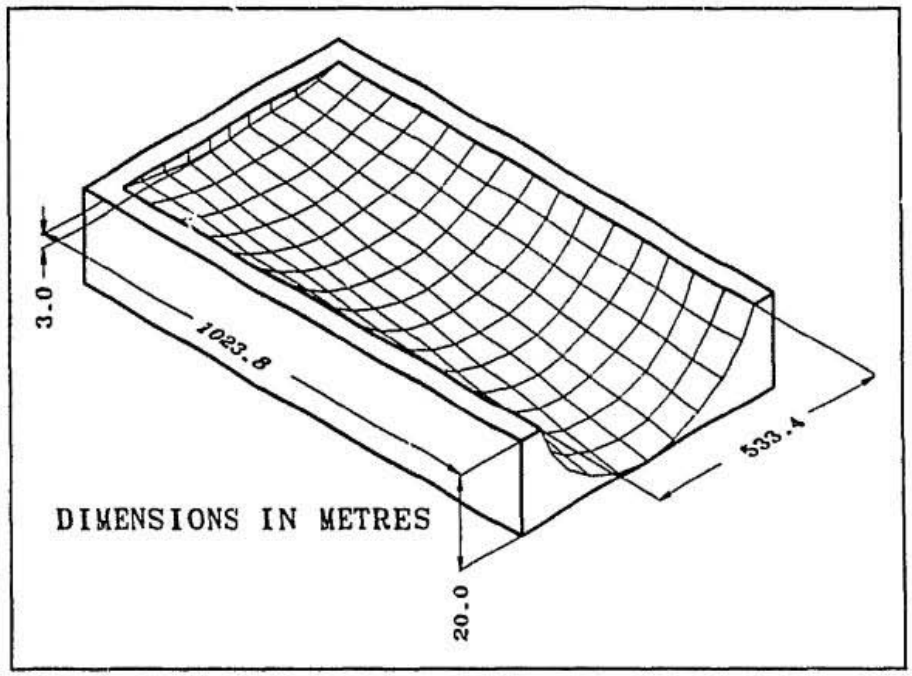

Fig. 6.7 - Idealized outer basin of SOHILCO Harbour Development (metres).

Similarly, the outer basin was idealized as having the cross sections as presented in Fig. 6.7. The equations for the fundamental response period differs in each direction (Dean and Dalrymple, 1985, pp.148-149).

The water basin was idealized as having a parabolic cross section in the east-west direction with an average depth of ten (10) metres in the north-south direction and triangular in the north-south direction with a maximum depth of twenty (20) metres.

The subsequent fundamental response period in the east-west , T_{FEW}, direction is estimated to be,

$$T_{FEW} = 1.110 \frac{2L}{\sqrt{gh}} = \frac{(1.110)(2)(533.4)}{\sqrt{(9.81)(10)}} = \underline{119.6}$$

and in the north-south direction, T_{FNS}, to be

$$T_{FNS} = 1.640 \frac{2L}{\sqrt{gh}} = \frac{(1.640)(2)(1023.8)}{\sqrt{(9.81)(20)}} = \underline{239.7}$$

The minimum grid spacings required to meet the computational resolution required by the program LONGWAVE for each of the inner and outer basins are presented in Table 6.3.

Table 6.3 - Grid spacing estimates for SOHILCO grid database development.

	T_{FEW} (SECS)	T_{FNS} (SECS)	DEPTH (M)	Δs_{EW} (M)	Δs_{NS} (M)
INNER BASIN	33.2	65.7	10	11.0	21.7
OUTER BASIN	119.6	239.7	20	55.8	111.9

The spacing selected for the creation of the grid databases for the inner and outer basin response analysis are ten (10) and thirty (30) metres respectively. These spacings conformed with the minimums required and permitted proper geometric representation of the water basins.

The file names and relative sizes of the grid databases prepared for the analyses are presented in Table 6.4.

Table 6.4 - Grid databases developed using CADGRID.

FILENAME	ROWS/COLUMNS	SIZE (bytes)
SJBY100 .DAT	88/57	45340
SJBY200A.DAT	81/76	55591
INNER010.DAT	22/43	8640
OUTER030.DAT	29/49	12923

6.4 Analysis using MUNWAVE

The analysis of water wave propagation from deep water into St. John's Bay was accomplished using the previously developed grid database titled SJBY200A.DAT as input for the program MUNWAVE. This analysis provided information as to the refraction coefficient encountered at the entrance of Freshwater Bay where the SOHILCO development is to be undertaken. The defaults were maintained constant throughout the refraction analysis (see Table 6.5). The coordinates for the specific points of interest were also kept constant (see Table 6.6).

Table 6.5 - MUNWAVE default parameter values.

DEFAULT PARAMETER	VALUE
Change in water depth (metre)	0
Wave period (seconds)	10
Point time increment	1
Plot crest every N time increments	60
Orthogonal spacing in grid space units	1
Deep water wave height (metre)	1

Table 6.6 - Specific point of interest coordinates in grid space units.

POINT	X	Y
1	8.51	31.51
2	10.46	34.12
3	20.23	37.59
4	15.02	36.72
5	33.25	37.59

The deep water wave crest position and angle was altered by ten degrees (10^{o}) starting at 90^{o} through 240^{o} (see Fig. A.1 to A.17, Appendix A). The combined refraction and shoaling coefficient at each specific point of interest for each wave angle was recorded (see Table 6.7).

The wave angle providing the maximum concentration of wave

energy at the mouth of Freshwater Bay appeared to be two hundred ten (210) degrees as indicated in Figs. A.12 to A.14 inclusive (see Appendix A). Further analysis was undertaken using this wave angle and altering the wave period (see Table 6.8 and Figs. A.18 to A.26, Appendix A).

These analyses were accomplished using a relatively large ray spacing which results in the recording of suspect refraction and shoaling coefficients as indicated in the two tables. A finer grid spacing would bring the wave orthogonals closer to the points of interest which in turn would also increase the computational time required.

A similar coefficient can be obtained using the LONGWAVE program and outputting the 'basin response' parameter or the ratio of incident to deep water surface elevations in the form of contour plots.

Table 6.7 - Combined refraction and shoaling coefficients for specific point of interest and deep water wave angle with a wave period of ten (10) seconds for the St. John's Bay analysis.

DEEP WATER ANGLE	COMBINED REFRACTION AND SHOALING COEFFICIENT, $K_r K_s$, FOR EACH POINT OF INTEREST				
	1	2	3	4	5
90	*0.146	**0.226**	*0.325	*0.385	*0.372
100	*0.324	*0.324	*0.276	*0.303	*0.462
110	*0.266	*0.252	*0.259	*0.284	**0.707**
120	*0.147	*0.165	**0.196**	*0.595	**0.992**
130	**0.065**	**0.151**	*0.239	**0.646**	**0.999**
140	*0.315	*0.315	*0.635	**0.900**	**0.999**
150	*0.505	**0.604**	**0.751**	**0.982**	**0.999**
160	*0.307	*0.804	**0.937**	**0.985**	**0.999**
170	*0.582	**0.930**	**0.959**	**0.990**	**0.999**
180	*0.589	**0.833**	**0.973**	**0.990**	**0.999**
190	**0.421**	**0.870**	**0.911**	**0.989**	**0.999**
200	*0.473	**0.743**	**0.930**	**0.989**	**0.999**
210	*0.345	**0.130**	**0.769**	**0.990**	**0.999**
220	*1.586	*1.652	*2.820	**0.990**	**0.999**
230	*0.557	*0.383	*0.337	**0.990**	**0.999**
240	*5.068	*5.068	**0.526**	**0.733**	**0.999**
250	*0.161	*0.174	*0.308	*0.317	**0.837**

(*) - indicates suspect values due to large distance between the point and nearest wave orthogonal point time increment. (see Figs. A.1 to A.17 in Appendix A)

Table 6.8 - Analysis with constant wave angle of 210° and varying wave period.

WAVE PERIOD (SECS)	COMBINED REFRACTION AND SHOALING COEFFICIENT, K_rK_s, FOR EACH POINT OF INTEREST				
	1	2	3	4	5
5	**0.503**	**0.995**	**0.999**	**1.000**	*1.000
15	*0.221	**0.242**	**0.302**	**1.109**	*0.887
20	*5.030	*1.083	**0.392**	**1.309**	*0.808
30	*1.985	*0.722	*0.047	**4.463**	*0.744
40	*0.952	*0.952	*0.575	**3.345**	*0.796
50	*1.512	*1.512	*0.658	**11.718**	*0.865
70	*0.484	*0.519	*0.810	**16.079**	*1.005
90	*0.486	*0.486	*0.895	**10.646**	*1.134
120	*1.165	*1.165	*1.097	**22.340**	*1.282

(*) - indicates suspect values due to large distance between the point and nearest wave orthogonal point time increment (see Fig. A.18 to A.26, Appendix A).

6.5 Analysis using LONGWAVE

The program LONGWAVE produces various forms of contour plots at user specified time intervals for a particular incident wave period at the entrance to a basin. A suitable data file for St. John's Bay, titled SJBY100.DAT, having a grid spacing of one hundred (100) metres, was developed as previously described and used as input for the LONGWAVE program. The basin response parameter contour and vector plots produced for a wave period of one hundred twenty (120) seconds are

presented in Appendix B. The plots were produced at fifteen (15) second time intervals sequentially through to three hundred sixty (360) seconds or three (3) wave lengths. The contour plots are self explanatory and trace the value of the response parameter over the period (see Appendix B). The computational sequence was terminated after three hundred sixty (360) seconds as this was felt to provide the necessary information for prediction of the response parameter at the points as specified in the analysis using the MUNWAVE program.

The overall response of the Freshwater Bay water basin can be observed using plots generated from the previous analysis of St. John's Bay basin by comparing the plots in Appendix B. However, information as to specific areas inside Freshwater Bay where potential problems might occur cannot be obtained with any degree of reliability from these plots. The analysis using finer grids developed for the Freshwater Bay area would provide a means to examine local disturbances due to encroaching waves.

Therefore, the two (2) grid database, OUTER030.DAT and INNER010.DAT, developed previously were used and plots obtained using the 120 second wave period for the open boundary condition at each grid.

The plots resulting from the analysis using the OUTER030.DAT

grid data file provide the means to examine the response of the SOHILCO development outer basin, created to protect the inner basin, to encroaching waves (see Appendix C). The plots resulting from the use of the INNER010.DAT grid database provide the means to examine the response of the inner basin to encroaching waves from the outer basin (see Appendix D).

Chapter 7
Discussion and Conclusions

7.0 Discussion

The analysis of wave propogation over varying bottom photography into water basins of irregular geometry requires the input of a large amount of physical data in the form of water depths or soundings. The data is readily available in the form of hydrographic or fair charts. The process of manually creating an equally spaced depth grid and producing the data in a suitable form for analyses is typically very tedious. The problem is further compounded if a number of grids of various spacings are required of the same area. The CADGRID program interfaces with a CADD package which can be used to digitize the data directly from the source chart producing a single database of information which can be used over and over. CADGRID can then be used to develop as many grids of any size required for the analysis of a particular area. These data grids are used as input for the MUNWAVE and LONGWAVE programs directly after production.

The program MUNWAVE can be used to examine the propogation of deep water waves on shore. The program is limited in the size of wave period used for the analyses. This is directly related to the average depth contained in the data file and the

Courant number of one (1). The constraints of linear wave theory have been incorporated which also limit the size of wave period used in any analysis.

The initial analysis of St. John's Bay using MUNWAVE was undertaken using an input wave period of ten (10) seconds to determine the wave direction which produces the most severe wave effects in the Freshwater Bay area (see Fig. A.1 to A.17). The direction was observed to be coincident with a wave angle of 210° based on the observation of wave ray spacings in the area of Freshwater Bay using Figs. A.12, A.13 and A.14.

Further analysis of St. John's Bay using MUNWAVE was undertaken to observe the effects of increasing wave period on wave propagation into Freshwater Bay using the wave angle of 210° (see Fig. A.18 to A.26). These outputs show that the long period waves shoal at a deeper depth off shore and the presence of caustics was also observed. The wide dispersion of wave rays gave rise to suspect readings in the Freshwater Bay area as recorded in Table 6.8. The problem tended to increase as the wave period increased and could be overcome by using a finer ray spacing on a trial and error basis.

The Program LONGWAVE is a better tool for examining the propagation of long period waves into a water basin. The program can also be used to examine the particular response

pattern of a water basin and produce contour plots of a response parameter equivalent to the combined refraction/shoaling coefficient as produced by the MUNWAVE program.

The LONGWAVE plots of St. John's Bay agree with the plots produced by the MUNWAVE program qualitatively. The areas of wave concentration on shore predicted by the refraction analysis are also the areas where high response parameters were observed in the outputs from the LONGWAVE program (see Appendices A & B).

The LONGWAVE plots produced for the outer basin of the SOHILCO Harbour Development show the response parameters and areas of problem which might occur upon completion. The mode two (2) response of the outer basin in the north-south, 'X', direction was found to be approximately one hundred twenty (120) seconds (compare Figs. C.4, C.7, C.11, C.13 & C.15) which was also the east-west, 'Y', direction mode one (1) response period (compare Figs. C.20 & C.24). A comparison of Figs C.1 to C.26 reveals the area with maximum response behaviour to be at the east side, lower 'Y' direction, of the outer basin.

The comparison of the plots produced for the inner basin indicate the first or flushing mode of the basin to be in the sixty (60) second range (compare Figs D.4, D.5, D.8, D.9,

D.17, D.18). The maximum effect occurs at the small craft moorings on the east and west side of the central pier where the 120 second period wave produces a sloshing effect between the two mooring locations or sub-basins.

7.1 Conclusion

The computer programs CADGRID, MUNWAVE and LONGWAVE presented in this thesis were developed with the aim to provide the coastal engineer with tools to ease the process of data manipulation and computation for typically simple coastal wave analyses. The analyses of long period wave phenomenon has been stressed in the thesis. However, the programs presented can be used for shorter period wave analyses with very few modifications.

The programs are meant to be tools for the coastal engineer and cannot take the place of the engineer's experience. The programs provide a plethora of data in a relatively short period of time when compared with the manual methods. The data output provides the coastal engineer with the necesary information to design new coastal structures as well as analyze existing facilities or improvements.

The full capabilities of the software packages were not

explained in this thesis. The description and usage provided was for the analysis of water basin response to long period water waves. The full capabilities of the programs can only be appreciated by the coastal engineer who, in the past, has been faced with the tedious process of manual analysis of ocean wave propagation.

The types of output available are suitable for written reports as well as demonstration tools in the education field.

The necessary verification of the software packages using other programs, physical models or field data was not conducted due to time and financial constraints.

References

Baker, R. (1989). Physical model laws for the study of harbour response to long period offshore waves entering a harbour (harbour seiching), Modelling and Similarity Techniques Course, Graduate Paper, Memorial University of Newfoundland, St. John's, Newfoundland.

Baker, R. and Allen, J.H. (1990). Water wave refraction & diffraction program MUNWAVE, Centre for Computer Aided Engineering, Faculty of Engineering, Memorial University of Newfoundland, St. John's, Newfoundland.

Barthel, V. and Funke, E.R. (1984). Estimates of long waves in the Weser Estuary, Proceedings of the 19th Coastal Engineering Conference, ASCE, September 3-7, Houston, Texas, vol.1, ch.53, pp.782-797.

Biesel, F. (1954). The similitude of scale models for the study of seiches in harbours, Proceedings of the 5th Coastal Engineering Conference, ed. J.W. Johnson, September, Grenoble, France, Council on Wave Research, The Engineering Foundation, Engineering Field Station, University of California, Richmond, California, ch.9, pp.95-118.

Berenguer, I., Madsen, P.A., Rubjerg, M. and Kej, A. (1986). Mathematical and physical wave disturbance modelling complimentary tools, Proceedings of the 20th Coastal Engineering Conference, ASCE, November 9-14, Taipei, Taiwan, vol.1, ch.3, pp.27-41.

Botes, W.A.M., Russell, K.S. and Huizinga, P. (1984). Model harbour seiching compared to prototype data, Proceedings of the 19th Coastal Engineering Conference, ASCE, September 3-7, Houston, Texas, vol.1, ch.57, pp.846-857.

Bowers, E.C. (1982). The modelling of waves and their effects in harbours, Hydraulic Modelling in Maritime Engineering, Proceedings of the Conference organized by the Institution of Civil Engineers, October 13-14, London, England, Thomas Telford Ltd., London, England, pp.121-127.

Cadkey (1989). Computer Aided Engineering Library, Version 3.5, vols.1 and 2, Cadkey Inc., Manchester, Connecticut.

Chen, H.S. (1981). A finite element model of storm surge and circulation for Chesapeake Bay and its Atlantic nearshore, Oceans 81 Conference, IEEE, September 16-18, Boston, Massachusetts, vol.2, pp.815-819.

Coeffe, Y., Dal Secco, S., Esposito, P. and Latteaux, B. (1984). A finite element method for storm surge and tidal computation, Proceedings of the 19th Coastal Engineering Conference, ASCE, September 3-7, Houston, Texas, vol.2, ch.82, pp.1209-1224.

Crookshank, H.L. (1975). Numerical calculation of refraction diagrams - program HYDRSDC, Hydraulics Laboratory Report HY-88, National Research Council of Canada.

Dean, R.G, and Dalrymple, R.A. (1984). Water wave mechanics for engineers and scientists, Prentice-Hall, Inc., Englewood Cliffs, New Jersey.

Douglas, J.F., Gasiorek, J.M. and Swaffield, J.A. (1979). Fluid mechanics, Copp Clark Pitman, Toronto.

Dronkers, J.J. (1972). The schematization for tidal computations in case of variable bottom shape, Proceedings of the 13th Coastal Engineering Conference, ASCE, July 10-14, Vancouver, B.C., vol.3, ch.136, pp.2379-2396.

Easton, A.K. (1984). Modelling seiches, Computational techniques & Applications CTAC-83, eds. J. Noye and C. Fletcher, Elsevier Science Publishers B.V. (North-Holland) pp.449-460.

Ebersole, B.A.(1985). Refraction-diffraction model for linear water waves, Journal of Waterway, Port, Coastal and Ocean Engineering, November, ASCE, vol.111, no.6, pp.939-953.

Falconer, R.A. and Mardapitta-Hadjipandeli, L. (1986). Application of a nested numerical model to idealized rectangular harbours, Proceedings of the 20th Coastal Engineering Conference, ASCE, November 9-14, Taipei, Taiwan, vol.1, ch.14, pp.176-192.

Gaillard, P. (1982). Numerical calculation of seiche motions in harbours of arbitrary shape, Proceedings of the 18th Coastal Engineering Conference, ASCE, November 14-19, Capetown, South Africa, vol.1, ch.11, pp.172-191.

Headland, J.R. and Chu, H.-L. (1984). A numerical model for refraction of linear and cnoidal waves, Proceedings of the 19th Coastal Engineering Conference, ASCE, September 3-7, Houston Texas, vol.2, ch.76, pp.1119-1131.

Hou, H.-S. (1985). Model investigation of wave-induced oscillations in Taichung Harbour, Taiwan, R.O.C., International Conference on Numerical and Hydraulic Modelling of Ports and Harbours, BHRA, April 23-25, Birmingham, England, Paper M1, pp.331-338.

Houston, J.R. (1977). Los Angeles Harbor and Long Beach Harbor: finite element numerical model of harbor resonance, Ports '77, 4th Annual Symposium of the Waterway, Port, Coastal and Ocean Division of ASCE, March 9-11, Long Beach, California, vol.1, pp.119-137.

HP-7475A (1983). Interfacing and programming manual, Hewlett-Packard Company, San Diego, California.

Hsaio, S.V. and Shemdin, O.H. (1978). Bottom dissipation in finite-depth water waves, Proceedings of the 16th Coastal Engineering Conference, ASCE, August 27 to September 3, Hamburg, Germany, vol.1, ch.24, pp.434-448.

International Association for Hydraulic Research (IAHR) Working Group on Wave Generation and Analysis (1989). List of sea-state parameters, Journal of Waterway, Port, Coastal, and Ocean Engineering, ASCE, vol.115, no.6, pp.793-808.

Ismail, N.M. (1984). Interaction of non-uniform currents and surface waves, Proceedings of the 19th Coastal Engineering Conference, ASCE, September 3-7, Houston, Texas, vol.1, ch.73, pp.1073-1089.

Jonsson, I.G. and Christoffersen, J.B. (1984). Current depth refraction of regular waves, Proceedings of the 19th Coastal Engineering Conference, ASCE, September 3-7, Houston, Texas, vol.2, ch.75, pp.1103-1117.

Kohlhase, S. and Dette, H.H. (1980). Models of wave induced phenomena, Hydraulic Modelling, ed. H. Kobas, International Association for Hydraulic Research and German Association for Water Resources and Land Improvement, Verlag Paul Parey, Hamburg, Germany, ch.9, pp.165-309.

Kohlhase, S., Daemrich, K.-F., Berger, U., Tautenhain, E. and Burkhardt, O. (1978). A Numerical approach for the determination of the wave height distribution in a harbour, Proceedings of the 16th Coastal Engineering Conference, ASCE, August 27 to September 3, Hamburg, Germany, vol.1, ch.37, pp.664-676.

Lee, L-L and Raichlen, F. (1970). Resonance in harbours of arbitrary shape, Proceedings of the 12th Coastal Engineering Conference, ASCE, September 13-18, Washington D.C., vol.3, ch.131, pp. 2163-2180.

Leendertse, J.J. (1967). Aspects of a computational model for long-period water-wave propagation, Memorandum RM-5294-PR, The Rand Corporation, Santa Monica, California.

Leendertse, J.J. (1968). Use of a computational model for two-dimensional tidal flow, Proceedings of the 11th Coastal Engineering Conference, ASCE, September, London, England, vol.2, ch.90, pp.1403-1420.

Leendertse, J.J. (1970). A water-quality simulation model for well- mixed estuaries and coastal seas: Volume I, Principles of computation, Memorandum RM-6230-RC, The Rand Corporation, Santa Monica, California.

List, J.H. (1986). Wave groupiness as a source of nearshore long waves, Proceedings of the 20th Coastal Engineering Conference, ASCE, November 9-14, Taipei, Taiwan, vol.1, ch.38, pp.497-511.

Liu, P.L.-F. and Tsay, T.-K. (1983). Water-wave motion around a breakwater on a slowly varying topography, Proceedings of Coastal Structures '83, ASCE, March 9-11, Arlington, Virginia, pp. 974-987.

Liu, P.L.-F. and Tsay, T.-K. (1985). Numerical prediction of wave transformation, Journal of Waterway, Port, Coastal and Ocean Engineering, September, ASCE, vol.111, no.5, pp.843-855.

Mansaard, E.P.D. and Barthel, V. (1984). Shoaling properties of bounded long waves, Proceedings of the 19th Coastal Engineering Conference, ASCE, September 3-7, Houston, Texas, vol.1, ch.54, pp.798-814.

Olliver, G.F. (1982). Harbours: the value of physical modelling, Hydraulic Modelling in Maritime Engineering, Proceedings of the Conference organized by the Institution of Civil Engineers, October 13-14, 1981, London, England, pp.129-133.

Ottesen Hansen, N.-E., Sand, E.S., Lundgren, H., Sorensen, T. and Gravesen, H. (1980). Correct reproduction of group-induced long waves, Proceedings of the 17th Coastal Engineering Conference, ASCE, March 23-28, Sidney, Australia, vol.1, ch.48, pp.784-800.

Panchang, V.G., Cushmin-Roisin, B. and Pearce, B.R. (1988). Combined refraction-diffraction of short-waves in large coastal regions, Coastal Engineering, Elsevier Science Publishers B.V., Amsterdam, The Netherlands, no.12, pp.133-156.

Panchang, V.G., Wei, G., Cushman-Roisin, B. and Pearce, B.R. (1990). Solution of the mild-slope wave problem by iteration, Applied Ocean Research, to appear.

Peregrine, D.H. (1986). Approximate descriptions of the focusing of water waves, Proceedings of the 20th Coastal Engineering Conference, ASCE, November 9-14, Taipei, Taiwan, vol.1, ch.51, pp.675-685.

Pipkin, B.W., Gorsline, D.S., Casey, R.E. and Hammond, D.E. (1987). Laboratory exercises in oceanography, 2nd Edition, W.H. Freeman and Company, New York.

Raichlen, F. and Lee, J.J. (1984). The interaction of small and finite amplitude long waves and currents, Proceedings of the 19th Coastal Engineering Conference, ASCE, September 3-7, Houston, Texas, vol.1, ch.67, pp.983-998.

Raney, D.C. (1977). Los Angeles Harbour and Long Beach Harbor: A numerical model for tidal circulation, Ports '77, 4th Annual Symposium of the Waterway, Port, Coastal and Ocean Division of ASCE, Long Beach, California, March 9-11, vol.1, pp.85-100.

Seelig, W.N. (1983). Wave reflection from coastal structures, Proceedings of Coastal Structures '83, ASCE, March 9-11,Arlington, Virginia, pp.961-973.

Sharp, J.J. (1981). Hydraulic modelling, Butterworth & Co., England.

Shemdin, O.H. and Forney, R.M. (1970). Tidal motion in bays, Proceedings of the 12th Coastal Engineering Conference, ASCE, September 13-18, Washington, D.C., vol.3, ch.134, pp.2225-2242.

Skovgaard, O., Behrendt, L. and Jonsson, I.G. (1984). A finite element model for wind wave diffraction, Proceedings of the 19th Coastal Engineering Conference, ASCE, September 3-7, Houston, Texas, vol.1, ch.74, pp.1090-1102.

Southgate, H.N. (1984). Techniques of ray averaging, International Journal for Numerical Methods in Fluids, John Wiley & Sons Ltd., Toronto, vol.4, pp.725-747.

SPM (1984). See U.S. Army Corps of Engineers.

Sundermann, J. and Vollmers, H. (1972). Mathematical and hydraulic models of tidal waves, Proceedings of the 13th Coastal Engineering Conference, ASCE, July 10-14, Vancouver, B.C., vol.3, ch.139, pp.2423-2437.

Thacker, W.C. (1978). Comparison of finite-element and finite-difference schemes. part II: two-dimensional gravity wave motion, Journal of Physical Oceanography, American Meteorological Society, Boston, July, vol.8, pp.680-689.

U.S. Army Corps of Engineers (1984). Shore protection manual (SPM), 4th edition, U.S. Government Printing Office, Washington, D.C.

Vis, F.C., Mol, A., Rita, M.M. and Deelan, C. (1985). Long waves and harbour design, International Conference on Numerical and Hydraulic Modelling of Ports and Harbours, BHRA, April 23-25, Birmingham, England, Paper J1, pp.249-256.

Wang, S-Y. and Christensen, B.A. (1986). Friction in hurricane-induced surges, Proceedings of the 20th Coastal Engineering Conference, ASCE, November 9-14, Taipei, Taiwan, vol.1, ch.62, pp.822-836.

Whalin R.W. and Chatham, C.E. (1974). Design of distorted harbor wave models, Proceedings of the 14th Coastal Engineering Conference, ASCE, June 24-28, Copenhagen, Denmark, vol.3, ch. 122, pp.2102-2121.

Wiegel, R.L. (1964). Oceanographical Engineering, Harbour oscillations, Prentice-Hall, Inc., Englewood Cliffs, New Jersey, sec. 4, ch. 5, pp.115-124.

Wilson, B.W., Hendricksen, J.A. and Jen, J. (1972). Surge in the southeast basin, Long Beach Harbor, Calif., Proceedings of the 13th Coastal Engineering Conference, ASCE, July 10-14, Vancouver, B.C., vol.3, ch.152, pp.2629-2678.

Yamaguchi, M. (1986). A numerical model of nearshore currents based on a finite amplitude wave theory, Proceedings of the 20th Coastal Engineering Conference, ASCE, November 9-14, Taipei, Taiwan, vol.1, ch.64, pp.849-863.

Yoo, D., O'Connor, B.A. and McDowell, D.M. (1989). Mathematical models of wave climate for port design, Proceedings of The Institution of Civil Engineers, The Institution of Civil Engineers, London, England, Part 1, no.86, June, pp.513-530.

Appendix A

MUNWAVE HARDCOPY OUTPUTS FOR ST. JOHN'S BAY REFRACTION ANALYSIS.

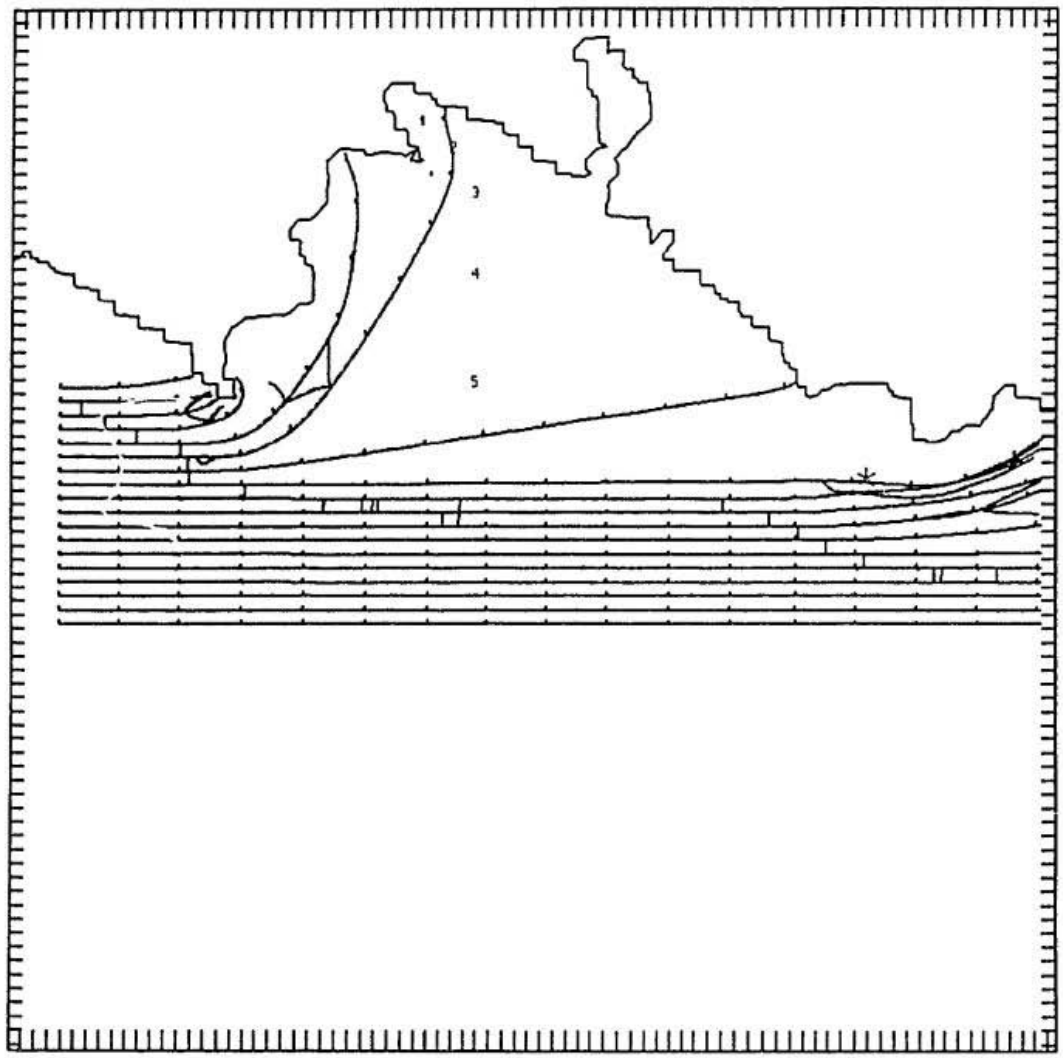

ST. JOHN'S BAY

WAVE ANGLE : 89.9 PERIOD : 10 sec.
CREST INTERVAL : 60 sec INITIAL WAVE HEIGHT 1 metre
ORTH SPACING : 200 metre GRID SPACING 200 metre
WATER DEPTH DATUM CHANGE : 0 metre

WAVE HEIGHTS CONTOURED : 1 metre.

Fig. A.1 - Refraction analysis output; T=10 sec., α_0=90°.

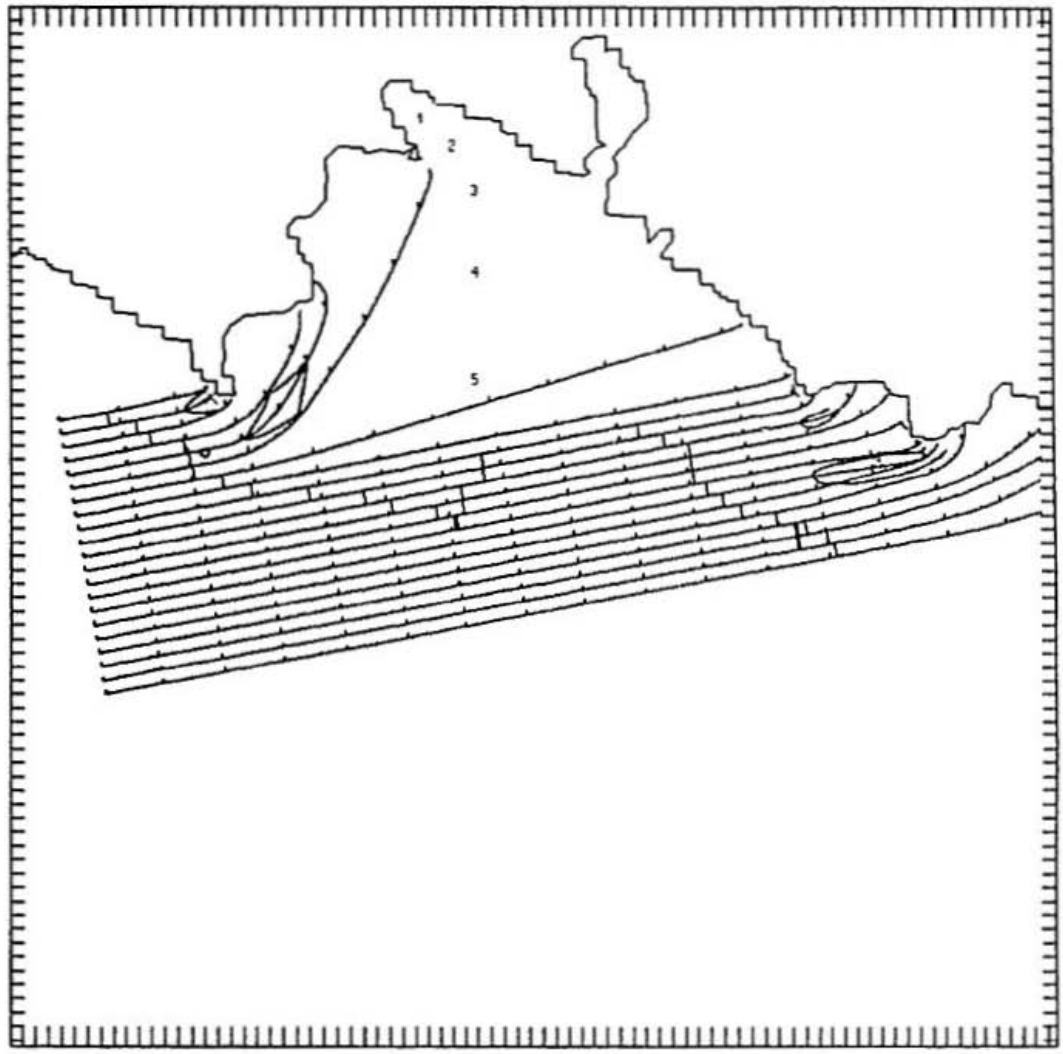

ST. JOHN'S BAY

WAVE ANGLE : 100 PERIOD : 10 sec
CREST INTERVAL : 60 sec INITIAL WAVE HEIGHT 1 metre
ORTH SPACING : 200 metre GRID SPACING 200 metre
WATER DEPTH DATUM CHANGE : 0 metre

WAVE HEIGHTS CONTOURED : 1 metre

Fig. A.2 - Refraction analysis output; T=10 sec., $\alpha_0=100^0$.

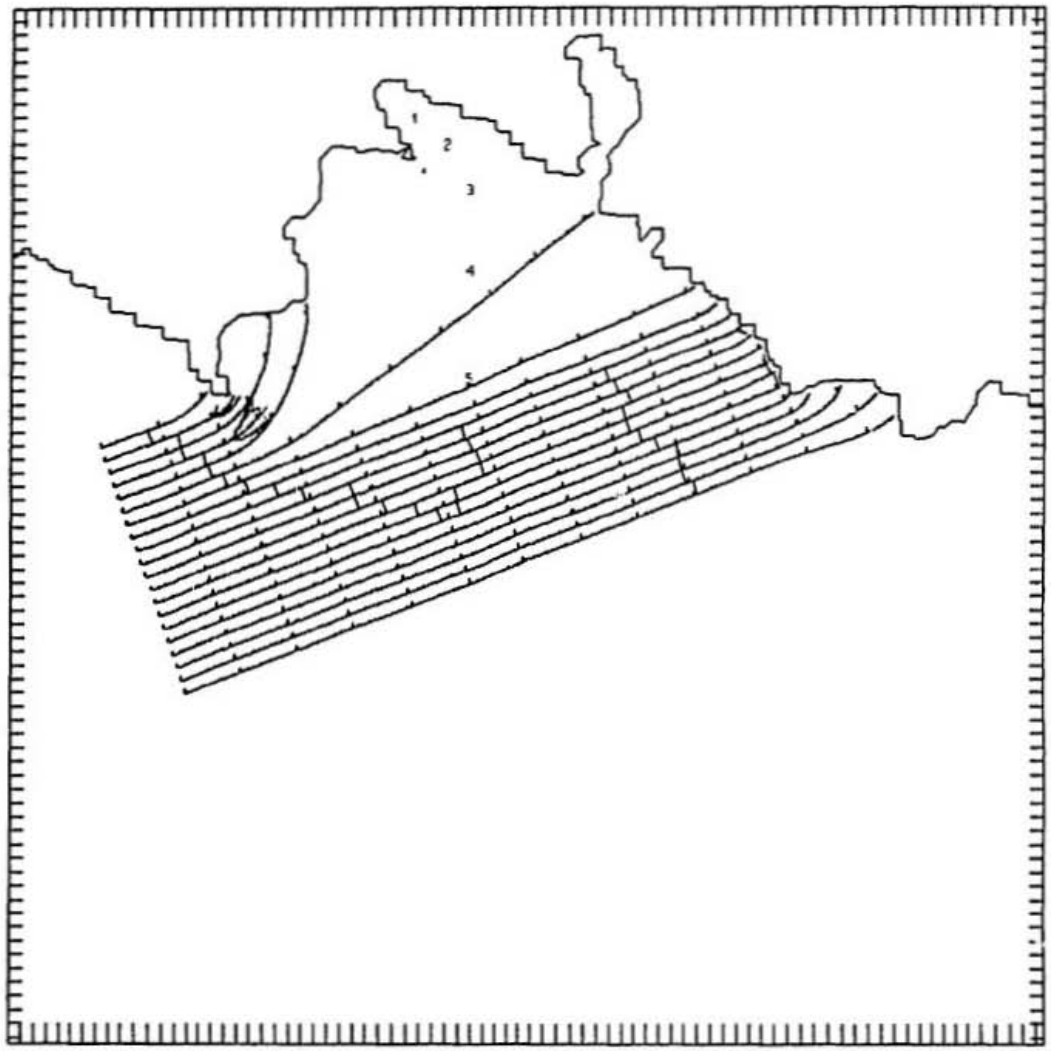

ST. JOHN'S BAY

WAVE ANGLE : 110 PERIOD : 10 sec.
CREST INTERVAL : 60 sec. INITIAL WAVE HEIGHT 1 metre.
ORTH SPACING : 200 metre GRID SPACING : 200 metre
WATER DEPTH DATUM CHANGE : 0 metre

WAVE HEIGHTS CONTOURED : 1 metre

Fig. A.3 - Refraction analysis output; T=10 sec., α_0=110°.

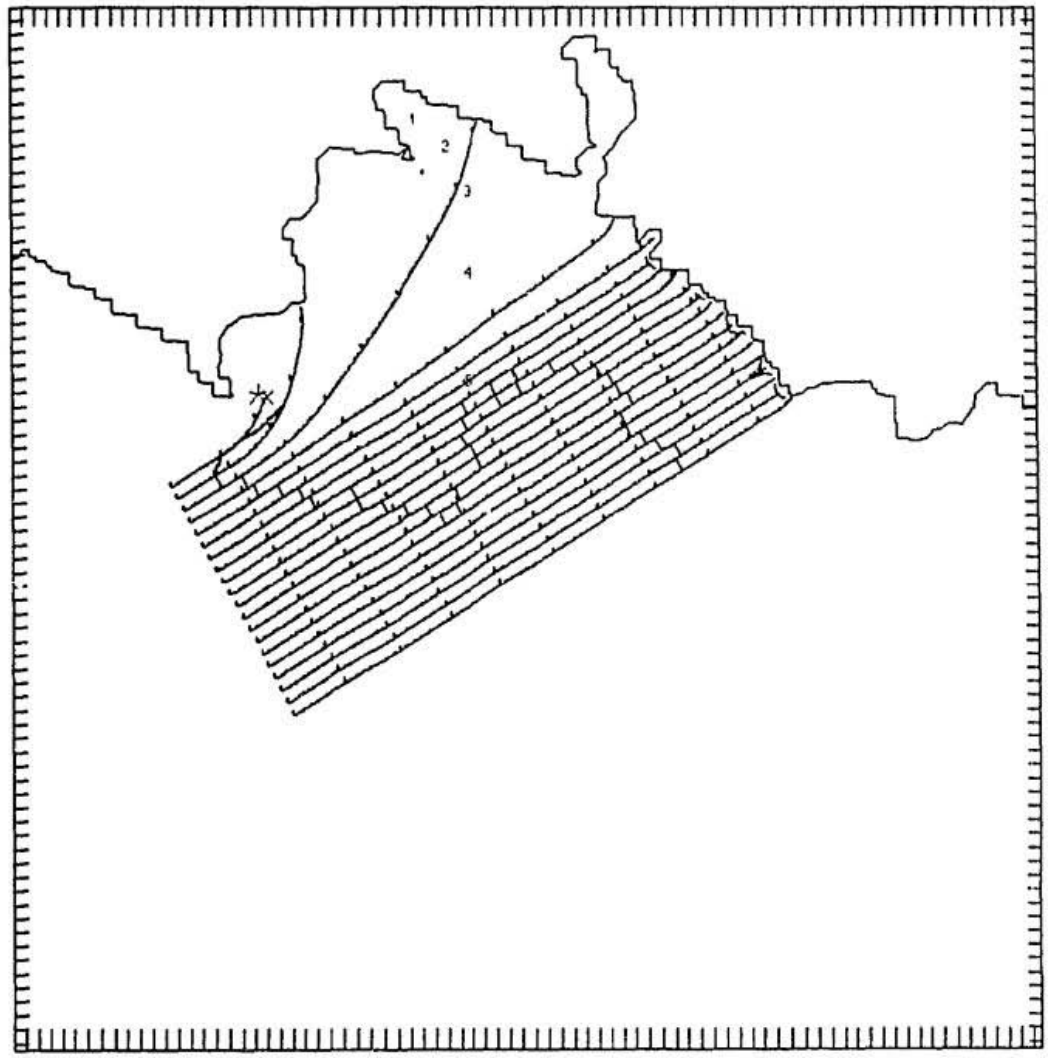

ST. JOHN'S BAY

WAVE ANGLE : 120 PERIOD : 10 sec
CREST INTERVAL : 60 sec. INITIAL WAVE HEIGHT : 1 metre
ORTH SPACING : 200 metre GRID SPACING 200 metre
WATER DEPTH DATUM CHANGE : 0 metre.

WAVE HEIGHTS CONTOURED : 1 metre.

Fig. A.4 - Refraction analysis output; T=10 sec., α_0=120°.

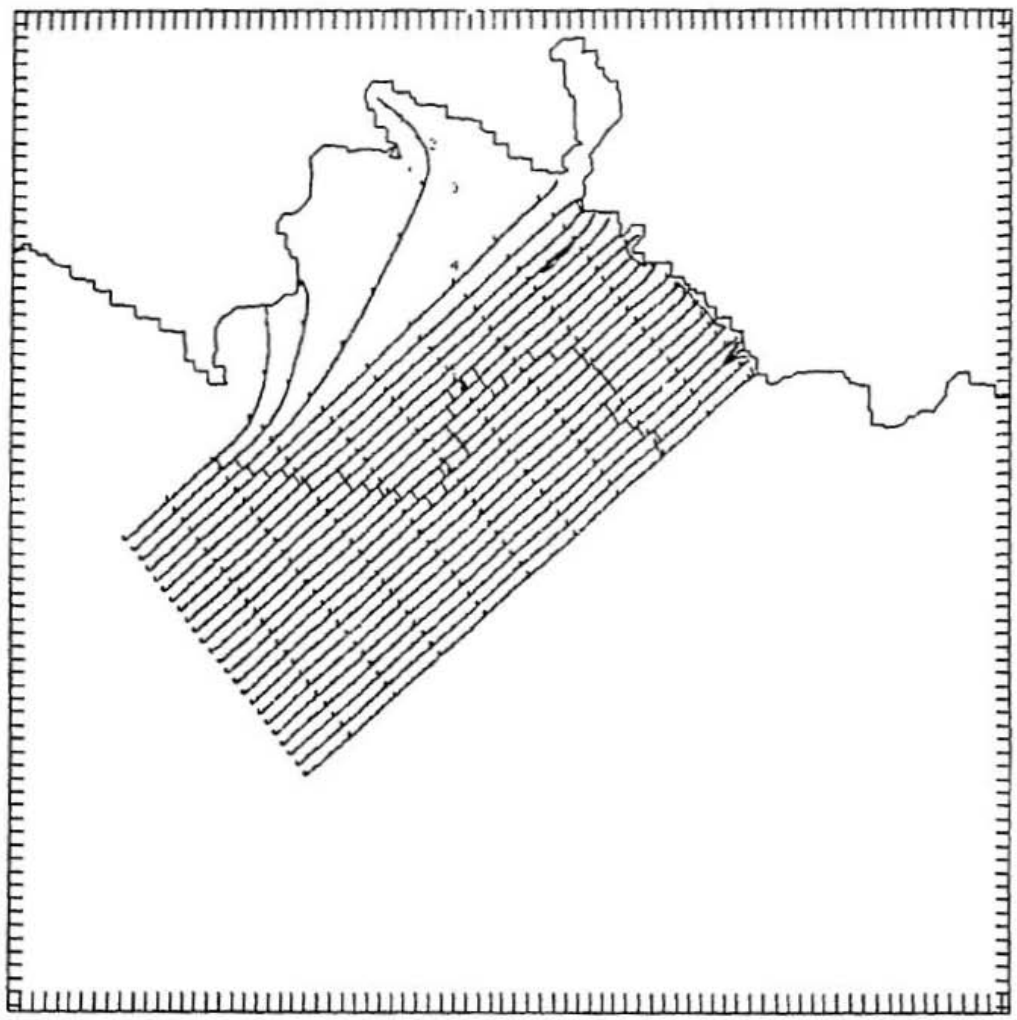

ST. JOHN'S BAY

WAVE ANGLE 130 PERIOD 10 sec
CREST INTERVAL 60 sec INITIAL WAVE HEIGHT 1 metre
ORTH SPACING · 200 metre GRID SPACING 200 metre
WATER DEPTH DATUM CHANGE · 0 metre

WAVE HEIGHTS CONTOURED · 1 metre

Fig. A.5 - Refraction analysis output; T=10 sec., α_0=130°.

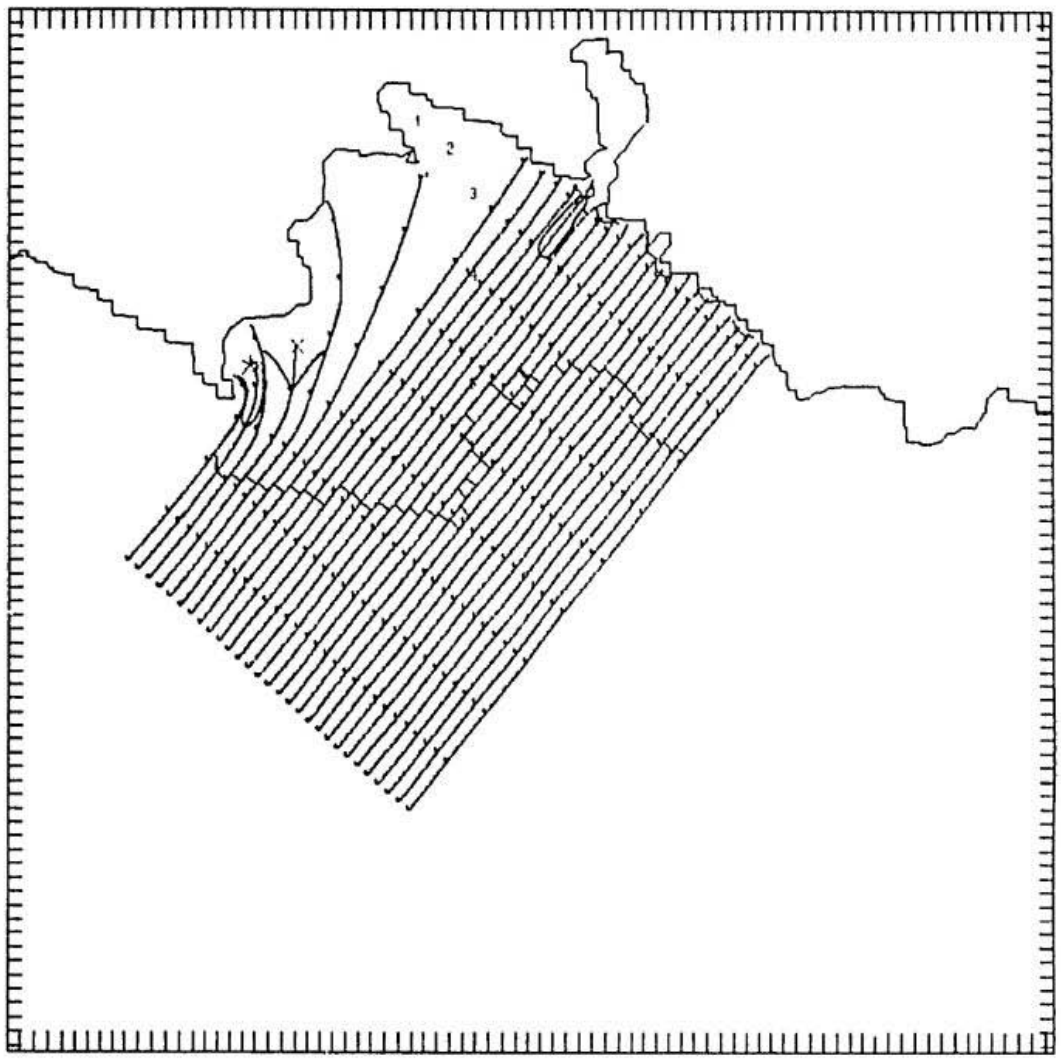

ST. JOHN'S BAY

WAVE ANGLE 140 PERIOD 10 sec
CREST INTERVAL 60 sec INITIAL WAVE HEIGHT 1 metre
ORTH SPACING 200 metre GRID SPACING 200 metre
WATER DEPTH DATUM CHANGE 0 metre

WAVE HEIGHTS CONTOURED 1 metre

Fig. A.6 - Refraction analysis output; T=10 sec., $\alpha_0=140^0$.

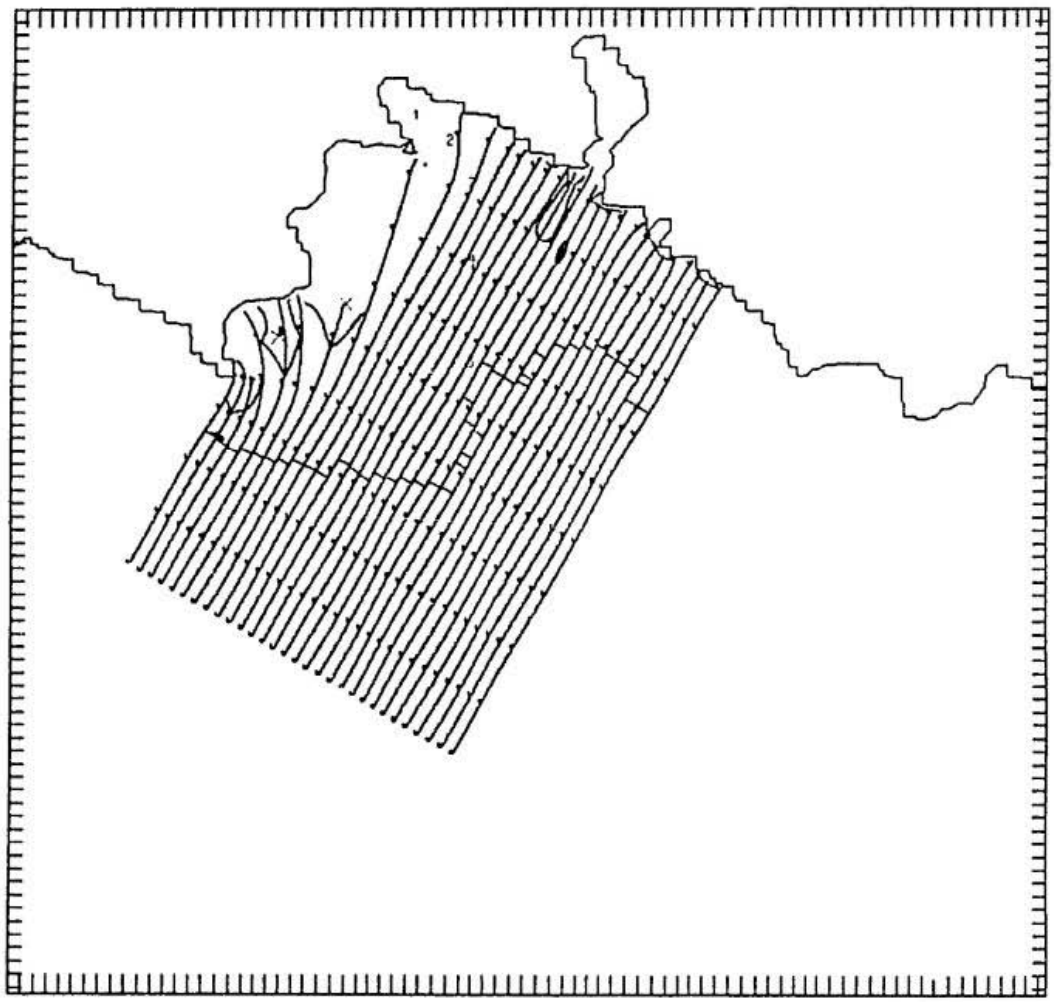

ST. JOHN'S BAY

WAVE ANGLE 150 PERIOD 10 sec
CREST INTERVAL 60 sec. INITIAL WAVE HEIGHT 1 metre
ORTH SPACING : 200 metre GRID SPACING 200 metre
WATER DEPTH DATUM CHANGE : 0 metre.

WAVE HEIGHTS CONTOURED : 1 metre.

Fig. A.7 - Refraction analysis output; T=10 sec., α_0=150°.

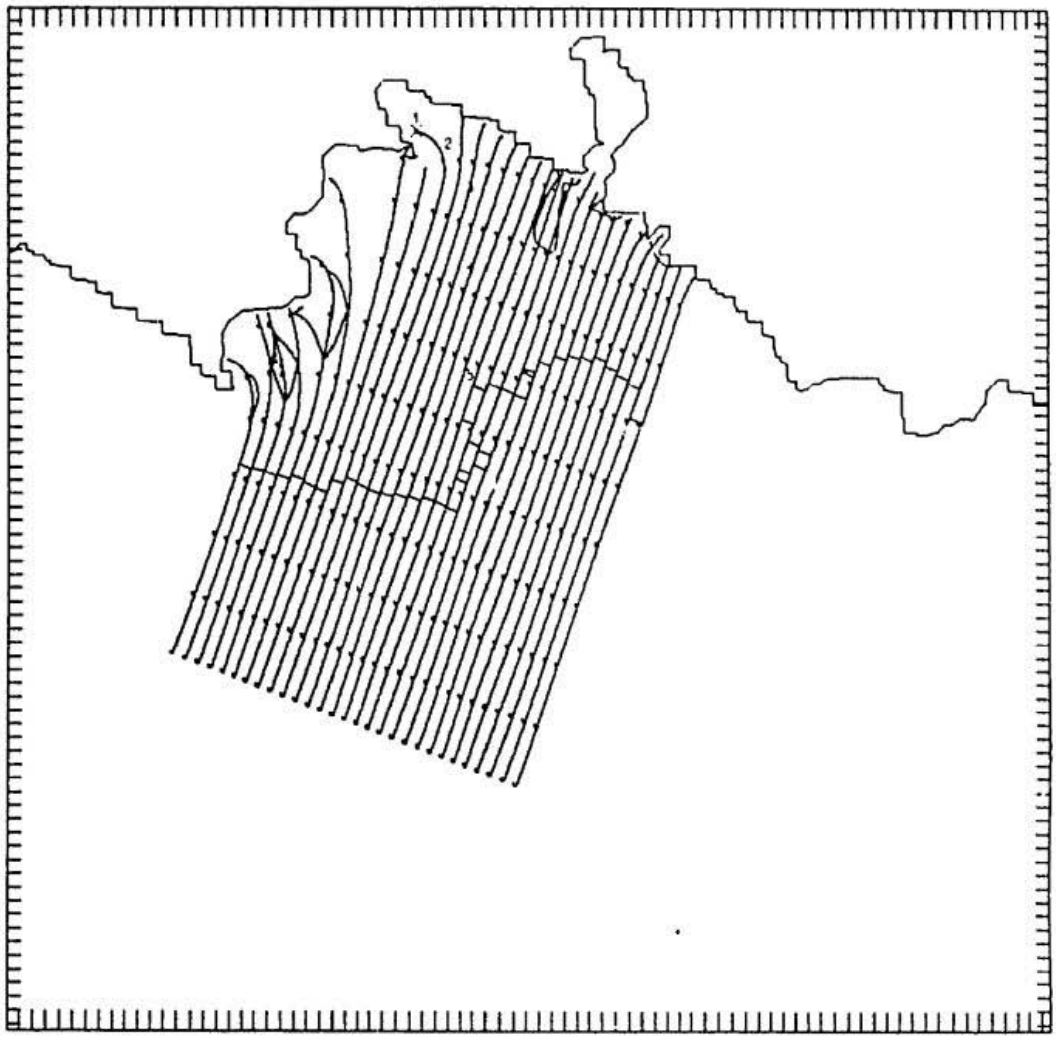

ST. JOHN'S BAY

WAVE ANGLE : 160 PERIOD : 10 sec
CREST INTERVAL : 60 sec INITIAL WAVE HEIGHT 1 metre
ORTH SPACING 200 metre GRID SPACING 200 metre
WATER DEPTH DATUM CHANGE : 0 metre

WAVE HEIGHTS CONTOURED : 1 metre

Fig. A.8 - Refraction analysis output; T=10 sec., α_0=160^0.

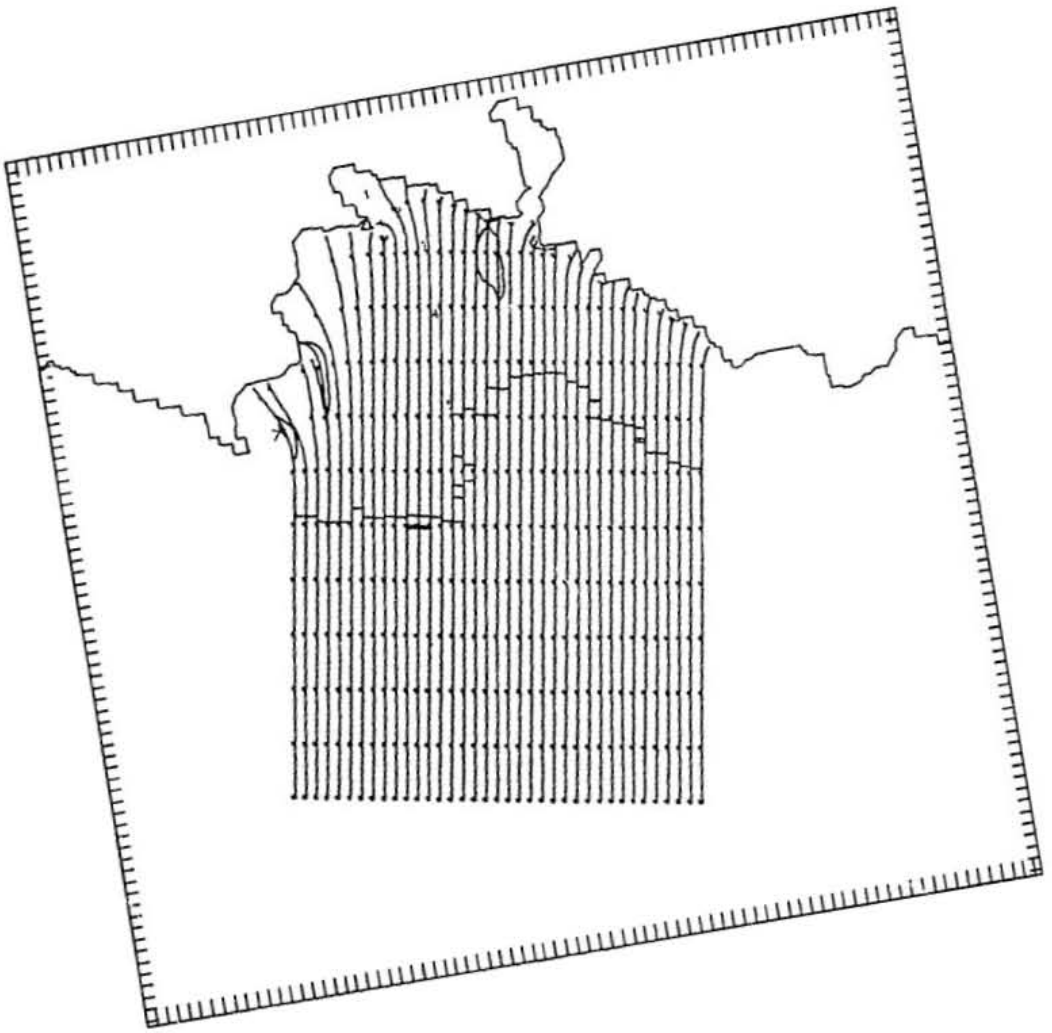

Fig. A.9 - Refraction analysis output; T=10 sec., α_0=170°.

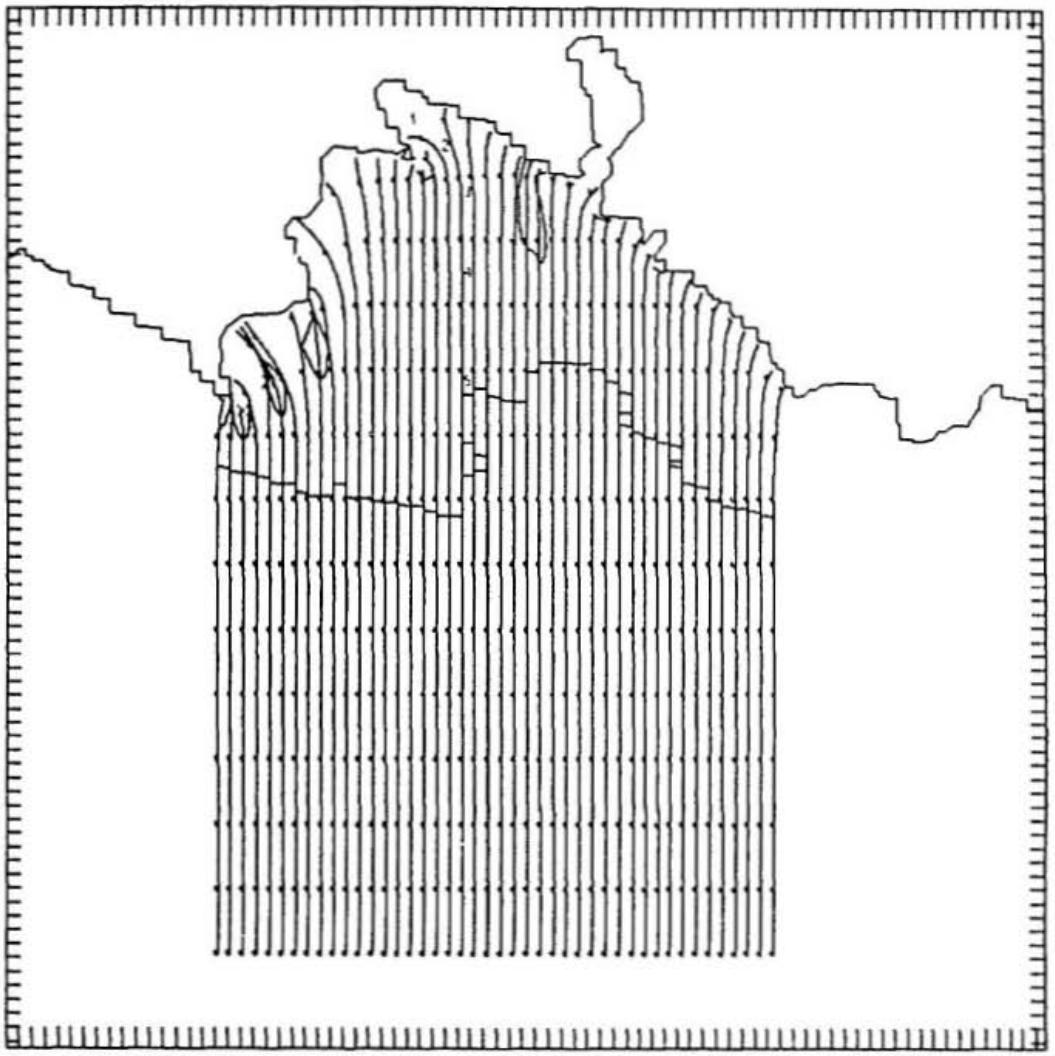

ST. JOHN'S BAY

WAVE ANGLE : 180 PERIOD . 10 sec
CREST INTERVAL : 60 sec. INITIAL WAVE HEIGHT 1 metre
ORTH SPACING : 200 metre GRID SPACING 200 metre
WATER DEPTH DATUM CHANGE : 0 metre

WAVE HEIGHTS CONTOURED : 1 metre

Fig. A.10 - Refraction analysis output; T=10 sec., α_0=180°.

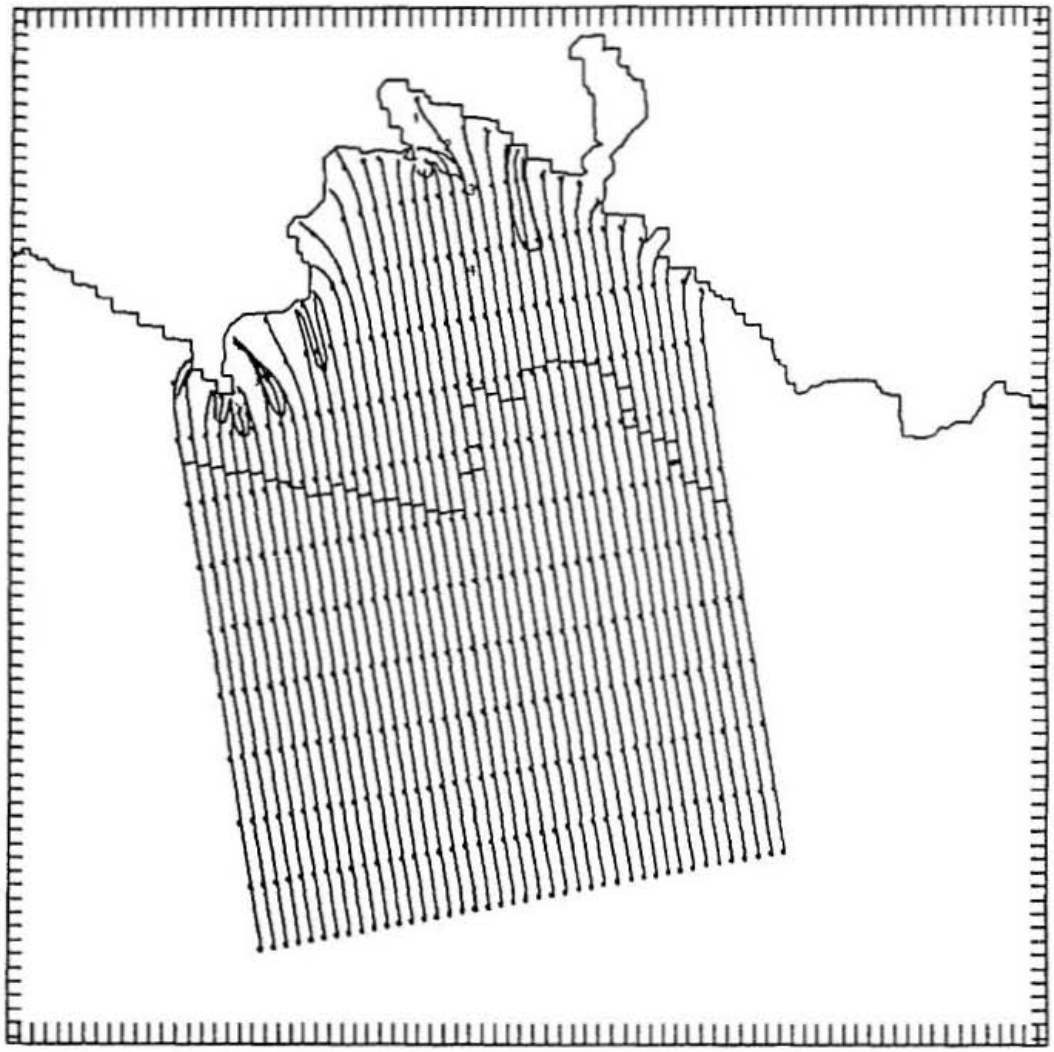

ST. JOHN'S BAY

WAVE ANGLE : 190 PERIOD 10 sec
CREST INTERVAL : 60 sec INITIAL WAVE HEIGHT 1 metre
ORTH SPACING : 200 metre GRID SPACING 200 metre
WATER DEPTH DATUM CHANGE : 0 metre

WAVE HEIGHTS CONTOURED : 1 metre

Fig. A.11 - Refraction analysis output; T=10 sec., α_0=190^0.

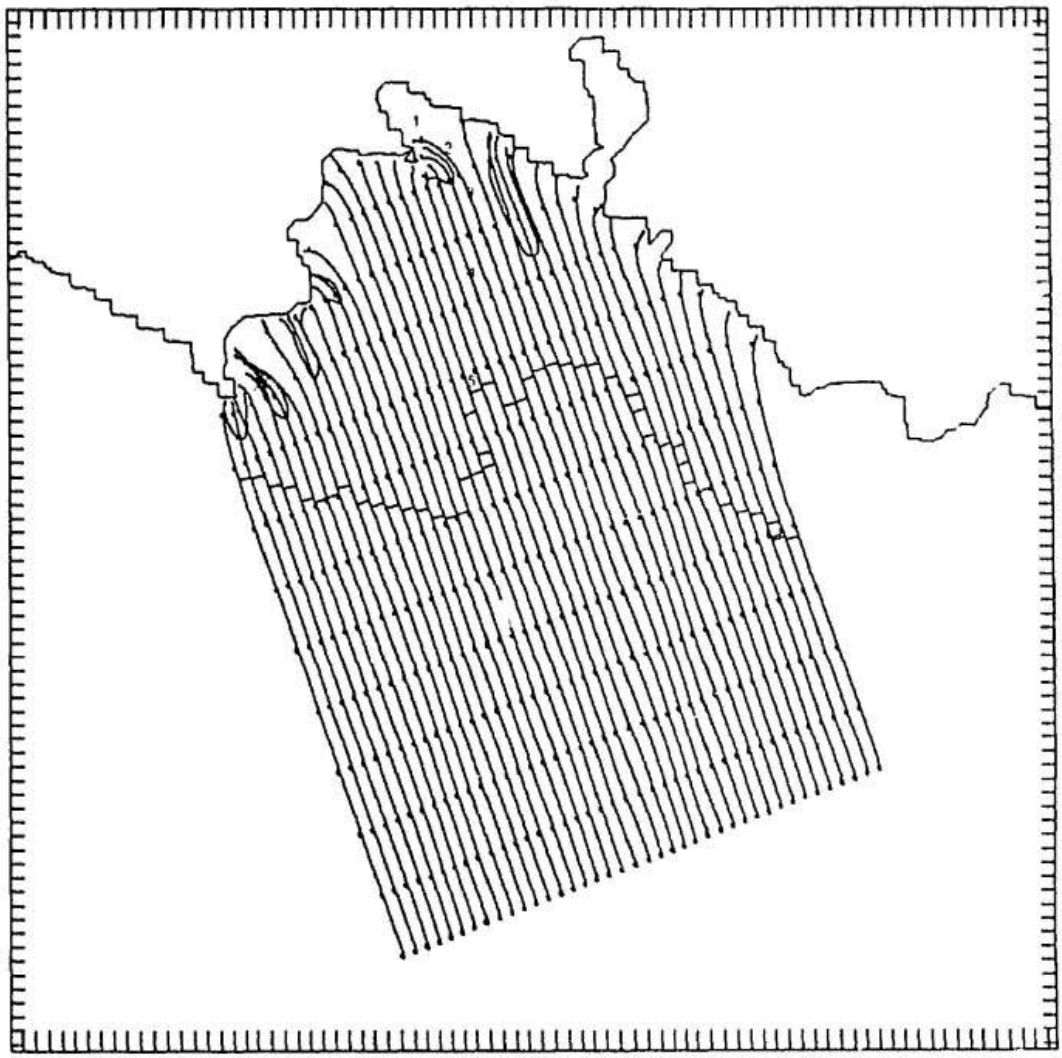

ST. JOHN'S BAY

WAVE ANGLE : 200 PERIOD : 10 sec
CREST INTERVAL : 60 sec. INITIAL WAVE HEIGHT 1 metre
ORTH SPACING : 200 metre GRID SPACING 200 metre
WATER DEPTH DATUM CHANGE : 0 metre.

WAVE HEIGHTS CONTOURED : 1 metre

Fig. A.12 - Refraction analysis output; T=10 sec., α_0=200°.

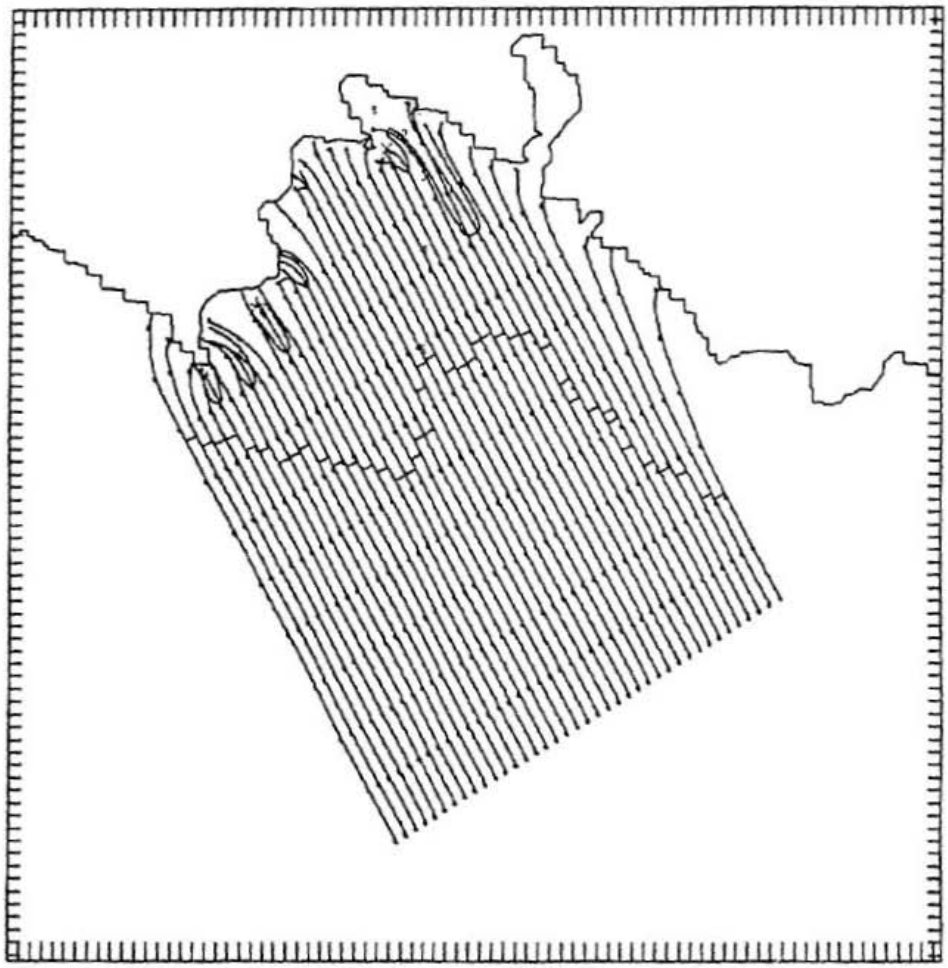

ST. JOHN'S BAY

WAVE ANGLE : 210 PERIOD . 10 sec
CREST INTERVAL . 60 sec. INITIAL WAVE HEIGHT 1 metre
ORTH SPACING · 200 metre GRID SPACING 200 metre
WATER DEPTH DATUM CHANGE · 0 metre.

WAVE HEIGHTS CONTOURED : 1 metre.

Fig. A.13 - Refraction analysis output; T=10 sec., α_0=210°.

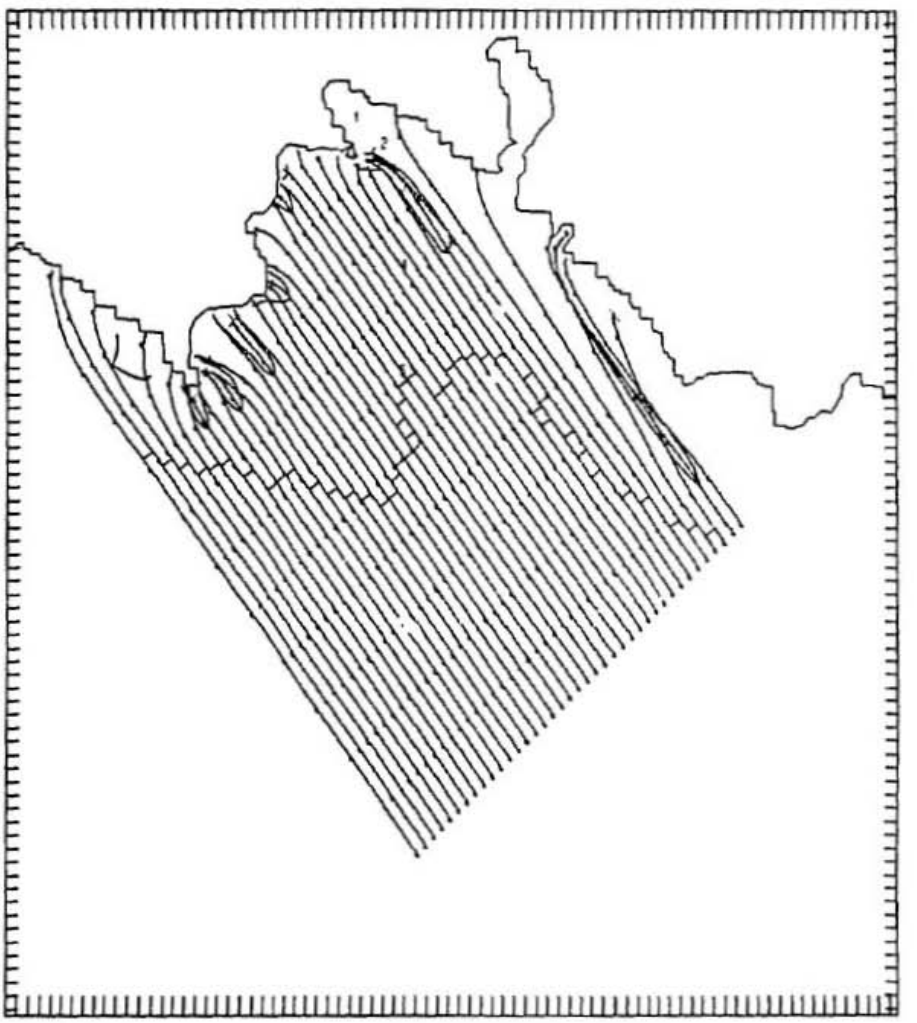

ST. JOHN'S BAY

WAVE ANGLE : 220 PERIOD 10 sec
CREST INTERVAL : 60 sec. INITIAL WAVE HEIGHT 1 metre
ORTH SPACING : 200 metre GRID SPACING 200 metre
WATER DEPTH DATUM CHANGE : 0 metre

WAVE HEIGHTS CONTOURED : 1 metre

Fig. A.14 - Refraction analysis output; T=10 sec., α_0=220^0.

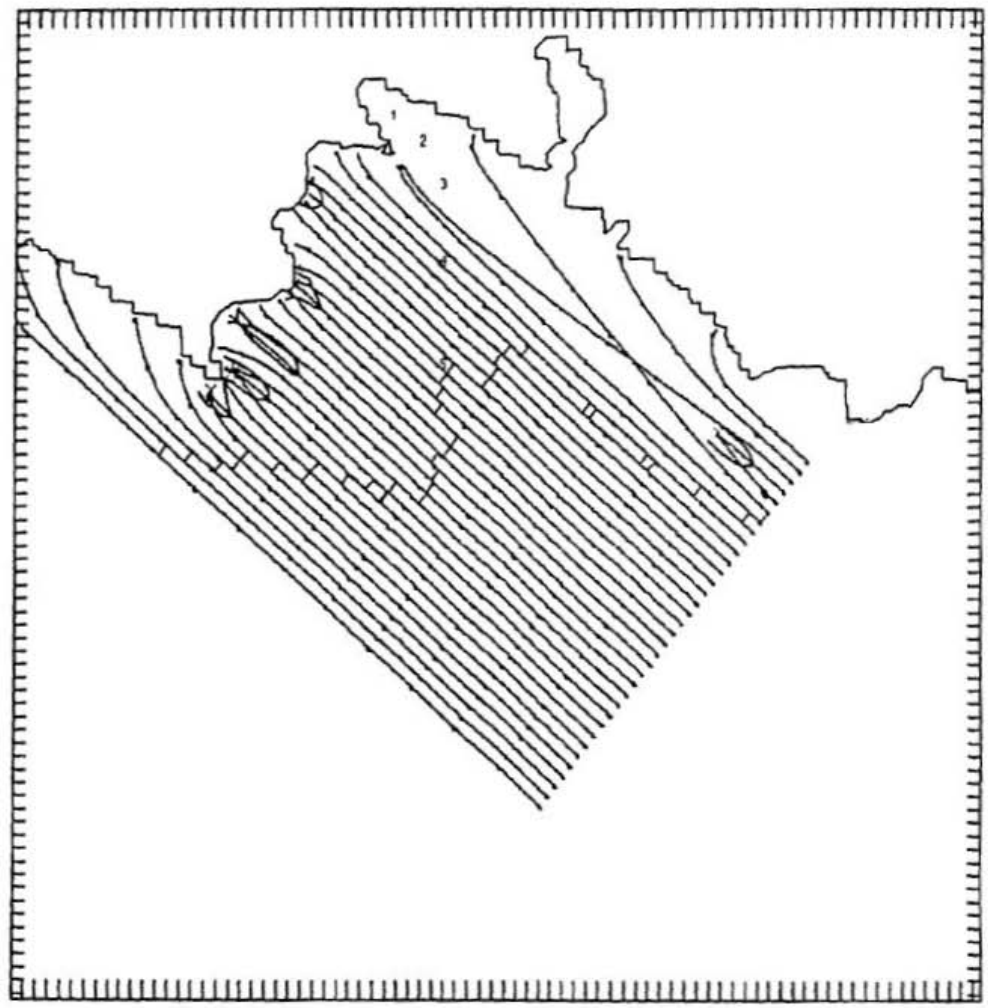

ST. JOHN'S BAY

WAVE ANGLE : 230 PERIOD : 10 sec
CREST INTERVAL : 60 sec INITIAL WAVE HEIGHT 1 metre
ORTH SPACING : 200 metre GRID SPACING 200 metre
WATER DEPTH DATUM CHANGE : 0 metre

WAVE HEIGHTS CONTOURED : 1 metre.

Fig. A.15 - Refraction analysis output; T=10 sec., α_0=230°.

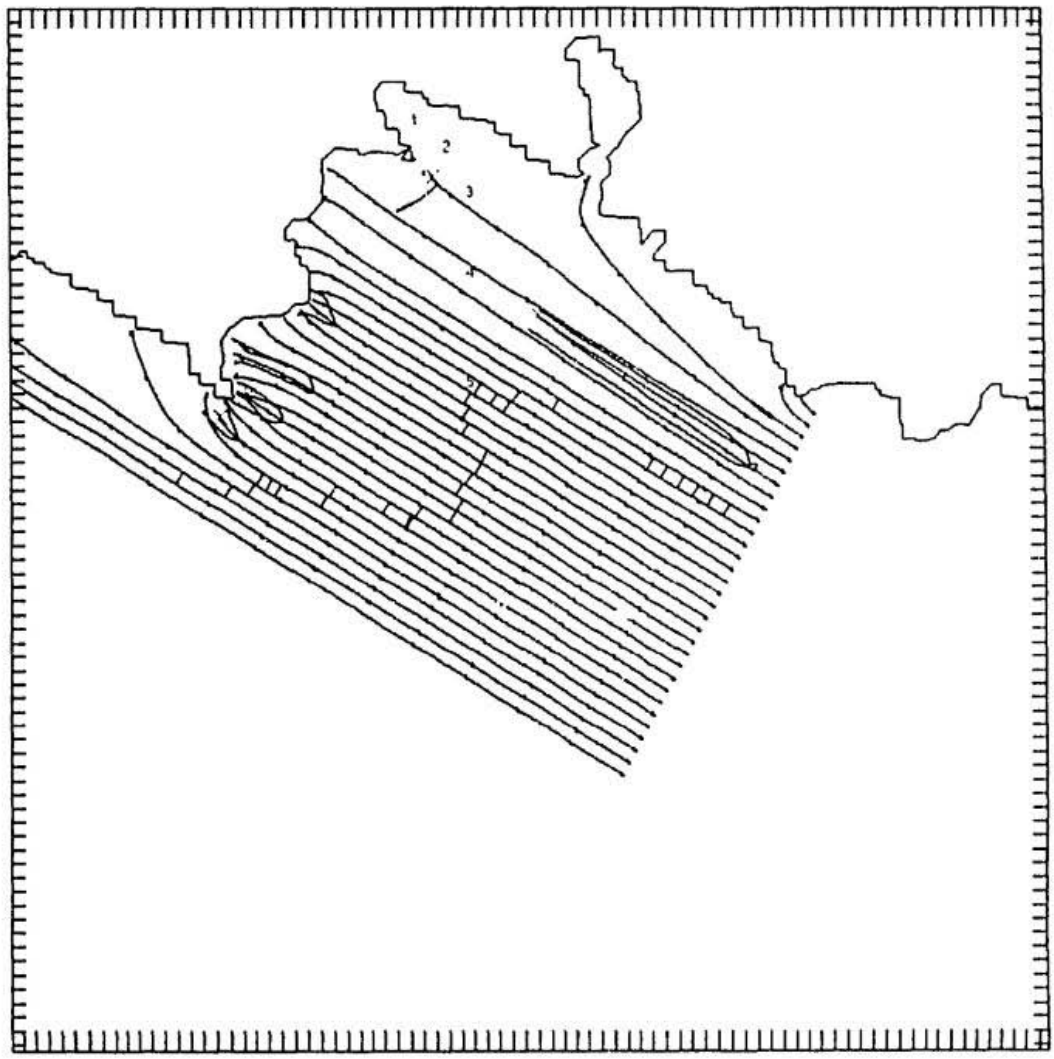

ST. JOHN'S BAY

WAVE ANGLE : 240 PERIOD : 10 sec.
CREST INTERVAL : 60 sec INITIAL WAVE HEIGHT : 1 metre
ORTH SPACING : 200 metre GRID SPACING : 200 metre
WATER DEPTH DATUM CHANGE : 0 metre

WAVE HEIGHTS CONTOURED : 1 metre

Fig. A.16 - Refraction analysis output; T=10 sec., α_0=240^o.

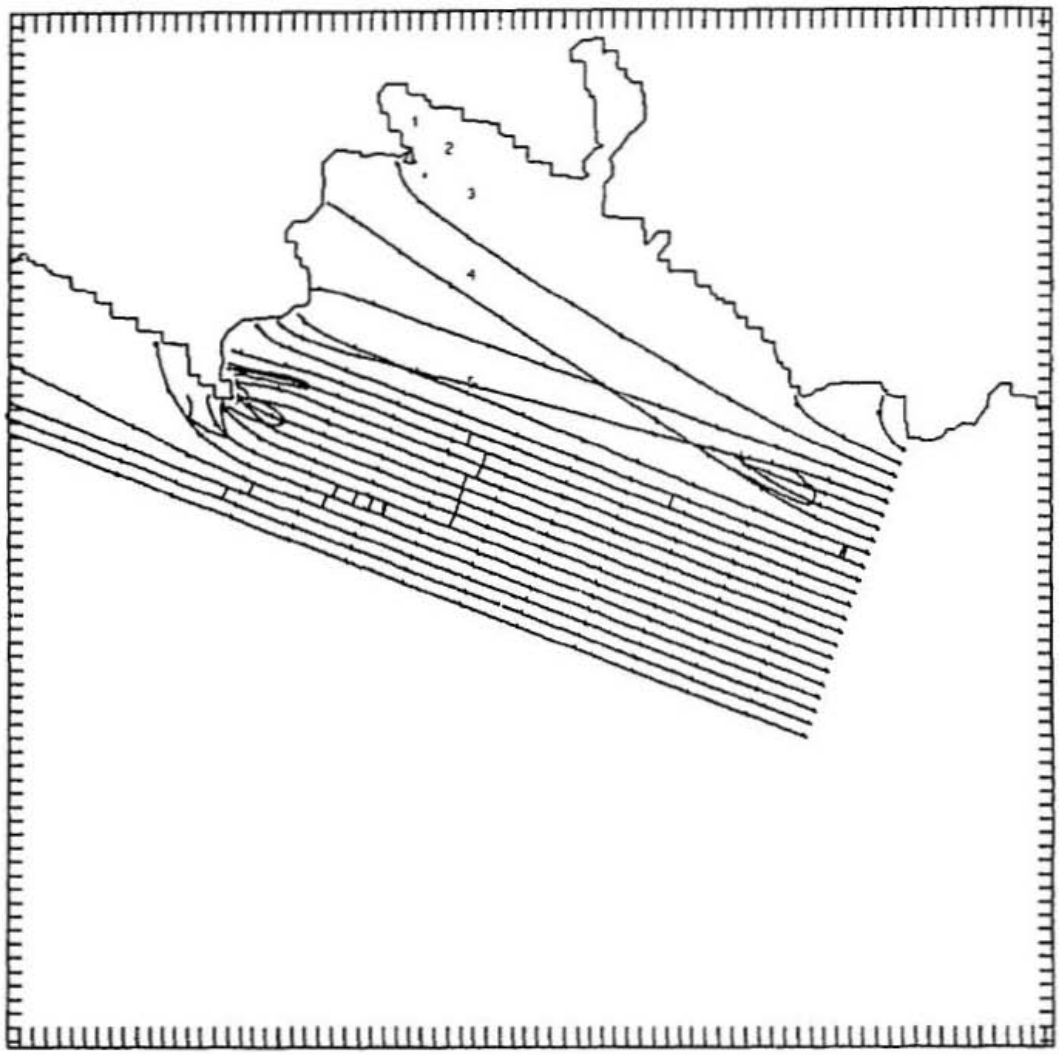

ST. JOHN'S BAY

WAVE ANGLE : 250 PERIOD : 10 sec.
CREST INTERVAL : 60 sec. INITIAL WAVE HEIGHT . 1 metre
ORTH SPACING : 200 metre GRID SPACING : 200 metre
WATER DEPTH DATUM CHANGE : 0 metre

WAVE HEIGHTS CONTOURED : 1 metre.

Fig. A.17 - Refraction analysis output; T=10 sec., α_0=250°.

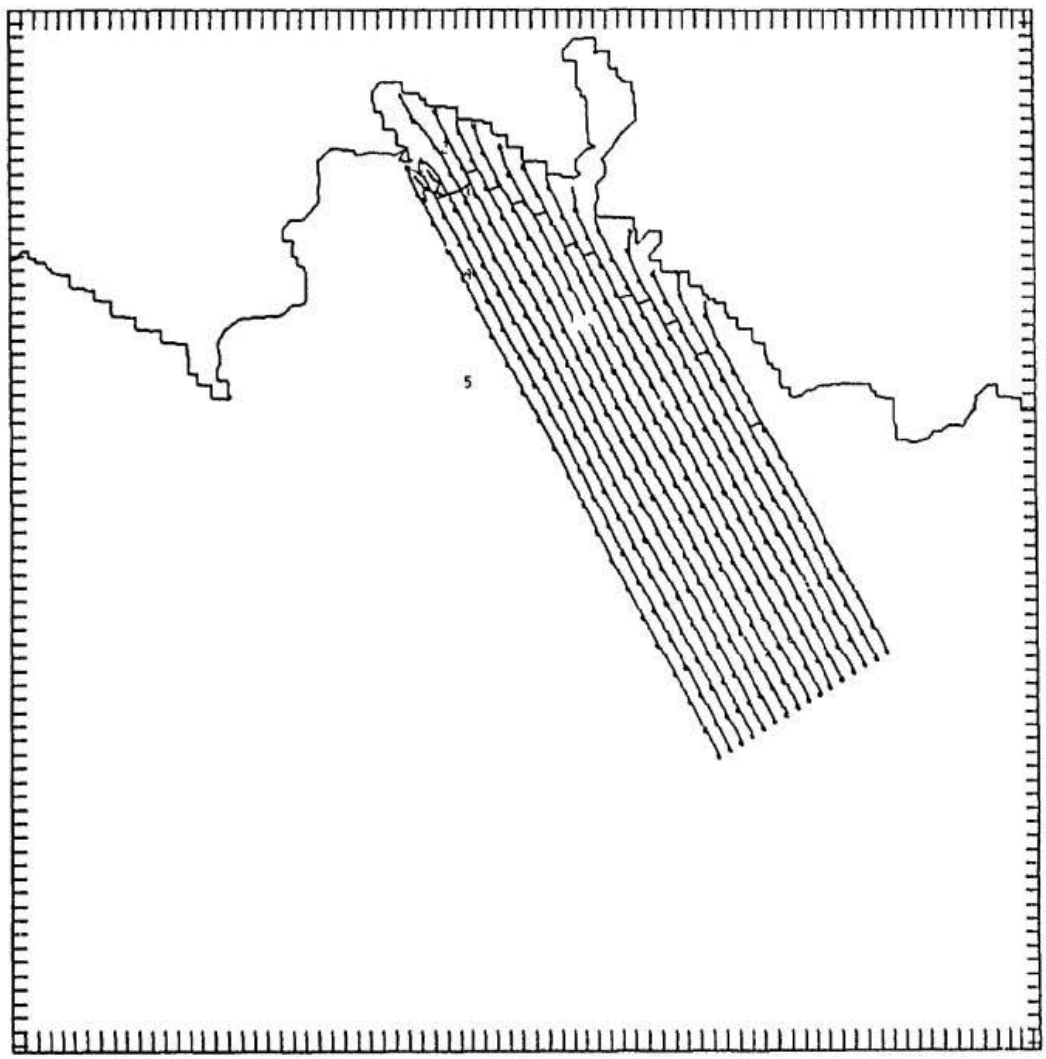

ST. JOHN'S BAY

WAVE ANGLE : 210 PERIOD : 5 sec
CREST INTERVAL : 60 sec INITIAL WAVE HEIGHT : 1 metre
ORTH SPACING 200 metre GRID SPACING 200 metre
WATER DEPTH DATUM CHANGE : 0 metre

WAVE HEIGHTS CONTOURED : 1 metre.

Fig. A.18 - Refraction analysis output; T=5 sec., α_0=210^o.

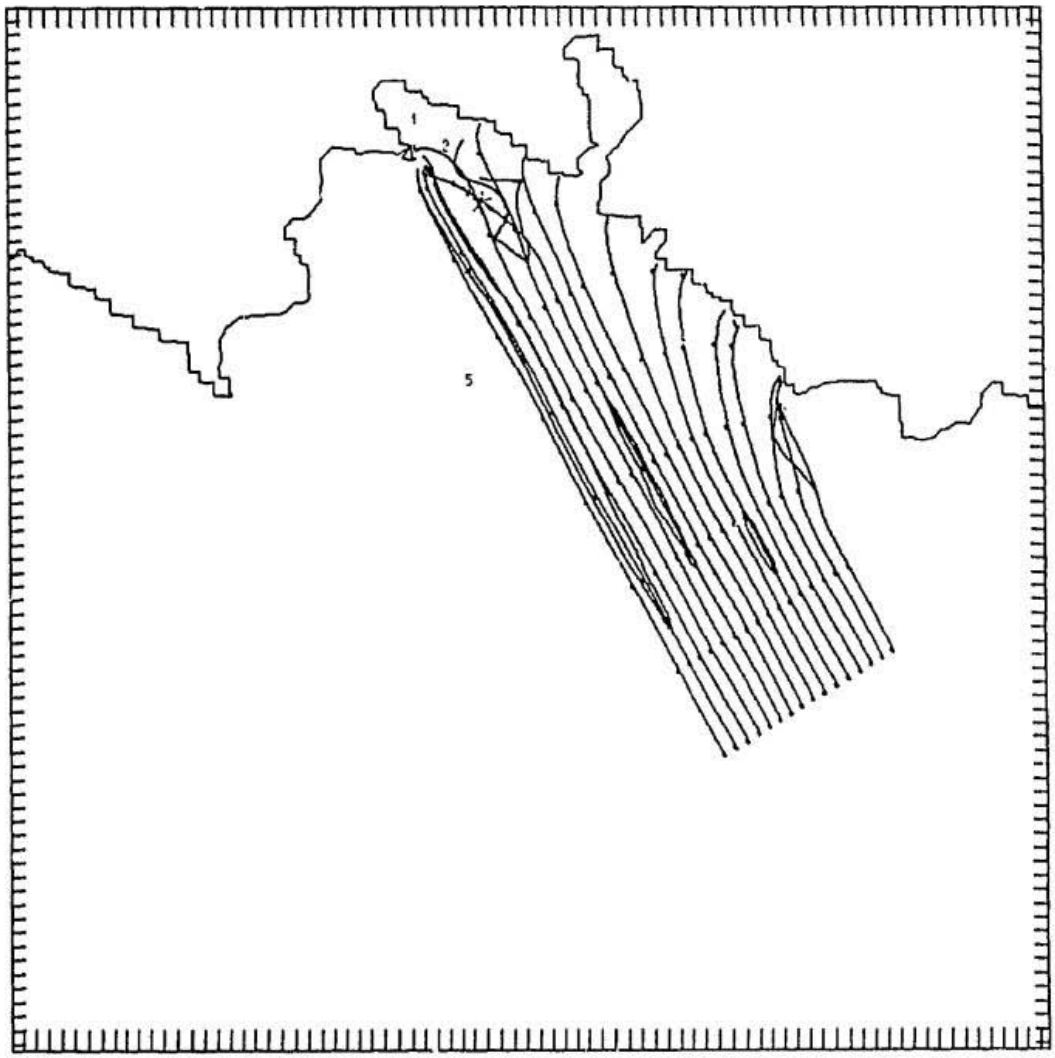

ST. JOHN'S BAY

WAVE ANGLE : 210 PERIOD : 15 sec.
CREST INTERVAL : 60 sec. INITIAL WAVE HEIGHT : 1 metre
ORTH SPACING : 200 metre GRID SPACING 200 metre
WATER DEPTH DATUM CHANGE : 0 metre

WAVE HEIGHTS CONTOURED : 1 metre.

Fig. A.19 - Refraction analysis output; T=15 sec., α_0=210°.

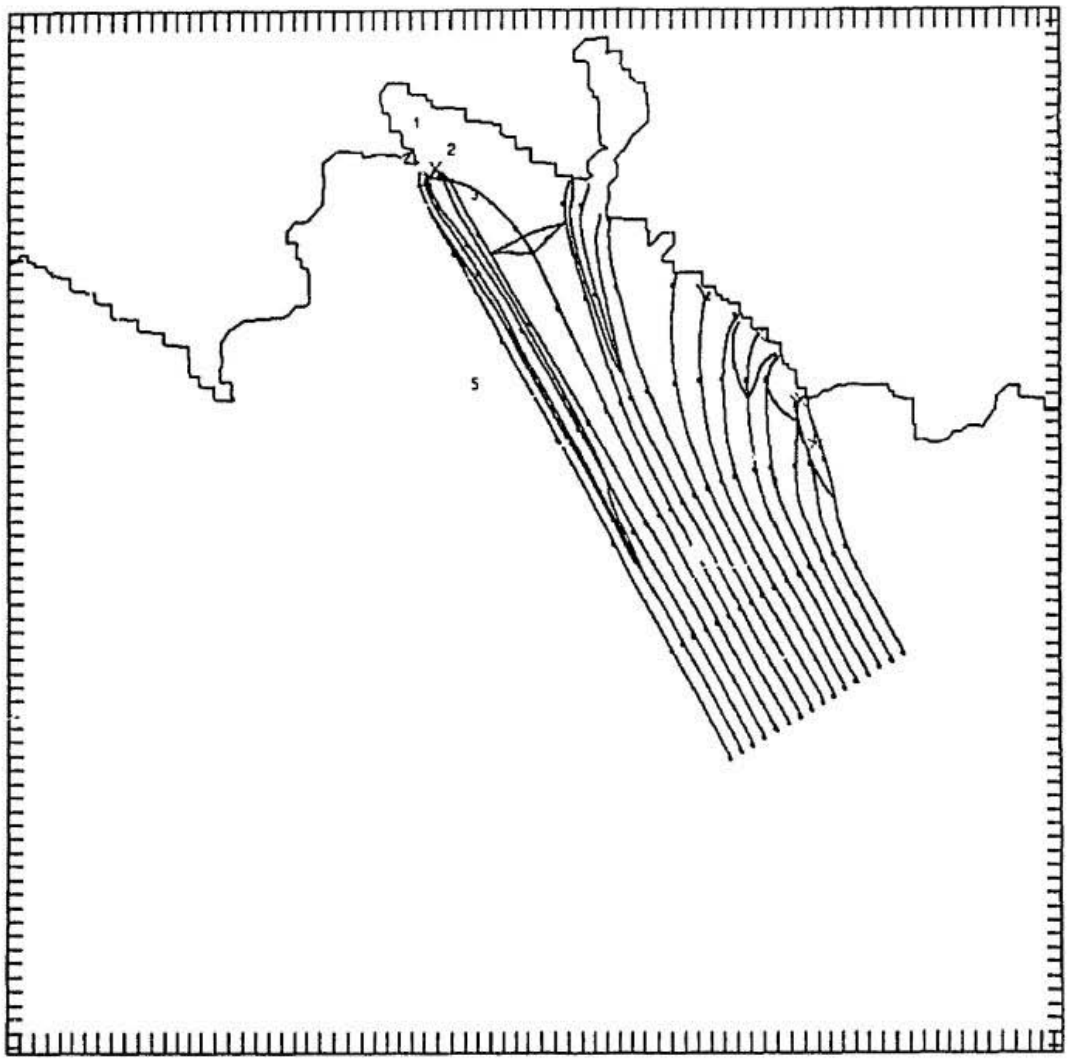

ST. JOHN'S BAY

WAVE ANGLE : 210 PERIOD : 20 sec.
CREST INTERVAL : 60 sec. INITIAL WAVE HEIGHT : 1 metre.
ORTH SPACING : 200 metre GRID SPACING : 200 metre
WATER DEPTH DATUM CHANGE : 0 metre.

WAVE HEIGHTS CONTOURED : 1 metre.

Fig. A.20 - Refraction analysis output; T=20 sec., α_0=210°.

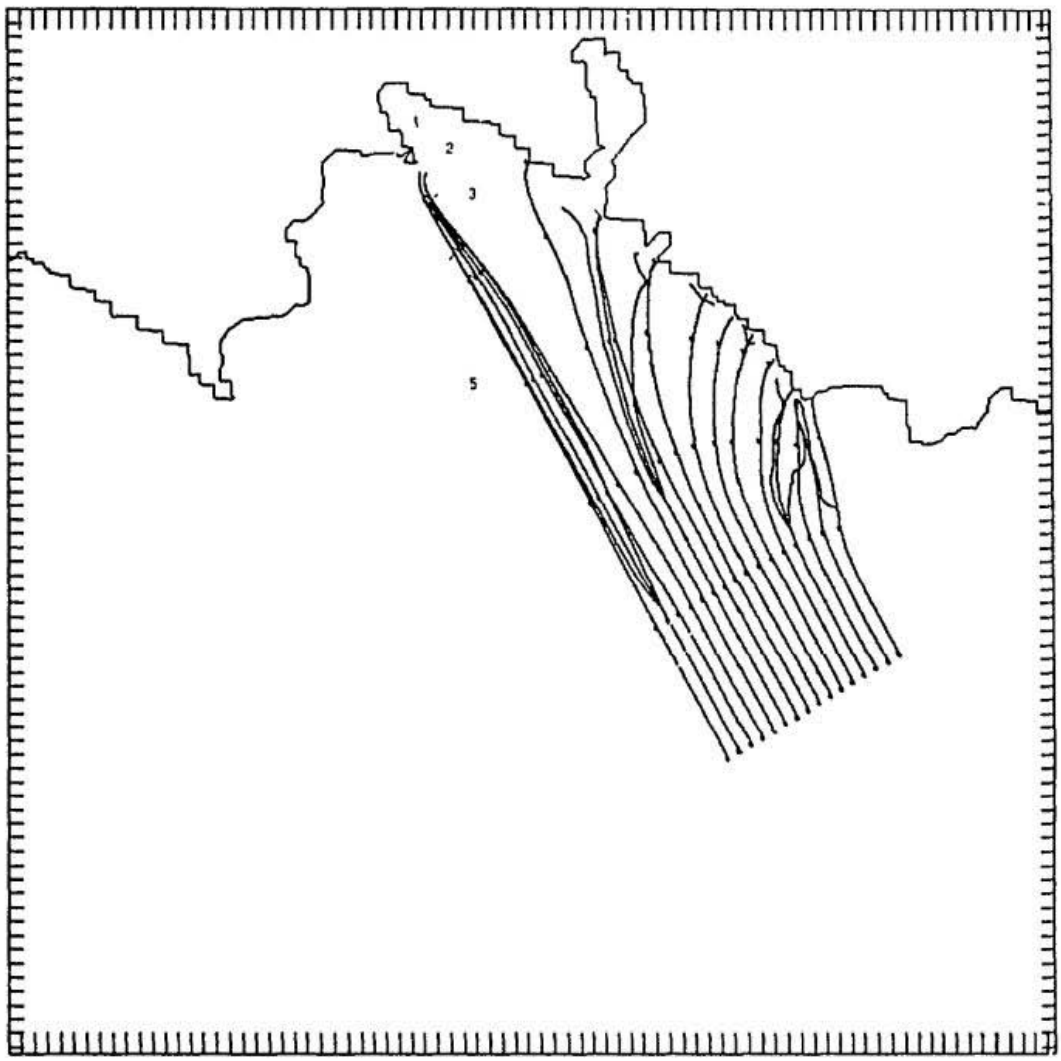

ST. JOHN'S BAY

WAVE ANGLE : 210 PERIOD : 30 sec.
CREST INTERVAL : 60 sec. INITIAL WAVE HEIGHT 1 metre
ORTH SPACING : 200 metre. GRID SPACING : 200 metre.
WATER DEPTH DATUM CHANGE : 0 metre.

WAVE HEIGHTS CONTOURED : 1 metre.

Fig. A.21 - Refraction analysis output; T=30 sec., α_0=210°.

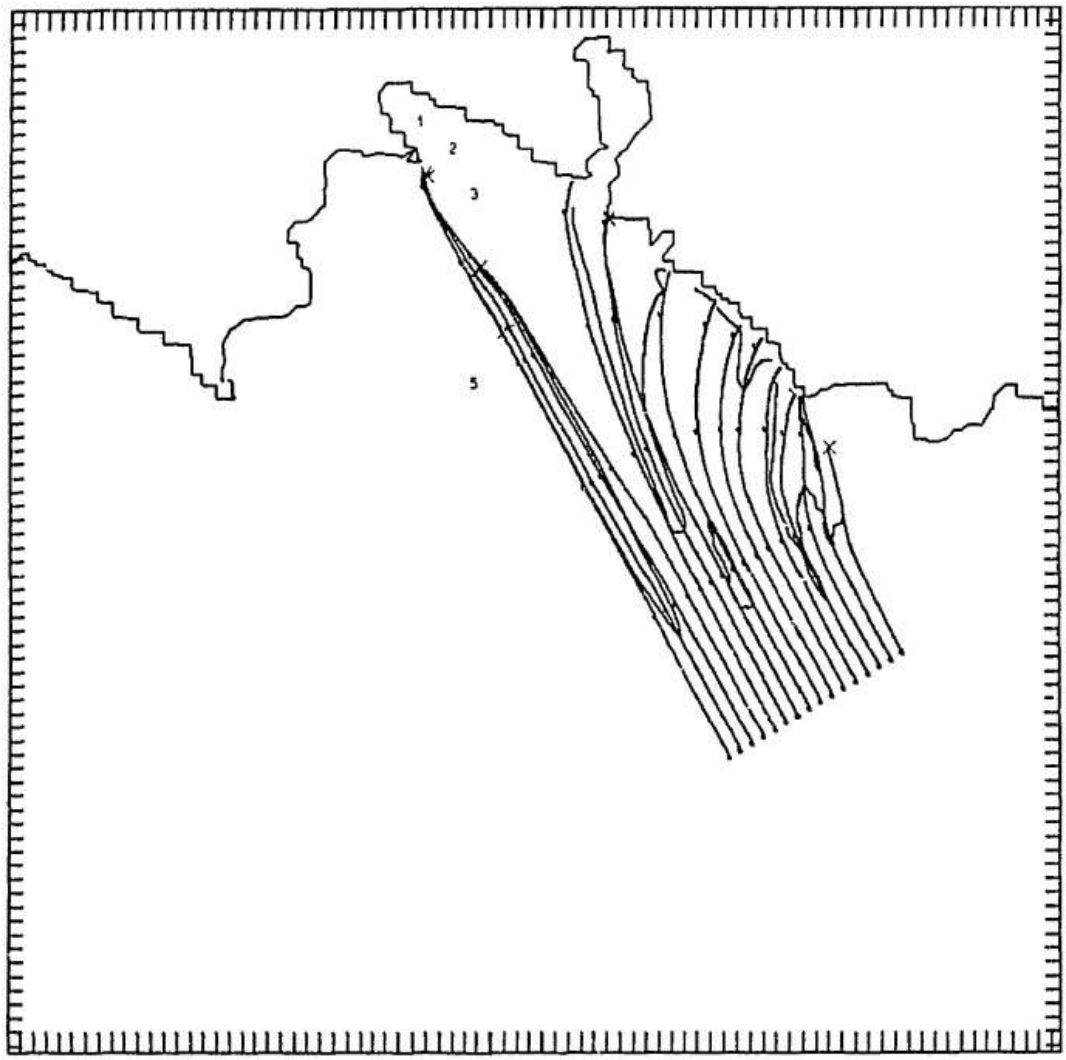

ST. JOHN'S BAY

WAVE ANGLE . 210 PERIOD . 40 sec.
CREST INTERVAL : 60 sec. INITIAL WAVE HEIGHT : 1 metre.
ORTH SPACING · 200 metre. GRID SPACING · 200 metre.
WATER DEPTH DATUM CHANGE : 0 metre.

WAVE HEIGHTS CONTOURED · 1 metre

Fig. A.22 - Refraction analysis output; T=40 sec., α_0=210°.

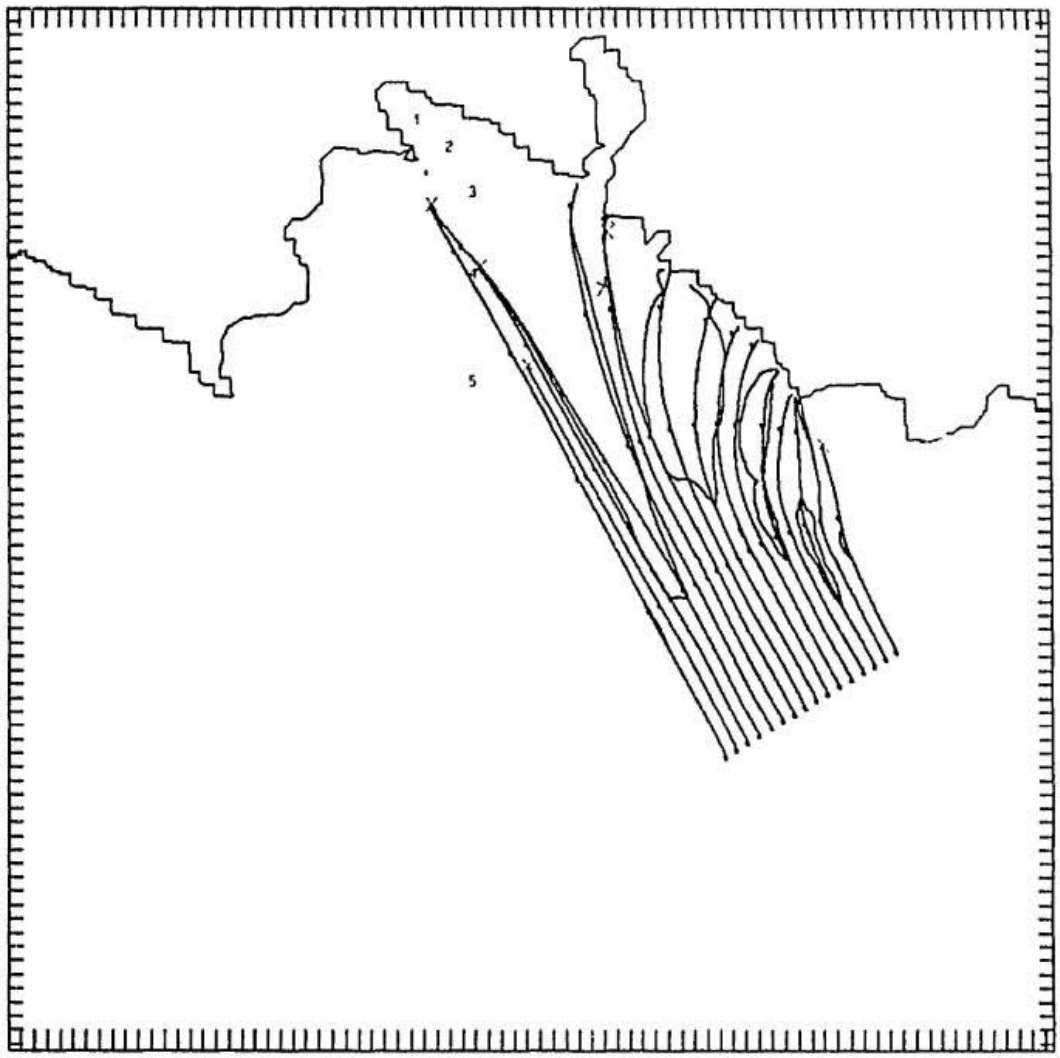

ST. JOHN'S BAY

WAVE ANGLE : 210 PERIOD : 50 sec.
CREST INTERVAL : 60 sec. INITIAL WAVE HEIGHT 1 metre.
ORTH SPACING : 200 metre. GRID SPACING : 200 metre
WATER DEPTH DATUM CHANGE : 0 metre

WAVE HEIGHTS CONTOURED : 1 metre

Fig. A.23 - Refraction analysis output; T=50 sec., α_0=210°.

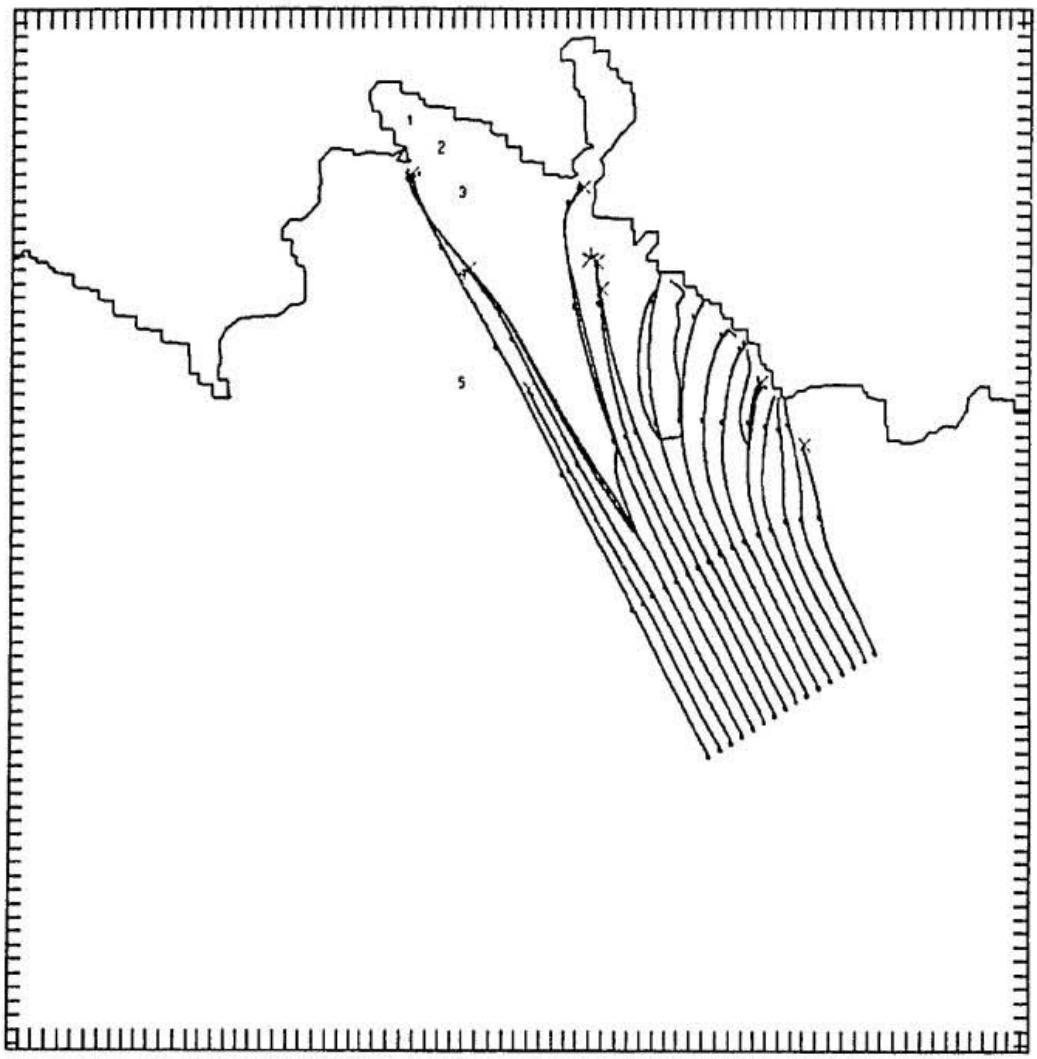

ST. JOHN'S BAY

WAVE ANGLE : 210 PERIOD : 70 sec.
CREST INTERVAL : 60 sec. INITIAL WAVE HEIGHT : 1 metre.
ORTH SPACING : 200 metre GRID SPACING : 200 metre
WATER DEPTH DATUM CHANGE : 0 metre

WAVE HEIGHTS CONTOURED : 1 metre.

Fig. A.24 - Refraction analysis output; T=70 sec., α_0=210°.

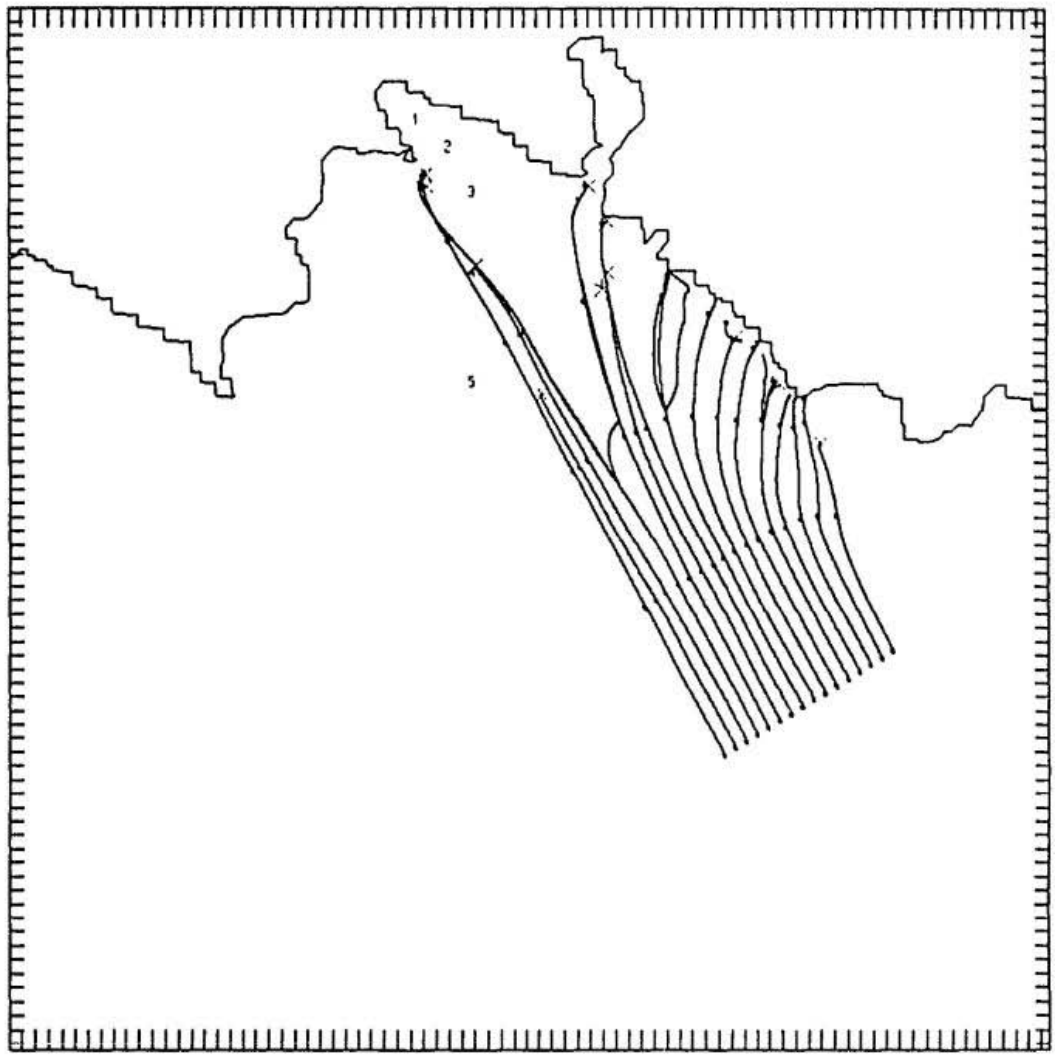

ST. JOHN'S BAY

WAVE ANGLE : 210 PERIOD . 90 sec
CREST INTERVAL : 60 sec. INITIAL WAVE HEIGHT 1 metre.
ORTH SPACING · 200 metre GRID SPACING · 200 metre
WATER DEPTH DATUM CHANGE · 0 metre

WAVE HEIGHTS CONTOURED : 1 metre

Fig. A.25 - Refraction analysis output; T=90 sec., α_0=210^0.

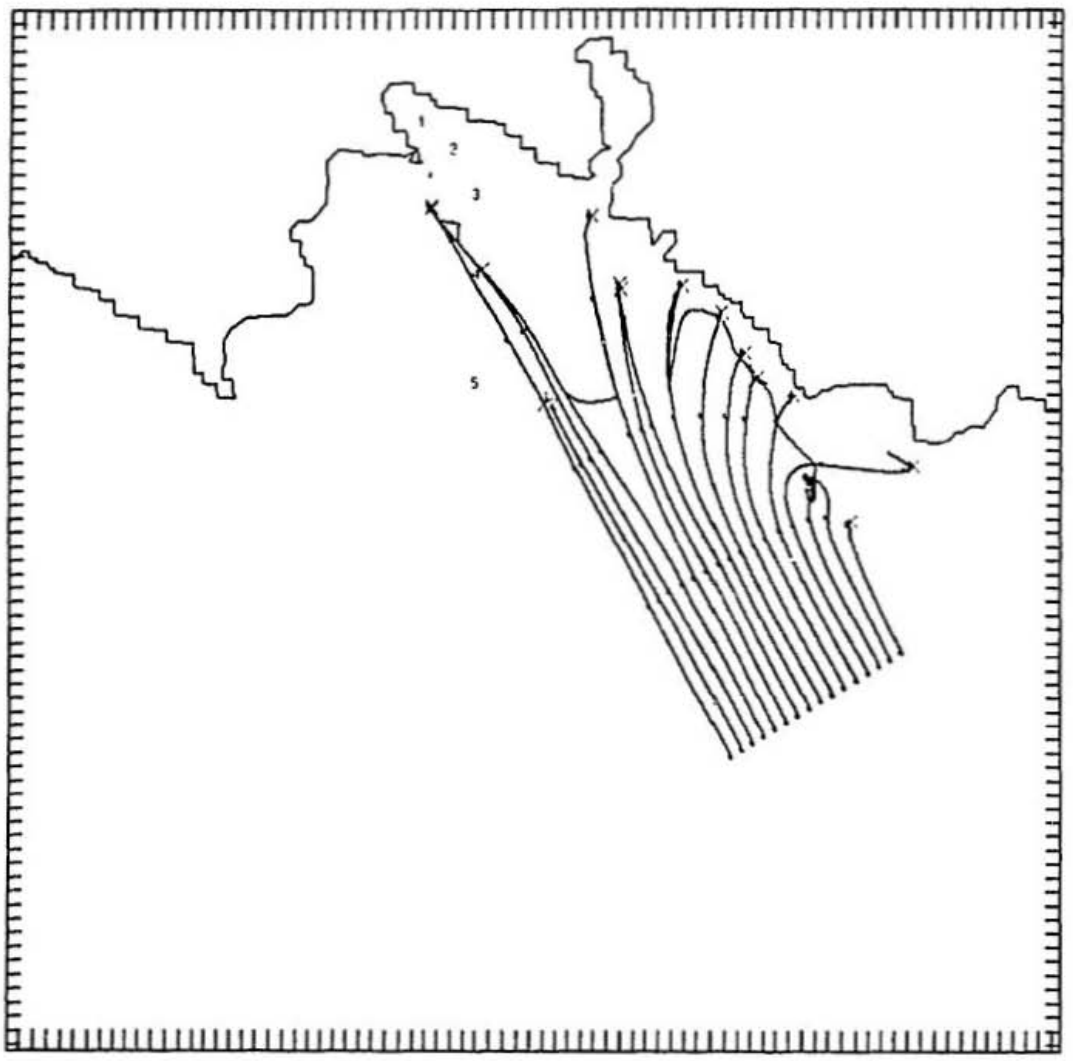

ST. JOHN'S BAY

WAVE ANGLE : 210 PERIOD . 120 sec.
CREST INTERVAL : 60 sec. INITIAL WAVE HEIGHT : 1 metre.
ORTH SPACING · 200 metre GRID SPACING · 200 metre
WATER DEPTH DATUM CHANGE : 0 metre.

WAVE HEIGHTS CONTOURED : 1 metre.

Fig. A.26 - Refraction analysis output; T=120 sec., α_0=210°.

Appendix B

LONGWAVE HARDCOPY OUTPUTS FOR ST. JOHN'S BAY RESPONSE PARAMETER ANALYSIS.

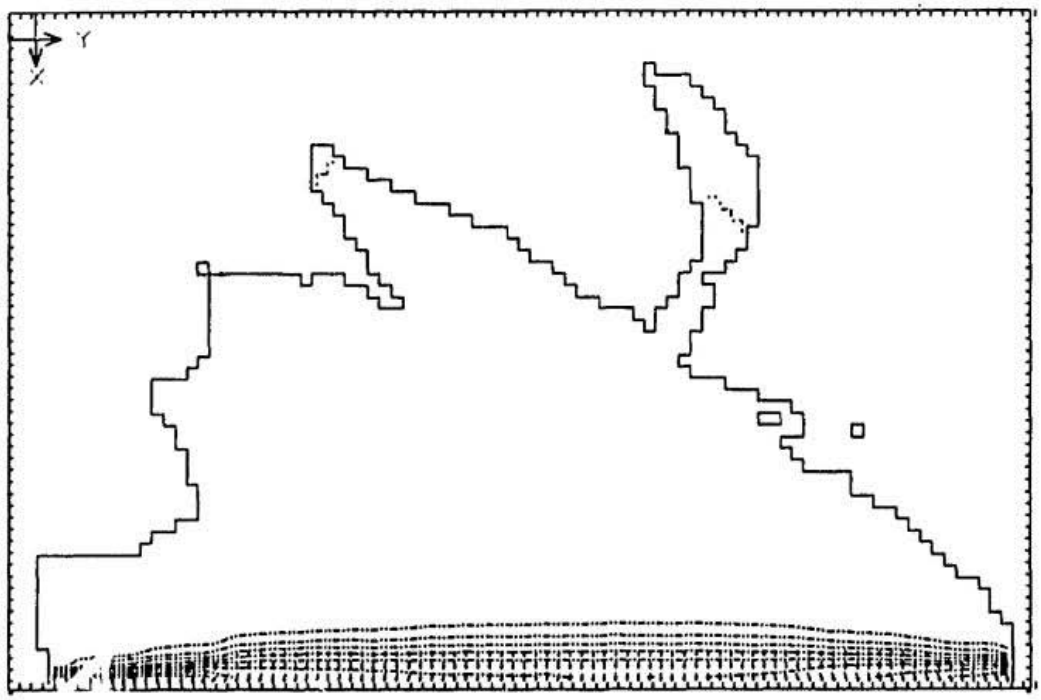

(·····) < 0 , (·····) = 0 , (———) > 0
RESPONSE PARAMETER CONTOURS , So= 1 42E-02, & VECTORS
WAVE PERIOD = 120 :: ITERATION TIME = 15
MAX/MIN = 0 / -.1516 :: INTERVAL = .015
GRID SPACE = 100 m
RUN DATE/TIME = 12-03-1991 / 11:00:44
Chezy Coefficient using Ganguillet & Kutter (1869), n= 03

Fig. B.1 - Response parameter, t=15 s, T=120 s.

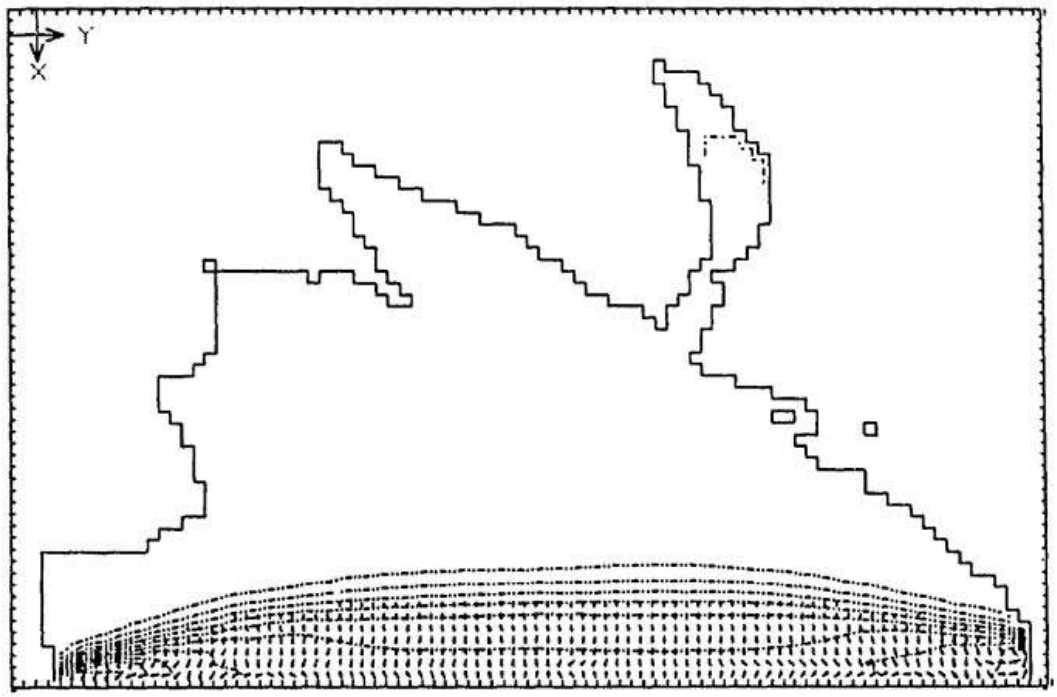

(----------)<0 , (----------)=0 , (————)>0
RESPONSE PARAMETER CONTOURS , So= 1 42E-02, & VECTORS
WAVE PERIOD = 120 ITERATION TIME = 30
MAX/MIN = 0 / - 2237 INTERVAL = 02
GRID SPACE = 100 m
RUN DATE/TIME = 12-03-1991 / 11 28 42
Chezy Coefficient using Ganguillet & Kutter (1869), n= 03

Fig. B.2 - Response parameter, t=30 s, T=120 s.

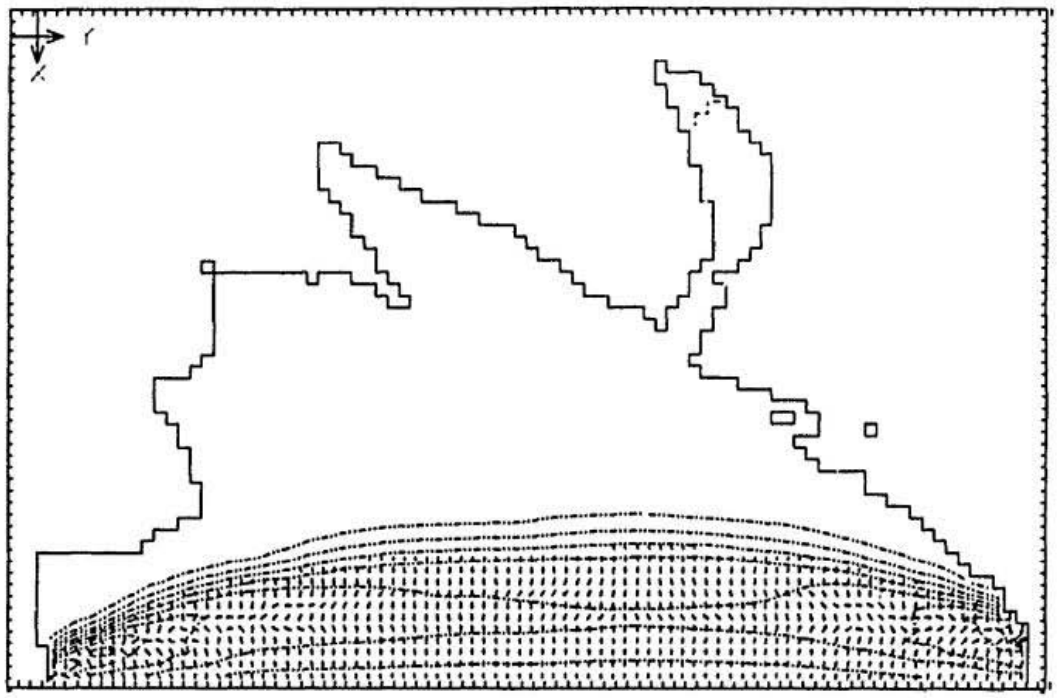

(----------)<0 , (----------)=0 , (————)>0
RESPONSE PARAMETER CONTOURS , So= 1.42E-02, & VECTORS.
WAVE PERIOD = 120 :: ITERATION TIME = 45
MAX/MIN = 0 /-.2658 :: INTERVAL = .025
GRID SPACE = 100 m
RUN DATE/TIME = 12-03-1991 / 12:02:56
Chezy Coefficient using Ganguillet & Kutter (1869), n=.03

Fig. B.3 - Response parameter, t=45 s, T=120 s.

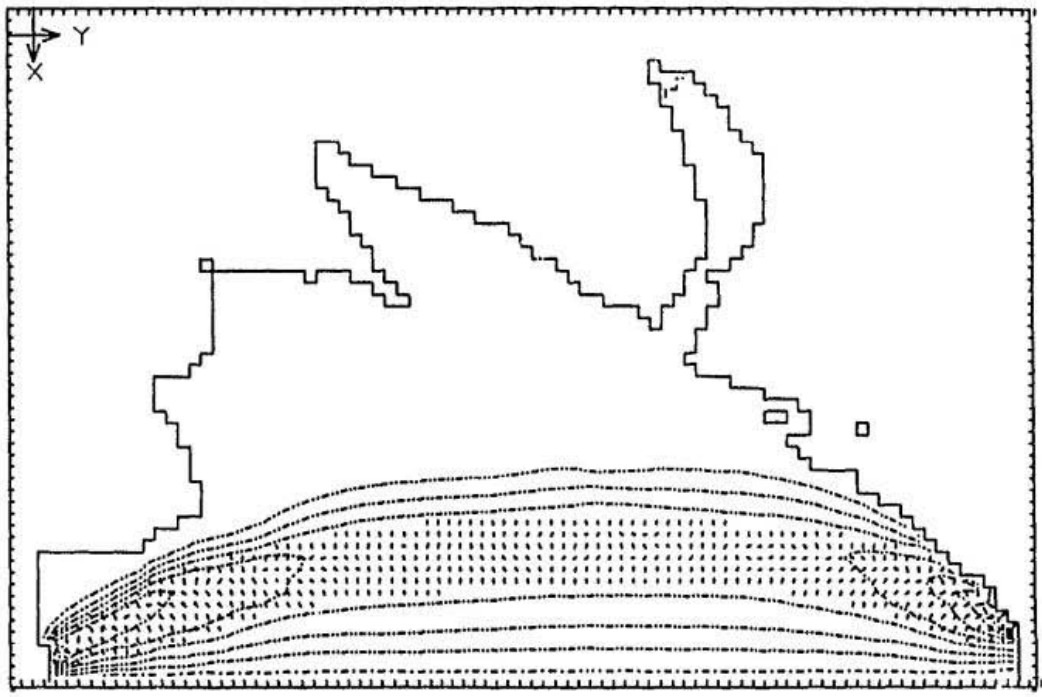

(----------)<0 , (----------)=0 , (————)>0
RESPONSE PARAMETER CONTOURS , So= 1.42E-02, & VECTORS
WAVE PERIOD = 120 :: ITERATION TIME = 60
MAX/MIN = 2.24E-02 /-.3965 :: INTERVAL = .035
GRID SPACE = 100 m
RUN DATE/TIME = 12-03-1991 / 12:23:05
Chezy Coefficient using Ganguillet & Kutter (1869), n= 03

Fig. B.4 - Response parameter, t=60 s, T=120 s.

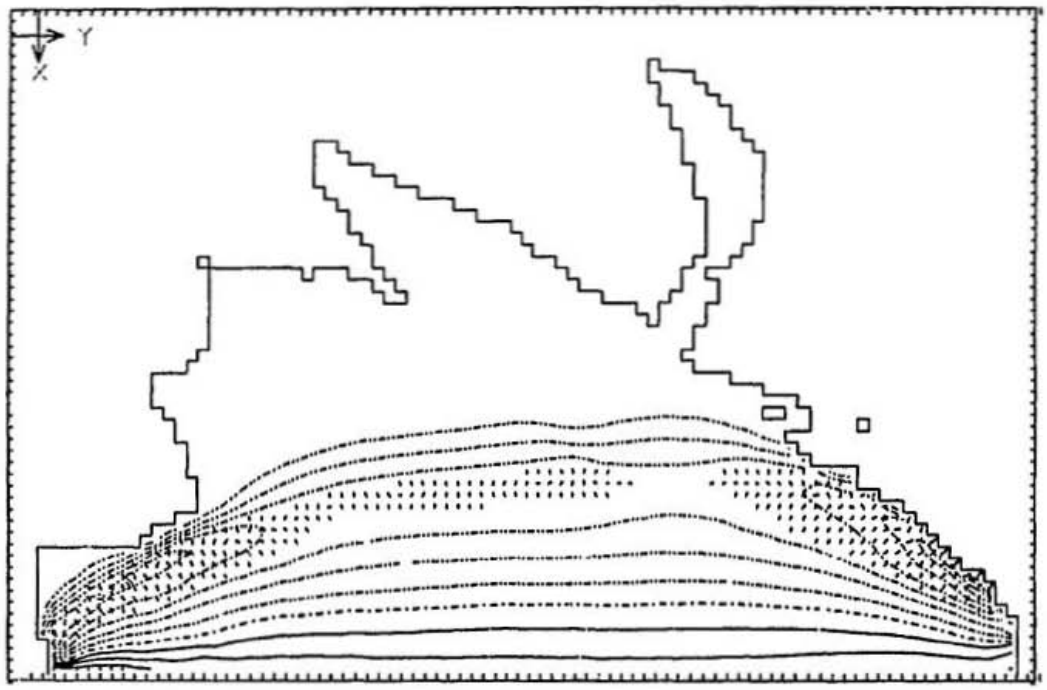

(————)<0 , (·····)=0 , (————)>0
RESPONSE PARAMETER CONTOURS , So= 1.42E-02, & VECTORS.
WAVE PERIOD = 120 :: ITERATION TIME = 75
MAX/MIN = .1674 /-.4406 :: INTERVAL = .04
GRID SPACE = 100 m
RUN DATE/TIME = 12-03-1991 / 12:53:15
Chezy Coefficient using Ganguillet & Kutter (1869), n=.03

Fig. B.5 - Response parameter, t=75 s, T=120 s.

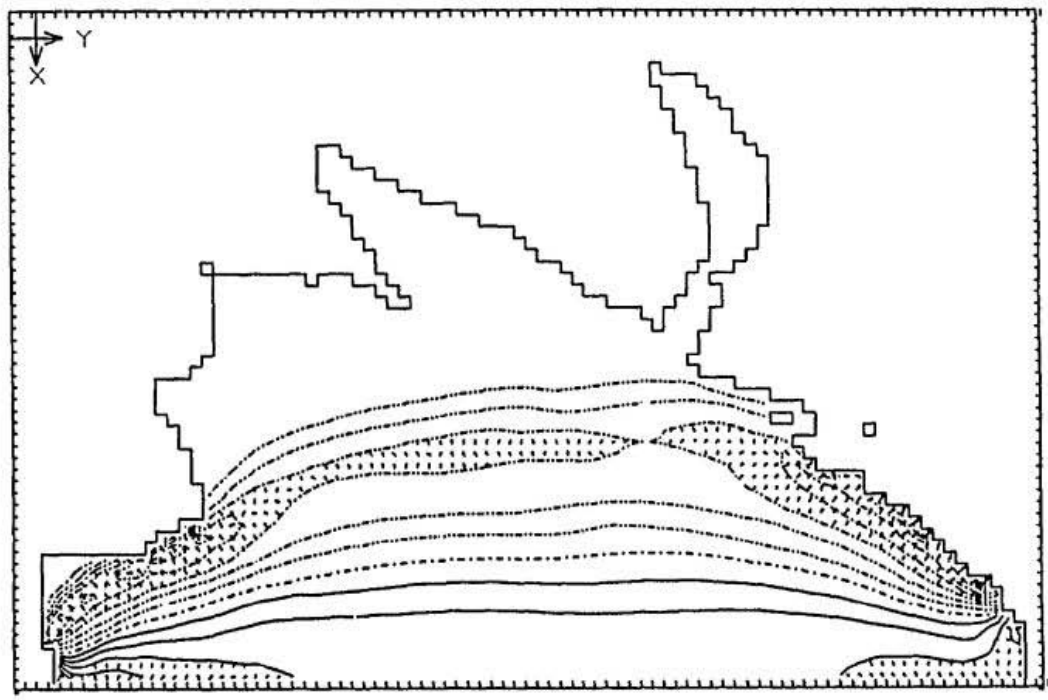

(----------)<0 , (----------)=0 , (————)>0
RESPONSE PARAMETER CONTOURS , So= 1.42E-02, & VECTORS
WAVE PERIOD = 120 :: ITERATION TIME = 90
MAX/MIN = .3046 / -.4527 :: INTERVAL = .045
GRID SPACE = 100 m
RUN DATE/TIME = 12-03-1991 / 13:32:58
Chezy Coefficient using Ganguillet & Kutter (1869), n= 03

Fig. B.6 - Response parameter, t=90 s, T=120 s.

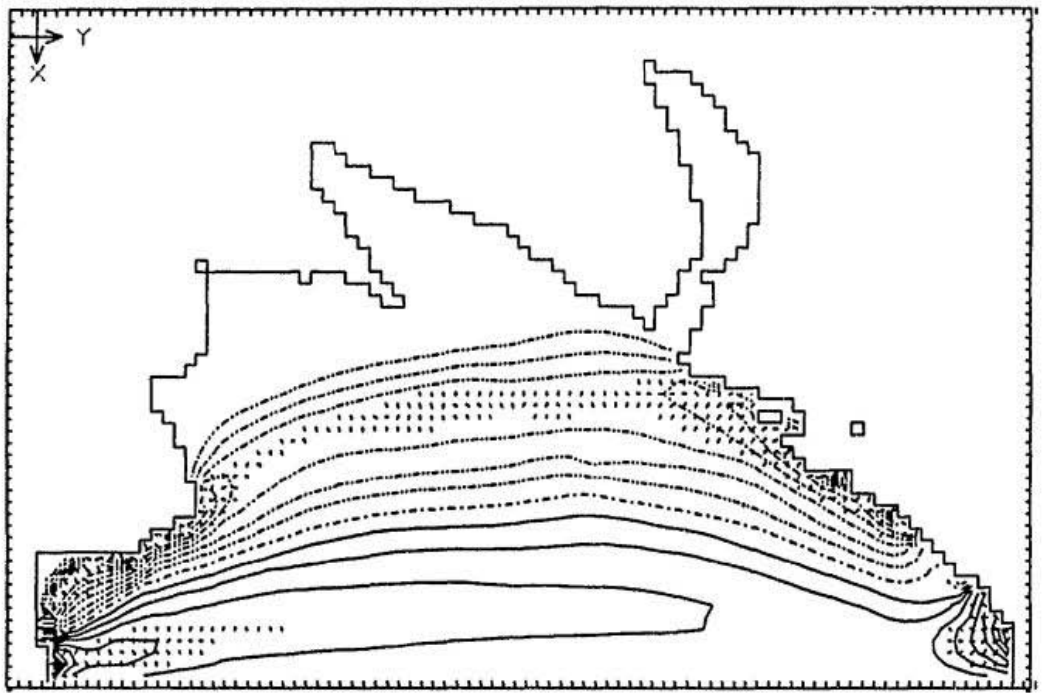

(·····) <0 , (·-·-·-·) =0 , (———) >0
RESPONSE PARAMETER CONTOURS , So= 1.42E-02, & VECTORS.
WAVE PERIOD = 120 :: ITERATION TIME = 105
MAX/MIN = .4167 / -.4636 :: INTERVAL = .04
GRID SPACE = 100 m
RUN DATE/TIME = 12-03-1991 / 13:54:16
Chezy Coefficient using Ganguillet & Kutter (1869), n=.03

Fig. B.7 - Response parameter, t=105 s, T=120 s.

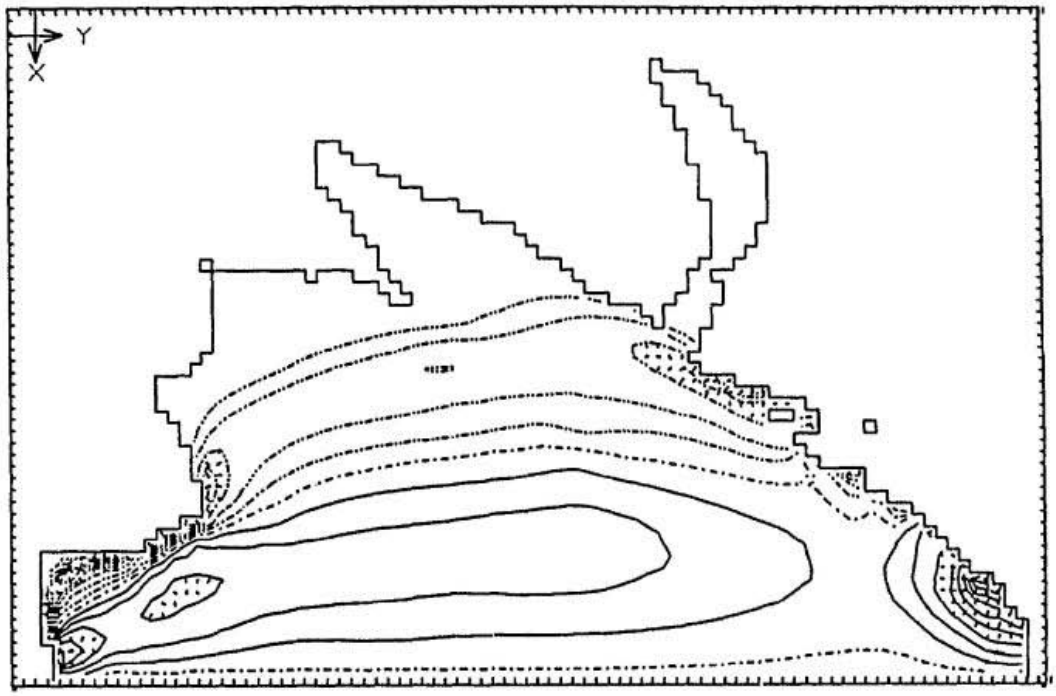

(·····) < 0 , (·····) = 0 , (———) > 0
RESPONSE PARAMETER CONTOURS , So= 1.42E-02, & VECTORS
WAVE PERIOD = 120 :: ITERATION TIME = 120
MAX/MIN = .5609 / -.4129 :: INTERVAL = .055
GRID SPACE = 100 m
RUN DATE/TIME = 12-03-1991 / 14:52:33
Chezy Coefficient using Ganguillet & Kutter (1869), n= 03

Fig. B.8 - Response parameter, t=120 s, T=120 s.

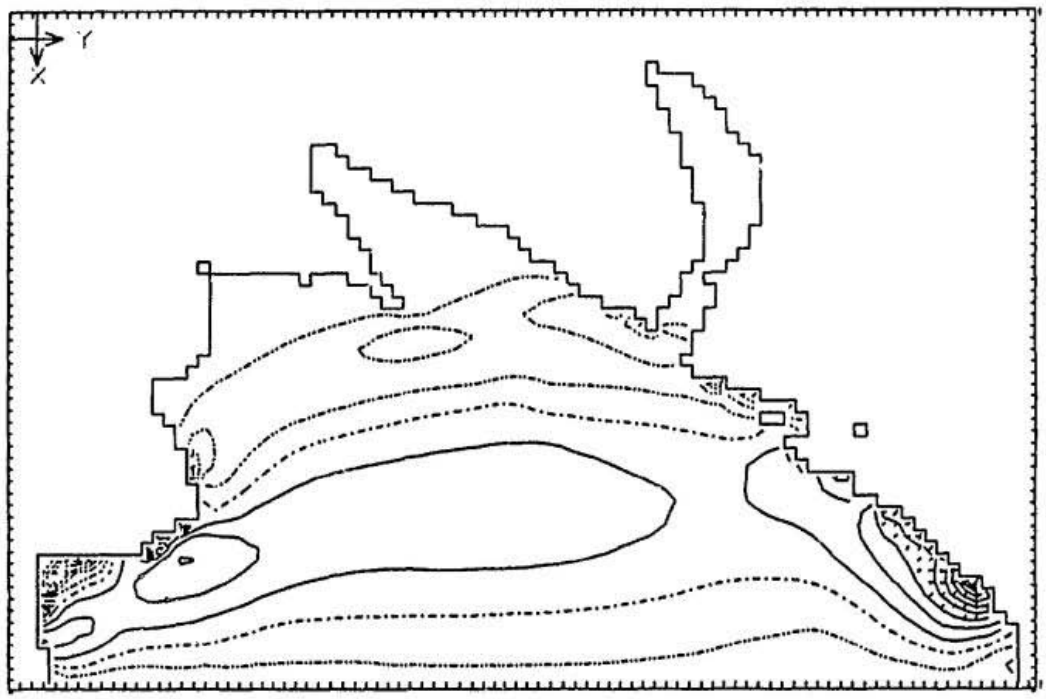

(·····) < 0 , (·····) = 0 , (———) > 0
RESPONSE PARAMETER CONTOURS , So= 1.42E-02, & VECTORS.
WAVE PERIOD = 120 :: ITERATION TIME = 135
MAX/MIN = .8393 / -.4343 :: INTERVAL = .08
GRID SPACE = 100 m
RUN DATE/TIME = 12-03-1991 / 15:47:02
Chezy Coefficient using Ganguillet & Kutter (1869), n=.03

Fig. B.9 - Response parameter, t=135 s, T=120 s.

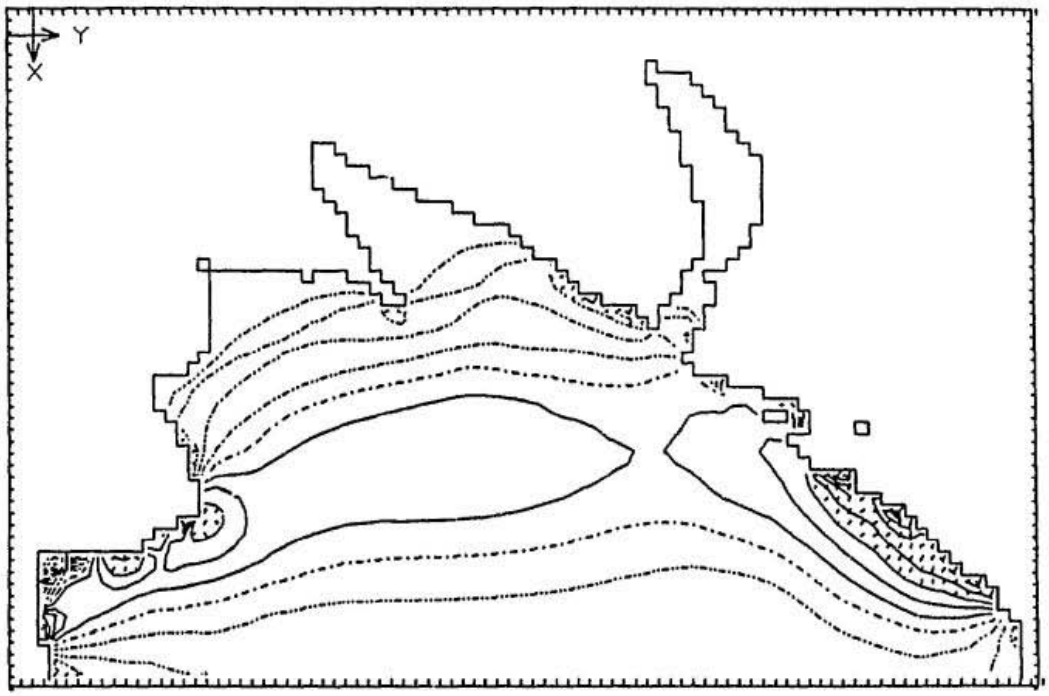

(·····)<0 , (·-·-·-·)=0 , (——)>0
RESPONSE PARAMETER CONTOURS , So= 1 42E-02, & VECTORS
WAVE PERIOD = 120 :: ITERATION TIME = 150
MAX/MIN = .7616 / -.4576 :: INTERVAL = .075
GRID SPACE = 100 m
RUN DATE/TIME = 12-03-1991 / 16:13:54
Chezy Coefficient using Ganguillet & Kutter (1869), n= 03

Fig. B.10 - Response parameter, t=150 s, T=120 s.

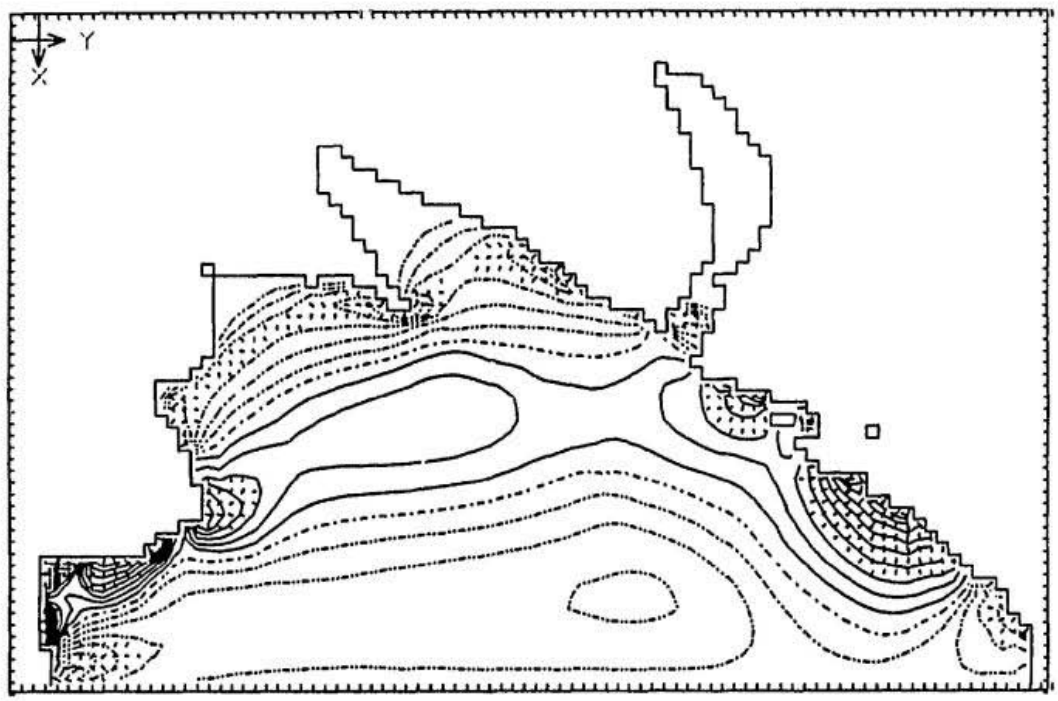

(----------)<0 , (----------)=0 , (----------)>0
RESPONSE PARAMETER CONTOURS , So= 1.42E-02, & VECTORS.
WAVE PERIOD = 120 :: ITERATION TIME = 165
MAX/MIN = .5322 /-.4521 :: INTERVAL = .05
GRID SPACE = 100 m
RUN DATE/TIME = 12-03-1991 / 16:37:29
Chezy Coefficient using Ganguillet & Kutter (1869), n=.03

Fig. B.11 - Response parameter, t=165 s, T=120 s.

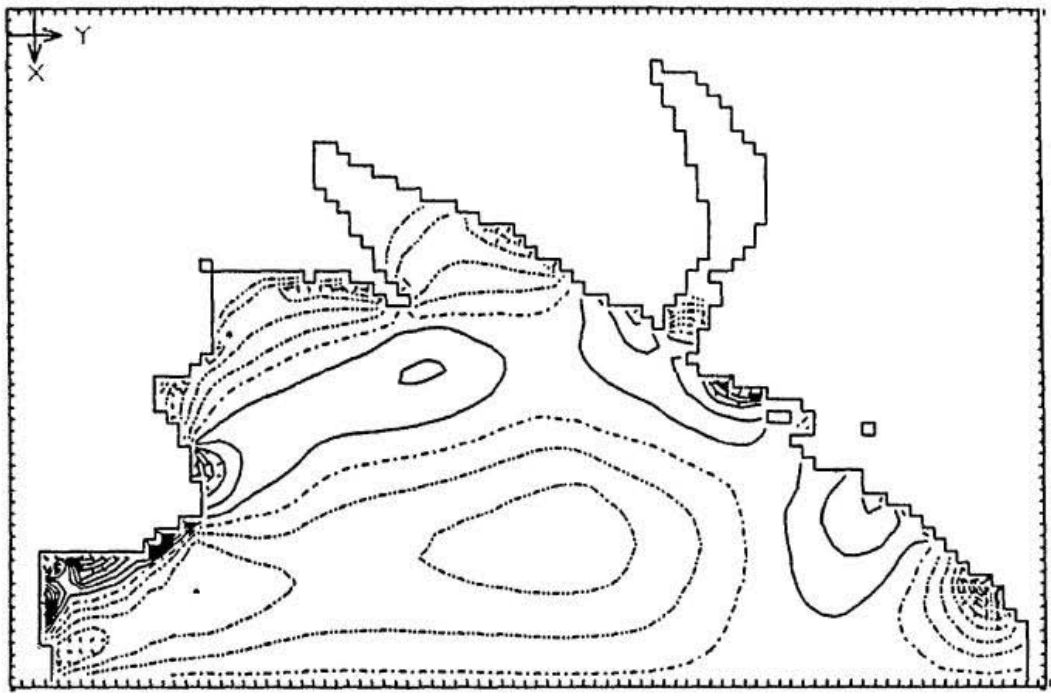

(----------)<0 , (----------)=0 , (----------)>0
RESPONSE PARAMETER CONTOURS , So= 1.42E-02, & VECTORS
WAVE PERIOD = 120 :: ITERATION TIME = 180
MAX/MIN = .6839 / -.7397 '' INTERVAL = .07
GRID SPACE = 100 m
RUN DATE/TIME = 12-03-1991 / 17:01:47
Chezy Coefficient using Ganguillet & Kutter (1869), n= 03

Fig. B.12 - Response parameter, t=180 s, T=120 s.

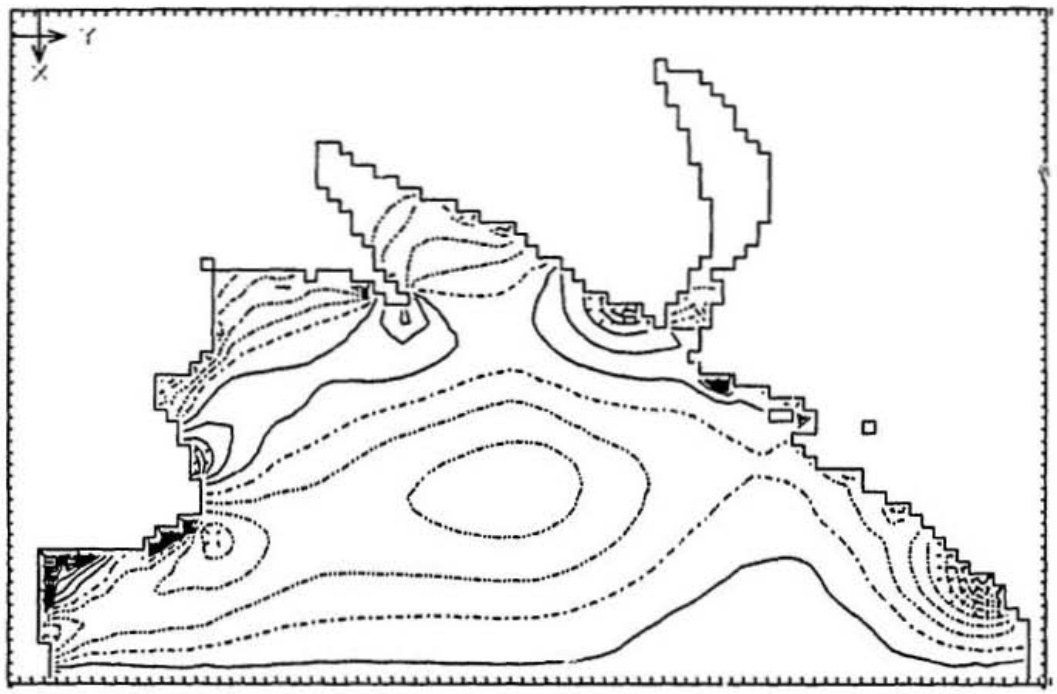

(————)<0 , (·····)=0 , (————)>0
RESPONSE PARAMETER CONTOURS , So= 1.42E-02, & VECTORS.
WAVE PERIOD = 120 :: ITERATION TIME = 195
MAX/MIN = .8370 /-.7423 :: INTERVAL = .08
GRID SPACE = 100 m
RUN DATE/TIME = 12-03-1991 / 17:32:31
Chezy Coefficient using Ganguillet & Kutter (1869), n=.03

Fig. B.13 - Response parameter, t=195 s, T=120 s.

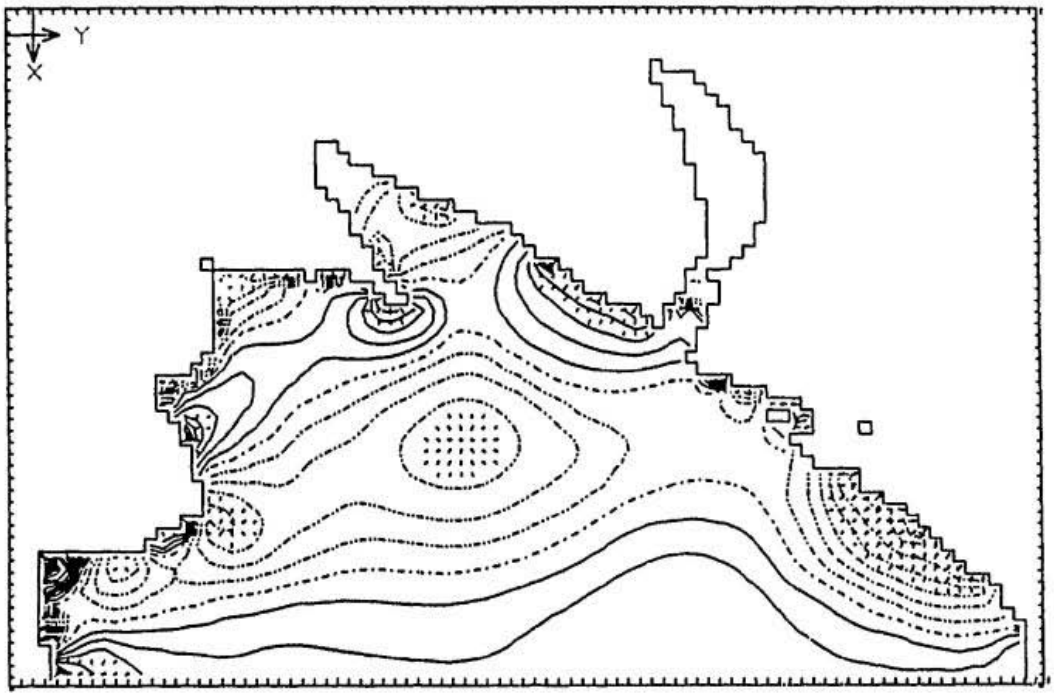

(·····) <0 , (·····) =0 , (———) >0
RESPONSE PARAMETER CONTOURS , So= 1 42E-02, & VECTORS
WAVE PERIOD = 120 : ITERATION TIME = 210
MAX/MIN = .5503 / -.6485 : INTERVAL = .06
GRID SPACE = 100 m
RUN DATE/TIME = 12-03-1991 / 18:27:09
Chezy Coefficient using Ganguillet & Kutter (1869), n= 03

Fig. B.14 - Response parameter, t=210 s, T=120 s.

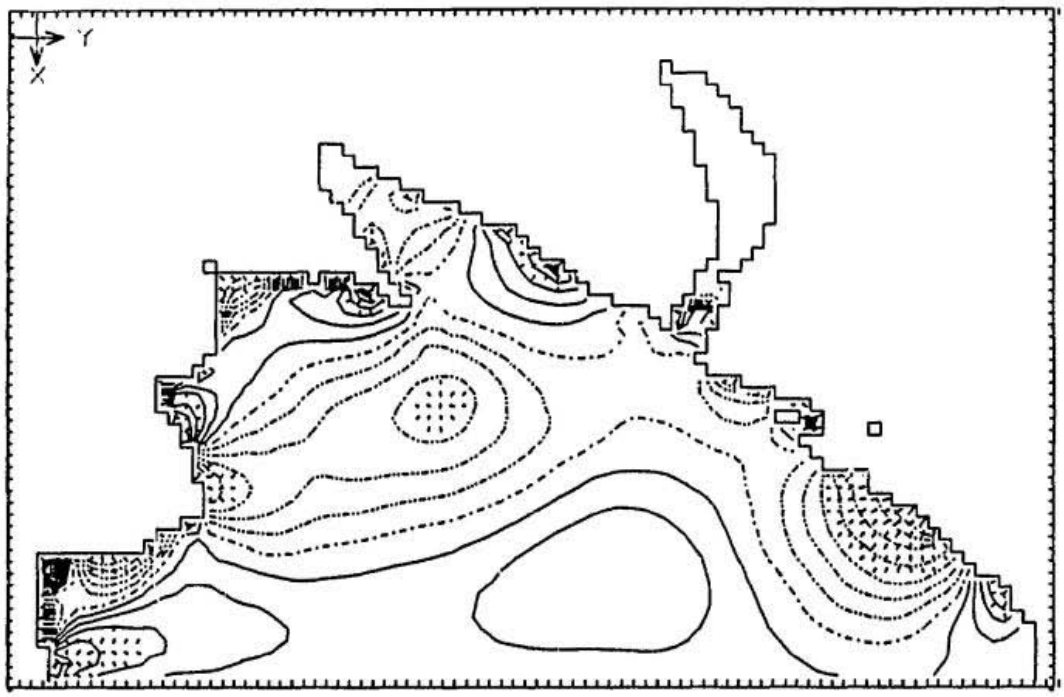

(·····) <0 , (·-·-·-·) =0 , (———) >0
RESPONSE PARAMETER CONTOURS , So= 1.42E-02, & VECTORS.
WAVE PERIOD = 120 :: ITERATION TIME = 225
MAX/MIN = .6960 /-.5860 :: INTERVAL = .065
GRID SPACE = 100 m
RUN DATE/TIME = 12-03-1991 / 18:51:25
Chezy Coefficient using Ganguillet & Kutter (1869), n=.03

Fig. B.15 - Response parameter, t=225 s, T=120 s.

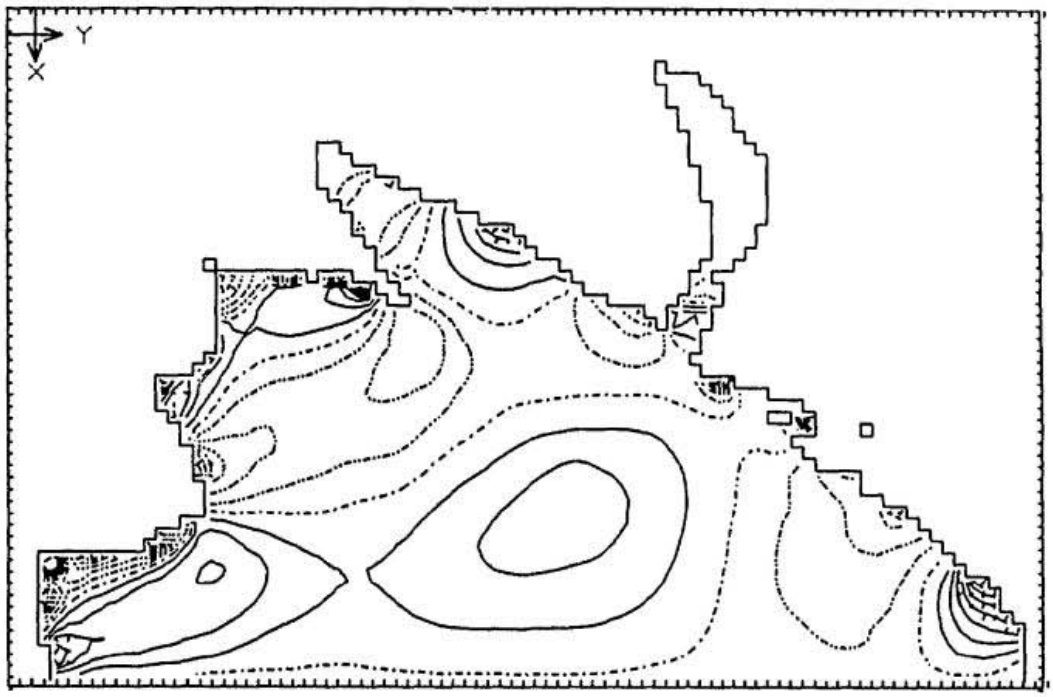

(----------)<0 , (·-·-·-·-)=0 , (———)>0
RESPONSE PARAMETER CONTOURS , So= 1.42E-02, & VECTORS
WAVE PERIOD = 120 : ITERATION TIME = 240
MAX/MIN = .8311 / -.9967 : INTERVAL = .09
GRID SPACE = 100 m
RUN DATE/TIME = 12-03-1991 / 19:19:50
Chezy Coefficient using Ganguillet & Kutter (1869), n= 03

Fig. B.16 - Response parameter, t=240 s, T=120 s.

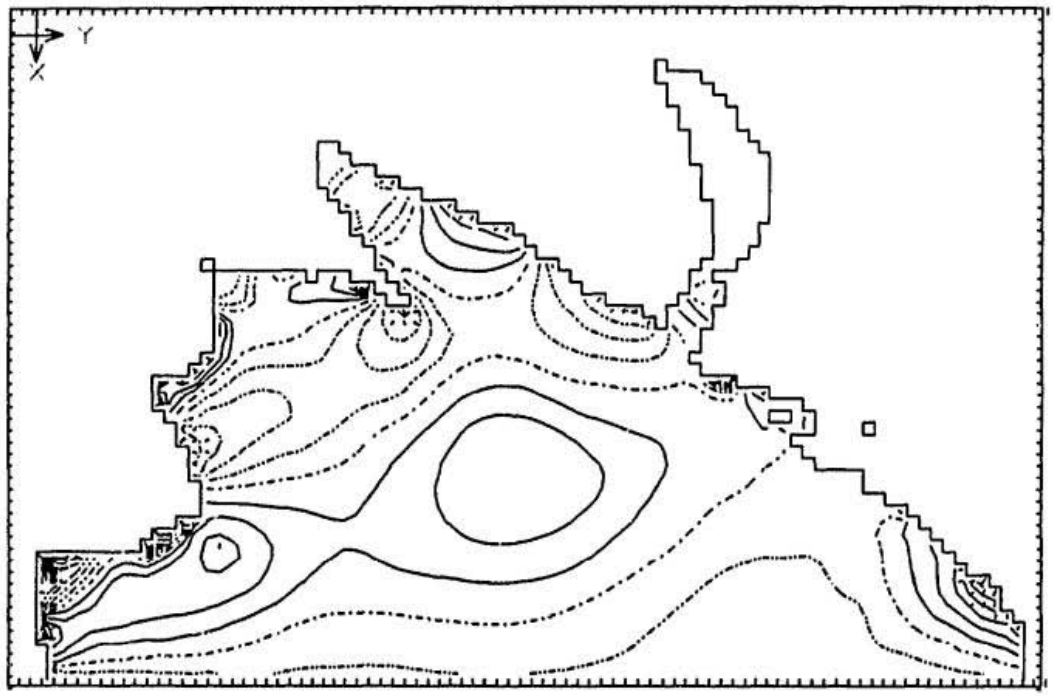

(·····) <0 , (·-·-·-·) =0 , (———) >0
RESPONSE PARAMETER CONTOURS , So= 1.42E-02, & VECTORS.
WAVE PERIOD = 120 :: ITERATION TIME = 255
MAX/MIN = .9738 /-.8873 :: INTERVAL = .09
GRID SPACE = 100 m
RUN DATE/TIME = 12-14-1991 / 20:32:34
Chezy Coefficient using Ganguillet & Kutter (1869), n=.03

Fig. B.17 - Response parameter, t=255 s, T=120 s.

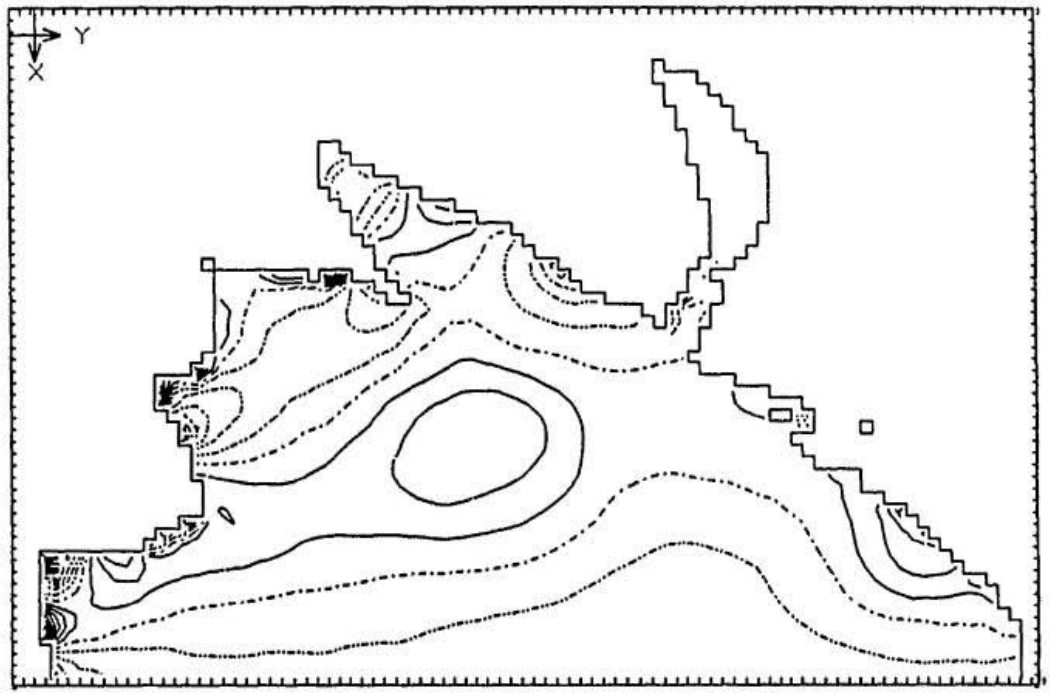

(·····) <0 , (·-·-·-·) =0 , (———) >0
RESPONSE PARAMETER CONTOURS , So= 1.42E-02, & VECTORS.
WAVE PERIOD = 120 :: ITERATION TIME = 270
MAX/MIN = 1.313 /-.7646 :: INTERVAL = .1
GRID SPACE = 100 m
RUN DATE/TIME = 12-14-1991 / 20:55:40
Chezy Coefficient using Ganguillet & Kutter (1869), n= 03

Fig. B.18 - Response parameter, t=270 s, T=120 s.

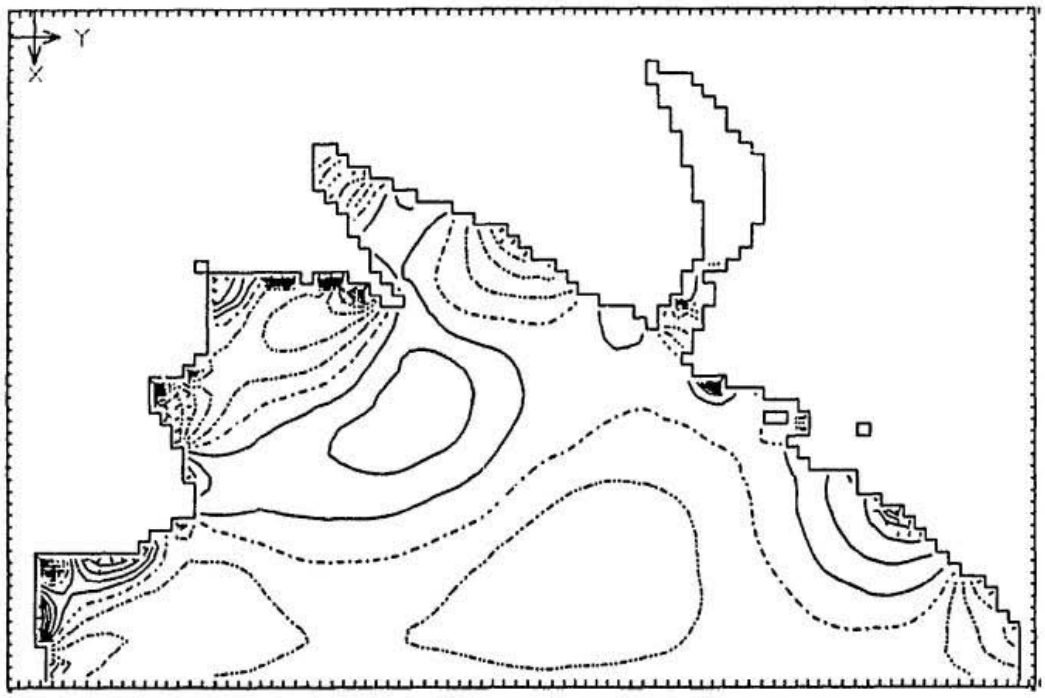

(----------)<0 , (----------)=0 , (————)>0
RESPONSE PARAMETER CONTOURS , So= 1.42E-02, & VECTORS.
WAVE PERIOD = 120 :: ITERATION TIME = 285
MAX/MIN = 1.082 /-1.055 :: INTERVAL = .1
GRID SPACE = 100 m
RUN DATE/TIME = 12-14-1991 / 21:19:24
Chezy Coefficient using Ganguillet & Kutter (1869), n=.03

Fig. B.19 - Response parameter, t=285 s, T=120 s.

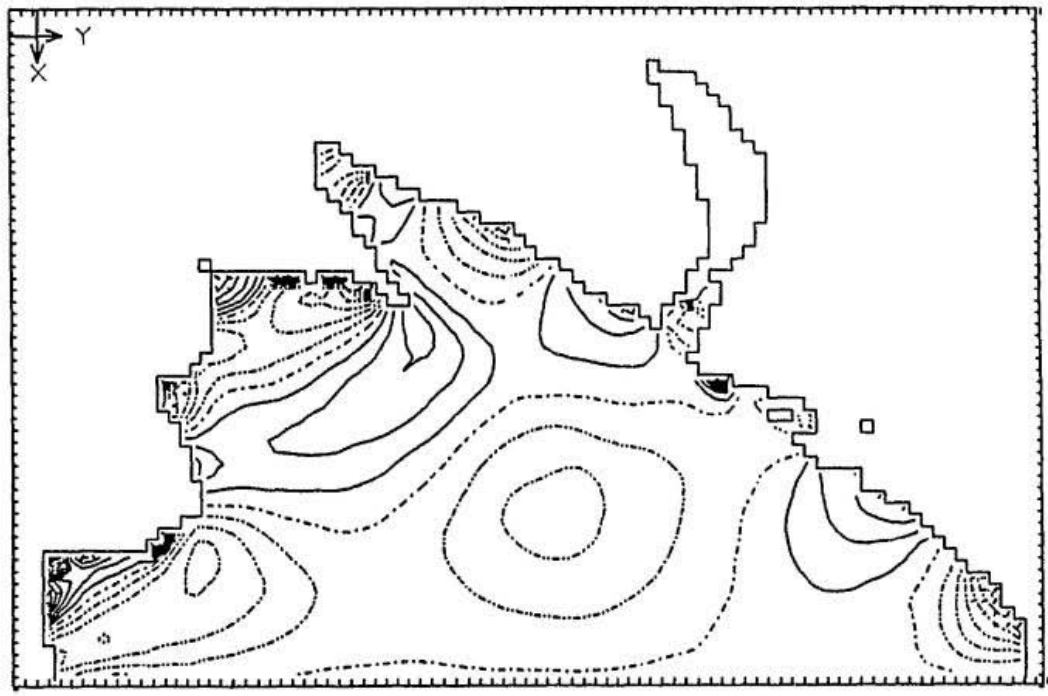

(·····) < 0 , (·····) = 0 , (———) > 0
RESPONSE PARAMETER CONTOURS , So= 1.42E-02, & VECTORS
WAVE PERIOD = 120 :: ITERATION TIME = 300
MAX/MIN = 1.204 / -1.009 :: INTERVAL = .1
GRID SPACE = 100 m
RUN DATE/TIME = 12-14-1991 / 21:45:31
Chezy Coefficient using Ganguillet & Kutter (1869), n= 03

Fig. B.20 - Response parameter, t=300 s, T=120 s.

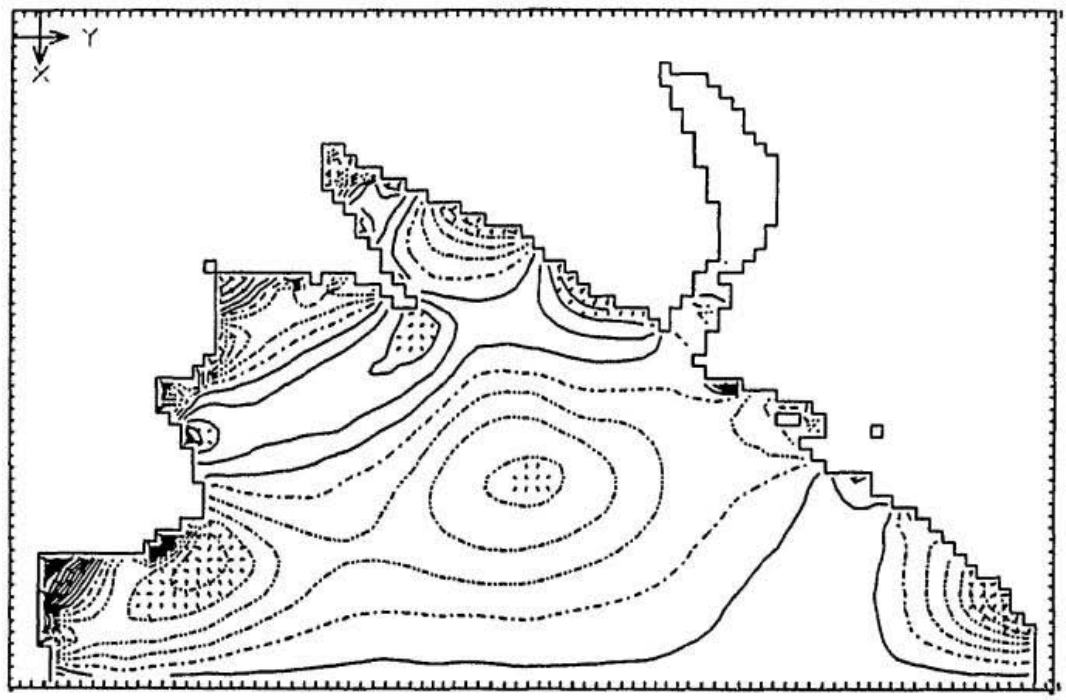

(·····) <0 , (·-·-·-·) =0 , (———) >0
RESPONSE PARAMETER CONTOURS , So= 1.42E-02, & VECTORS.
WAVE PERIOD = 120 :: ITERATION TIME = 315
MAX/MIN = .7540 /-.8329 :: INTERVAL = .08
GRID SPACE = 100 m
RUN DATE/TIME = 12-14-1991 / 22:10:09
Chezy Coefficient using Ganguillet & Kutter (1869), n=.03

Fig. B.21 - Response parameter, t=315 s, T=120 s.

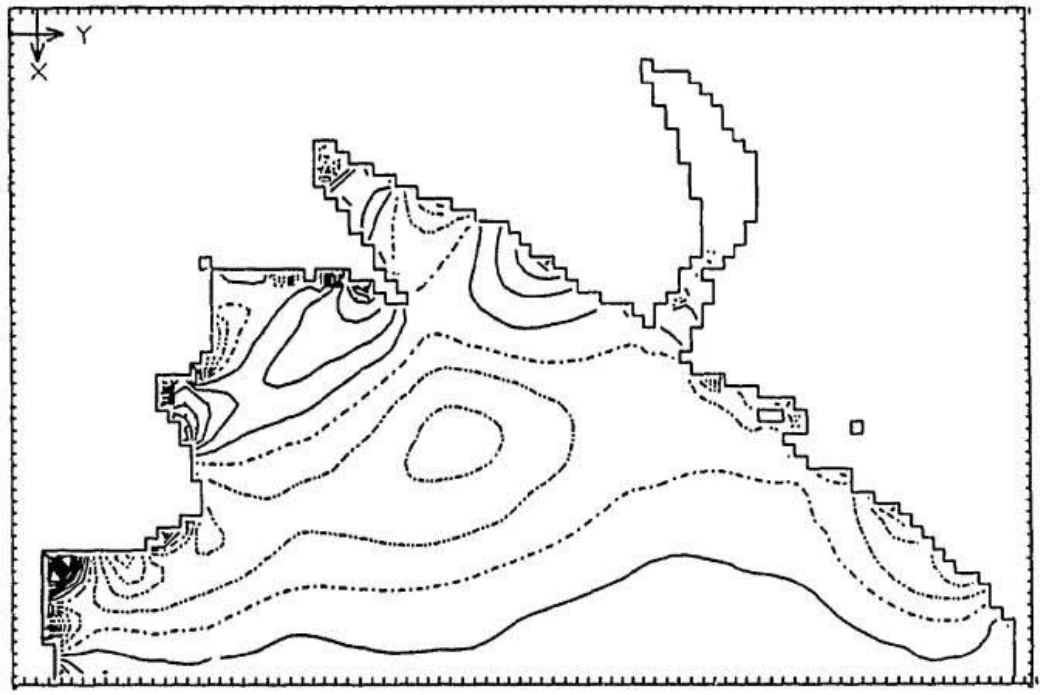

(————)<0 , (····)=0 , (—— ——)>0
RESPONSE PARAMETER CONTOURS , So= 1.42E-02, & VECTORS.
WAVE PERIOD = 120 :: ITERATION TIME = 330
MAX/MIN = 1.335 / -1.104 :: INTERVAL = 1
GRID SPACE = 100 m
RUN DATE/TIME = 12-14-1991 / 22:31:43
Chezy Coefficient using Ganguillet & Kutter (1869), n= 03

Fig. B.22 - Response parameter, t=330 s, T=120 s.

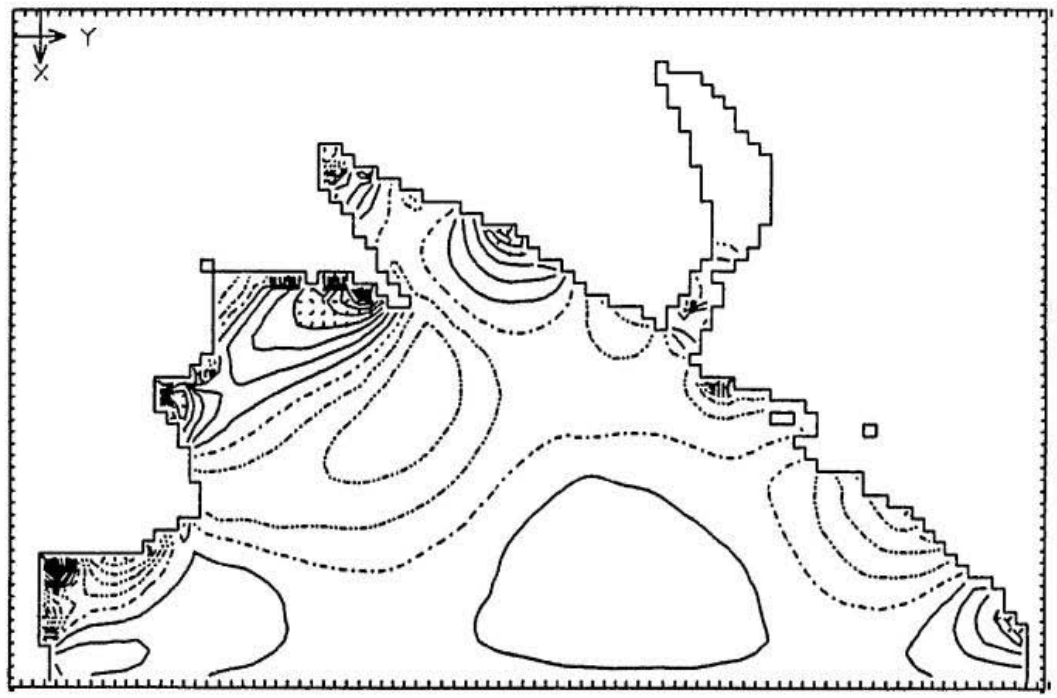

(·····) < 0 , (·-·-·-·) = 0 , (——) > 0
RESPONSE PARAMETER CONTOURS , So= 1.42E-02, & VECTORS.
WAVE PERIOD = 120 :: ITERATION TIME = 345
MAX/MIN = 1.324 /-1.319 :: INTERVAL = .1
GRID SPACE = 100 m
RUN DATE/TIME = 12-14-1991 / 22:57:48
Chezy Coefficient using Ganguillet & Kutter (1869), n=.03

Fig. B.23 - Response parameter, t=345 s, T=120 s.

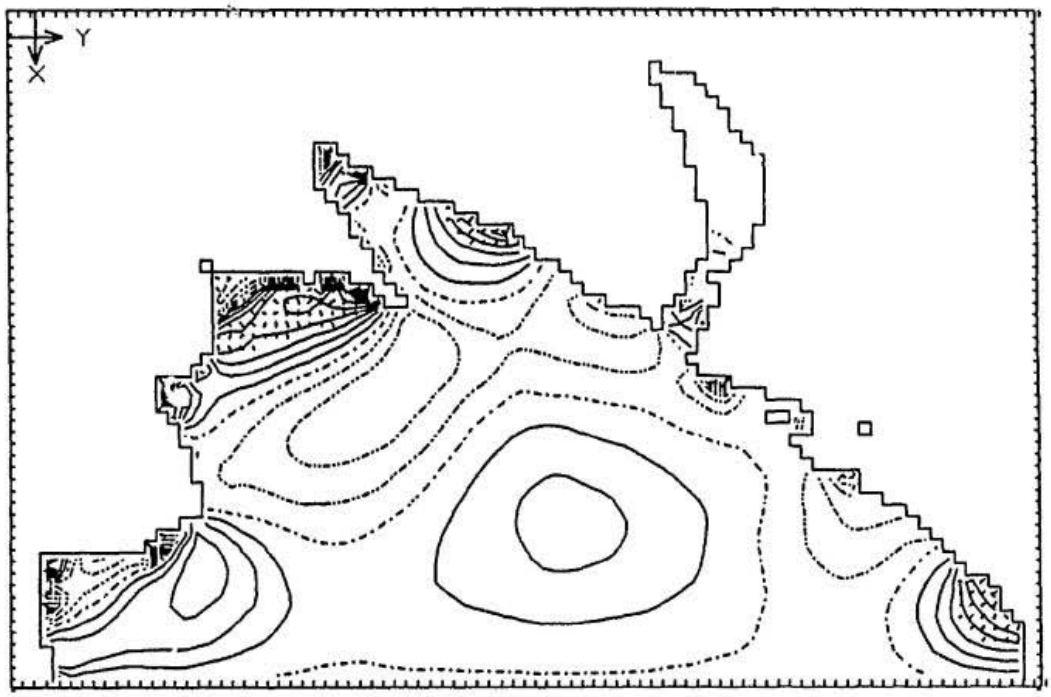

(·····)<0 , (·-·-·-·)=0 , (———)>0
RESPONSE PARAMETER CONTOURS , So= 1.42E-02, & VECTORS
WAVE PERIOD = 120 :: ITERATION TIME = 360
MAX/MIN = 1.154 /-1.086 :: INTERVAL = .1
GRID SPACE = 100 m
RUN DATE/TIME = 12-14-1991 / 23:21 08
Chezy Coefficient using Ganguillet & Kutter (1869), n= 03

Fig. B.24 - Response parameter, t=360 s, T=120 s.

Appendix C

LONGWAVE HARDCOPY OUTPUTS FOR SOHILCO HARBOUR DEVELOPMENT, FRESHWATER BAY, OUTER BASIN, RESPONSE PARAMETER ANALYSIS.

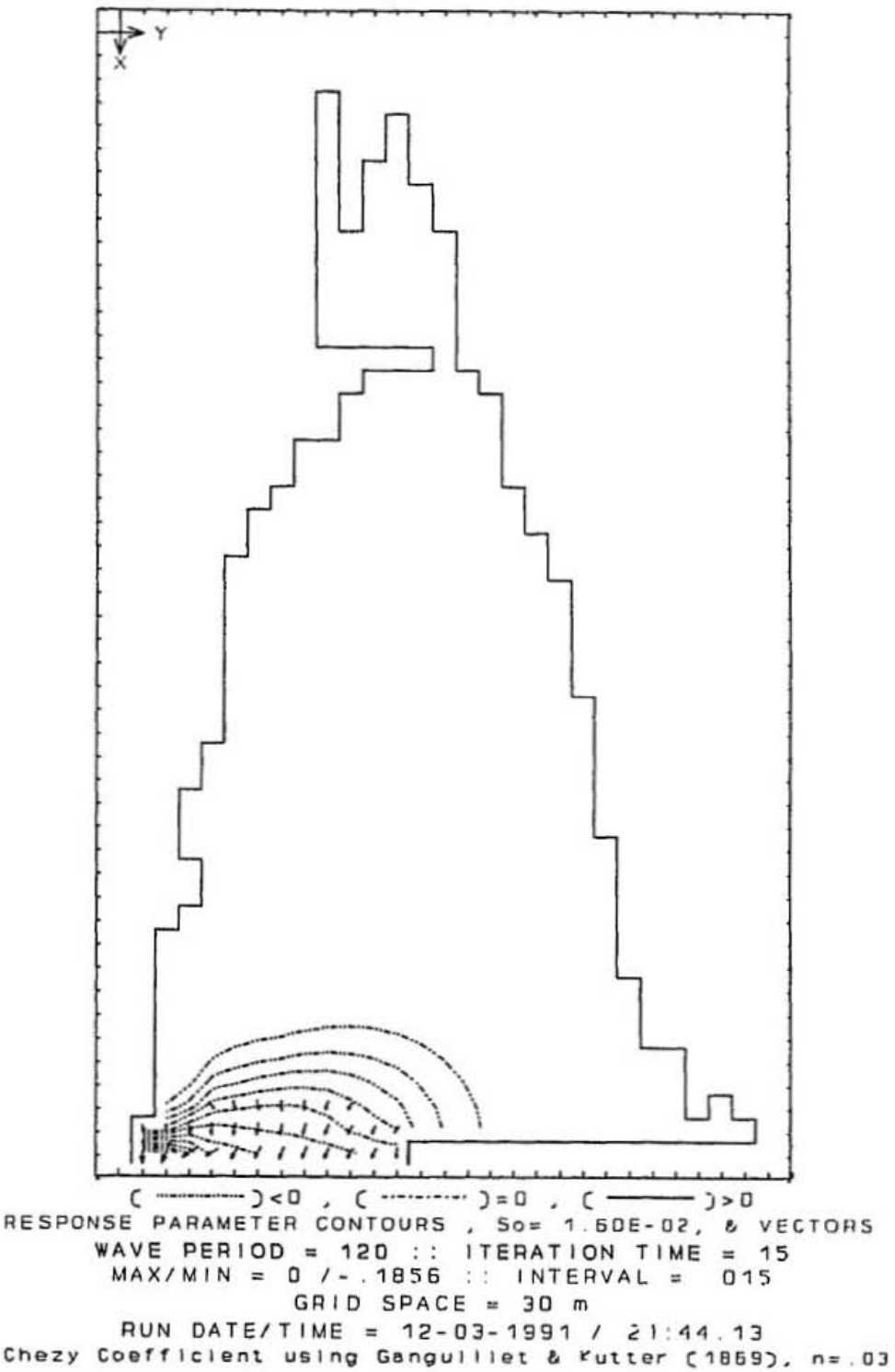

Fig. C.1 - Basin response, t=15 s, T=120 s.

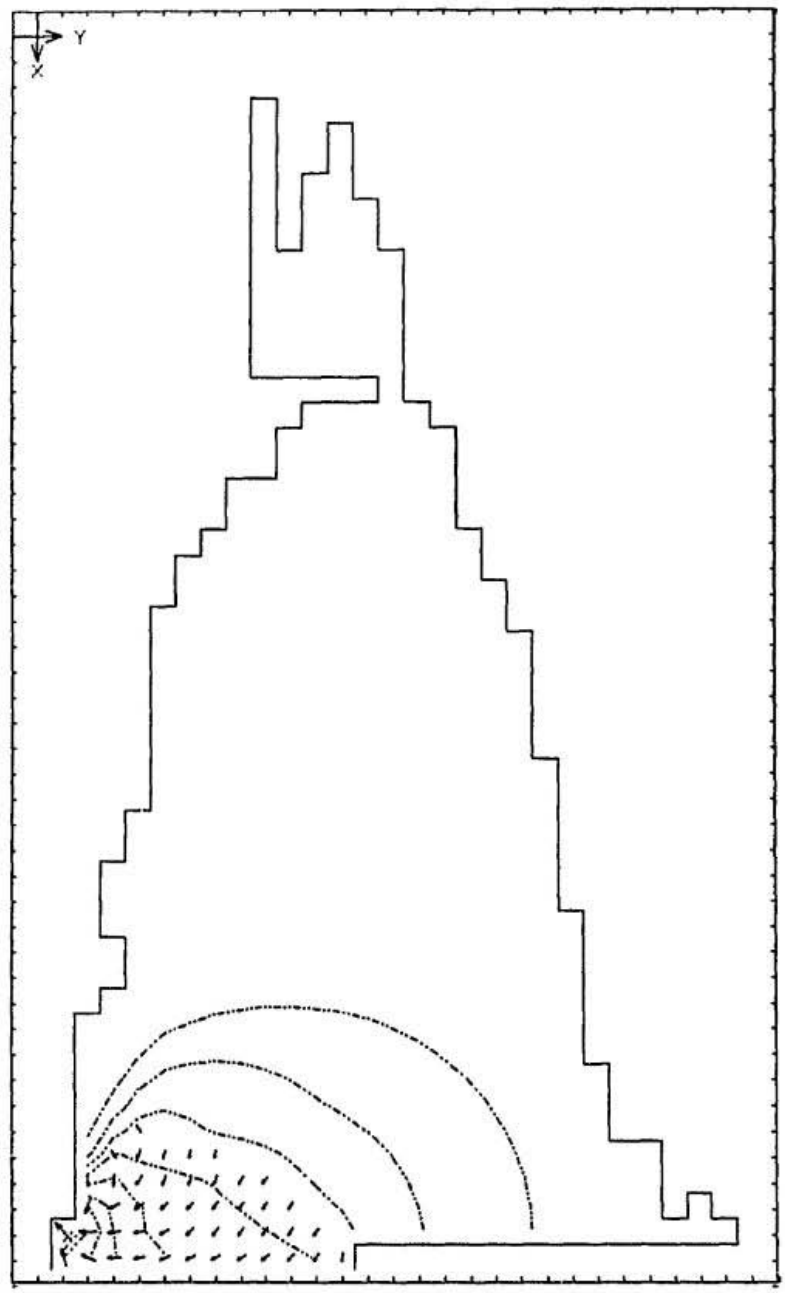

Fig. C.2 - Basin response, t=30 s, T=120 s.

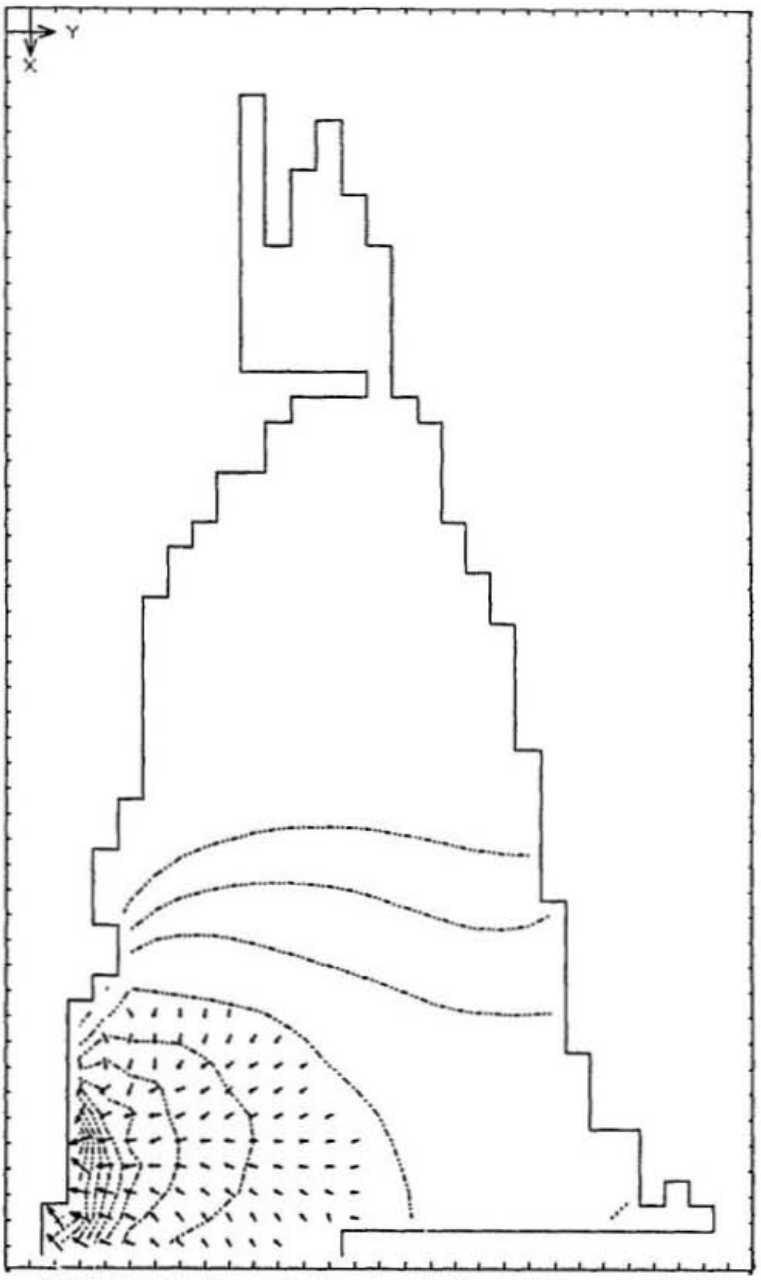

Fig. C.3 - Basin response, t=45 s, T=120 s.

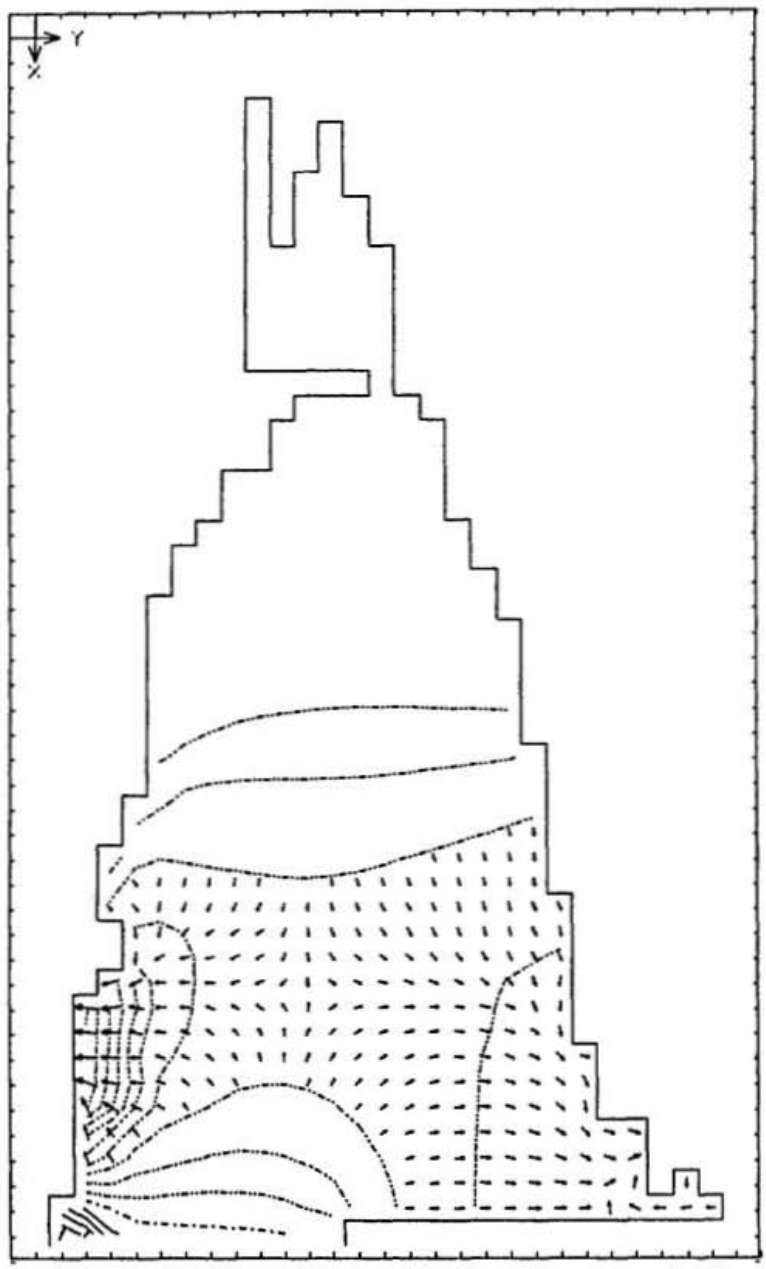

Fig. C.4 - Basin response, t=60 s, T=120 s.

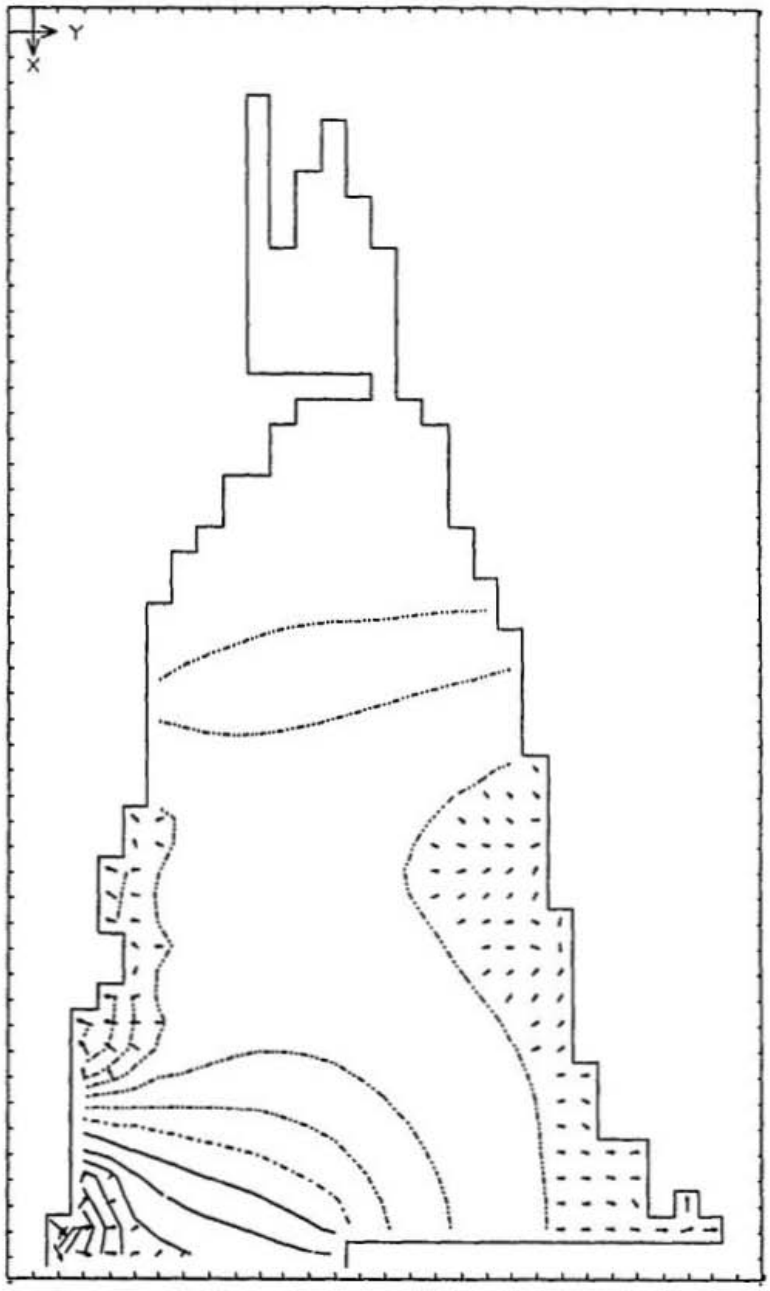

Fig. C.5 - Basin response, t=75 s, T=120 s.

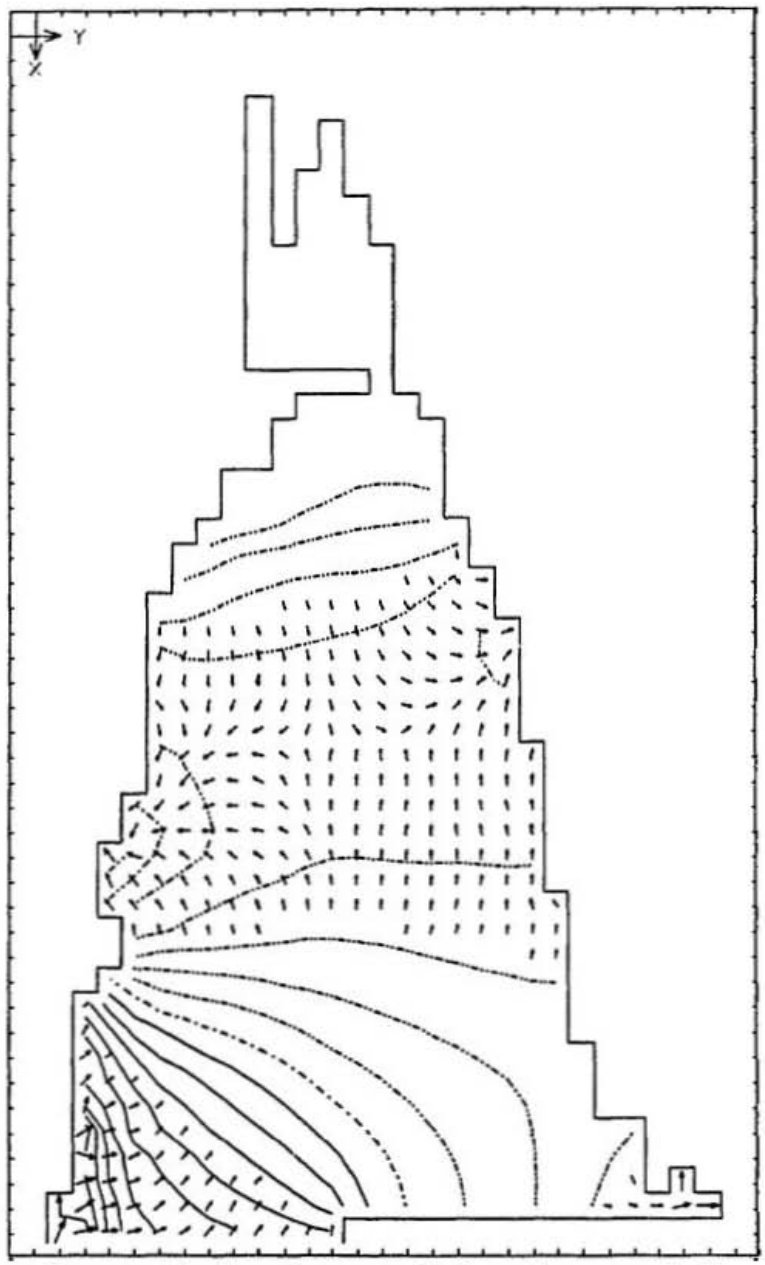

Fig. C.6 - Basin response, t=90 s, T=120 s.

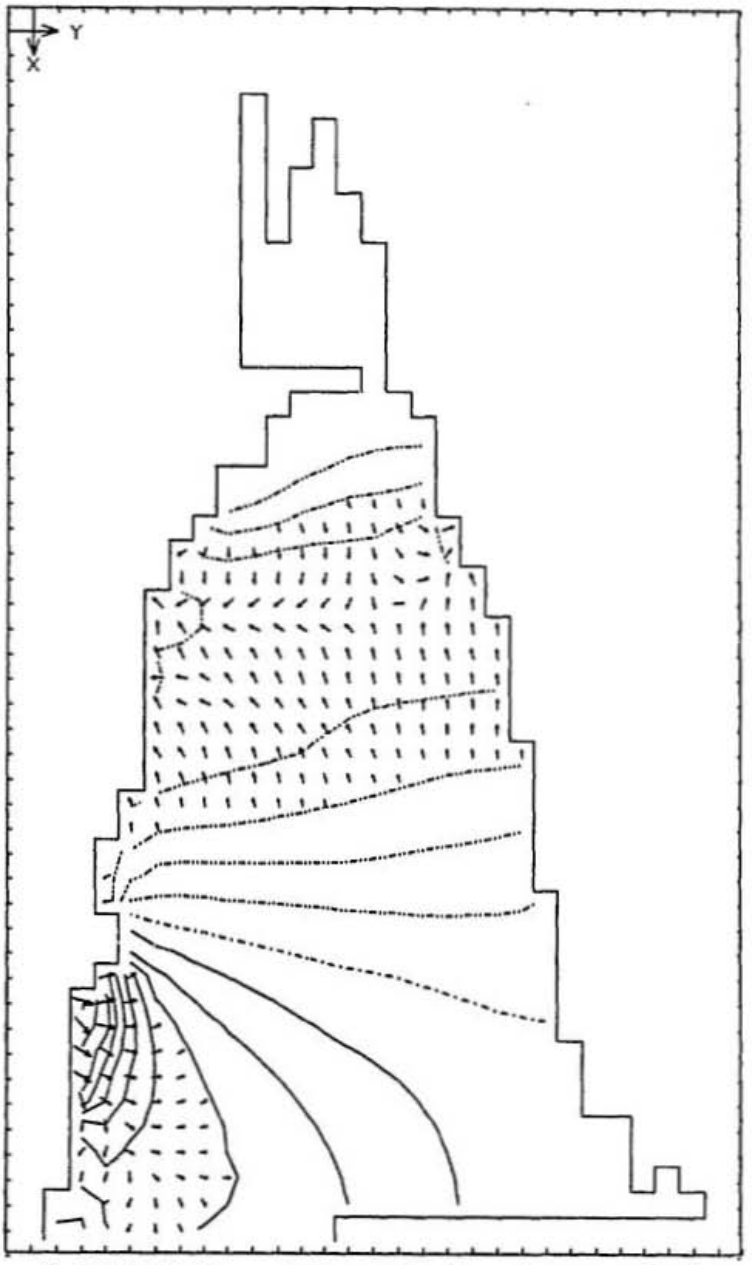

Fig. C.7 - Basin response, t=105 s, T=120 s.

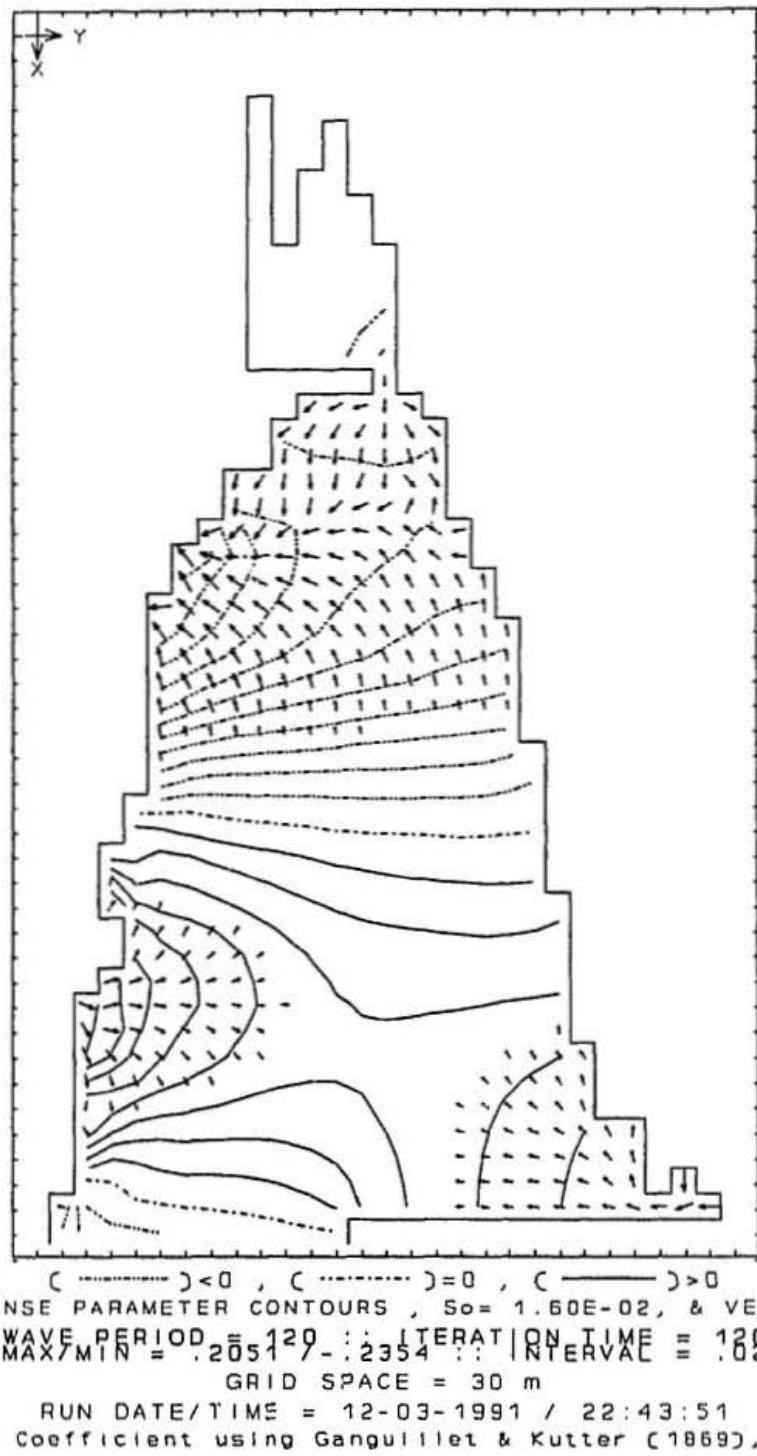

Fig. C.8 - Basin response, t=120 s, T=120 s.

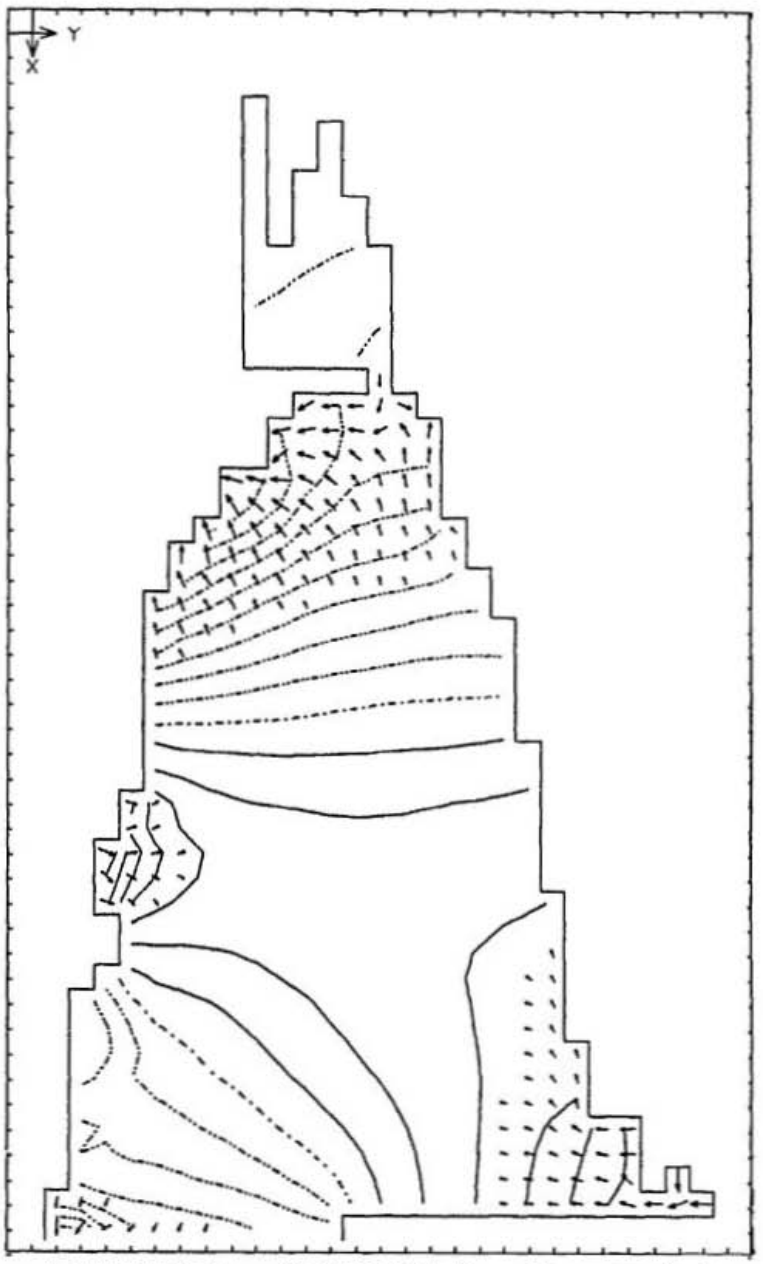

Fig. C.9 - Basin response, t=135 s, T=120 s.

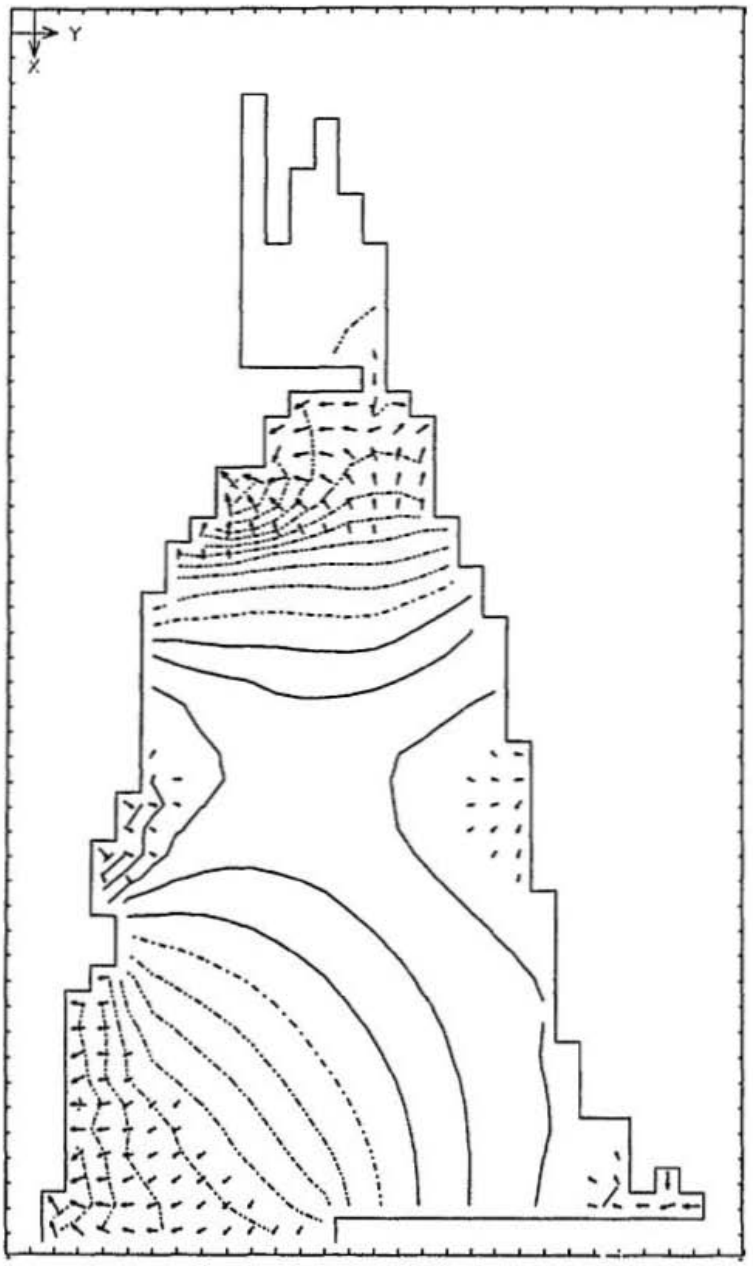

Fig. C.10 - Basin response, t=150 s, T=120 s.

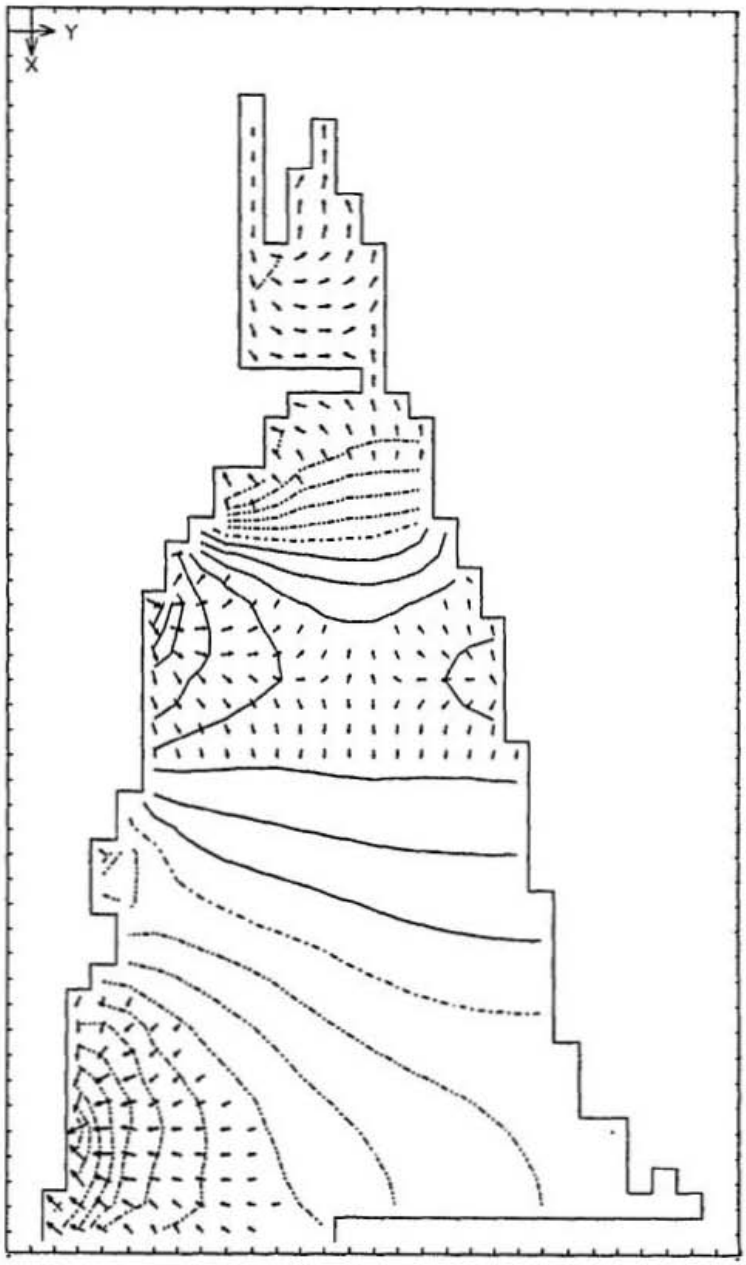

Fig. C.11 - Basin response, t=165 s, T=120 s.

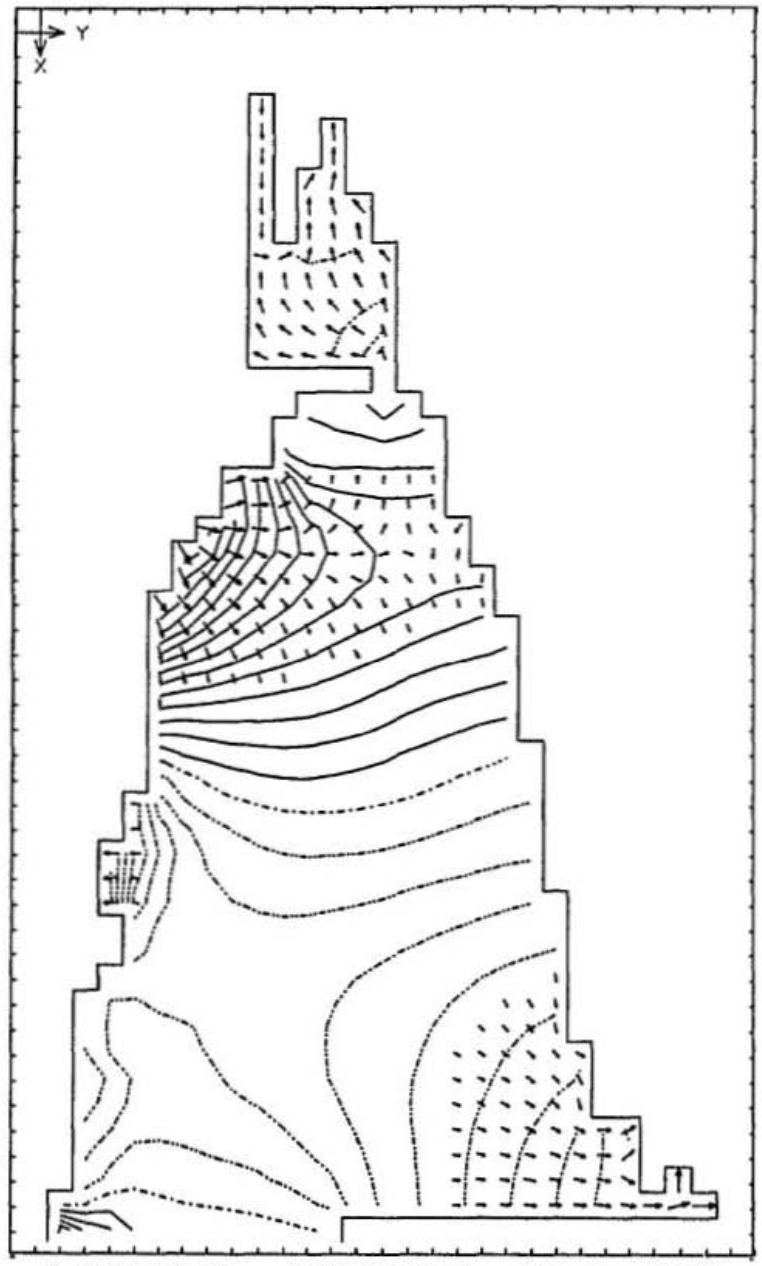

Fig. C.12 - Basin response, t=180 s, T=120 s.

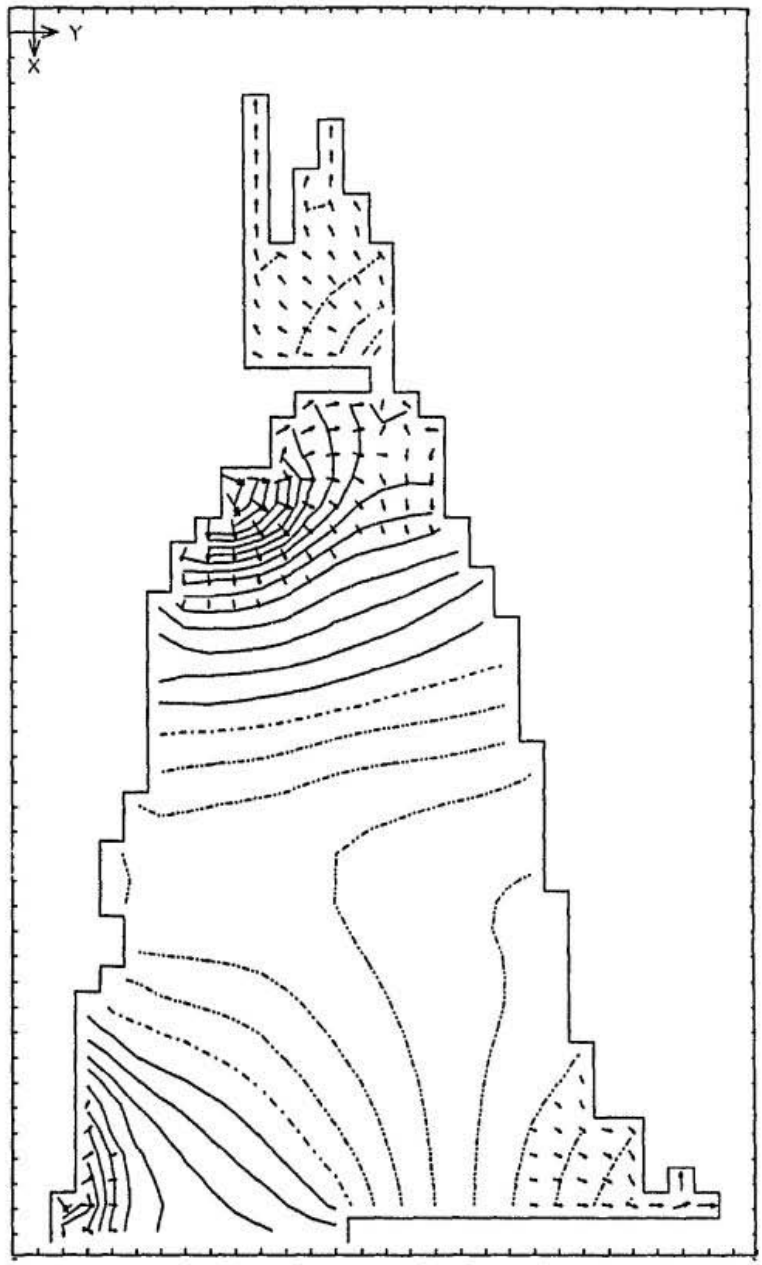

Fig. C.13 - Basin response, t=195 s, T=120 s.

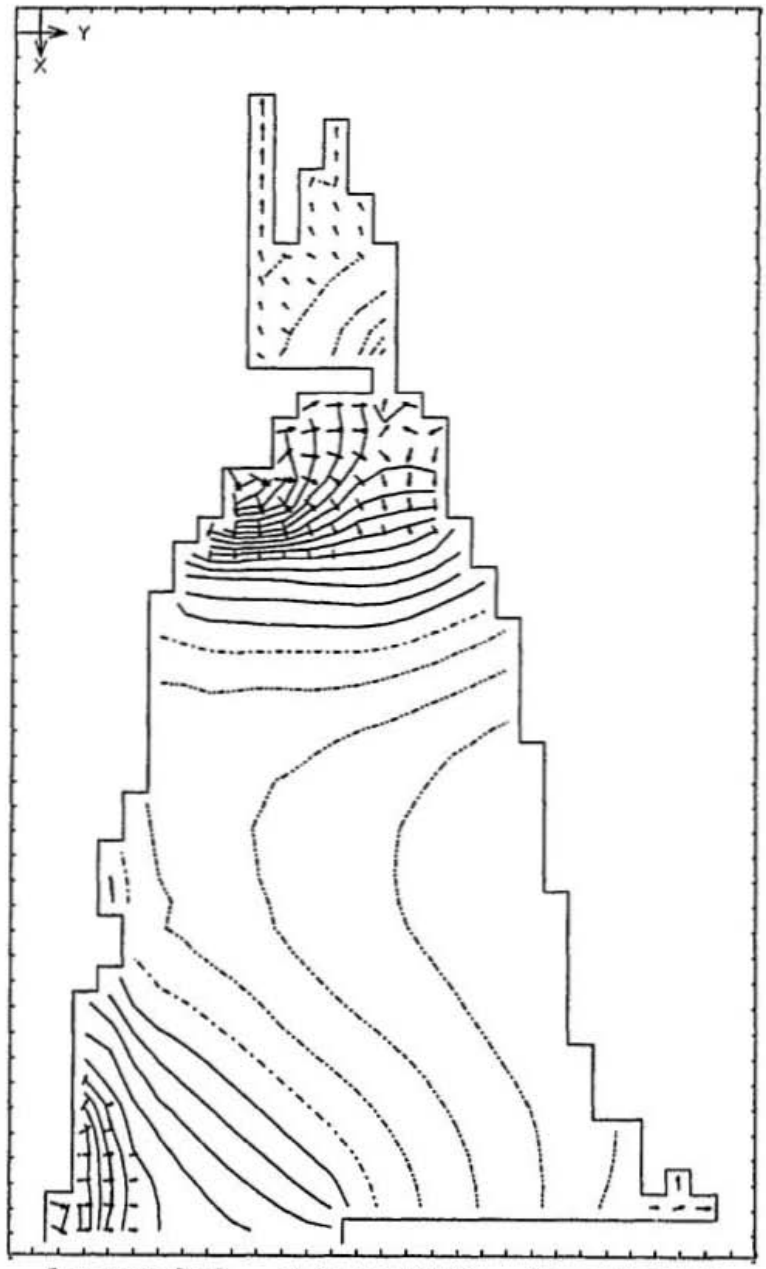

Fig. C.14 - Basin response, t=210 s, T=120 s.

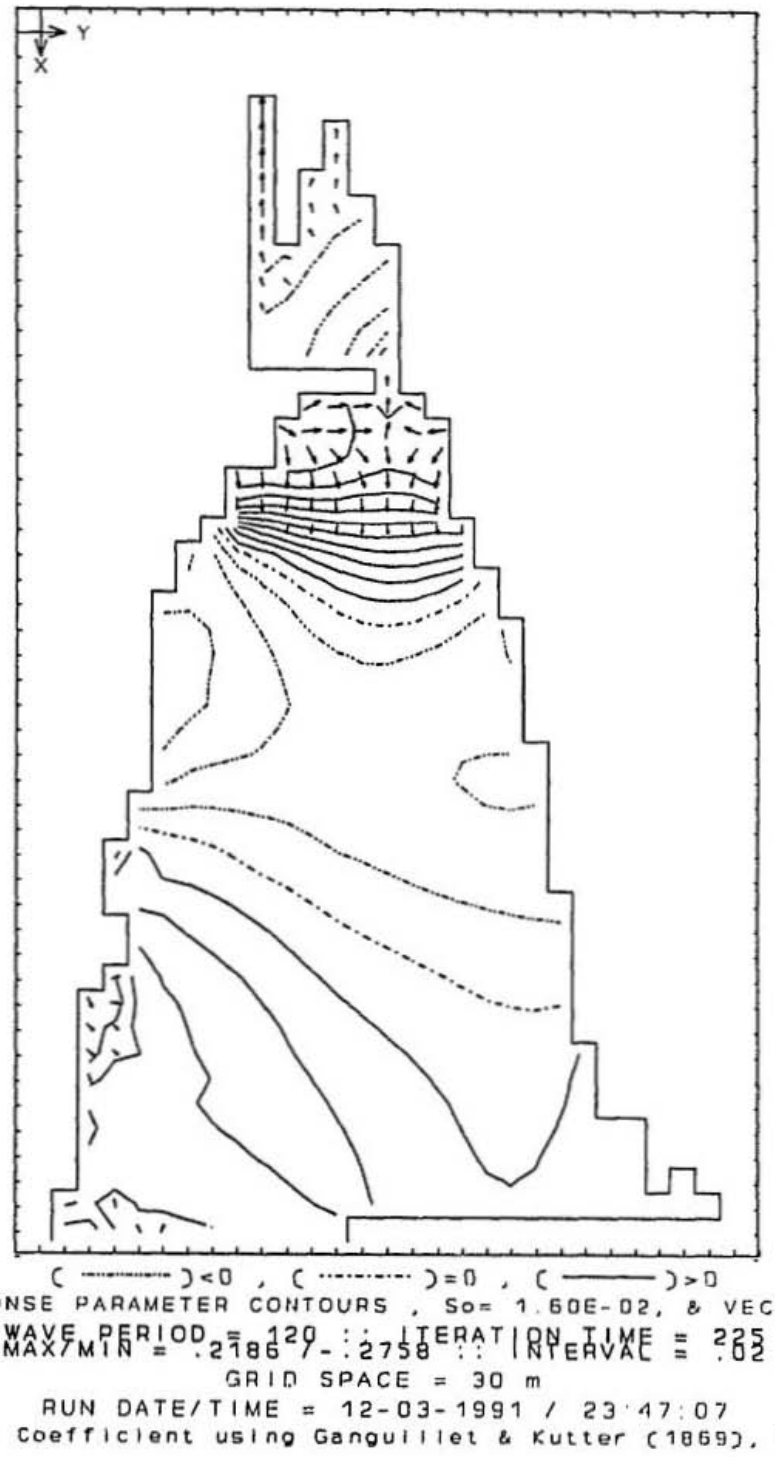

Fig. C.15 - Basin response, t=225 s, T=120 s.

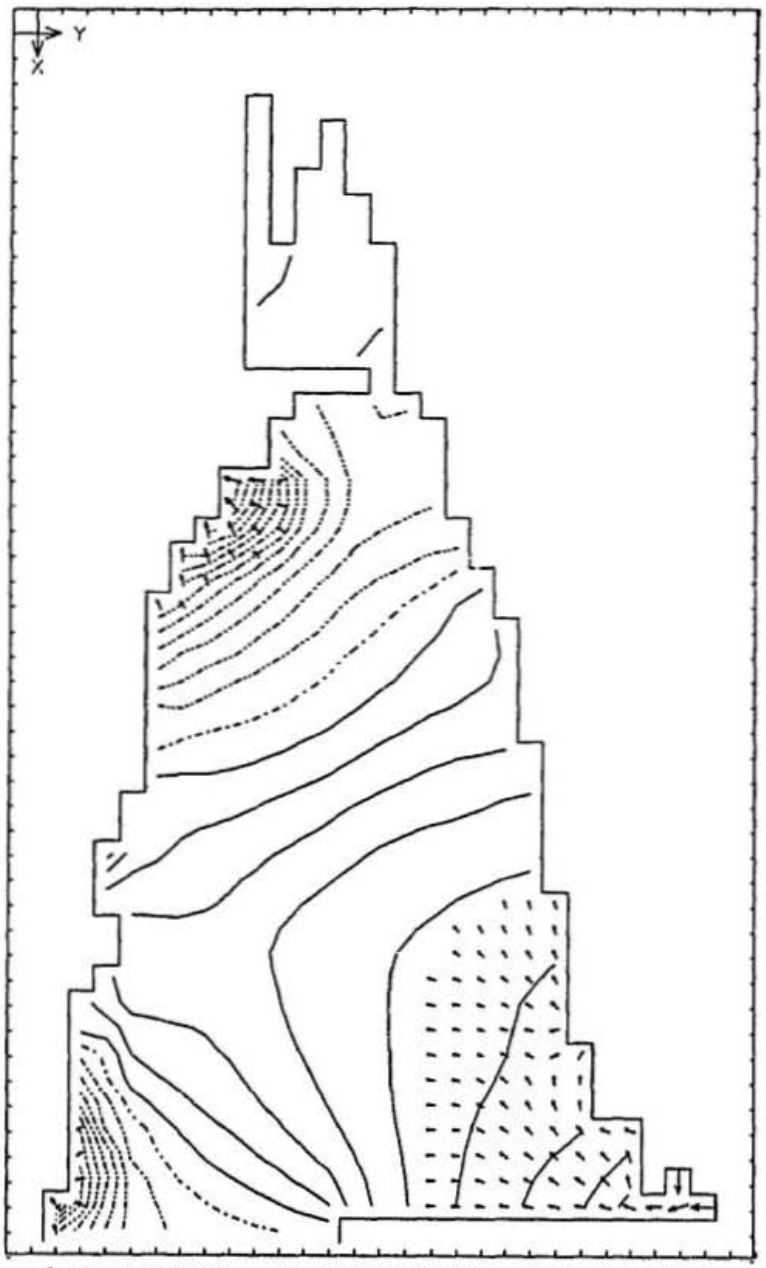

Fig. C.16 - Basin response, t=240 s, T=120 s.

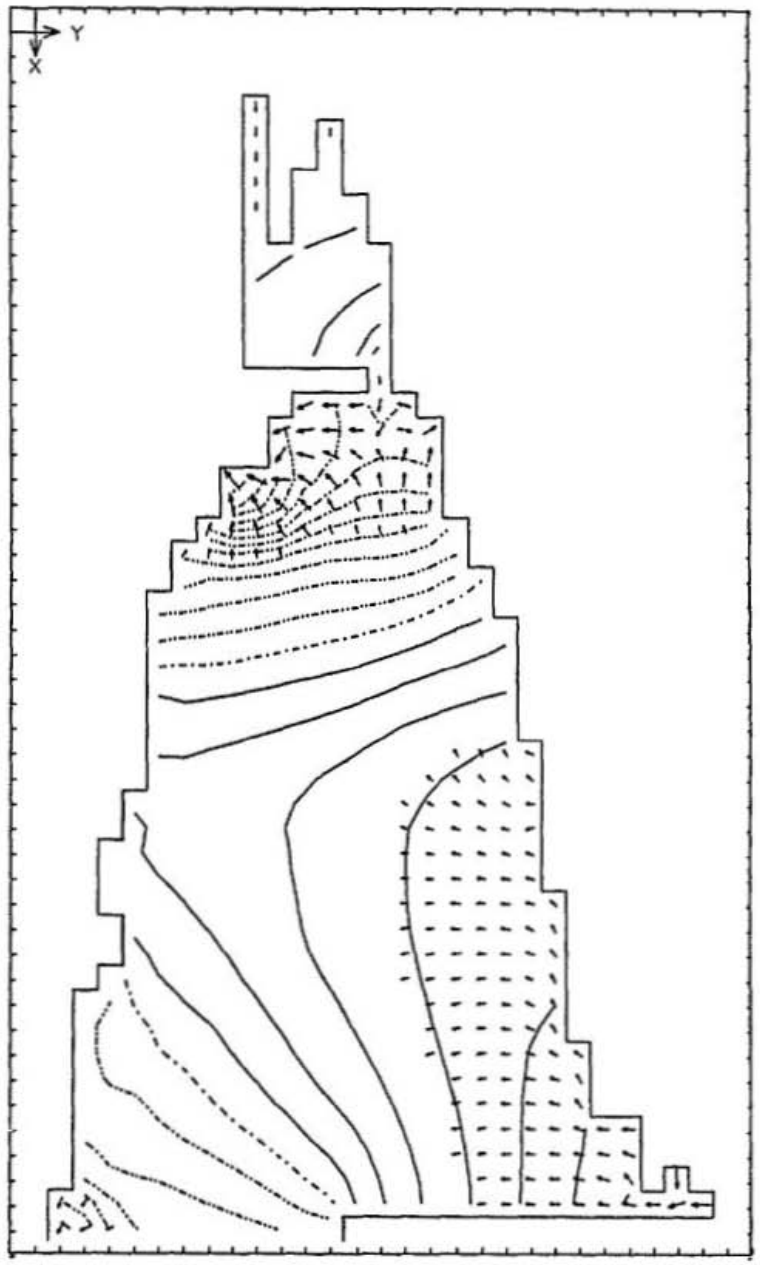

Fig. C.17 - Basin response, t=255 s, T=120 s.

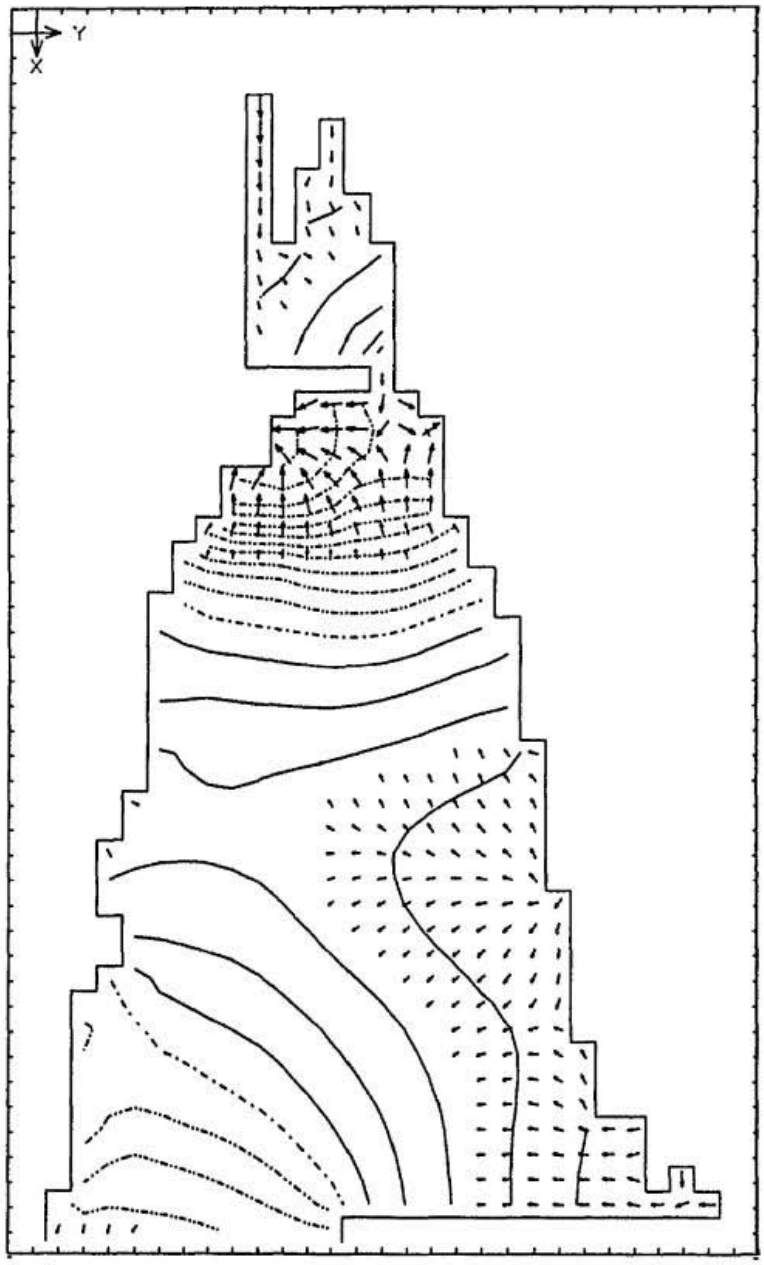

Fig. C.18 - Basin response, t=270 s, T=120 s.

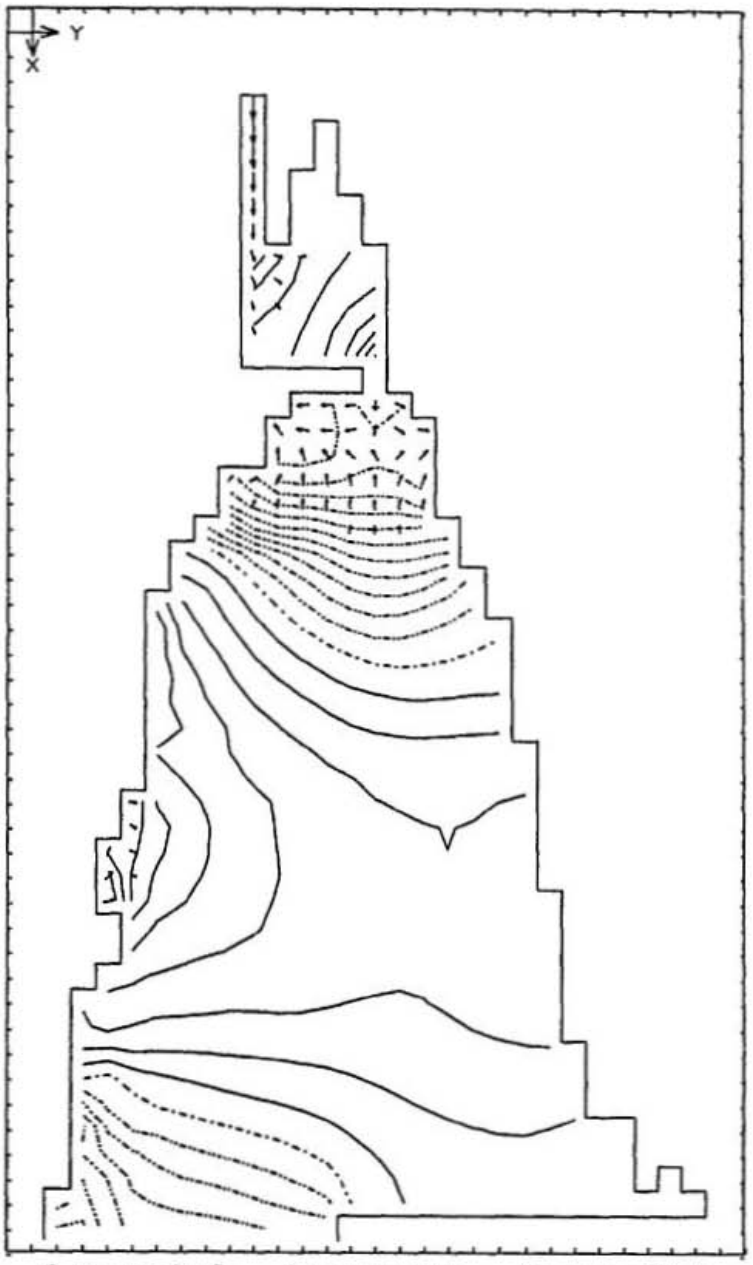

Fig. C.19 - Basin response, t=285 s, T=120 s.

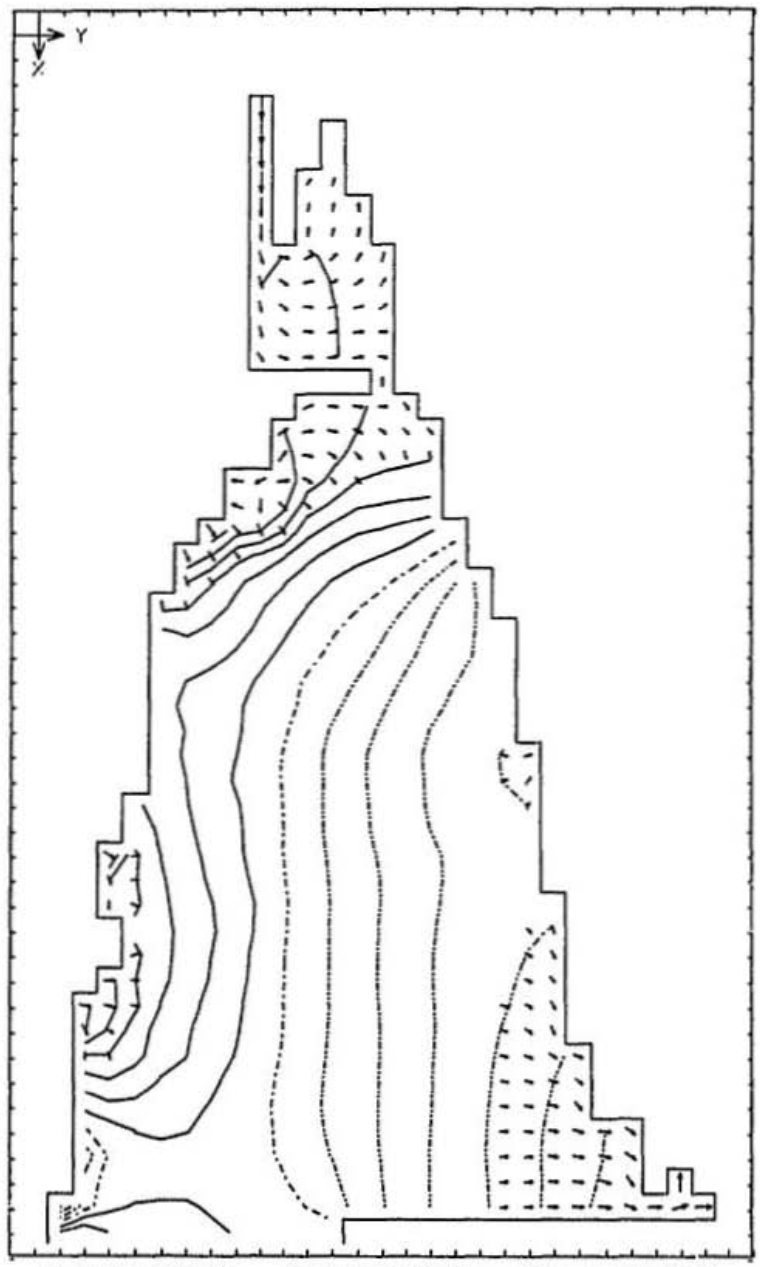

Fig. C.20 - Basin response, t=300 s, T=120 s.

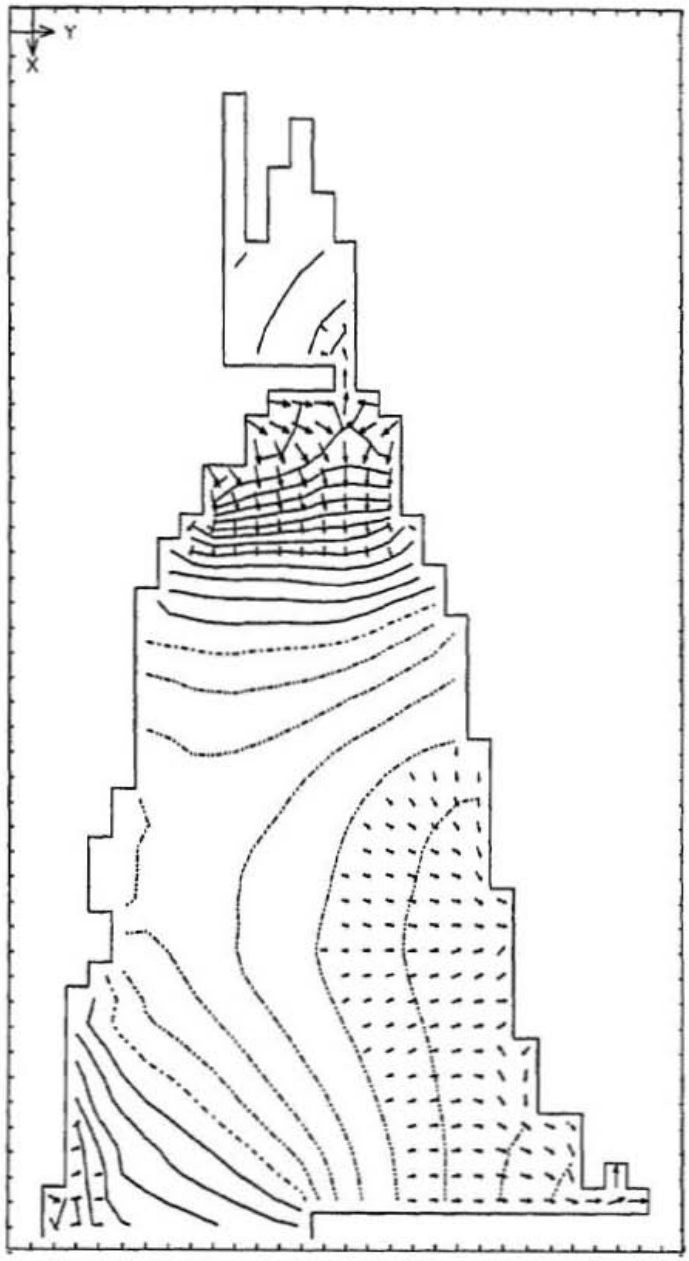

Fig. C.21 - Basin response, t=315 s, T=120 s.

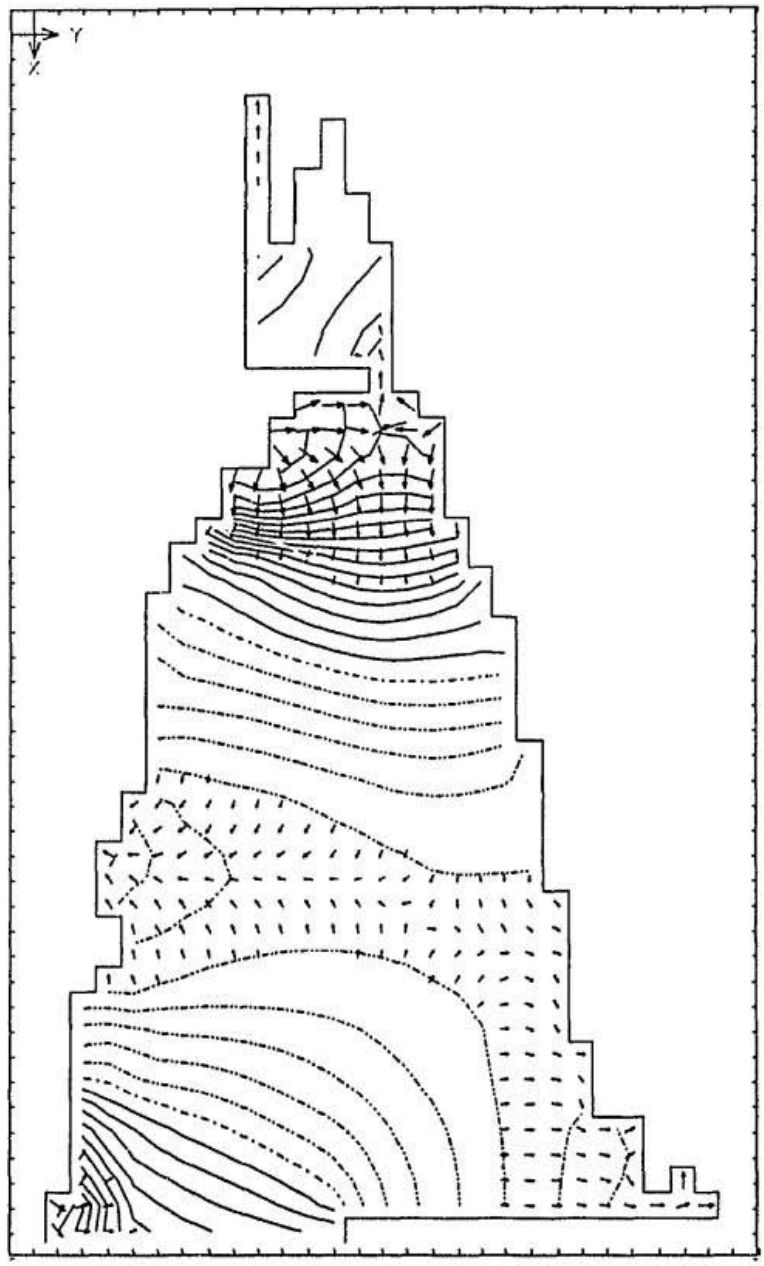

Fig. C.22 - Basin response, t=330 s, T=120 s.

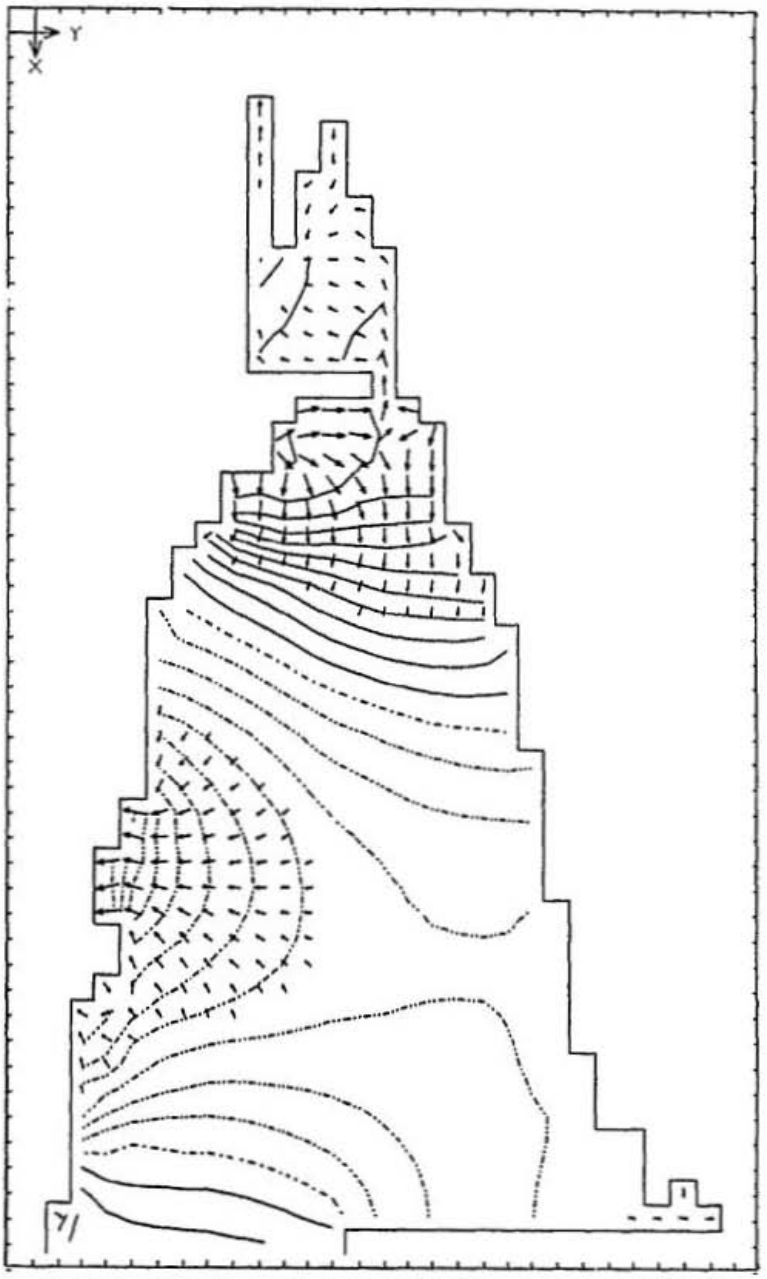

Fig. C.23 - Basin response, t=345 s, T=120 s.

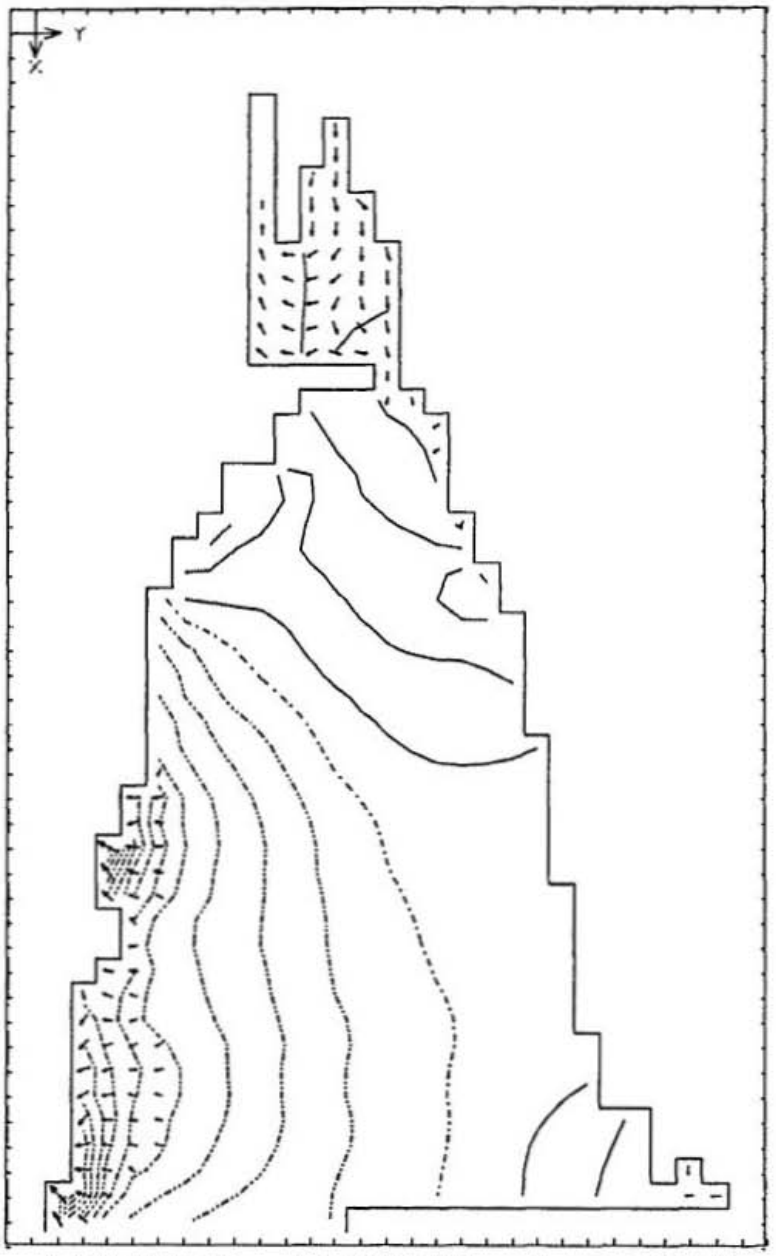

Fig. C.24 - Basin response, t=360 s, T=120 s.

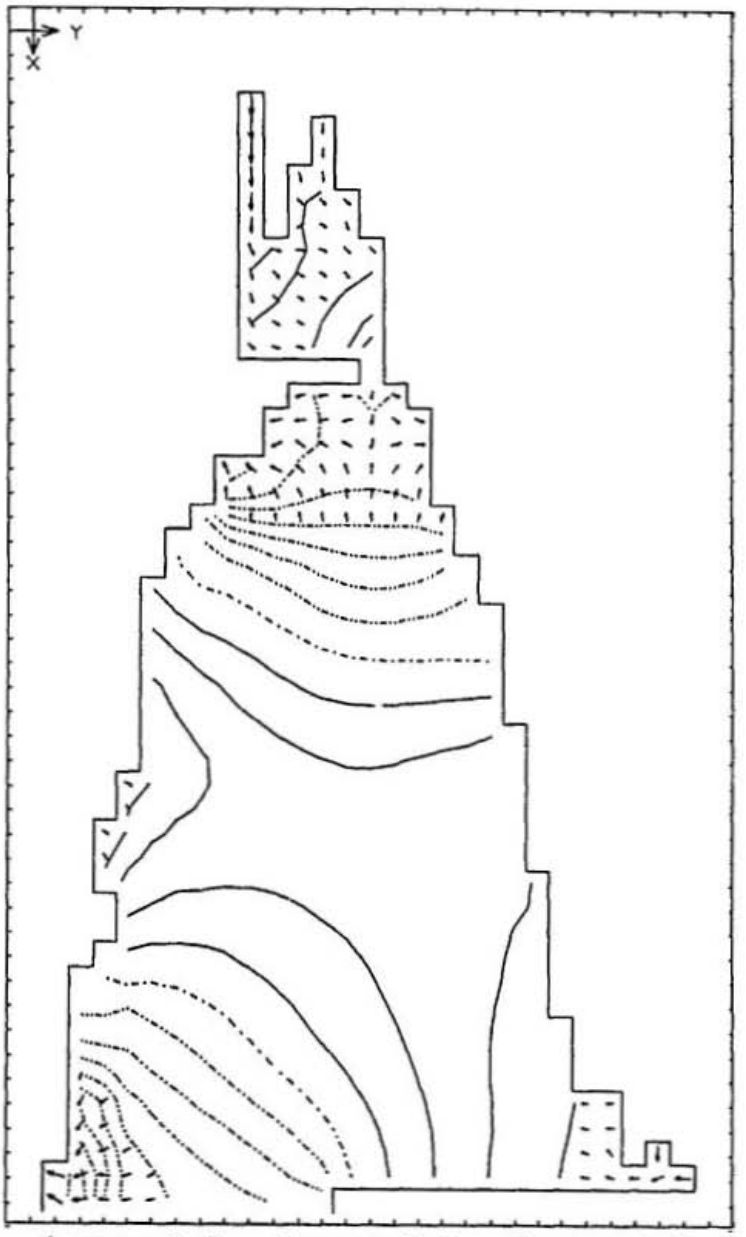

Fig. C.25 - Basin response, t=375 s, T=120 s.

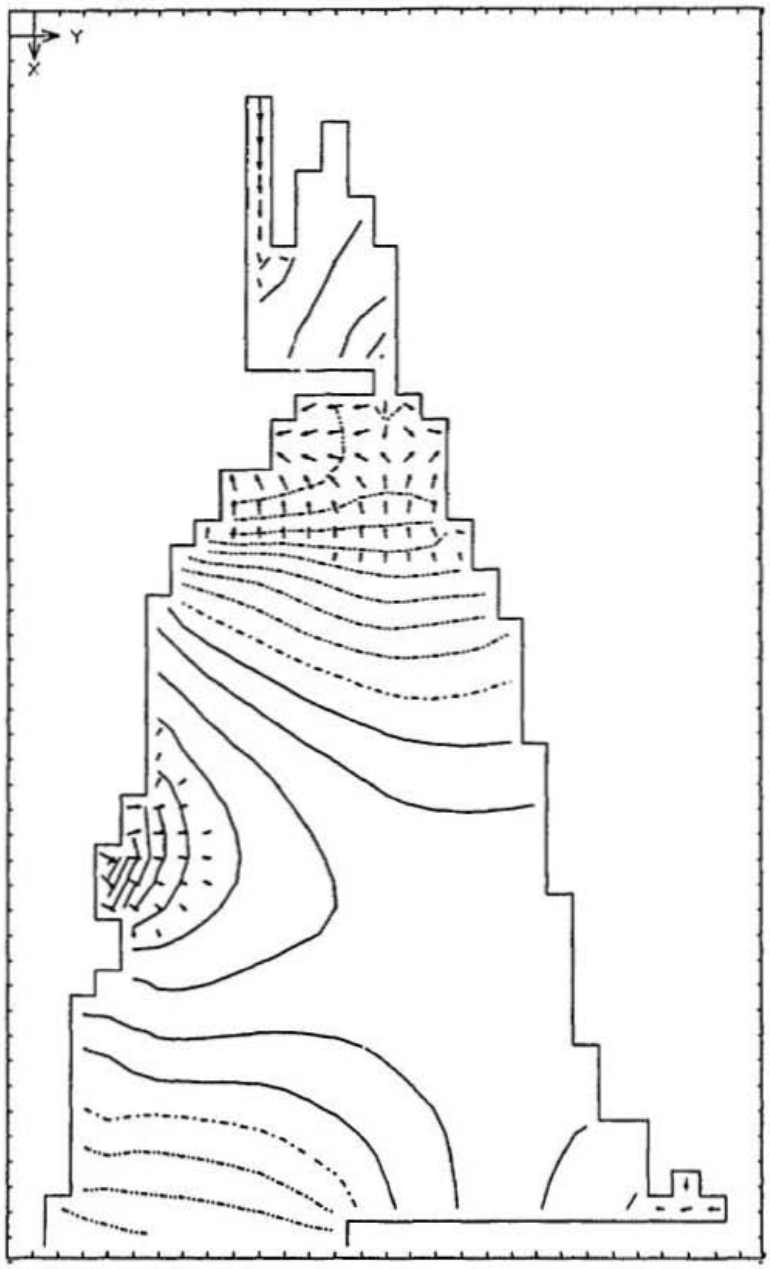

Fig. C.26 - Basin response, t=390 s, T=120 s.

Appendix D

LONGWAVE HARDCOPY OUTPUTS FOR SOHILCO HARBOUR DEVELOPMENT, FRESHWATER BAY, INNER BASIN, RESPONSE PARAMETER ANALYSIS.

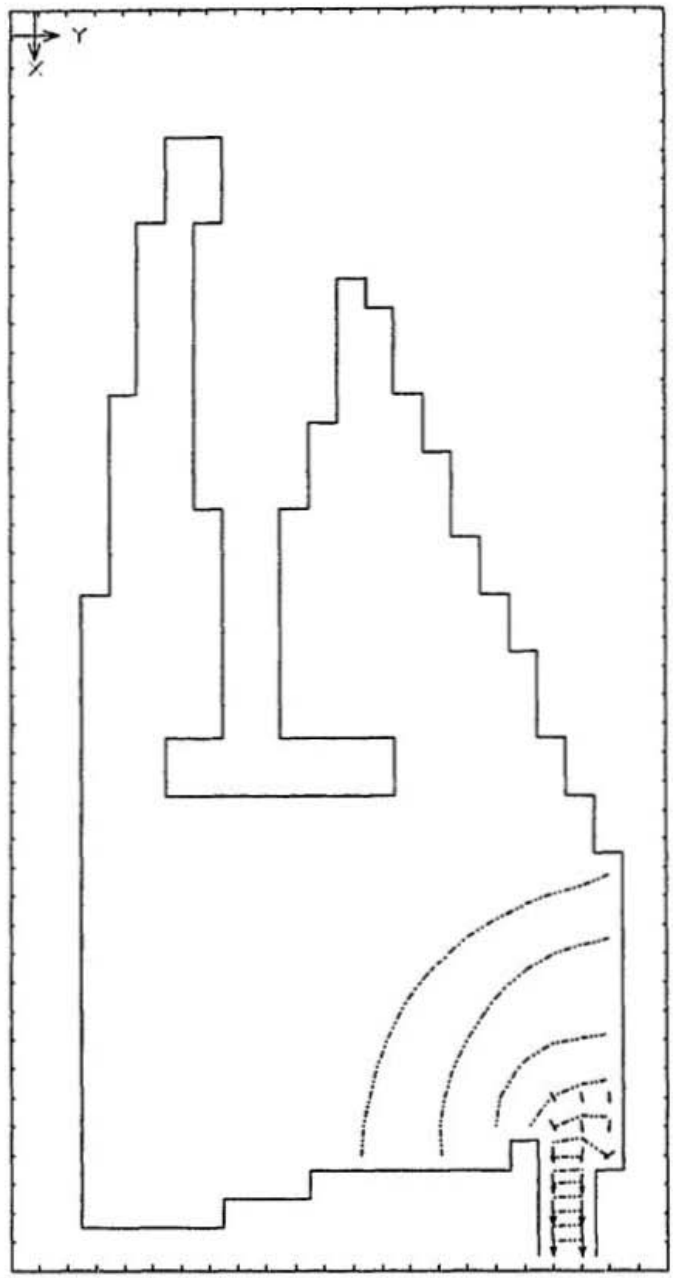

(·····)<0 , (·-·-·-·)=0 , (———)>0
RESPONSE PARAMETER CONTOURS , So= 1.86E-02, & VECTORS.
WAVE PERIOD = 120 :: ITERATION TIME = 15
MAX/MIN = 0 / -3.94E-02 :: INTERVAL = .003
GRID SPACE = 10 m
RUN DATE/TIME = 12-05-1991 / 19:27:52
Chezy Coefficient using Ganguillet & Kutter (1869), n=.03

Fig. D.1 - Response parameter, t=15 s, T=120 s.

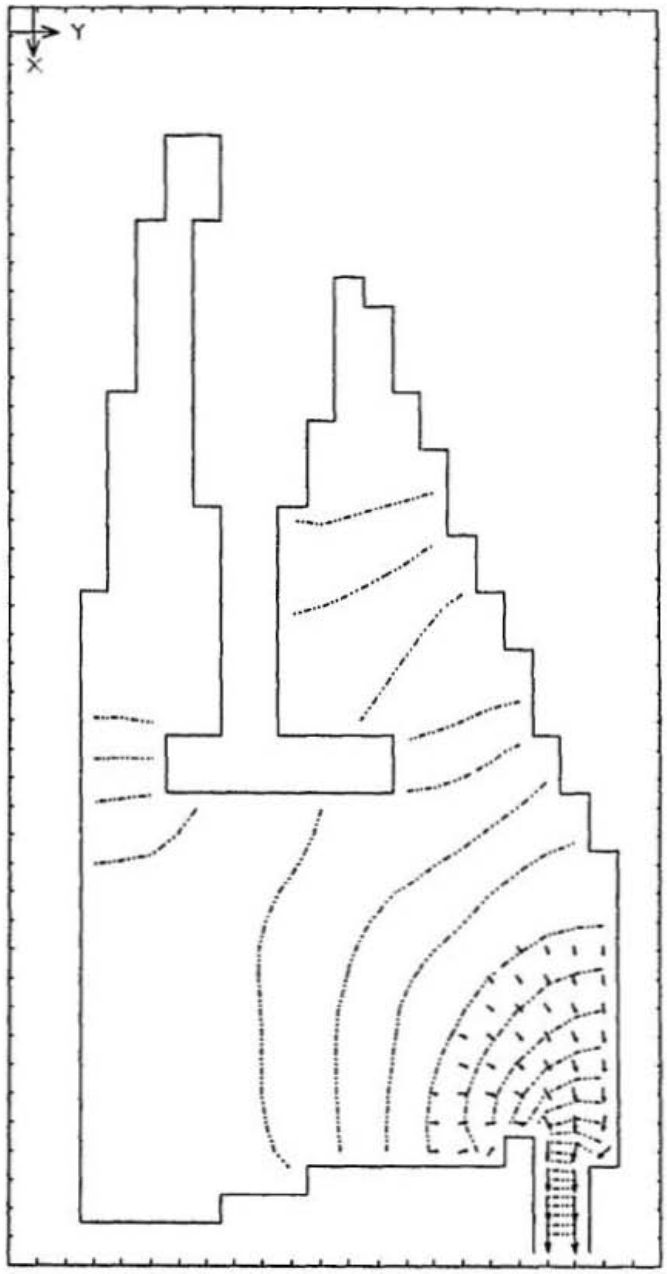

Fig. D.2 - Response parameter, t=30 s, T=120 s.

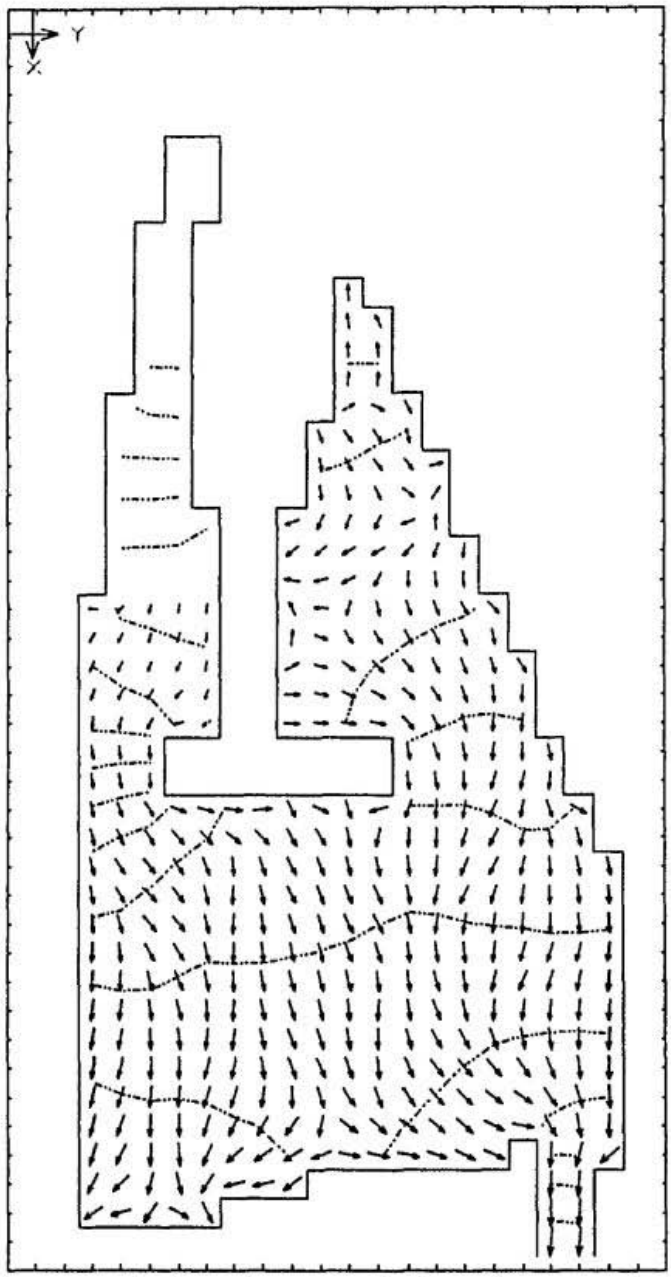

(·····)<0 , (·····)=0 , (———)>0
RESPONSE PARAMETER CONTOURS , So= 1.86E-02, & VECTORS.
WAVE PERIOD = 120 :: ITERATION TIME = 45
MAX/MIN = 0 /-3.73E-02 :: INTERVAL = .002
GRID SPACE = 10 m
RUN DATE/TIME = 12-05-1991 / 19:59:54
Chezy Coefficient using Ganguillet & Kutter (1869), n=.03

Fig. D.3 - Response parameter, t=45 s, T=120 s.

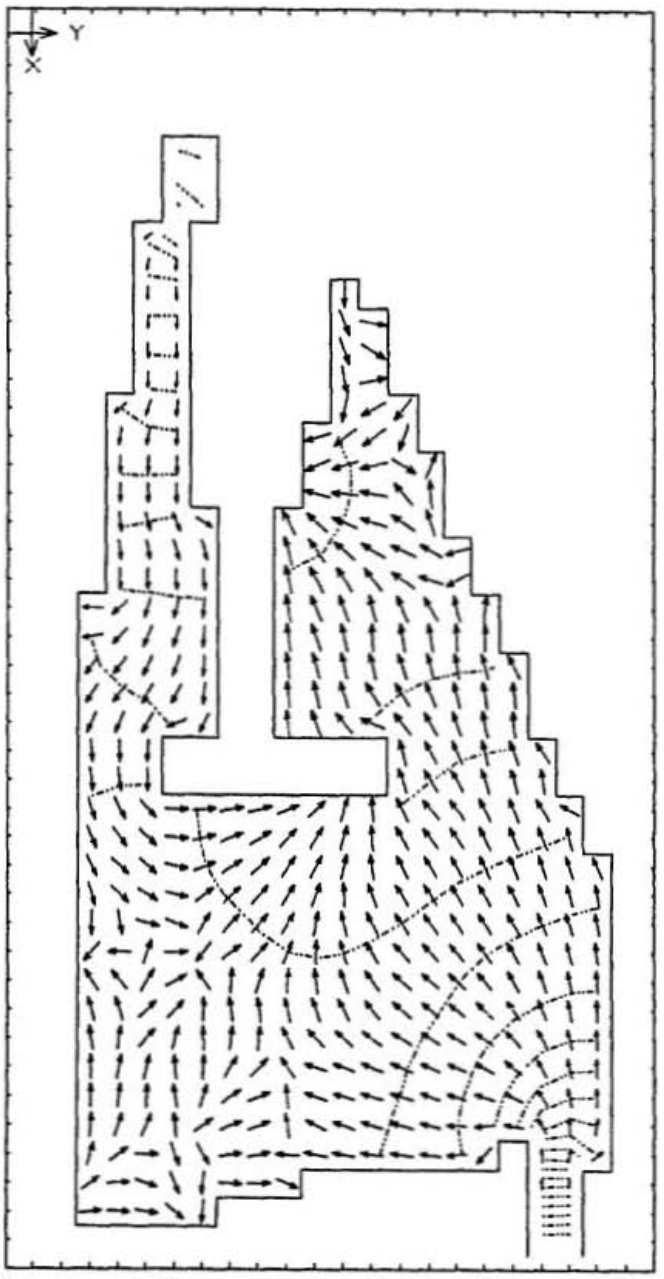

Fig. D.4 - Response parameter, t=60 s, T=120 s.

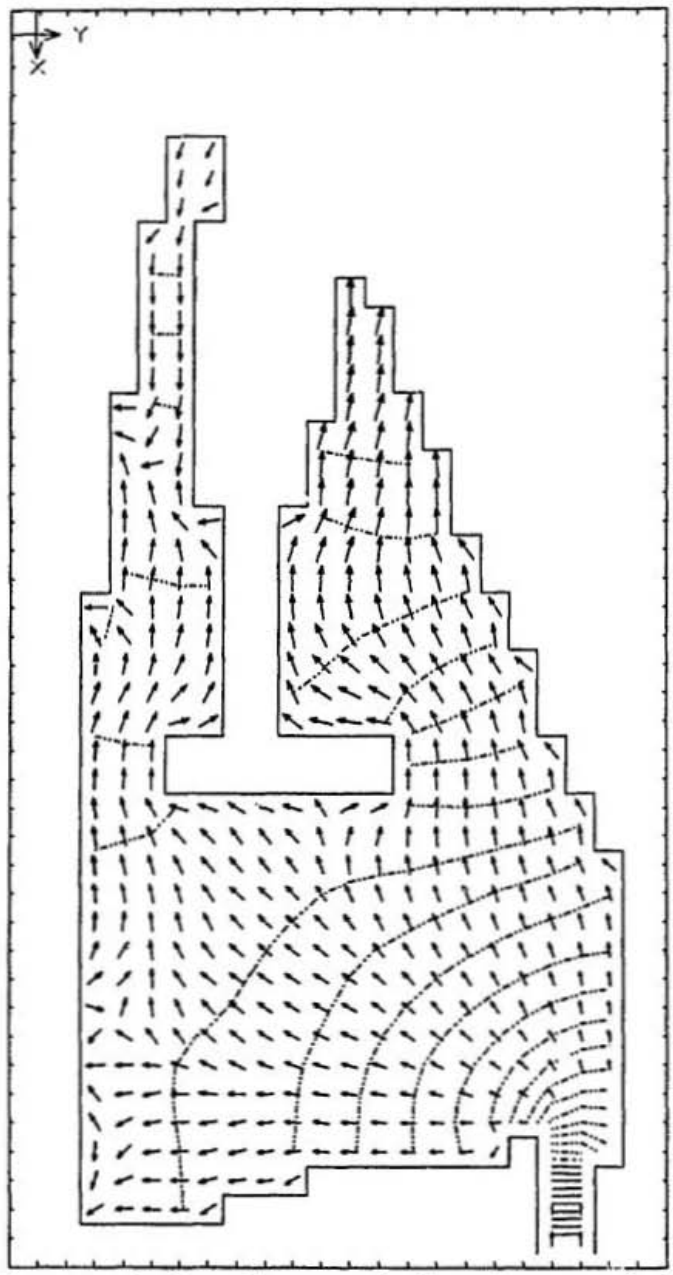

(·····)<0 , (·····)=0 , (———)>0
RESPONSE PARAMETER CONTOURS , So= 1.86E-02, & VECTORS.
WAVE PERIOD = 120 :: ITERATION TIME = 75
MAX/MIN = 3.21E-02 /-6.57E-02 :: INTERVAL = .003
GRID SPACE = 10 m
RUN DATE/TIME = 12-05-1991 / 20:33:15
Chezy Coefficient using Ganguillet & Kutter (1869), n=.03

Fig. D.5 - Response parameter, t=75 s, T=120 s.

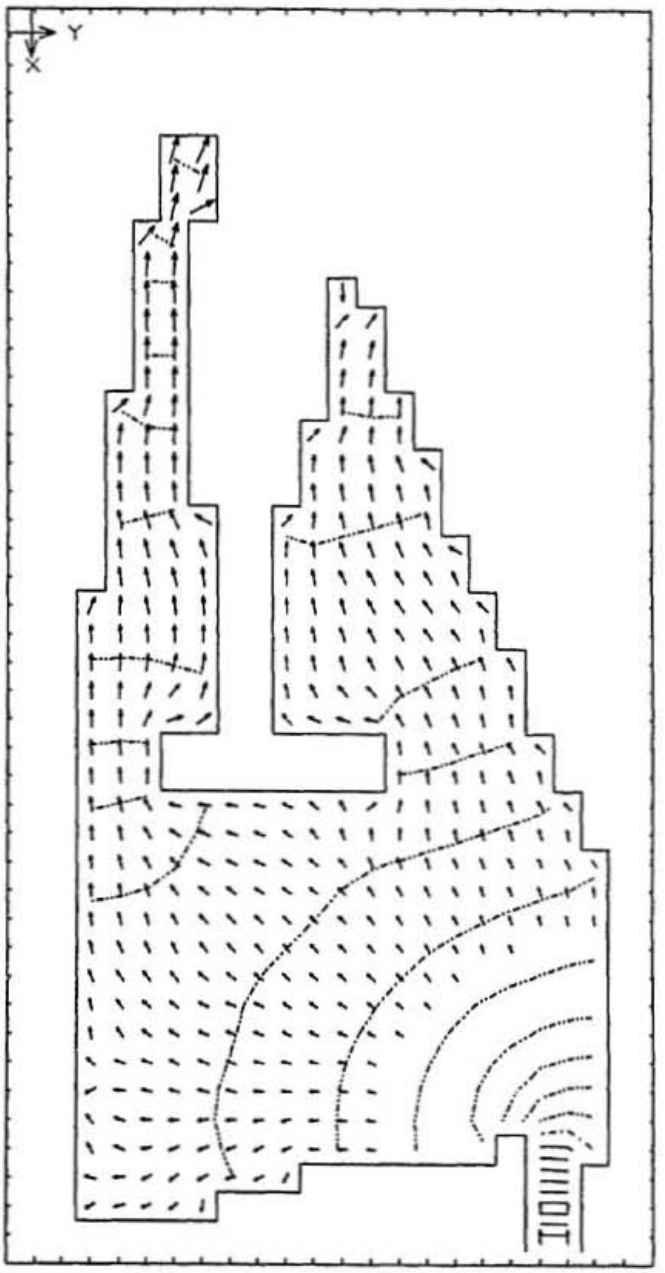

Fig. D.6 - Response parameter, t=90 s, T=120 s.

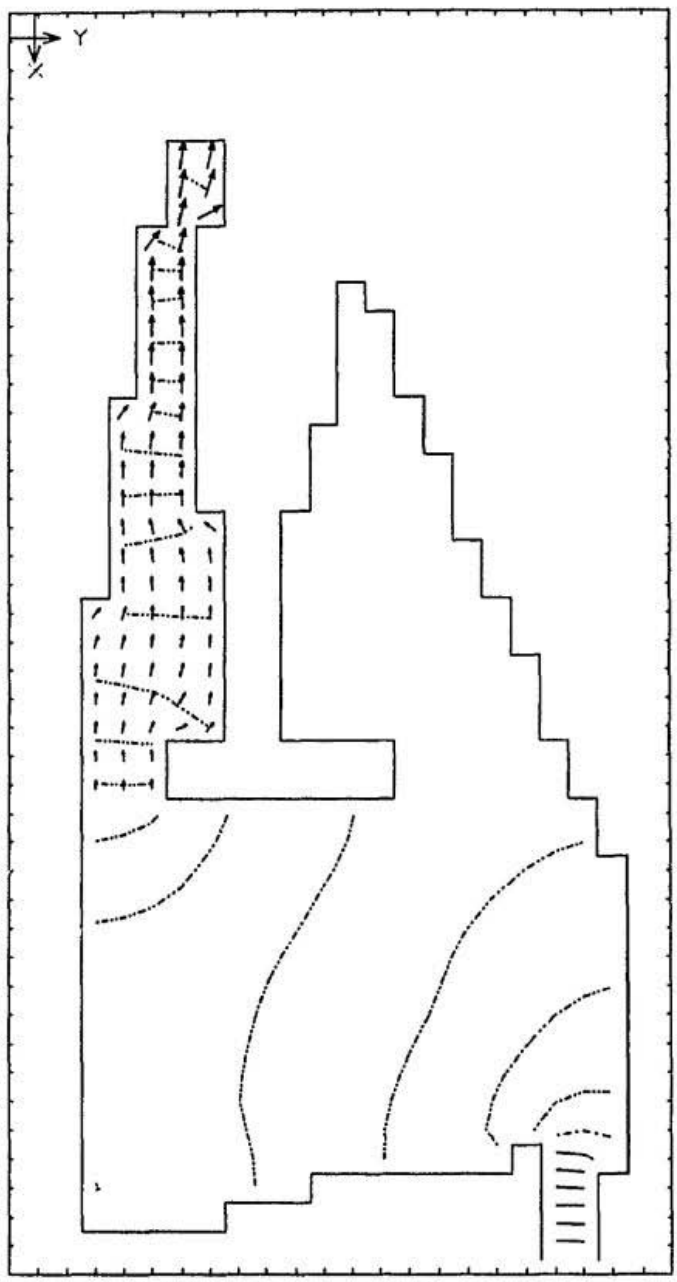

Fig. D.7 - Response parameter, t=105 s, T=120 s.

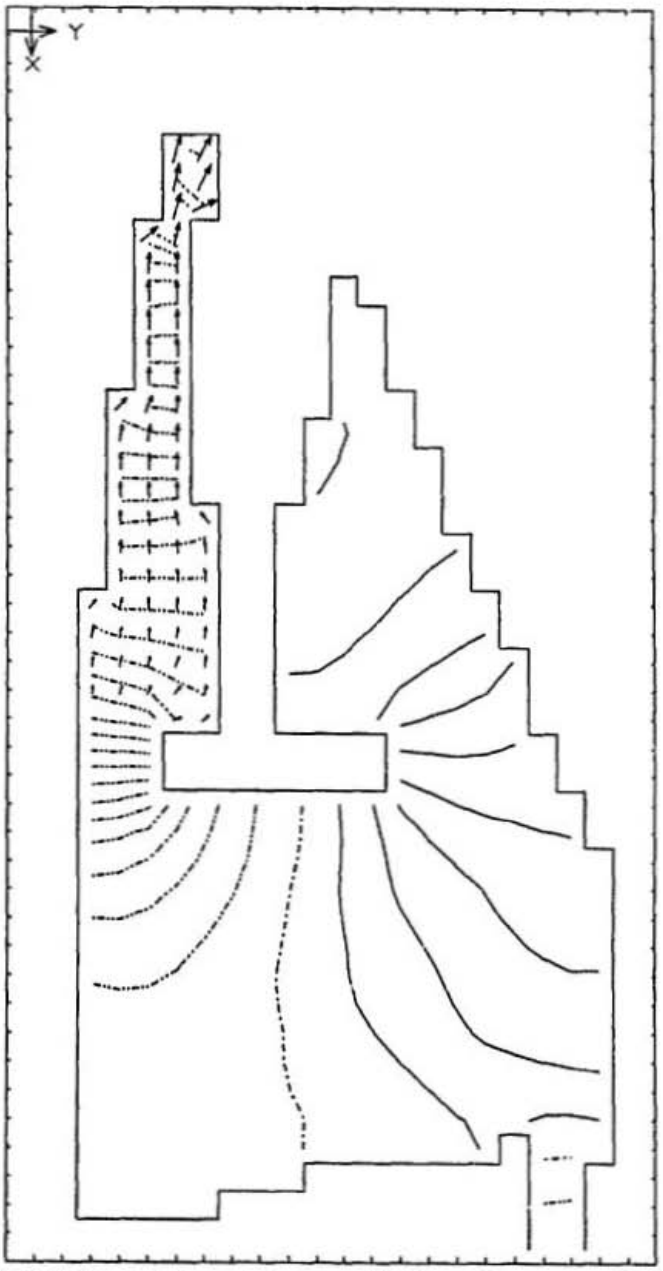

Fig. D.8 - Response parameter, t=120 s, T=120 s.

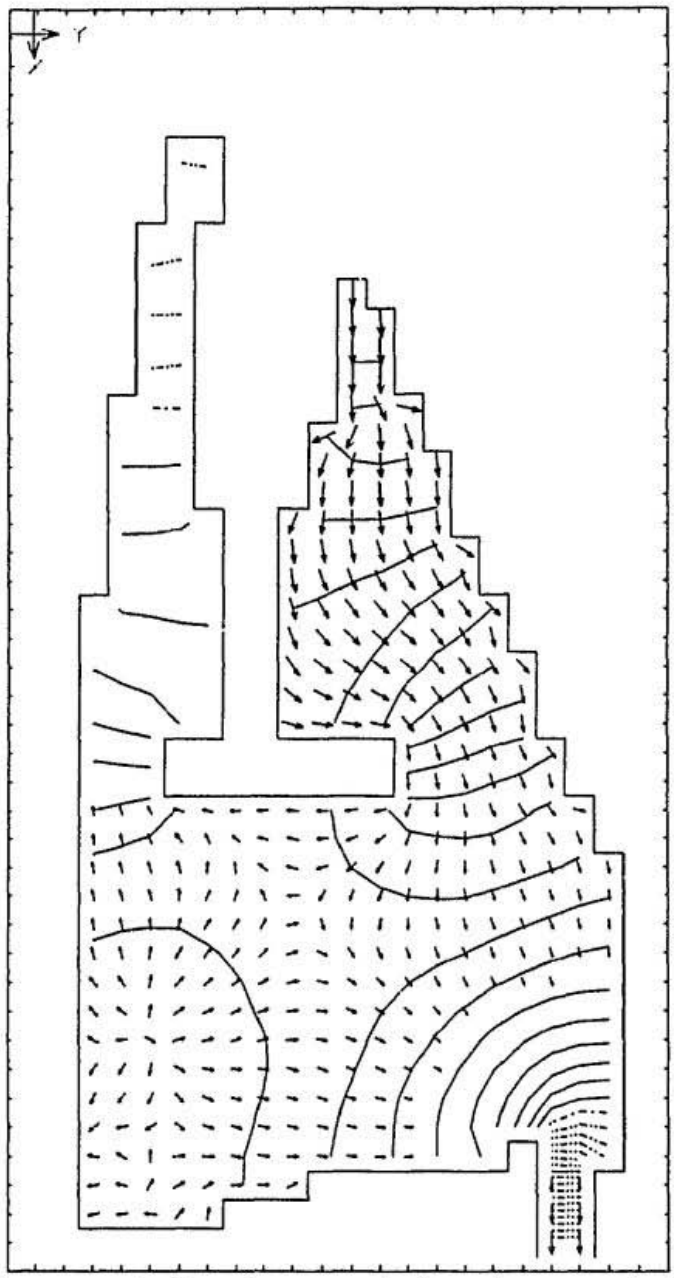

Fig. D.9 - Response parameter, t=135 s, T=120 s.

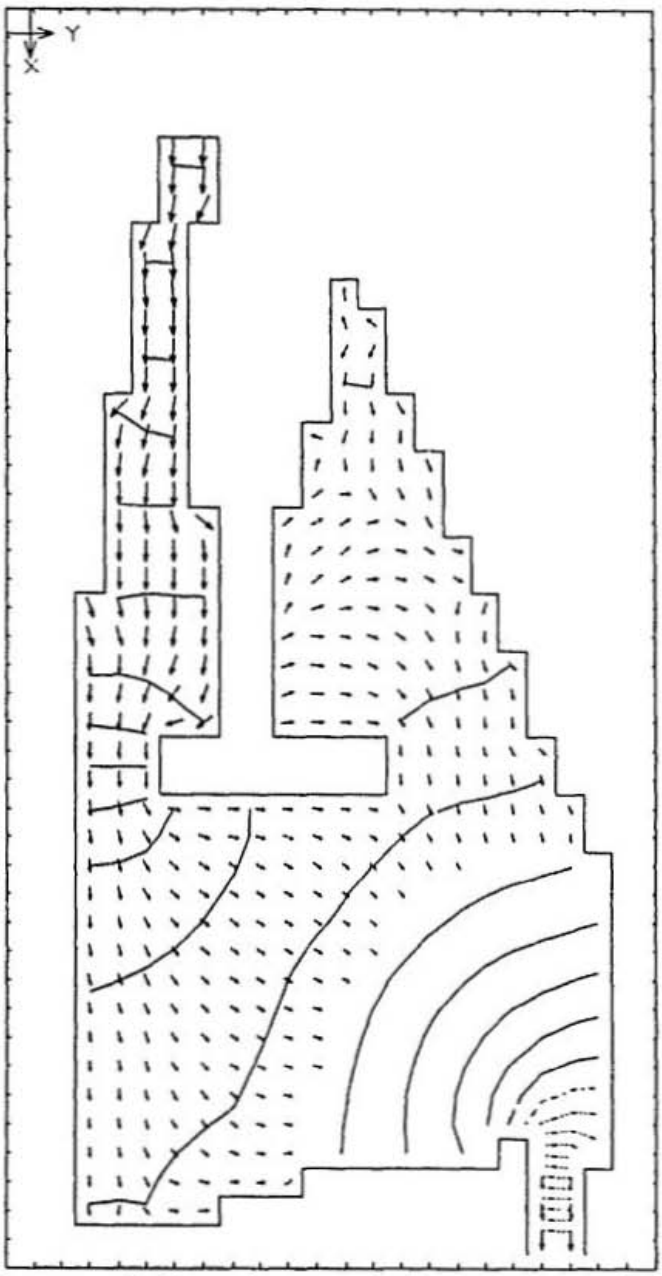

Fig. D.10 - Response parameter, t=150 s, T=120 s.

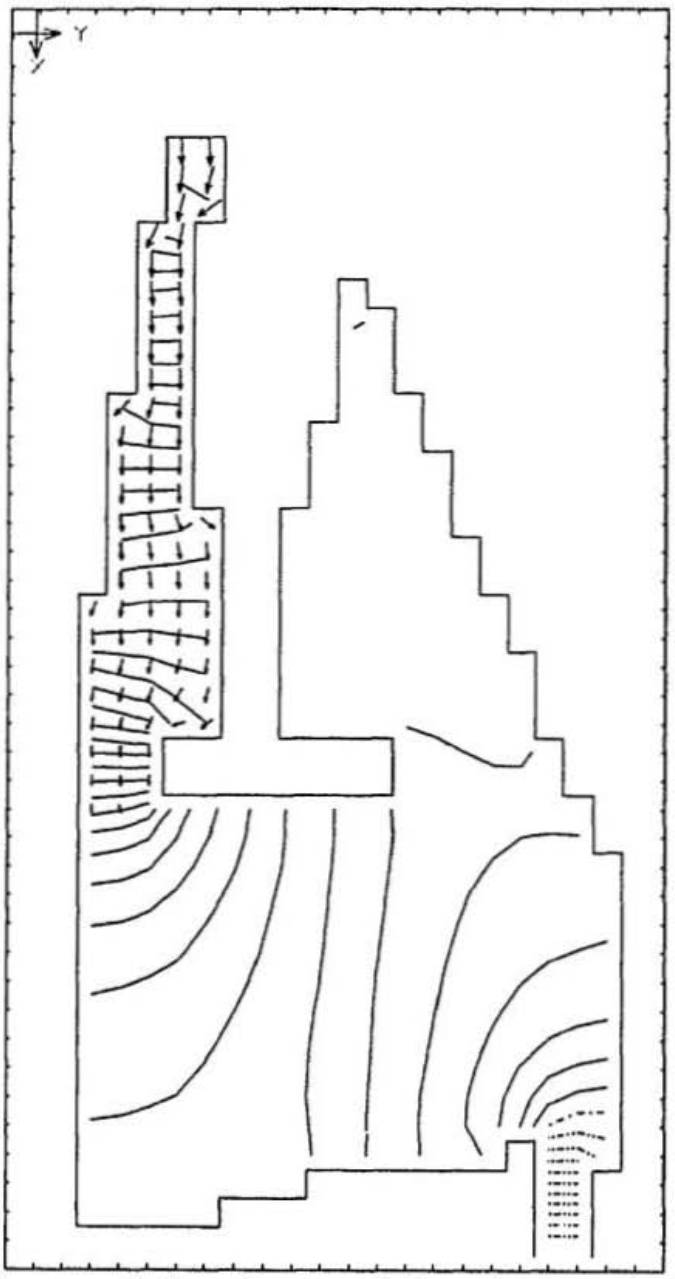

(·····)<0 , (·····)=0 , (———)>0
RESPONSE PARAMETER CONTOURS , So= 1.86E-02, & VECTORS.
WAVE PERIOD = 120 ITERATION TIME = 165
MAX/MIN = 1368 /-3 18E-02 INTERVAL = .003
GRID SPACE = 10 m
RUN DATE/TIME = 12-05-1991 / 22:22:17
Chozy Coefficient using Ganguillet & Kutter (1869), n= 03

Fig. D.11 - Response parameter, t=165 s, T=120 s.

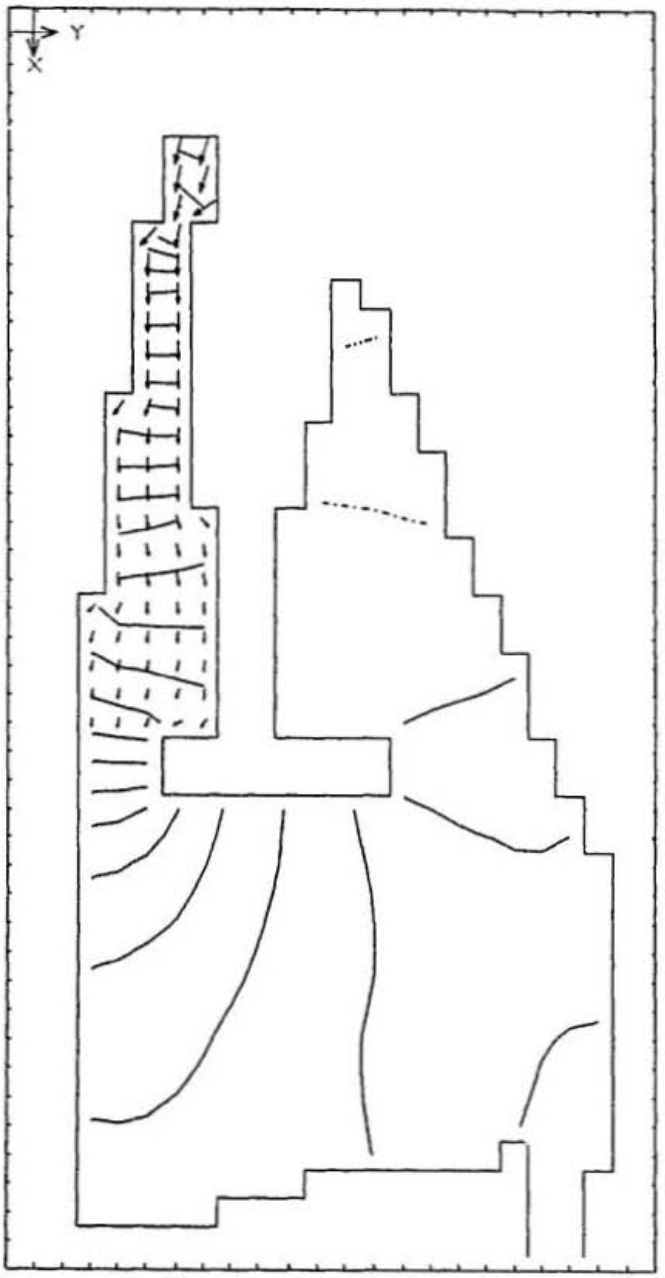

Fig. D.12 - Response parameter, t=180 s, T=120 s.

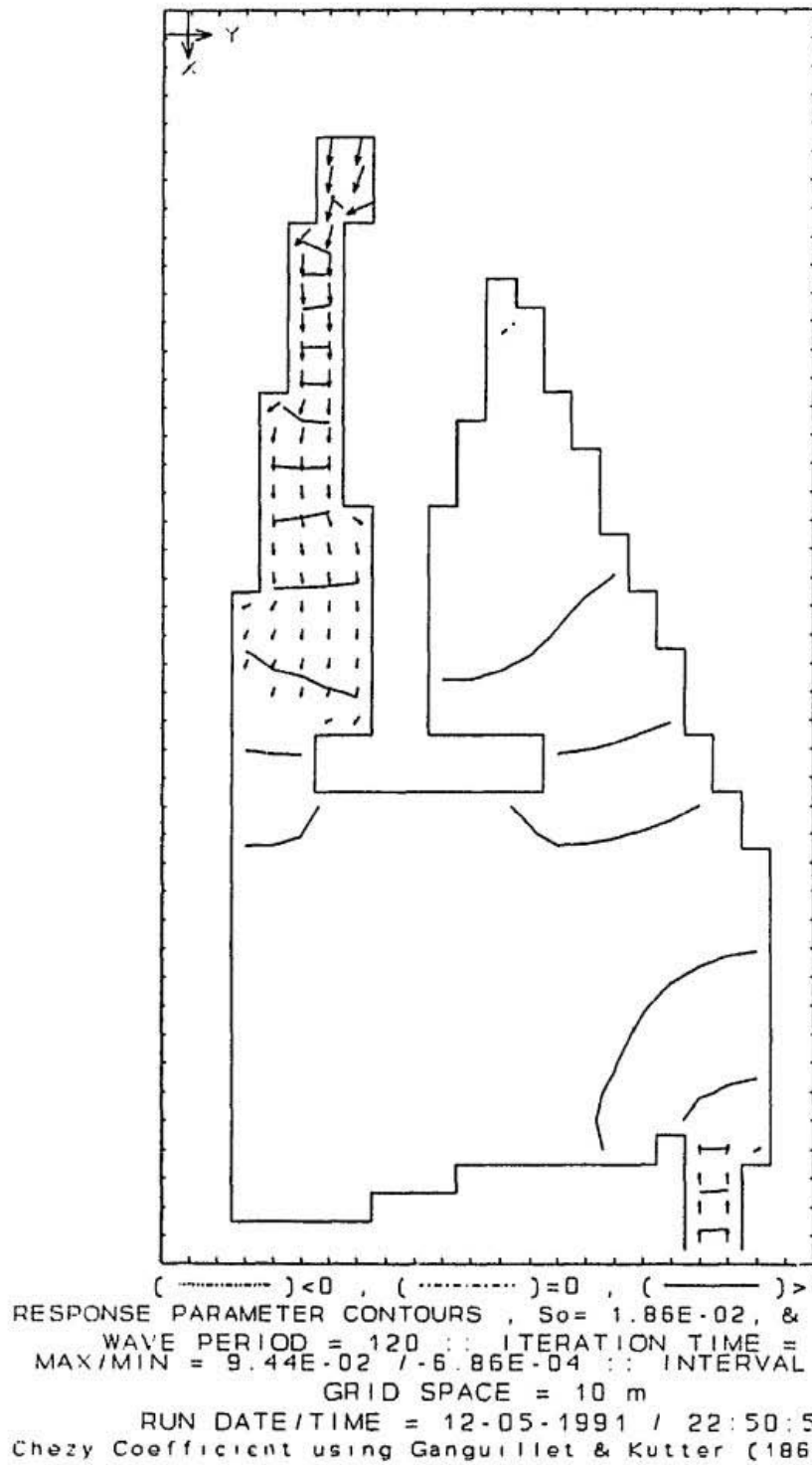

Fig. D.13 - Response parameter, t=195 s, T=120 s.

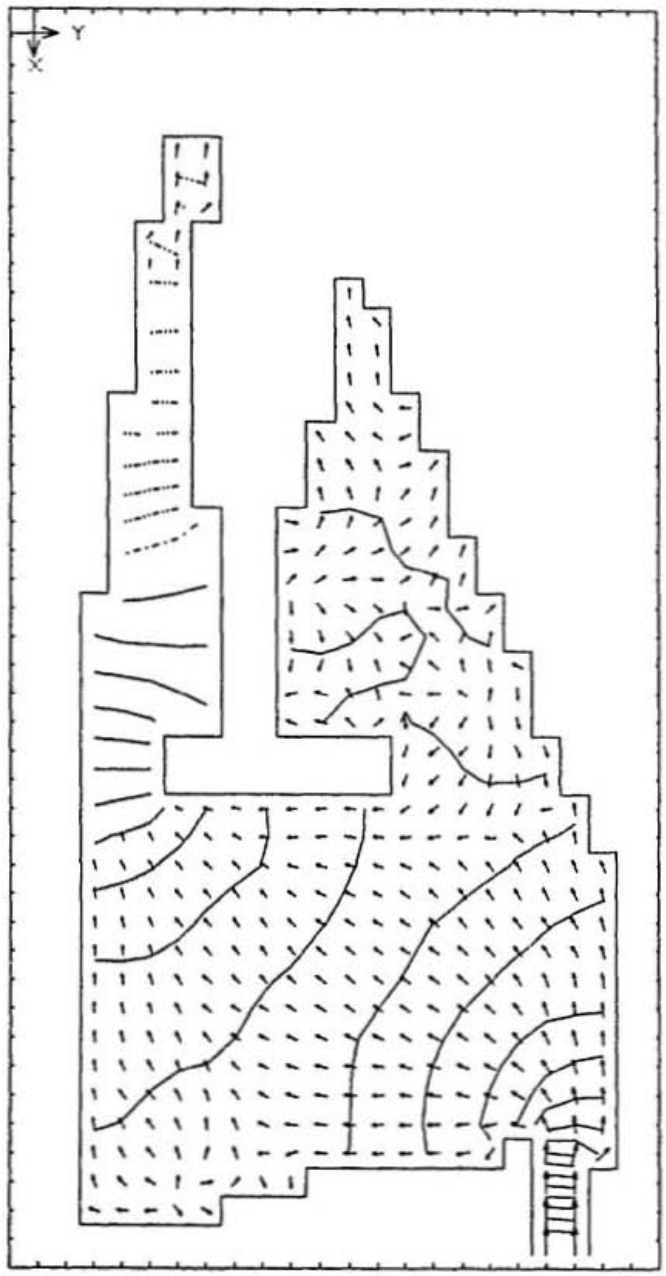

(————)<0 , (·····)=0 , (————)>0
RESPONSE PARAMETER CONTOURS , So= 1.86E-02, & VECTORS
WAVE PERIOD = 120 ITERATION TIME = 210
MAX/MIN = 5.36E-02 / -2.71E-02 INTERVAL = .002
GRID SPACE = 10 m
RUN DATE/TIME = 12-05-1991 / 23 04 39
Chezy Coefficient using Ganguillet & Kutter (1869), n= 03

Fig. D.14 - Response parameter, t=210 s, T=120 s.

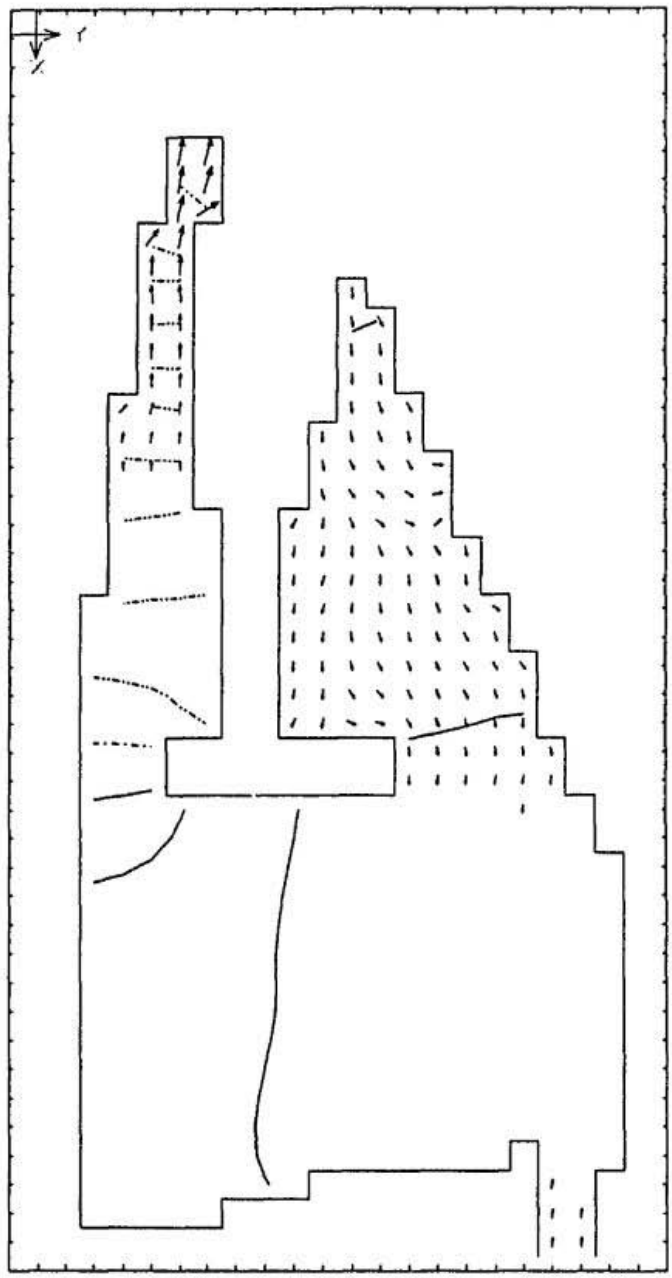

Fig. D.15 - Response parameter, t=225 s, T=120 s.

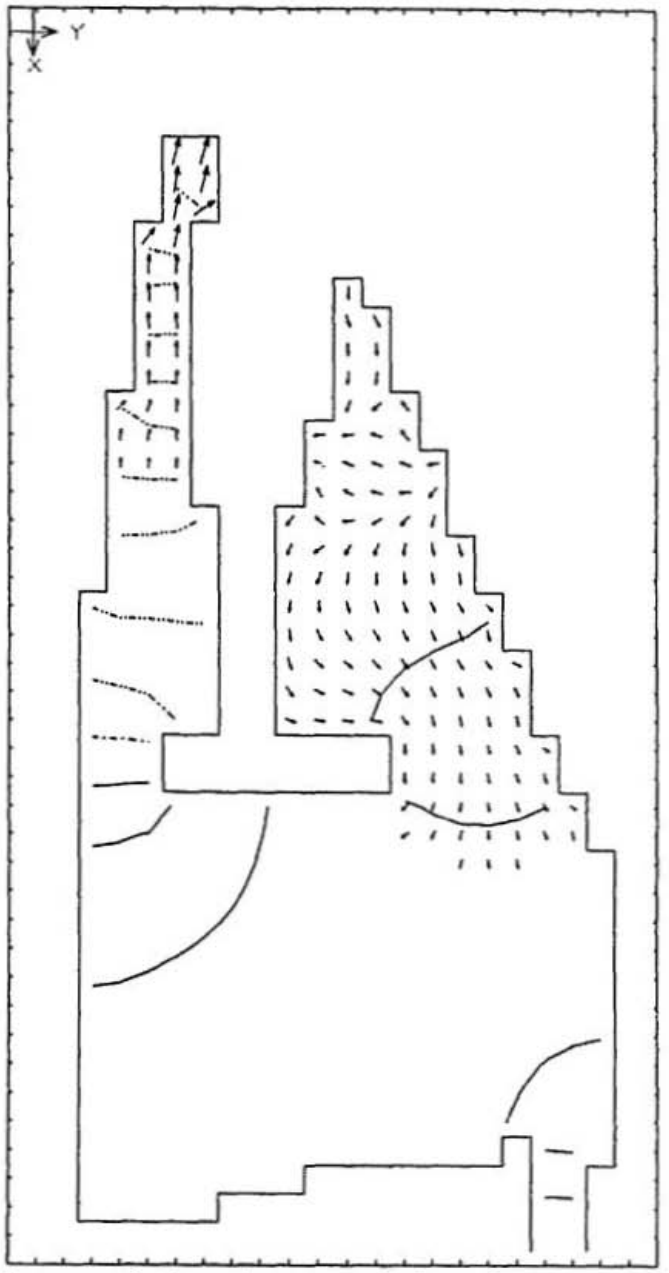

Fig. D.16 - Response parameter, t=240 s, T=120 s.

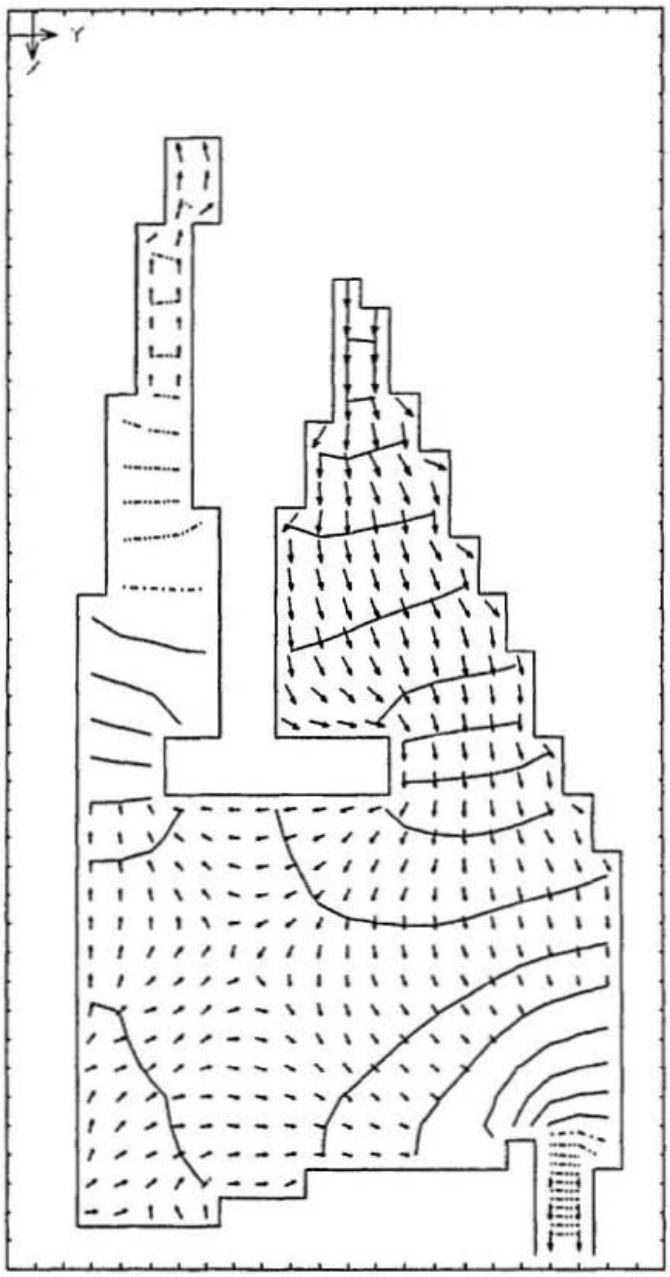

Fig. D.17 - Response parameter, t=255 s, T=120 s.

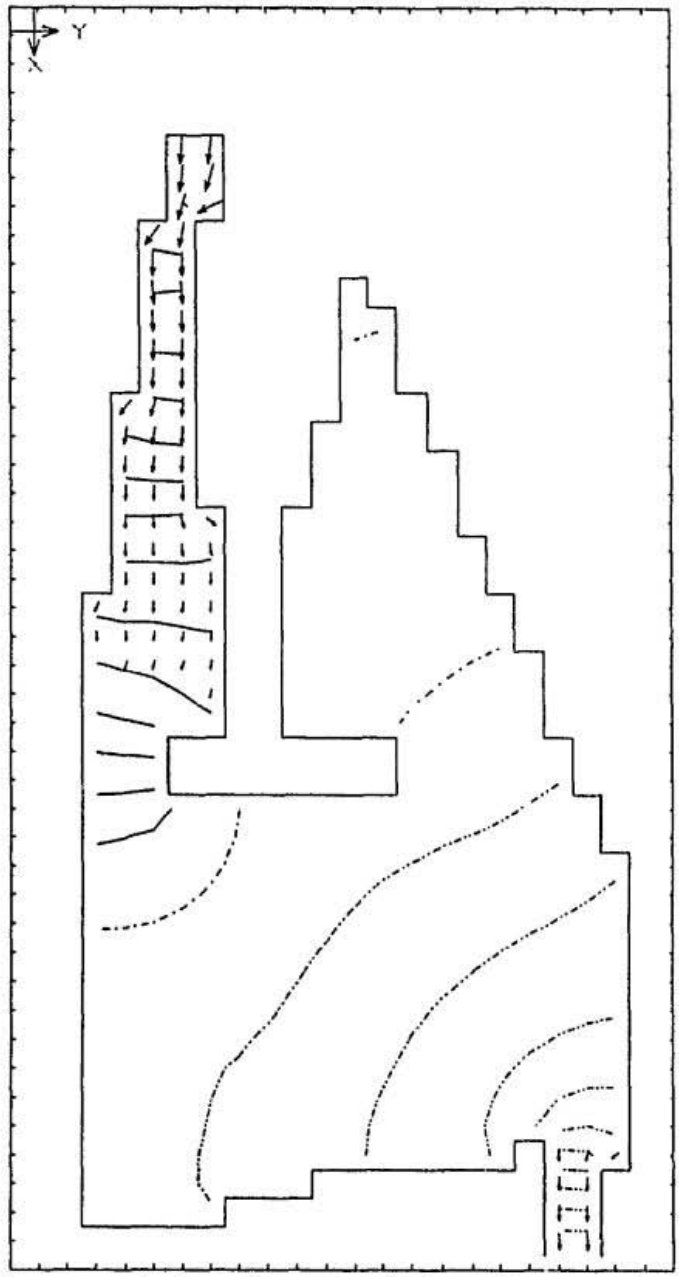

Fig. D.18 - Response parameter, t=270 s, T=120 s.

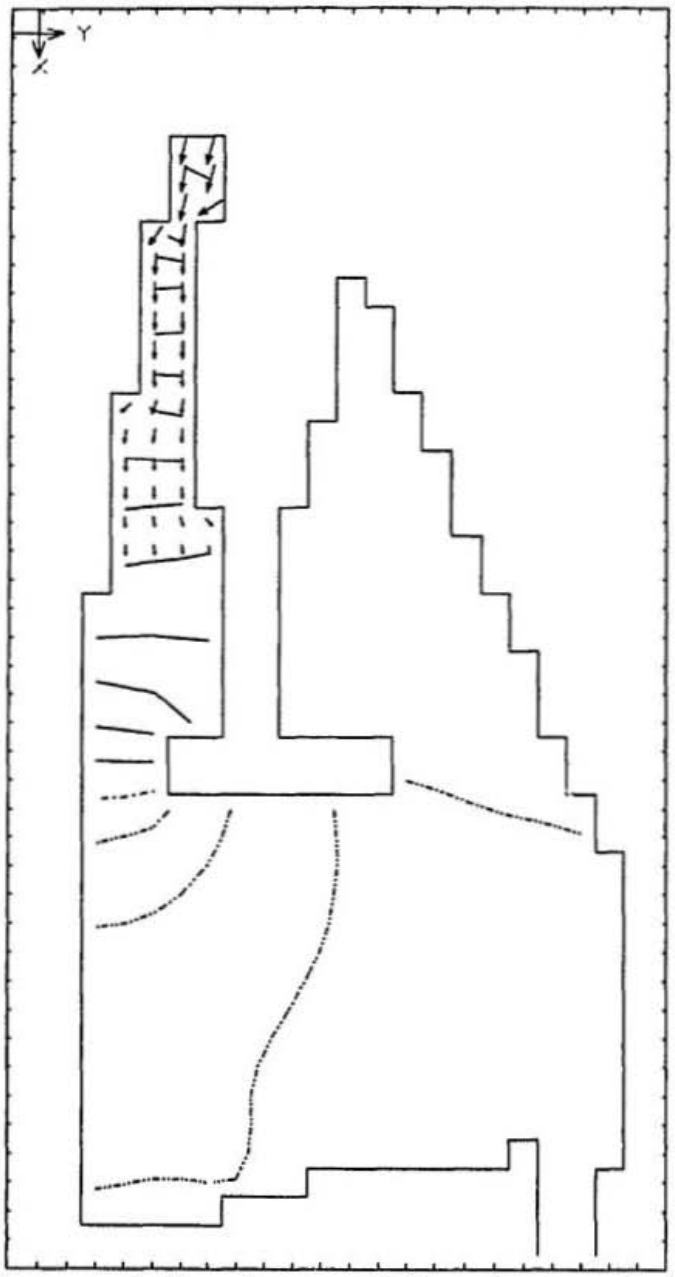

(·····)<0 , (·-·-·-)=0 , (———)>0
RESPONSE PARAMETER CONTOURS , So= 1.86E-02, & VECTORS.
WAVE PERIOD = 120 :: ITERATION TIME = 285
MAX/MIN = 1626 / -4.82E-02 :: INTERVAL = .01
GRID SPACE = 10 m
RUN DATE/TIME = 12-06-1991 / 00:23:03
Chezy Coefficient using Ganguillet & Kutter (1869), n=.03

Fig. D.19 - Response parameter, t=285 s, T=120 s.

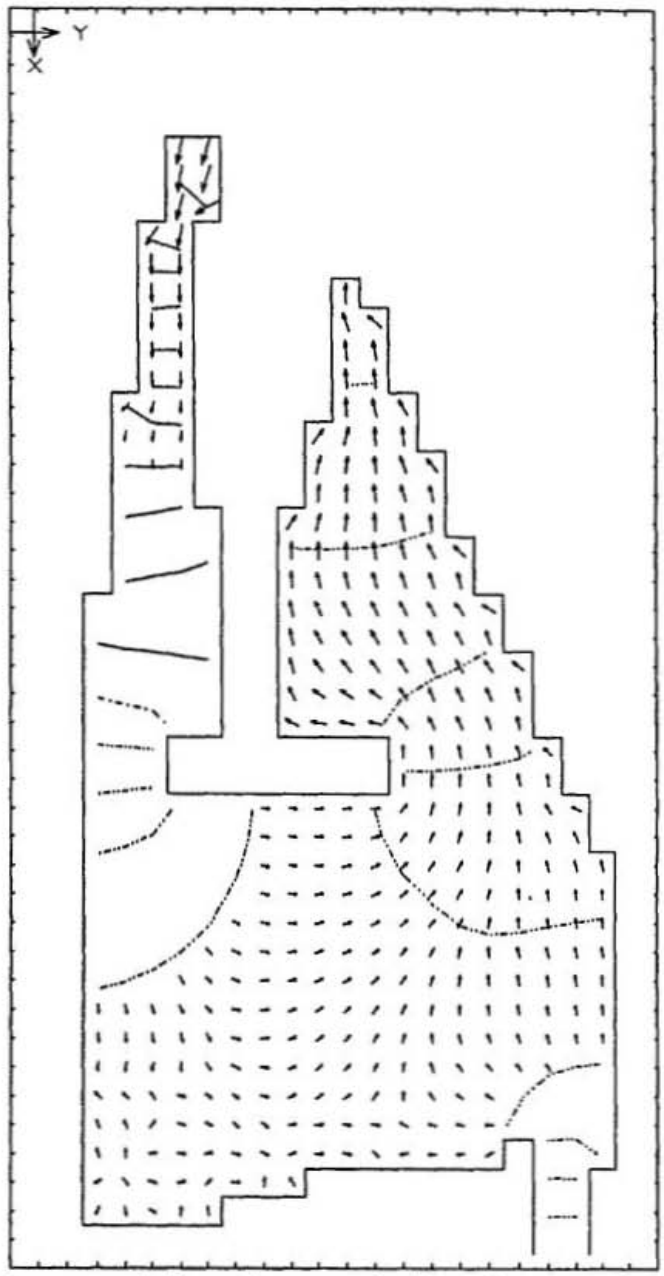

Fig. D.20 - Response parameter, t=300 s, T=120 s.

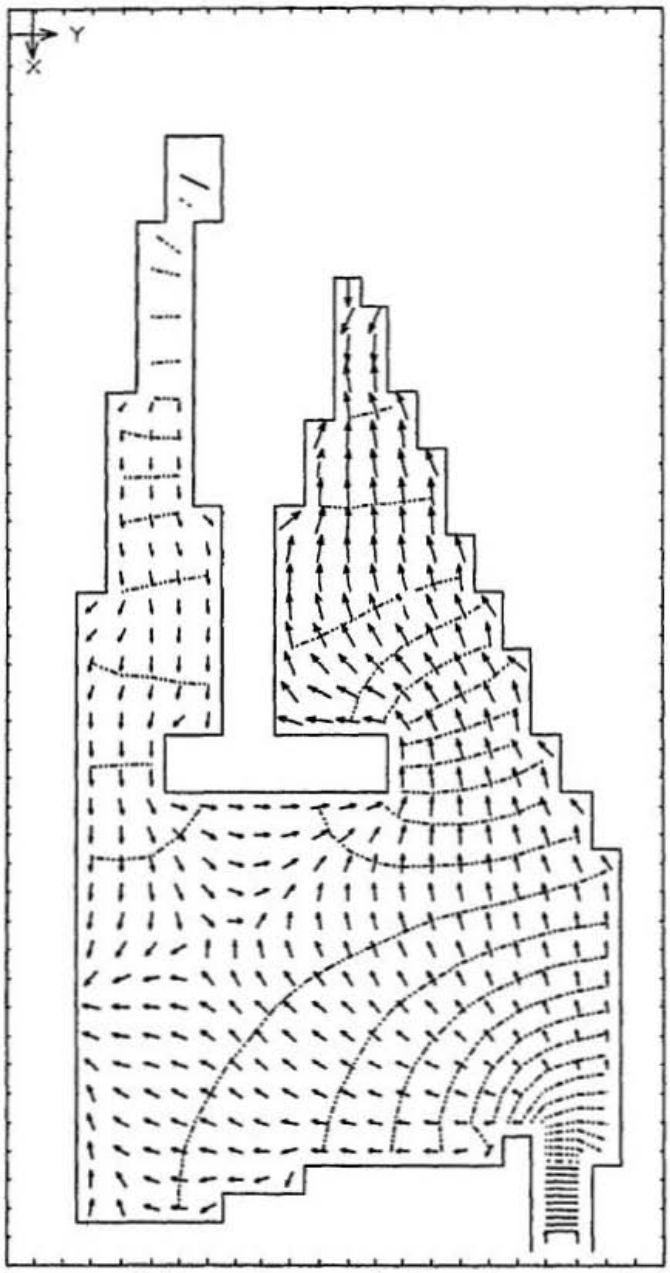

(·····)<0 , (·-·-·-·)=0 , (———)>0
RESPONSE PARAMETER CONTOURS , So= 1.86E-02, & VECTORS.
WAVE PERIOD = 120 :: ITERATION TIME = 315
MAX/MIN = 3.25E-02 / -.0787 :: INTERVAL = .003
GRID SPACE = 10 m
RUN DATE/TIME = 12-06-1991 / 00:50:05
Chezy Coefficient using Ganguillet & Kutter (1869), n=.03

Fig. D.21 - Response parameter, t=315 s, T=120 s.

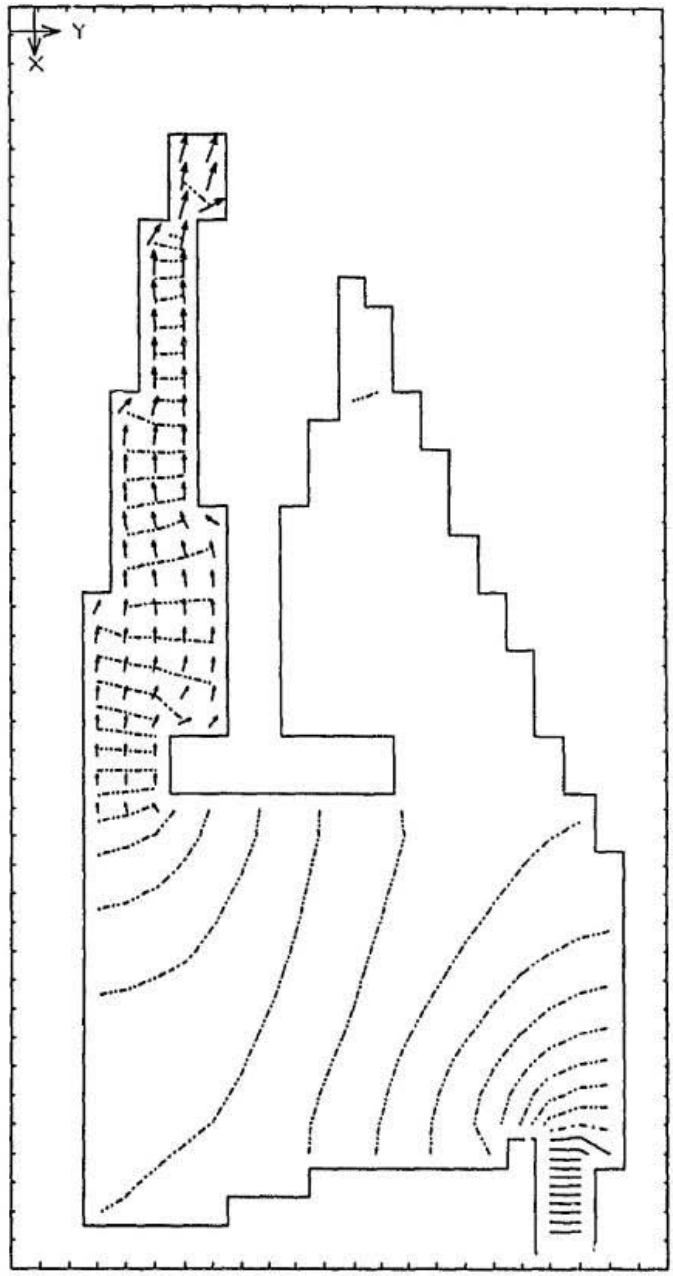

Fig. D.22 - Response parameter, t=330 s, T=120 s.

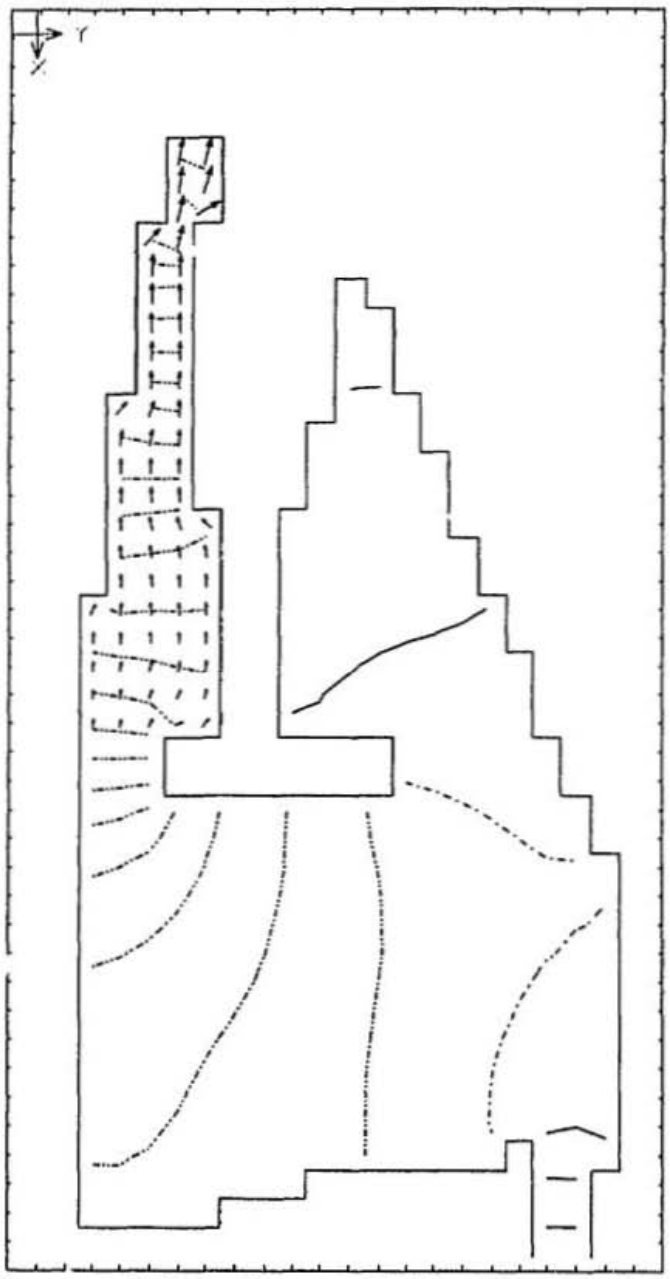

Fig. D.23 - Response parameter, t=345 s, T=120 s.

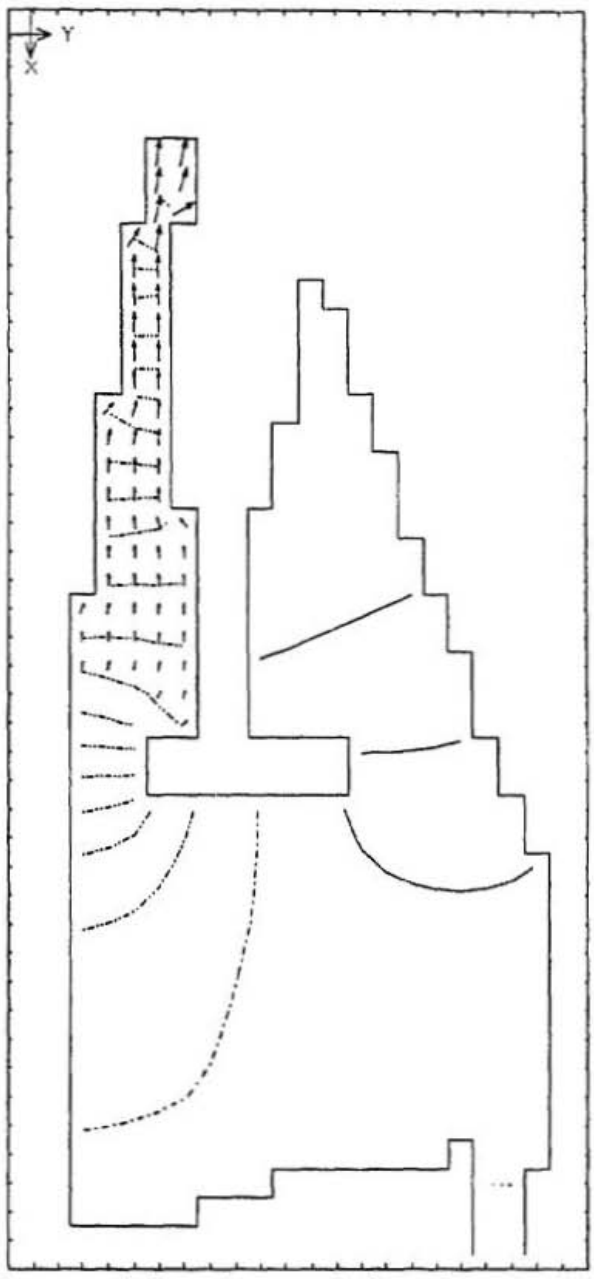

(———)<0 , (·-·-·-·)=0 , (———)>0
RESPONSE PARAMETER CONTOURS , So= 1.86E-02, & VECTORS
WAVE PERIOD = 120 ITERATION TIME = 360
MAX/MIN = 3.81E-02 / 2293 INTERVAL = 01
GRID SPACE = 10 m
RUN DATE/TIME = 12-06-1991 / 01 29 26
Chezy Coefficient using Ganguillet & Kutter (1869), n= 03

Fig. D.24 - Response parameter, t=360 s, T=120 s.